Coarse-Grained Simulation Studies of Self-Organization in Soft Matter Systems Interacting *via* Dynamic Bonds

by

Gaurav Mitra

A dissertation submitted in partial fulfillment

of the requirements for the degree of

Doctor of Philosophy

Department of Chemistry

New York University

September, 2024

Prof. Glen M. Hocky

DEDICATION

To my dear parents for being there unconditionally...

ACKNOWLEDGEMENTS

I extend my heartfelt gratitude to the many individuals who have contributed to the successful completion of this dissertation. First and foremost, I express profound thanks to both my parents for their unwavering support and love throughout this journey. As an international student, pursuing my Ph.D. required me to reside several thousand miles away from my family in India. I can only fathom the excruciating pain they endured dealing with this separation. Nonetheless, they embraced it with a singular hope in their hearts — to witness my success in any career path I choose. I dedicate this thesis to their boundless faith and unwavering perseverance.

My mother is not just a parent but my closest confidante, unconditional advisor, and well-wisher. She possesses an innate ability to understand me better than I know myself. Her wisdom and guidance have been the bedrock of my strength and resilience. Through her, I've learned the art of dealing with situations calmly, especially in the face of adversity. More importantly, she has instilled in me the strength to navigate through encounters with individuals who seek to bring me down. Her teachings resonate in my every step, a testament to the profound impact she has had on shaping my character and approach to life. I am truly blessed to have a mother who supports me relentlessly.

I express deep gratitude to Professor Glen M. Hocky, my Ph.D. dissertation advisor, for consistently serving as an inspiring and supportive mentor throughout my doctoral journey. Even during moments of profound self-doubt and uncertainty about completing a Ph.D. in a field far removed from my comfort zone, Professor Hocky demonstrated unwavering faith in my abilities.

Having been primarily trained in Chemistry during my undergraduate studies, transitioning into the realms of Physics and Material Science for my Ph.D. presented significant challenges. None of this would have been possible without Professor Hocky's invaluable guidance and support.

Being among your first Ph.D. students fills me with immense pride, and the wealth of knowledge I've gained from you is immeasurable. Professor Hocky's proficiency in coding, particularly in Python and Bash, has been a tremendous source of learning for me, considering I was a novice in these areas when I commenced my journey at NYU. Beyond coding skills, I've absorbed his exceptional scientific curiosity and the ability to pose rational questions about any system or topic. These attributes have become integral aspects of my own approach over time.

One of the qualities I've diligently tried to cultivate is the excessive patience demonstrated by Professor Hocky, a crucial trait for any researcher. Observing your ability to remain calm yet determined in the face of overwhelming situations has been instructive. Professor Hocky's clear and strategic thinking, avoiding overwhelm and consistently focusing on the best solutions, has been a guiding principle for me in learning to overcome challenges throughout my academic journey.

I extend my sincere gratitude to the esteemed members of my thesis committee: Prof. Mark E. Tuckerman, Prof. Yingkai Zhang, Prof. Nate Traaseth, and Prof. Alexej Jerschow. Throughout my Ph.D. journey, I have been incredibly fortunate to receive invaluable advice and insights from each of these esteemed scholars.

Prof. Mark E. Tuckerman has played a pivotal role in my academic development. Taking his Advanced Statistical Mechanics course in my second semester proved to be a transformative experience. His exceptional ability to elucidate complex concepts in a clear and understandable manner set a high standard for teaching, which I have rarely encountered elsewhere. Serving as a Teaching Assistant for his Mathematics for Chemistry course in my first year further enriched my learning experience. Prof. Mark's unwavering availability for discussions and guidance, right from my initiation at NYU, has been a cornerstone of my academic journey.

Prof. Yingkai Zhang's course on Machine Learning in my second semester significantly contributed to my academic and professional growth. I am deeply thankful for the clarity and depth of understanding I gained, providing me with a valuable toolset for potential transitions into industry. Prof. Yingkai's approachability and willingness to offer guidance on my Ph.D. endeavors at any point during graduate school have been immensely appreciated.

Prof. Nate Traaseth, serving as the Director of Graduate Studies in Chemistry for most of my time in grad school, has been a constant source of support. His availability to address my questions and concerns regarding my Ph.D. and the valuable insights and suggestions provided during my Ph.D. Candidacy examination in my second year have been instrumental to my academic progress.

Prof. Alexej Jerschow is the Reader of my Dissertation Committee, and my experience as a Teaching Assistant for his Physical Chemistry Lab course has been equally rewarding. His consistent support and kindness have created a positive and conducive environment for me in grad school.

In summary, I consider myself exceptionally fortunate to have had such a remarkable and supportive thesis committee, each member contributing significantly to my academic and professional journey.

I would like to express my profound gratitude to my esteemed collaborators throughout my thesis projects—Prof. Jasna Brujic from CSMR and the Department of Physics at NYU, Prof. Liam J. Holt from NYU Langone School of Medicine, and Prof. Thomas Truskett from the Department of Chemical Engineering at UT Austin. I am incredibly fortunate to have had the opportunity to work with these brilliant minds and the dedicated graduate students and post-doctoral researchers in their respective research groups.

My initial thesis project, conducted in collaboration with Prof. Brujic's lab, was a significant learning experience. The inspiration for the simulation model stemmed from the experiments of Dr. Angus McMullen, a postdoctoral researcher in the group. The invaluable insights and guidance provided by both Jasna and Angus were instrumental in shaping the model and crafting a compelling narrative for my first publication, making it possible to successfully complete this challenging project in my fifth year of graduate school. I am deeply indebted to both of them.

In addition, a special mention goes to Dr. Kartikeya Pratap Singh, a senior graduate student in Prof. Brujic's lab. Beyond our professional collaboration, Kartikeya has been an unwavering source of support and friendship, transcending the boundaries of work. I am grateful for the bond we've formed, and he remains one of my closest confidantes.

For my second project in cellular biophysics and soft biological matter, I had the pleasure of working with Prof. Liam J. Holt and his postdoctoral scholar, Dr. Tong Shu. Liam's genuine sweetness, humility, and unwavering dedication to scientific research made the collaboration both interesting and enjoyable. Liam and Tong were always available to answer questions and provided invaluable ideas for setting up the coarse-grained simulation platform for modeling Liquid-Liquid Phase Separation in a different biological system. My collaboration with Tong has been seamless and beautiful, characterized by her exceptional work ethic and humanity.

Recently, we embarked on a collaboration with Prof. Thomas Truskett's research group, contributing to a larger project funded by a substantial NSF grant—Designing Materials to Revolutionize and Engineer our Future (DMREF). Prof. Truskett, or Tom, has proven to be a gem of a mentor—kind, patient, and supportive. Our collaboration, initiated right after the acceptance of my first publication, has been a delightful journey. Working with his graduate student, Tanner Wilcoxson, has been an unparalleled experience. Tanner's intelligence, communication skills, and expertise in soft matter physics, coupled with his coding prowess, have enriched the collaborative effort. I feel truly blessed for the unmatched experiences gained through collaborations with Tong and Tanner, making this academic journey even more rewarding.

I extend my sincere gratitude to my thesis advisors during my undergraduate (B.Sc.) studies at St. Xavier's College, Kolkata, and my Masters (M.Sc.) studies at IIT Kanpur. The decision to pursue a Ph.D. in Computational Chemistry, focusing on Statistical Mechanics and Soft Matter, has been shaped significantly by their unwavering encouragement and support. They have played a pivotal role in influencing my career trajectory and guiding my scientific choices.

I would like to express heartfelt appreciation to my undergraduate thesis advisor, Prof. Rahul Sharma. His exceptional kindness, care, support, and humility have left a lasting impression on me. Prof. Sharma recognized my potential for research in Chemical Physics and encouraged me to explore Ph.D. programs in Computational Chemistry abroad. His guidance has been instrumental in my academic journey.

During my Masters project at IIT Kanpur, I had the privilege of working under the tutelage of Prof. Keshavamurthy Srihari, an eminent theoretical chemist. His unparalleled guidance and teaching have been transformative, defying mere verbal expression. Prof. Srihari, an outstanding mentor, conducted two remarkable courses during my time at IIT Kanpur. His ability to simplify complex concepts by drawing parallels to everyday life is unparalleled. Prof. Srihari's influence has been a significant motivating force that has shaped my current position, and I am eternally grateful to him.

I wish to convey my profound gratitude to both of my mentors from the summer research internship programs during my undergraduate and Masters studies. In 2016, I had the privilege of working with the globally renowned physical chemist and pioneer of single-molecule spectroscopy, the late Prof. Kankan Bhattacharyya, at IACS, Kolkata. Beyond being a close family friend, he played a pivotal role as a caring and fatherly figure in my life. Prof. Bhattacharyya not only motivated me to nurture my passion for science but also embodied exceptional kindness and compassion. His untimely departure is a source of occasional sorrow, but I believe he watches over me from above, forever blessing my journey. He was more than a mentor; he was my guiding light.

In 2017, I embarked on a summer internship at IIT Bombay under the guidance of Prof. Rajarshi Chakrabarti, a celebrated scientist in the field of Statistical Mechanics and Soft Matter. Our personal camaraderie enriched the experience, turning the summer project into a masterclass that honed my analytical tools and advanced mathematics skills for solving intriguing problems in Non-Equilibrium Statistical Physics. Prof. Chakrabarti, along with his incredibly talented graduate students, Soham and Subhashish, contributed significantly to my learning. The three golden months spent in Mumbai hold a special place in my memory, and I am grateful for the lasting impact of that experience. Prof. Chakrabarti remains a constant source of support, always just a call or text away. I am fortunate to have had the opportunity to work under his guidance, and his pivotal role in supporting my graduate school application process in 2017 is deeply appreciated.

I want to express my gratitude to several professors from both of my undergraduate institutions who played a crucial role in shaping my interest and motivation for Theoretical Physical Chemistry. Professors Madhav Ranganathan and Pratik Sen, who instructed me in various courses during my M.Sc. at IIT Kanpur, focusing on Theoretical and Experimental Physical Chemistry, as well as Mathematics for Chemistry, significantly influenced me with their brilliance and meticulous teaching methods. Their unwavering support and valuable suggestions, particularly during my graduate school applications, were instrumental.

I also want to acknowledge Prof. Rina Ghosh, who introduced me to Quantum Mechanics and Spectroscopy during my B.Sc. degree. Her commitment to perfection left a lasting impression on me. Her dedication and passion for science, coupled with a special emphasis on accuracy and perfection, have become invaluable lessons that I will carry with me throughout my lifetime. These qualities are particularly essential for a computational chemist dealing with a multitude of numbers, figures, and units on a daily basis.

I want to express my heartfelt gratitude to Shenglong Wang, our incredibly helpful and supportive HPC Manager at NYU. Throughout my graduate school journey, Shenglong played a pivotal role in providing support at every stage. Whether it was assisting with the compilation of software/plugins or efficiently allocating resources for the multitude of GPU jobs required for my simulations across various projects, his contribution was indispensable. Shenglong, your presence and support were integral to the completion of my Ph.D., and I am immensely thankful for that!

I also extend a special note of thanks to Prof. Enrique (Rico) Rojas and Dr. Katie Johnson for their invaluable assistance and support during my job search. Both of you are truly exceptional individuals, and I feel incredibly fortunate to have crossed paths with you during my time in graduate school. My gratitude for your guidance and support knows no bounds.

I want to express my sincere appreciation to our exceptional graduate program administrators, Jennifer, Julia, and Yadira, for their unwavering guidance throughout our journey in graduate school. They have been consistently available to address any questions or concerns we may have, whether related to Ph.D. requirements, departmental policies, or other logistical matters. Their support has played a crucial role in navigating the complexities of our academic pursuits.

Lastly, I extend immense gratitude to Kathleen, our administrator at the Simons Center for Computational Chemistry. Kathleen has been an invaluable source of support and care for each member of the Theoretical and Computational Suite. Acting as a maternal figure, she has gone above and beyond to ensure the smooth functioning of all proceedings and seminars in the Theoretical Suite. Kathleen has personally taken measures to facilitate seamless operations to the best of her ability. Moreover, she has organized delightful happy hours and departmental outings, providing much-needed breaks from the routine aspects of research life. Her efforts have created a nurturing and supportive environment that enhances our overall graduate experience.

A decade ago, right after high school in 2013, I took my first steps into college life at St. Xavier's College, Kolkata. At the age of 18, I found myself surrounded by friends like Debankur, Sujit, Farha, Payal, Saibal, Rituparna, Devesh, Ayendrila and many more, whose sheer presence made those college days so memorable. We were all so naive back then, and little did I know that these relationships would withstand the test of time. The camaraderie from those three years of my college days has significantly contributed to my personal development. These friendships, formed in the crucible of early adulthood, played a crucial role in shaping who I am today. It's been a decade since we first forged these bonds, and the memories and connections created during that time continue to be a meaningful part of my life. My friends from college sometimes understand me better than I do myself. Even though we are geographically located in different parts of the world, the bond we share remains unbroken, a testament to the enduring strength of our friendships. Debankur, Sujit, Farha, and Payal have been my closest confidants, and even after a decade, they still stand as some of my most reliable support systems.

My two years pursuing a Master's degree at the Indian Institute of Technology, Kanpur, were undeniably the highlight of my life so far. I owe an immense debt of gratitude to this premier institute for technology and research, as it played a pivotal role in providing me unparalleled exposure and fostering personal development. The cosmopolitan environment, coupled with exceptional teaching quality, a holistic curriculum emphasizing problem-solving skills over rote learning, and extensive exposure to the outside world, as well as integrated co-scholastic activities, collectively contributed to the all-round development of every student fortunate enough to study here.

IIT Kanpur not only offered academic excellence but also provided an atmosphere that allowed the formation of priceless bonds of friendship. The friendships forged during this time are invaluable and, I hope, will remain an integral part of my life forever. This was my first experience living away from my family, and I was fortunate to find a closely-knit community of friends who made the transition easier, ensuring that I never felt too far from home.

The two years passed in the blink of an eye, and as it came to an end, I felt as though a part of myself was being taken away. I want to take this moment to express my heartfelt love and gratitude to those who made my life at IIT Kanpur more beautiful.

Among them, Sampreeti stands out as my closest friend (in fact, my best friend!), hailing from the same city as me (Kolkata). She has been the person I share every major event of my life with, and I hope our unconditional bond of friendship endures a lifetime. Her unmatched emotional quotient, intelligence, sense of empathy and intricate sensitivity have been a constant source of support, making the challenging aspects of life seem more manageable. I consider myself incredibly fortunate to have a friend like her in my life. Naveen, another dear friend, has imparted a profound lesson in appreciating life's simplicity amidst a materialistic world. A lover of poetry and an inspiring photographer, he ignited my own passion for photography. His deep compassion for dogs and for those facing life's toughest battles are qualities I admire greatly. Naveen's influence has not only enriched my creative pursuits but has also instilled in me a genuine appreciation for life's simple joys and the importance of empathy.

Anita is a friend who is always helpful and caring, and approaches life with a pragmatic mindset, offering valuable insights and support in a way that is both reassuring and thoughtful. Sampreeti, Anita and I have also shared some incredible and hilarious memories together which have turned my two years at IIT Kanpur into a collection of moments that are truly worth cherishing. Sachin, my roommate at IIT Kanpur, is a true gem of a friend — kind, compassionate, and incredibly understanding. He has been an invaluable support system during our time in Kanpur. Despite being in geographically distant parts of the world now, we continue to stay connected through WhatsApp. One of Sachin's most admirable qualities is his simplicity and the absence of unnecessary complexity in his character, a trait rarely absent in most people these days.

Neeti, Sampreeti's roommate at IIT Kanpur, is a genuinely sweet person and a very calming influence as a friend. Our shared experiences include countless hangouts, and I will always remember our spontaneous last-minute trips to New Delhi (Sampreeti, Neeti and myself) for our GRE and TOEFL exams. Those crazy moments created lasting memories that I'll cherish forever. I am immensely grateful for friends like Chetan and Saksham from the Mathematics and Statistics departments at IIT Kanpur. The memories we created during our time in the hostel, the late-night walks, and canteen visits are unforgettable. Special thanks also go to Kapil (for being the dearest elder brother to me I had always missed in life and for being an absolute gem of a person—kind, empathetic and so emotionally sensitive) and the incredible team at the Counseling Service Team, IIT Kanpur (Praharsh, Siddharth, Rupesh, Mayank, and many others) for ensuring our transition into this new environment was welcoming and seamless. Their support has been invaluable, and I'll always appreciate their role in making my IIT Kanpur experience so enriching.

In reflecting on my six-year journey at New York University within the Hocky Research Group, I am compelled to express my deep appreciation to several members who have played instrumental roles in shaping my experience.

First and foremost, I am grateful for the friendship of Yuvraj, a great companion throughout my grad school journey. Yuvraj's unwavering support, intelligence, and rational thinking have left an indelible mark on me. His transparency and open-hearted nature were a breath of fresh air. Yuvraj's exceptional empathy and sensitivity during challenging times have made him an invaluable and caring friend. The countless late nights in the lab with Yuvraj as a constant companion will forever be etched in my memory.

Equally significant is my connection with Willmor, a fellow Ph.D. student who has shared innumerable engaging conversations, memorable dinners and drinks with me. As a matter of fact- Yuvraj, Willmor, and I are the first students to graduate under Professor Hocky's supervision, embarking on this collective journey back in 2018.

I extend my gratitude to other members of the Hocky Research Group who have contributed to the enjoyable and fulfilling nature of this journey. Triasha and Nicodemo, in their second and third years of Ph.D. respectively, have been really great labmates with whom I could have stimulating conversations, and shared moments of fun. I would also like to thank some of the current group members Kangxin, Nicole, Abby, Fatemah and JP for their contributions to create a positive and wholesome environment.

A special acknowledgment is reserved for Dr. Michael Hartmann, the former postdoctoral researcher in our group. Despite his one-year tenure, the wealth of knowledge I gained from him in the domain of research is immeasurable. Michael's cheerful disposition, unwavering focus, and exceptional work ethic were truly inspiring. Beyond work, our camaraderie added a special dimension to my initial years in graduate school, as he was always available to offer any assistance I needed.

I am deeply thankful for the presence of our Simons Center Postdoctoral Researchers- Philipp, Michael and Muhammad, who have enriched my experience with their insightful conversations and valuable contributions. In particular, my connections with Philipp and Michael have been very special, as they both are incredibly kind and extremely supportive people to be around with. The meaningful exchanges and camaraderie we share have added a positive dimension to my grad school experience.

I would like to extend my heartfelt thanks to the exceptionally bright and engaging high school (GSTEM) and REU students I've had the privilege to mentor or advise, namely Sara (2023), Lauren (2023), Matilda (2022), Deborah (2022), Alexandra (2022), Hitangee (2019), Daniela (2020) and Chuan (2019). Chuan has played an indispensable role in setting up the python framework for my very first project and I shall be forever indebted to him for this. Working with these brilliant minds has been a rewarding experience, and I am confident that they will continue to excel on their journeys upwards. It was truly my pleasure and privilege to get to know these exceptionally talented students. They have undoubtedly set a benchmark with the enthusiasm they displayed for research at such a young age. Wishing each of them the very best in all their future endeavors.

I would like to express my gratitude to my colleagues and acquaintances in the NYU Chemistry department, including Richard, Amiel, Tommy, Hafsah, Stephanie, Leslie, Irene, Markus and Tom (Egg). Richard, despite being away in Chicago for most of his grad school, has been one of the most helpful friends I've had during this journey. I am forever indebted to him for his unwavering support, especially during my job search. The memories of our first year of grad school, filled with shared struggles and triumphs in coursework, are unforgettable. I want to express my sincere appreciation for the wonderful times spent with Richard and Amiel during those challenging moments. Wishing both of them the very best on their journeys ahead. I am grateful for the numerous insightful conversations I've had with the postdocs in our Theory Suite, namely Stephanie, Leslie, and Irene. Their brilliance and exceptional intelligence shine through, and they have consistently offered me invaluable solutions on how to navigate various challenges during my time in grad school. Tommy and Hafsah stand out as some of the nicest individuals I've encountered on this journey. Their sense of responsibility and commitment to the department is truly commendable. Both have shown initiative in planning various activities and events, contributing significantly to the overall positive atmosphere within our community. Their kindness extends beyond their roles, and I consider myself incredibly fortunate to have encountered such amazing individuals during my grad school experience. Finally, I would like to extend my thanks to the fantastic additions to our Theory Suite this year (2023), Markus and Tom. Markus, a visiting research student from Austria in Prof. Tuckerman's group, and Tom (Egg), a first-year graduate student, have both proven to be exceptionally bright individuals with a wonderful sense of humor. Despite the relatively short time that we had together, I have developed an amazing camaraderie with both of them. Our outings for drinks on several occasions have been memorable, and what sets Markus and Tom apart is their social outgoing nature and excellent communication skills. I extend my heartfelt wishes to both Markus and Tom, hoping for the very best on their journeys forward.

Lastly, I want to express my gratitude to all my friends whom I met here in the United States. They have made these long six years of my PhD a truly worthwhile and enriching journey. From countless trips and party nights with Sheenam and Arpan to sharing jokes and memes with Harnoor and Arpan, experiencing countless drunk nights (with Ankan) and waking up completely wasted the next morning, to engaging in the deepest and most fulfilling conversations about life, love, poetry, science, career, friends, ambitions, and everything in between with Satyam and Asit—these moments have defined the richness and depth of my grad school experience.

Sheenam and I have nurtured a friendship that spans over 6 years, dating back to our first meeting during our subject GRE exam in New Delhi. Throughout this time, she has consistently been a kind, empathetic, and helpful friend, for which I am truly thankful. We have shared some of the most splendid memories together in New York, living here for more than 6 years now. Arpan has been more than a friend; he has been my closest companion throughout most of my grad school journey, akin to a big brother. He stood by me during my worst and most vulnerable times, especially when I battled depression and faced the hopelessness of losing people close to me. Arpan has provided me with the most practical and useful advice on life, teaching me the importance of prioritizing myself over anyone else. His support as a friend has been invaluable. I was so sad when he had to leave earlier in 2023 for Mexico to stay there for a year, and I cannot wait for him to return back to the United States in a few months. Harnoor and I share a great friendship and his sense of humor and wittiness is just perfect. Our thoughts align so seamlessly that I understand exactly where he comes from; our frequencies of thought match exceptionally well. He is very sorted and disciplined as an individual, and I truly appreciate his maturity and growth.

Satyam and Asit, both PhD students in the Center for Soft Matter Research at NYU, exhibit a remarkable combination of emotional and intellectual intelligence. This is commendable at their age, considering that they are 3-4 years younger than me. I have formed strong connections with Satyam and Asit across various aspects of life. Their impeccable taste in music, food, and art has further strengthened our bond. Some of my best memories of grad school has been spending time in Newport, Jersey City at their residence with some of their other lab members. Talking to Satyam and Asit always makes me feel like I can truly be myself. Both of them are very consistent and determined about their choices in life, and I really admire that.

Nitin and Praful are also cherished friends of mine. Having been in the same cohort at IIT Kanpur, Nitin and I share a history from our Masters program from 2016-2018. Our camaraderie has extended to some of the best trips here, creating enjoyable and lasting memories. I first met Praful when I visited Buffalo in 2021 to see Nitin, and since then, he has become a great friend. Praful has provided me with invaluable advice on strategically approaching the job search game.

I consider myself fortunate to have met Lohit at the APS March Meeting 2023 and Parth, a friend of Sujit at the University of Miami. Both of them are truly amazing individuals, and our conversations have provided me with new perspectives on life. During the APS March Meeting in Las Vegas in 2023, Nitin, Lohit, and I embarked on a completely impromptu road trip across Arizona and Nevada. I must admit, it turned out to be one of the most treasured and unforgettable experiences of my life so far. It became a bonding experience for all three of us on a personal level. During another summer trip to upstate NY (2023) with Parth and Sujit, I had the opportunity to overcome one of my greatest fears – of heights, by trying out parasailing — thanks to Parth's motivation and insistence. Their presence has added significant value to my personal and adventurous experiences. Parth and I share a profound personal connection, and our bond was instant. Both of us have had uncomfortable experiences in the past, and talking to him during the trip felt like therapy or catharsis for me.

I have to give a special recognition to my incredibly selfless friend, Dhwanit, whom I've come to know properly only within the past year. The level of support and assistance he has provided as a friend goes beyond any measure. His guidance has been invaluable, especially in my search for a postdoctoral position, and I am truly grateful for his support!

And finally, I wish to conclude this *long* note by thanking the place where I have spent all these 6 years – New York City. New York, you've been more than a city to me; you've been a teacher, a friend, and a home. As I move forward, I carry with me the lessons learned on your streets—the value of perseverance, the beauty of diversity, and the strength that comes from embracing change. Thank you for being the backdrop to countless experiences, shaping my journey in ways I could have never anticipated. Thank you for being a part of my story, you will remain the most special to me.

Abstract

This thesis aims to comprehend the physics underlying self-organization phenomena in diverse soft matter systems, spanning materials and biology. The systems under scrutiny exhibit binders (or "active" binding sites) with dynamic interactions leading to aggregation. Our study investigates the dynamics of binder adhesion, utilizing Coarse-Grained Molecular Dynamics simulations. A pivotal component of our simulation platform is a dynamic binding and unbinding model, implemented as an open-source custom plugin to HOOMD-blue. This model allows stochastic binding and unbinding of particles, with optional temperature-dependent rates to capture cooperative melting. Through this approach, we strive to provide insights into the self-aggregation mechanisms in soft matter systems with binders, connecting materials and biological sciences. First, we study the self-assembly of colloidal particles with *explicit mobile binding molecules*, such as DNA-coated emulsion droplets, that allows for spontaneous valence control by tuning parameters such as the interaction strength between the particles and the concentration of the binders. This valence control can be used to optimize the yield of droplet polymer chains called *colloidomers*, and our coarse-grained MD simulation model can further guide programmable design in experiments such as folding of *colloidomer* chains. Next, we explore the dynamics involved in the formation of adhesion patches between these droplets. Additionally, we examine how adjusting the molecular features of the system can influence the growth and shape of the adhesion patch. Subsequently, our investigation delves into the formation of both equilibrium and kinetically arrested gels originating from ligated nanoparticles and macromers featuring distinct functionalities. These functionalities involve dynamic binding and unbinding, and our coarse-grained simulation platform allows us to gain insights into the impact of binding and unbinding kinetics in the design of such assemblies. Finally, we also establish an *in silico* model for a synthetic LLPS phase separation system called "synDrops" to study how the active, crowded cellular environment affects biomolecular condensate formation.

Contents

LIST OF FIGURES

List of Tables

CHAPTER 1

INTRODUCTION

1.1 MOTIVATION

Macroscopic properties of materials rely on the strength of intermolecular interactions [1, 2] and length scales. A gas condenses into liquid as intermolecular forces prevail over thermal motion. Further cooling yields a solid, with molecules fixed in definite locations. Liquids [3], held by intermolecular forces, exhibit fluidity, contrary to the indefinite shape of solids [4]. This interplay of attractive forces and thermal motion yields varied mechanical properties. Liquids flow (irreversible deformation) [3, 5–7], whereas solids exhibit elastic behavior (reversible deformation) under shear forces [4–7].

But what happens in a scenario where the distinction between solid and liquid becomes *blurred*? An interesting class of materials with mechanical properties intermediate between the two emerges! *Soft materials* [8–11] encompass a class of materials known for their flexibility, deformability, and low mechanical stiffness. They can readily undergo deformation in response to thermal or mechanical stresses, typically on the scale of thermal fluctuations. This category includes a wide range of materials, such as polymers, colloids, surfactants, foams, granular materials [12, 13], liquid crystals [14], gels, tissues, and biological/active materials e.g. bacteria [15, 16], active colloidal swimmers [17–19] and microtubules [20, 21] inside the cytoplasm of eukaryotic cells (which have a vital role in genomic organization). Everyday items, including various food products like mayonnaise, chocolate, and jelly are representative of soft materials.

The physical quantity that can predict how 'hard' or 'soft' a material is its shear modulus, obtained from rheological [5, 7] measurements. In contrast to traditional hard materials like metals and ceramics, soft materials can undergo significant deformations without breaking or losing their structural integrity. They retain their form temporarily, behaving similar to elastic solids, yet with the passage of time, they behave like fluids [8, 9, 11]. This dual nature of momentarily appearing as elastic solids and eventually exhibiting the properties of viscous liquids results in them being labeled as *viscoelastic materials* [22]. One common feature in all these materials is that they are composed of units at the *mesoscopic* length scale [23].

Building blocks of soft materials experience intermolecular forces [1, 2, 8, 9] similar to atoms or molecules, with their strength and scale influenced by particle size and the surrounding medium. These include electrostatic interactions [24], polarization forces [2, 25], and quantum mechanical forces (such as covalent bonds [26–28], hydrogen bonds [29, 30], and charge transfer interactions [31]). Additionally, soft materials involve other interactions like depletion [32–35] and hydrophobic forces [36].

What constitutes the motivation for exploring the properties and self-aggregation behavior of this *very* interesting class of systems known as *soft materials*? Such materials have very intriguing properties, and invite us to explore a field where flexibility and responsiveness [8, 9] transcends being just a mere attribute, evolving into a strategically harnessed advantage. Drawing inspiration from biological tissues and cells [37], soft materials serve as a key source of insight into the complexities of living organisms [8]. This exploration finds its use in biomimetics [38–40] and tissue engineering [41], offering a deeper understanding of how soft materials interact. Soft materials play a pivotal role in the field of manufacturing — particularly in shaping flexible electronics, wearable devices, and soft robotics [42, 43] (due to their adaptability); as well as in consumer products — ranging from clothing to packaging to personal care items. The significance of soft materials extends into medical applications, influencing drug delivery systems and implantable devices. The responsiveness of soft materials to external stimuli, such as temperature, or light, paves the way for the design of *smart* materials [44–47] capable of adapting to changing conditions, such as in sensors. Understanding the aggregation behavior of soft materials can also contribute to design of energy-efficient, recyclable, and eco-friendly materials which can promote environmental sustainability.

Soft materials are interesting systems to probe for gaining an understanding of the intricate world of structural arrangements at the molecular and nano-scale. Exploring these materials provides valuable insights into the interplay of forces, energy dissipation, and deformation, contributing significantly to our understanding of rheology [5, 7]. Moreover, the study of soft materials sheds light on the underlying physics of phase transitions and critical phenomena [48, 49] within these systems, enhancing our broader comprehension of fundamental physics principles. This knowledge extends beyond commercial applications, laying the groundwork for innovations in fields such as materials science and biophysics. In this thesis, I have outlined an in-depth study of the self-assembly phenomena in soft matter systems with a diverse range of properties, using computational simulations that involve coarse-grained modeling [50, 51].

1.2 Self-Assembly: a Brief Overview

Self-assembly is defined as a natural process where individual components spontaneously come together to form an organized structure or pattern due to specific interactions among the components [52]. The range of scales on which self-assembly occurs is vast: here, we primarily focus on assembly of components that range in size from a few angstroms (such as atoms and molecules) to a few micrometers (such as colloids) [53, 54]. This phenomenon can be used to design nanomaterials [55, 56] such as metals, alloys, and semiconductors, as well as supramolecular and biological materials. The driving force for self-organization phenomena range from multiple non-covalent interactions, such as hydrogen bonding, electrostatic association, and van der Waals forces, and hydrophobic interactions [57]. Self-assembly has indispensable applications in fields such as engineering of bio-inspired materials, drug delivery and pharmaceuticals. It can also be harnessed in the design of dynamic and self-healing [58, 59] materials.

This process has been particularly relevant in the synthesis of functional biomaterials [60] at mimic the natural extracellular environment and provide biological signals to guide cell behavior. Self-assembled biomaterials [61, 62] often incorporate at least one biological component to guide assembly. Prominent examples of self-assembly in materials science include the formation of molecular crystals [63, 64], colloidal aggregates [65–67], lipid bilayers [68–70], phase-separated polymers [71], etc., and there exists a vast reserve of literature on each of them. In this thesis, we mostly focus on non-driven systems [72] that do not receive any external energy and inactive components driven solely by thermal fluctuations from the solvent, and having a diffusive motion not involving any energy consumption.

1.3 Dynamic Bonds in Self-Assembly

Self-assembly is broadly classified into two types — *static* and *dynamic* [52, 54, 57, 73, 74]. Static self-assembly leads to the formation of thermodynamically stable structures, achieving rapid equilibrium with limited possibilities of spontaneous rearrangements [52, 54, 57]. In contrast, dynamic self-assembly is characterized by reversible processes, involving continual association and dissociation, thereby permitting the system to dynamically explore various configurations over time. The thermodynamics of dynamic self-assembly are complicated, and involve both enthalpy and entropy considerations within a non-equilibrium framework. Dynamic self-assembly can provide flexibility and responsiveness [28] to the self-assembled structures, unlike static assembly.

Dynamic bonds are instrumental in both assembly and disassembly of supramolecular structures [75]. These bonds, whether they are dynamic covalent or non-covalent interactions [28], exhibit reversibility — they can form or break in response to external stimuli. This inherent reversibility enables self-assembled structures to dynamically adapt and undergo alterations in reaction to different external conditions. Within self-assembling materials, dynamic bonds facilitate rearrangements, leading to the creation of adaptive (reconfigurable) structures [28, 76, 77]. This proves essential in applications such as drug delivery, nanotechnology, and the design of responsive materials [77] characterized by high fidelity.

Dynamic bonds can be classified into two broad categories — *dynamic supramolecular, non-covalent interactions*, and *dynamic covalent bonds (DCBs)* [28]. The former are relatively weaker as compared to DCBs and include hydrogen bonds, metal-ligand coordination bonds [78, 79], π-π stacking [80, 81], and host-guest interactions [82, 83]. Dynamic covalent bonds (DCBs) [28, 84] confer a dynamic quality to self-assembled structures through their capacity for the reversible exchange of covalent bonds, and such exchanges usually occur *via* associative or dissociative pathways. Examples of DCBs include transesterification reactions, disulfide exchange and reversible imine formation reactions [28, 77]. Recently, there have been tremendous advancements in design of polymeric materials [77, 85–87] through dynamic covalent bonds. These materials come with unique features like flexibility, self-healing [58, 59, 86], adaptability and responsiveness [58, 77].

1.3.1 Examples of dynamic bonds in assembly of biological systems

Dynamic bonds within biological assemblies are vital for maintaining structural integrity [88], promoting molecular interactions, and fostering adaptability. These bonds allow biomolecular structures to undergo necessary conformational changes [89, 90], respond to environmental stimuli, and fulfill their functional roles within living organisms. Discussed in the following sections

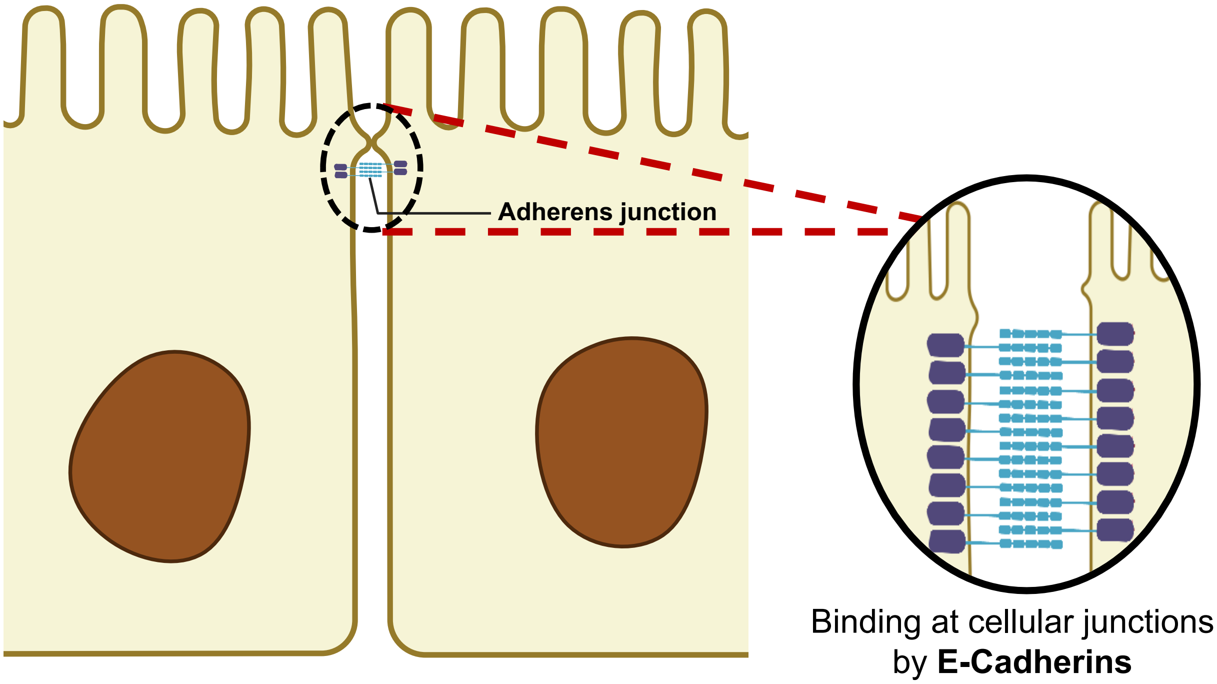

Figure 1.1: Schematic representing the intercellular junction of epithelial cells where E-cadherin proteins help in cell-cell adhesion (Figure created using `https://biorender.com/`).

are some examples of dynamic bonding in biological assemblies.

1.3.1.1 CELL-CELL ADHESION *VIA* JUNCTION PROTEINS SUCH AS CADHERINS

Cadherins are transmembrane proteins [91, 92] that mediate cell-cell adhesion in animals (Fig. 1.1 shows cadherin mediated cell-cell adhesion for epithelial cells). Cadherins from two opposing cells form *trans*-bonds at the cellular interface [38, 39, 93], controlling adhesion by reducing interfacial tension directly and indirectly through actomyosin signaling [94–96]. The cadherin adhesion complex links cells to the cytoskeleton [94], ensuring mechanical coupling crucial for tissue stability and cell mobility [96]. Adhesion is dynamic, with cadherins adapting to mechanical changes. They can form various adhesive dynamic bonds, like *catch* [39, 93, 97, 98] and *slip* bonds [99, 100], enabling them to modulate adhesion strength in response to force [101]. This modulation is critical for maintaining tissue integrity and regulating developmental morphogenetic processes [96, 102] in multicellular organisms.

1.3.1.2 Dynamic binding of actin filaments to myosin motors and crosslinkers

The dynamic binding of actin filaments with myosin motors and cross-linkers [103–107] is crucial for cell morphology, stiffness, and response to mechanical signals. Myosin motors are motor proteins that interact dynamically with actin filaments [104, 108–110] in a cyclic process known as the *cross-bridge cycle*, to facilitate cellular movement and muscle contraction. The binding process involves the myosin motor domain attaching to a specific actin-binding site (shown in Fig. 1.2 [A]), with ATP hydrolysis [109–111] powering a movement along the actin filament. Actin cross-linking proteins [112, 113] such as α-Actinin [114] and Fascin [115] stabilize actin filament interactions (binding of actin filaments with α-Actinin shown in Fig. 1.2 [B]) and tune the mechanical properties of the actin network [103–106, 116–121] (by providing structural stability to actin filaments), thus contributing to the regulation of actomyosin contraction [122] *in vivo*. The force-sensitive binding kinetics of cross-linkers [112, 113] further underscore their role in governing cell mechanics and behavior. The properties of these cross-linked cytoskeletal networks have been extensively studied *via* coarse-grained-simulations employing explicit cross-linkers [103–106, 118, 119], and these systems serve as good biological analogues for cross-linked polymeric gel networks (formed by dynamic covalent chemistry [28, 77, 84–87]), a topic explored in detail in Chapter 4. Simulation models used to study assembly of networks formed from microtubules and motor proteins [123] were also later adapted to study the assembly of cytoskeletal actin networks with dynamic cross-linking [124].

1.3.1.3 Reversible hydrogen bonds between complementary strands in a DNA Double Helix

In a DNA double strand, hydrogen bonds form between complementary base pairs [125–128] (as shown in Fig. 1.3). Adenine (A) forms two hydrogen bonds with thymine (T), and guanine

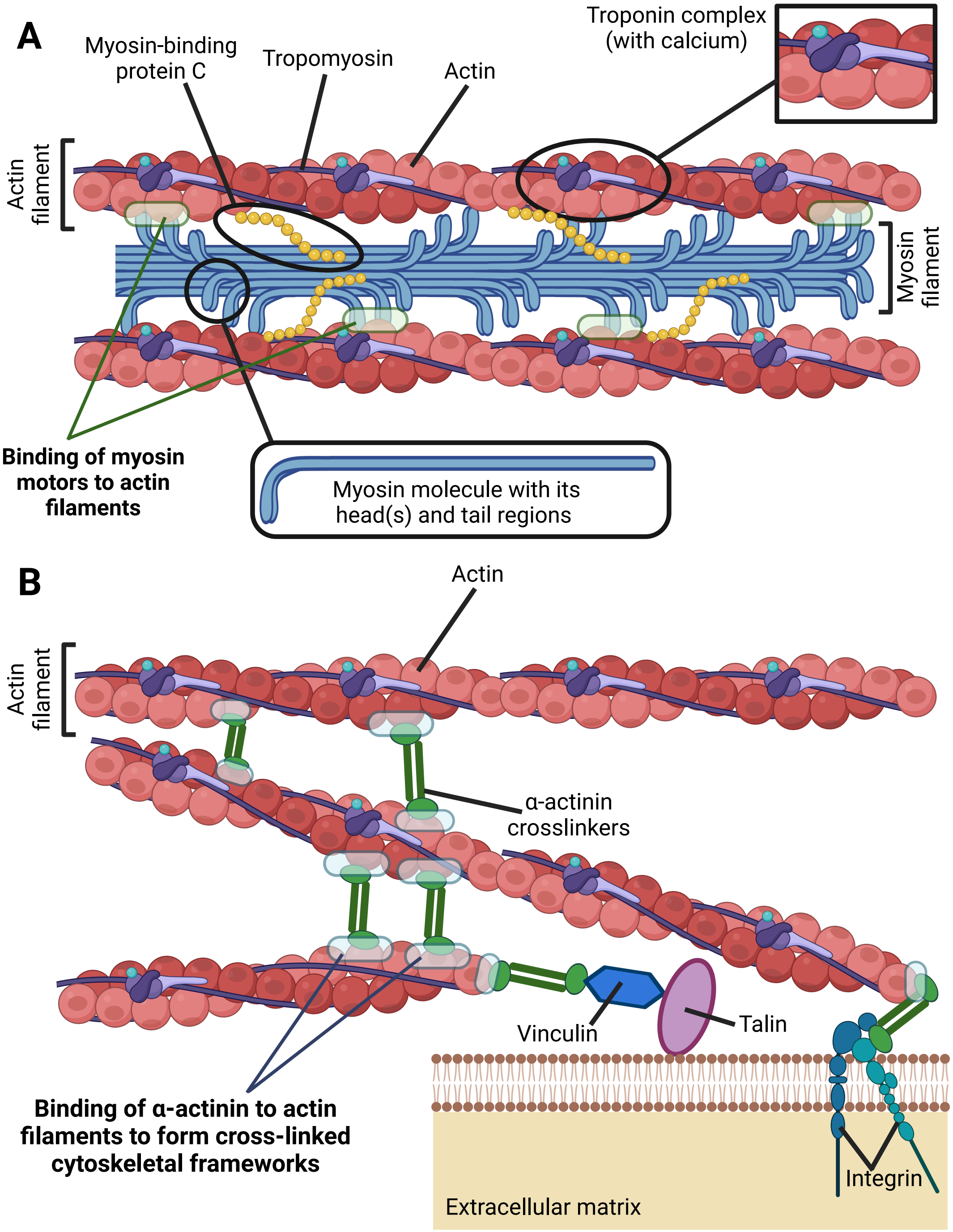

Figure 1.2: Schematic(s) representing the dynamic binding of actin filaments to (A) myosin motors (B) cross-linkers such as α-actinin to form the cytoskeletal framework (Figure created using `https://biorender.com/`).

(G) forms three hydrogen bonds with cytosine (C). This precise base pairing is pivotal for maintaining the specificity of the DNA structure. Notably, the hydrogen bonds in DNA are dynamic, allowing for processes like DNA replication [129–131] and transcription [132–134], during which the strands undergo temporary separation and subsequent rejoining. Hydrogen bonds, being relatively weak compared to covalent bonds, play a critical role in ensuring the stability and functionality of the DNA double helix. The stability of these hydrogen bonds is sensitive to temperature, and their nature is thermo-reversible. In instances of DNA denaturation [135, 136] at elevated temperatures, the hydrogen bonds between base pairs undergo breakage, leading to the separation of the DNA strands. It is noteworthy that this process is not isolated to individual segments; instead, if one region of the DNA initiates denaturation, it can promote the cooperative melting [137–139] of adjacent regions, contributing to the overall denaturation of the entire DNA molecule.

1.3.1.4 DYNAMIC BINDING IN LIGAND-RECEPTOR SYSTEMS

Ligand-receptor systems [140, 141] play critical roles in numerous biological processes, facilitating regulation within individual cells as well as between different cells. A general prototype of a ligand binding to a receptor to form a *ligand-receptor complex* [141–143] is shown in the schematic Fig. 1.4. Upon binding, both the ligand and the receptor may undergo changes in conformation. The binding process is frequently characterized by two rate constants: association (k_{on}) and dissociation (k_{off}). The relationship between these rates, expressed as the dissociation constant ($K_d = k_{\text{off}}/k_{\text{on}}$), serves as an indicator of the stability [142, 143] of the ligand-receptor complex.

Dynamic bonds in ligand-receptor systems involve non-covalent interactions like hydrogen bonds [29, 30], ionic bonds [144–146], and van der Waals forces [147, 148], which are reversible. Illustrative examples include antibody-antigen interactions [149] in the immune system, enzyme-substrate binding in catalysis [150–152], G protein-coupled receptor signaling [153–155], hormone-

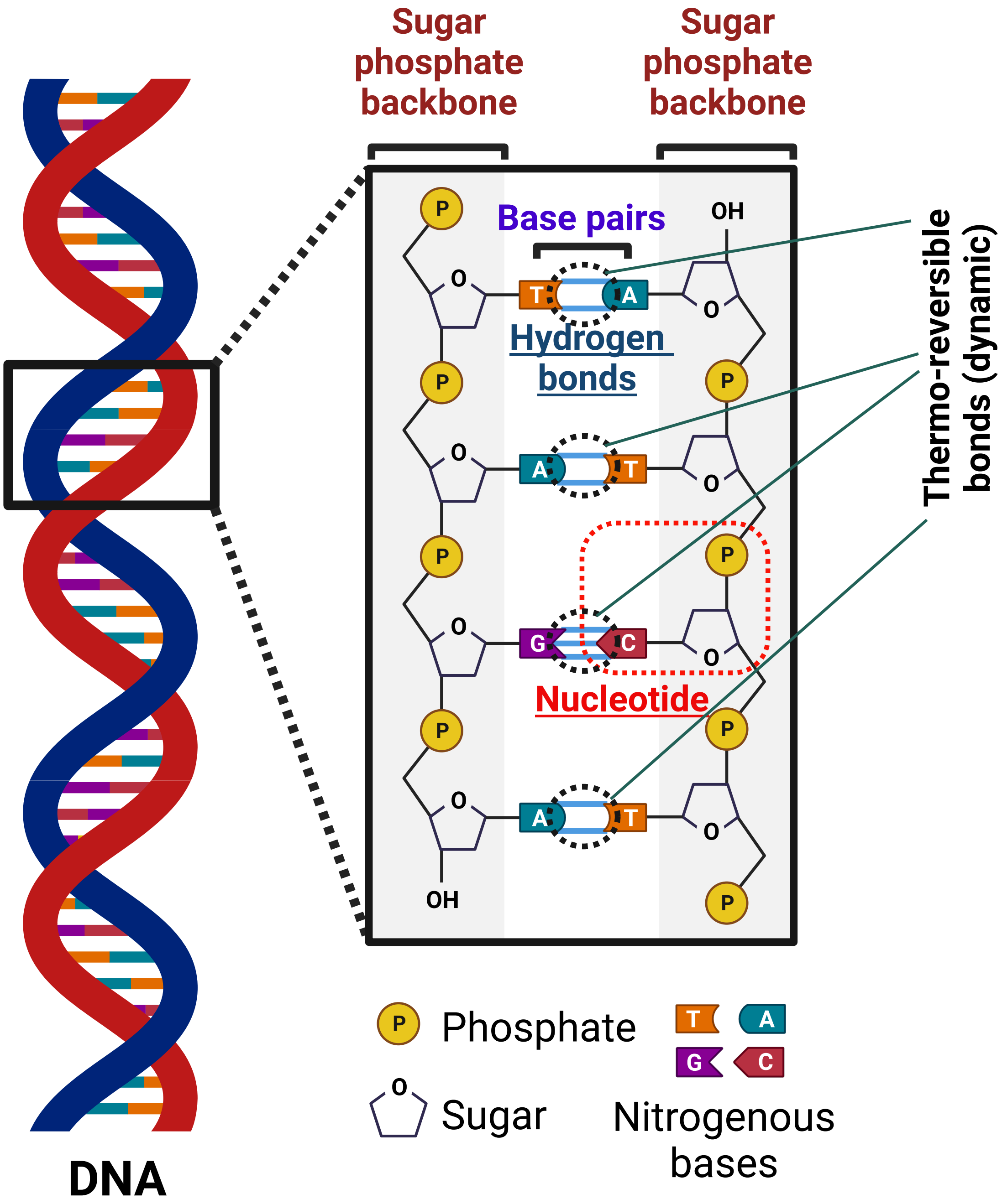

Figure 1.3: Diagram showing a double-stranded DNA strand and the hydrogen bonds formed between complementary base pairs (that keeps the double strand intact). These dynamic hydrogen bonds are thermo-reversible (Figure created using `https://biorender.com/`).

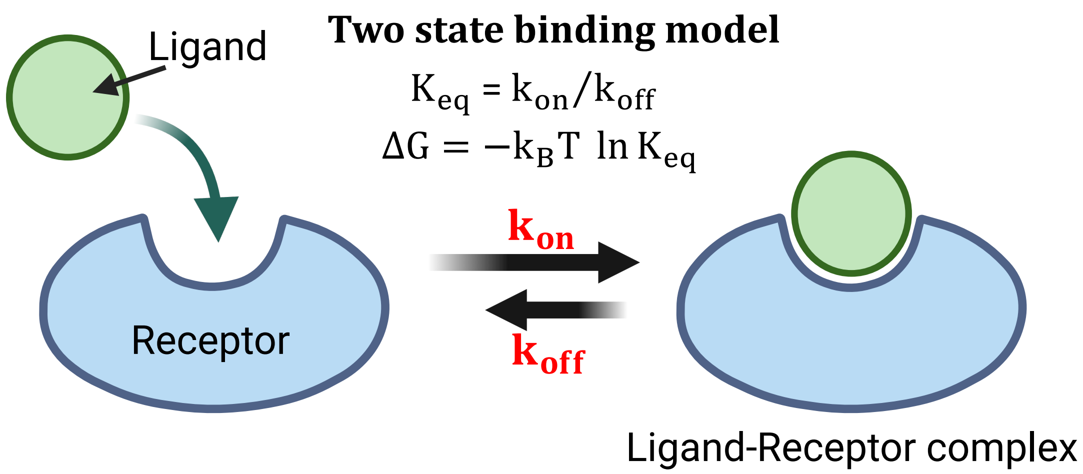

Figure 1.4: Schematic representing the reversible dynamic binding / unbinding of a ligand molecule to / from a receptor in a standard biophysical system of interest, with an equilibrium constant $K_{eq} = \frac{k_{on}}{k_{off}}$, the ratio of the forward and backward reaction rates (Figure created using `https://biorender.com/`).

receptor interactions [156–158] and many more. The robustness and specificity of these dynamic bonds contribute to the overall function of these biological systems. These dynamic interactions play crucial roles in cellular processes, facilitating reversible binding and unbinding, and are essential for diverse physiological functions such as immune response and enzymatic activity [159].

1.3.2 Examples of dynamic binding in soft materials

There is a diverse range of soft materials that leverage dynamic binding to achieve properties like self-healing, adaptability, and responsiveness to environmental stimuli [28, 58, 59, 77] as well as to mimic the mechanics of adhesive systems in cellular biology [38, 39, 93]. Some examples are mentioned in the following sections.

1.3.2.1 Dynamic binding in complementary emulsion droplets encapsulated with binders / ligands

Emulsion droplets [160–163], featuring binders that can establish complementary bonds with neighboring droplets, offer significant potential in designing intricate self-assembled structures.

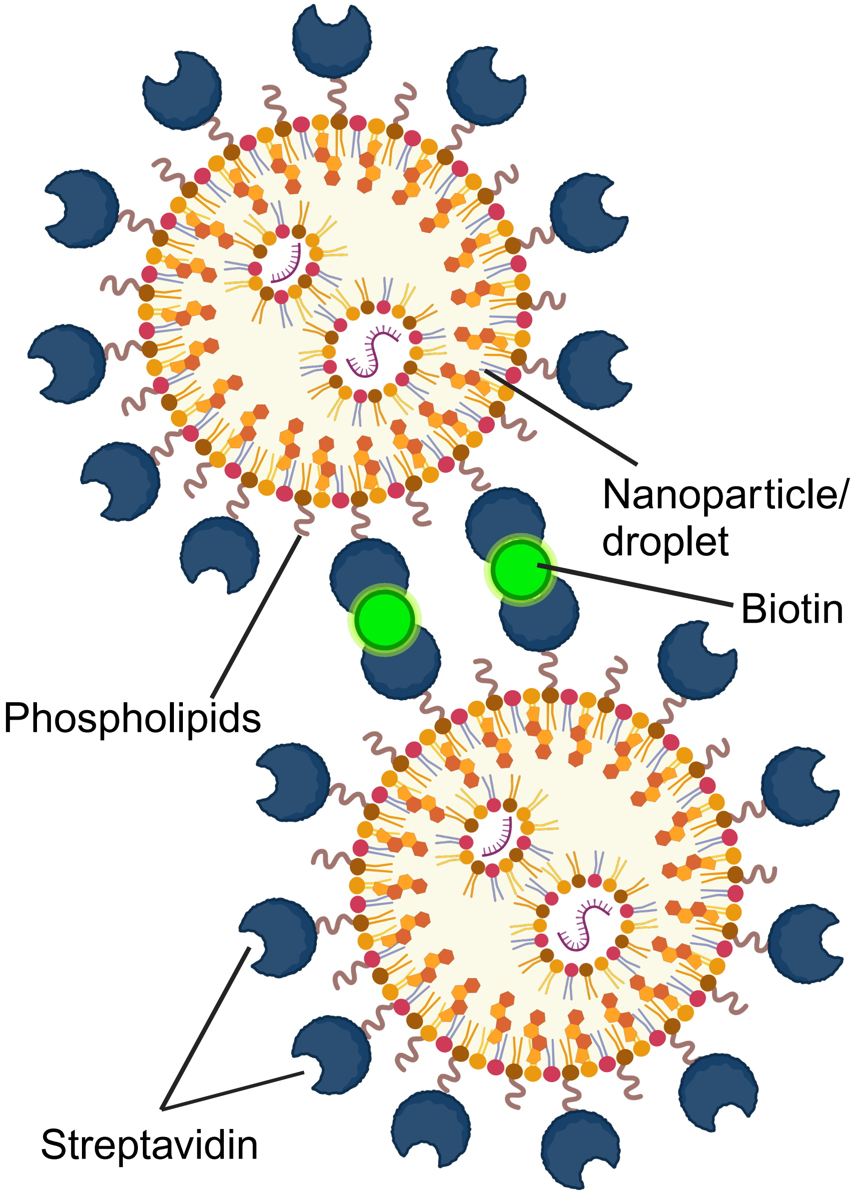

Figure 1.5: A schematic showing the adhesion of biomimetic emulsion droplets via the formation of dynamic covalent linkages between biotin and streptavidin. Here, cellular adhesion mediated by self-complementary cadherin proteins is replaced by a SA-biotin-SA complex bridging two droplet interfaces [38]. The binding energy associated with forming such *ligand-receptor* type bonds is on the same order as that of adhesions at cellular junctions, thus making this system a good *biomimetic* (Figure created using `https://biorender.com/`).

These binders engage in specific interactions, initiating a dynamic binding process [50, 161, 164] that provides a remarkable level of specificity and selectivity to the resulting structures. DNA serves as a versatile binder capable of facilitating programmable interactions, playing a crucial role in diverse applications such as drug delivery and the construction of three-dimensional materials [165]. Another promising avenue where such systems can explore dynamic binding is in mimicking the cellular adhesion mechanics [100] through design of biomimetic emulsion droplets [38, 39, 93] coated with dynamic binding agents that can mimic the adhesive properties of biological cells. Actual adhesion proteins such as cadherins could be used or receptors such as streptavidin [38, 166] which are known to bind covalently to ligands like biotin, as demonstrated in Fig. 1.5.

1.3.2.2 REVERSIBLE HYDROGELS AND POLYMERIC NETWORKS FORMED BY DYNAMIC BONDS

Dynamic covalent chemistry (DCC) [28, 77] is a fundamental strategy for crafting reversible hydrogels and polymer networks, utilizing bonds such as disulfide, boronic ester, imine, and thiol-ene reactions [28, 77, 84–86]. These bonds possess a distinctive ability to break and re-establish under particular conditions, enabling ongoing rearrangement within the polymer network. This leads to the development of materials characterized by adaptability, responsiveness, and the ability to undergo self-healing [28, 58, 59]. These systems find applications in drug delivery, and are also employed in tissue engineering [41], with notable instances such as pH-responsive hydrogels [167] incorporating imine bonds [77], allowing reversible changes in response to fluctuations in pH. Additionally, polymer networks with disulfide bonds [168] exhibit self-healing properties, aiding in material recovery following damage. Fig. 1.6 shows a schematic showing the formation of a reversible hydrogel network mediated by dynamic covalent linkages.

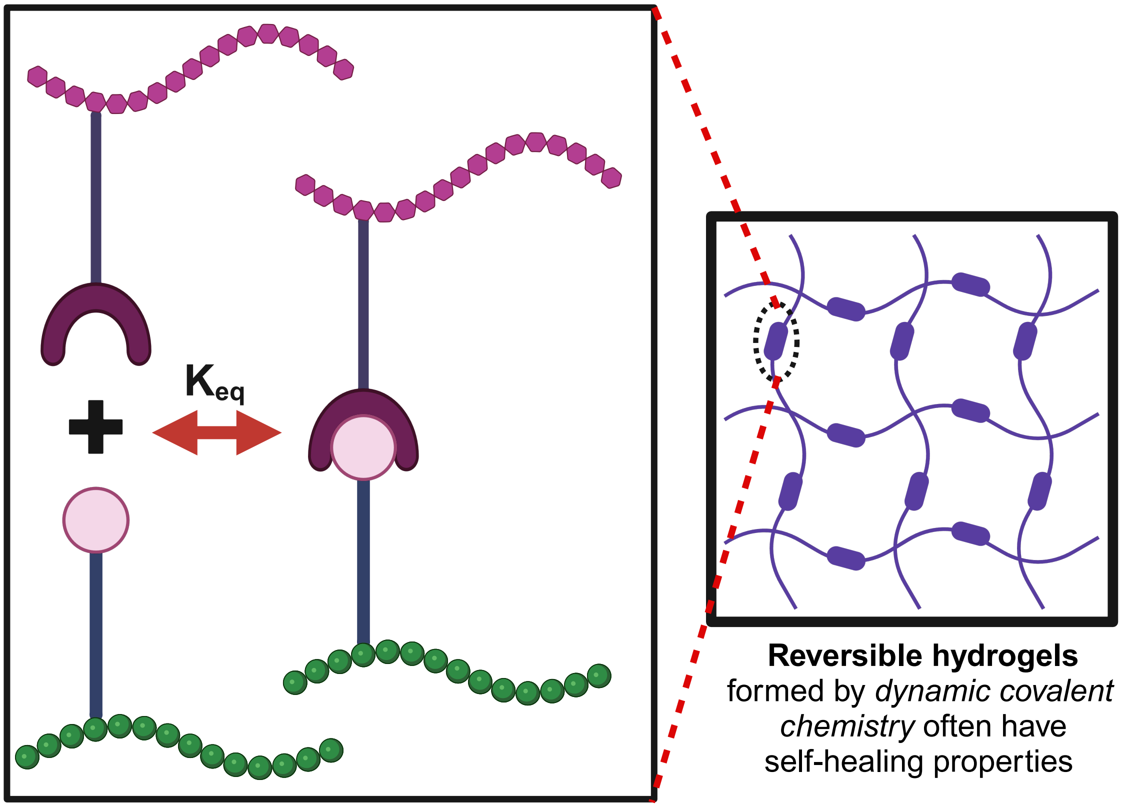

Figure 1.6: A schematic showing the formation of a reversible hydrogel network through dynamic bonds, that often have self-healing properties because of the dynamic covalent bonding (Figure created using `https://biorender.com/`).

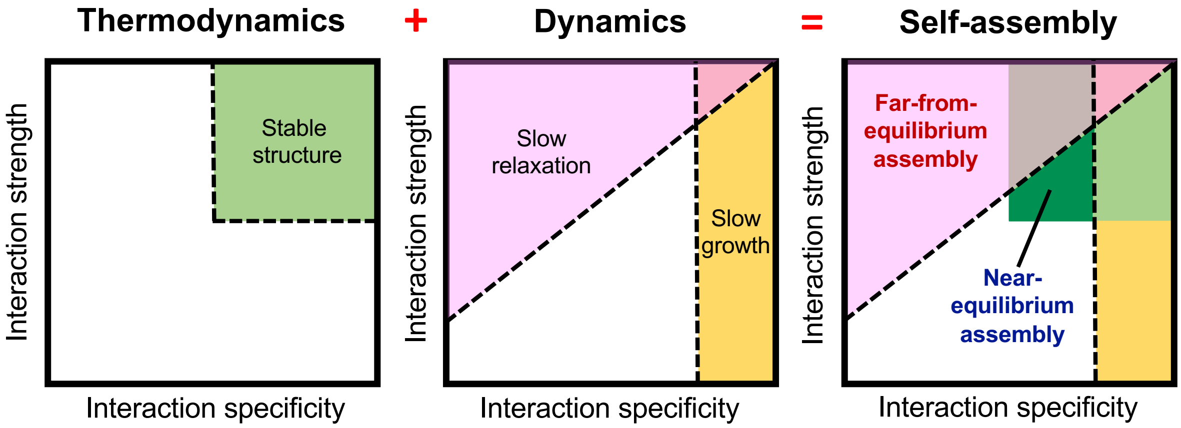

Figure 1.7: Schematic phase diagram illustration of the conflict between thermodynamic and kinetic requirements for self-assembly (this figure has been adapted from [57]). Only for a very narrow range of interaction parameters determined from the competing thermodynamic and dynamical effects, near-equilibrium self-assembly is favored (indicated by the dark green shaded region in the square on the right).

1.4 Thermodynamic and Kinetic Considerations in Self-Assembly

There are two distinct behavioral patterns observed in self-assembling systems [52, 57]: *near-equilibrium* assembly, guided by thermodynamics, and *far-from-equilibrium* assembly, characterized by the crucial role of dynamic effects in the resulting structures obtained. Dynamic effects [169, 170] usually result from the microscopic motion of the assembling particles, resulting in a competition between several slow timescales [171, 172] in such systems.

To maintain the stability of the desired thermodynamically stable structure, optimally strong and specific interactions among components (achieved through directional [66, 173–176] or selective complementary [160, 161, 163, 177–179] binding) are essential. These interactions guarantee that the assembled structure exhibits lower free energy than its unassembled counterparts, thereby outcompeting alternative assemblies [52, 57, 169].

Conversely, strong binding energies impede the equilibration dynamics [180]. Very strong interactions swiftly lead to the formation of metastable and *kinetically trapped* configurations [181–183]. The stronger drive for optimal binding is counteracted by the slow escape from stuck configurations (due to large energy barriers), resulting in a time-dependent dependence of the observed yield [57, 184] on the interaction strength.

The interplay between thermodynamic and kinetic effects suggests that the formation of a thermodynamically stable structure, also known as *near-equilibrium* assembly [52, 57, 184, 185], generally occurs within a limited portion of the available parameter space, as shown in Fig. 1.7.

Fig. 1.8 shows a schematic demonstrating two possible routes of self-assembly from a mixture of self-complementary nanoparticles encapsulated by ligands such as DNA [160, 177, 178] — (i) *near-equilibrium* assembly, leading to the formation of a stable thermodynamic phase, and (ii) *far-from-equilibrium* assembly which forms a kinetically trapped structure [181–183]. Kinetic trapping occurs because of *slow* relaxation of the internal degrees of freedom [160–163, 186, 187]. Here, the DNA binders explore different arrangements more slowly than the timescale of formation of structures [188]. Other examples of kinetic trapping includes cases where arrested gels [189, 190] are formed due to strong particle interactions, and errors that cannot reconfigure and equilibrate to form a stable phase at the timescale of observation.

1.5 Kinetic Rates and Preservation of Detailed Balance

For two given particles *1* and *2* that can bind to each other with an *on* rate k_{on} and an *off* rate k_{off}, the rates should be described in a way that can preserve *Detailed Balance* [118, 191–193], if the system is present at equilibrium. If the equilibrium distributions for the two possible states *on* (bound) and *off* (unbound) are π_b and π_u respectively, then the criterion of *Detailed Balance* requires

$$\pi_u(\vec{r}_1, \vec{r}_2) k_{\text{on}}(\vec{r}_1, \vec{r}_2) = \pi_b(\vec{r}_1, \vec{r}_2) k_{\text{off}}(\vec{r}_1, \vec{r}_2) \tag{1.1}$$

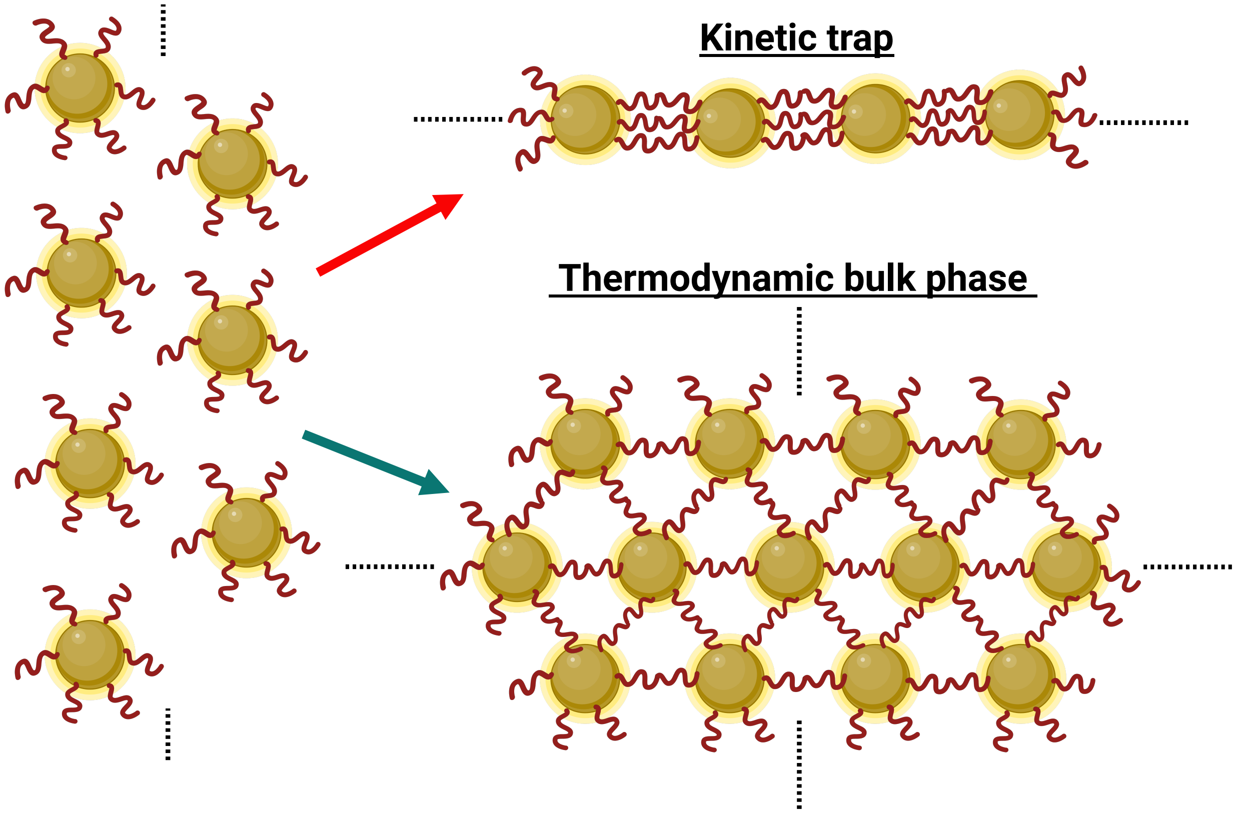

Figure 1.8: Schematic showing two possible routes of self-assembly from a mixture of self-complementary ligated nanoparticles, one resulting in a kinetically trapped structure and the other in the thermodynamically favored phase (Figure created using `https://biorender.com/`).

i.e. there is equilibrium between the rates of forward and backward transitions within a system (stemming from microscopic reversibility [194]), leading to a stable state where the populations of different states remain constant over time.

Here,

$$\pi_u(\vec{r}_1, \vec{r}_2) = \frac{1}{Z_u} \exp\left(-\frac{U(\vec{r}_1, \vec{r}_2)}{k_\mathrm{B}T}\right) \tag{1.2}$$

and

$$\pi_b(\vec{r}_1, \vec{r}_2) = \frac{1}{Z_b} \exp\left(-\frac{U(\vec{r}_1, \vec{r}_2) + E_0(\vec{r}_1, \vec{r}_2)}{k_\mathrm{B}T}\right) \tag{1.3}$$

where, $E_0(\vec{r}_1, \vec{r}_2)$ is the energy for the formation of the bond between *1* and *2*.

$$\frac{\pi_b(\vec{r}_1, \vec{r}_2)}{\pi_u(\vec{r}_1, \vec{r}_2)} = \frac{Z_u}{Z_b} \exp\left(-\frac{E_0(\vec{r}_1, \vec{r}_2)}{k_\mathrm{B}T}\right) \tag{1.4}$$

But from Equation 1.1, we have

$$\frac{\pi_b(\vec{r}_1, \vec{r}_2)}{\pi_u(\vec{r}_1, \vec{r}_2)} = \frac{k_\mathrm{on}}{k_\mathrm{off}} \tag{1.5}$$

If we redefine $Z_u = Z$ and $Z_b = Z\frac{k^0_\mathrm{off}}{k^0_\mathrm{on}}$, then from Equation 1.4 and Equation 1.5, we derive

$$\frac{k_\mathrm{on}}{k_\mathrm{off}} = \frac{k^0_\mathrm{on}}{k^0_\mathrm{off}} \exp\left(-\frac{E_0(\vec{r}_1, \vec{r}_2)}{k_\mathrm{B}T}\right) \tag{1.6}$$

According to Equation 1.6, there are several choices [50, 99, 118, 193, 195, 196] of specifying the rates k_on and k_off such that Detailed Balance is consistent, but at least one of the two rates has to *always* depend on the spatial positions of the particles. Some of the possibilities include—

Model 1: Binding rate is constant and the unbinding is space dependent, commonly used in cases where force-dependent unbinding kinetics are modeled [99, 197, 198].

$$k_{\mathrm{on}} = k_{\mathrm{on}}^{0}$$

$$k_{\mathrm{off}} = k_{\mathrm{off}}^{0} \exp\left(-\frac{E_0(\vec{r}_1, \vec{r}_2)}{k_{\mathrm{B}}T}\right)$$

Model 2: Unbinding rate is constant and the binding rate is space dependent, which we have used for designing our dynamic binding/unbinding model [50, 51] discussed later in this thesis (Chapter 2).

$$k_{\mathrm{on}} = k_{\mathrm{on}}^{0} \exp\left(-\frac{E_0(\vec{r}_1, \vec{r}_2)}{k_{\mathrm{B}}T}\right)$$

$$k_{\mathrm{off}} = k_{\mathrm{off}}^{0}$$

Model 3: Both the binding and unbinding rates depend on space.

$$k_{\mathrm{on}} = \frac{k_{\mathrm{on}}^{0}}{1 + \exp\left(\frac{E_0(\vec{r}_1,\vec{r}_2)}{k_{\mathrm{B}}T}\right)}$$

$$k_{\mathrm{off}} = \frac{k_{\mathrm{off}}^{0}}{1 + \exp\left(-\frac{E_0(\vec{r}_1,\vec{r}_2)}{k_{\mathrm{B}}T}\right)}$$

1.6 COMPUTATIONAL TECHNIQUES TO MODEL AND STUDY SOFT MATERIALS

Modeling and studying *soft materials* heavily rely on computational techniques [199–204], offering valuable insights into their behavior, properties, and possible applications. The choice of computational technique depends on (i) the specific characteristics of the system and (ii) the length and time scales of interest. Often, a combination of these techniques is used to provide a more comprehensive understanding of self-assembly and other important phenomena.

Molecular Dynamics (MD) [205–208] simulations are indispensable tools for elucidating the behavior of soft materials at the molecular level and their structural and dynamical properties. The typical procedure for a molecular dynamics (MD) simulation includes creating a system model and iteratively solving Newton's equations of motion over numerous time steps. This process generates a collection of microscopic configurations or MD trajectories which can be used to study the formation of self-assembled structures from a collection of interacting particles. All my projects described in this thesis have used MD simulations as the primary tool for studying self-aggregation in different soft material systems.

Monte Carlo simulations [209–211] offer a versatile and powerful approach for studying soft materials, adept at capturing the intrinsic complexity and randomness within such materials. They involve defining the material system, creating a mathematical model to represent its behavior, introducing randomness through random sampling [212], simulating the dynamical evolution of the system, collecting data on structural or thermodynamic properties, analyzing the results, and refining the model. The *Metropolis-Hastings criterion* [213, 214] is integral to Monte Carlo simulations, dictating the acceptance or rejection of proposed changes to a system's configuration. It allows the simulation to explore new states while ensuring detailed balance [191] for an equilibrium distribution. These simulations offer valuable insights into molecular configurations and phase transitions.

Soft materials often display intricate and complex behaviors at the microscopic level. However, conducting simulations of these systems at the atomic scale can be computationally *very* expensive. In *coarse-grained models*, groups of atoms or molecules are lumped together into a single interaction site or bead, effectively reducing the number of degrees of freedom [215–217]. These models use simplified potentials derived from microscopic interactions to capture essential system dynamics. Coarse-grained modeling [217] helps bridge the gap between molecular level details and macroscopic properties (emerging from collective behavior of many particles), thus providing insights into the material's overall behavior.

Stochastic reaction-diffusion modeling is another approach used to study the behavior of soft materials by considering both spatial diffusion and random, stochastic reactions at the molecular level [218–220]. It enables the exploration of spatial and temporal heterogeneity [221], small number effects [222], nonlinear reactions, and fluctuations, providing valuable insights into self-assembly and diffusion [223] especially in biological contexts. *Lattice Boltzmann Method* is another computational technique that simulates fluid flow [224–226] by representing the movement and interactions of particles on a lattice, to capture essential hydrodynamic effects [227, 228]. Other relevant approaches such as *Kinetic Monte Carlo* simulations [229, 230] of individual stochastic events (e.g. particle jumps) that occur during the system's evolution, can be used to study the stepwise assembly of structures and surface reactions.

Soft matter systems, such as polymers, colloids, and biomolecules, exhibit complicated dynamics influenced by both thermal fluctuations [9, 11] and hydrodynamic interactions. *Brownian Dynamics (BD)* [231–234] is a powerful simulation technique that effectively captures these key aspects. Brownian dynamics [231–234] simulates the motion of particles in a fluid by incorporating thermal random forces. These forces mimic the impacts of random collisions with solvent molecules, influencing the Brownian motion of particles. The Langevin [234] equation of motion is given by

$$M\ddot{\vec{r}}(t) = \vec{F} - \gamma\dot{\vec{r}}(t) + \sqrt{2\gamma k_{\mathrm{B}} T}\,\vec{\eta}(t) \tag{1.7}$$

where, M is the mass of the particle, k_{B} is the Boltzmann constant, γ_i is the drag coefficient, $\dot{\vec{\boldsymbol{r}}}(t)$ is the velocity of the particle, $\vec{F} = -\nabla U$ is the force on the particle derived from the total potential energy function of the system, and $\eta(t)$ is a delta-correlated random white noise [235], which accounts for thermal fluctuations. In Brownian dynamics [231, 234], the inertial force term $M\ddot{\vec{r}}(t)$ is so much smaller than the other three that it is considered negligible. In this case, the equation is approximately

$$0 = \vec{F} - \gamma\dot{\vec{r}}(t) + \sqrt{2\gamma k_\mathrm{B}T}\vec{\eta}(t) \tag{1.8}$$

1.7 Some Theoretical Models for Soft Materials that interact via Binding Sites

Exploring systems composed of soft materials featuring either stationary or mobile binding sites presents intriguing avenues for investigating their aggregation or assembly behavior [73]. The mobility of these binding sites [236] is particularly noteworthy as it can significantly influence the types of structures that emerge from the assembly process [237]. *Static* binders that remain relatively stationary or fixed in their positions [173, 176, 238, 239], usually result in the formation of a more rigid and well-defined structure. Conversely, *mobile* binders [50, 161, 195, 240–242], capable of movement or rearrangement throughout the self-assembly process, introduce dynamic [243] reconfigurability and responsiveness [28, 77, 244, 245] into the self-assembled structures. Various theoretical models have been proposed in the past to model and simulate systems of this nature. In this section, I will provide a brief overview of a few notable ones.

1.7.1 Frenkel and Kern's model for simulating *patchy* colloids

Employing a model based on hard spheres with isotropic short-range attractions [246–250] is a valuable initial approach for characterizing the phase behavior of globular proteins [251, 252], and this strategy aligns with colloidal systems [66, 238, 253]. However, it's crucial to recognize that this simplified model lacks complete justification for protein interactions, given their inherent anisotropy.

Kern and Frenkel developed a model [246] (2003) to model *patchy* particles [66, 173, 175, 176, 238, 253] with directional interactions that give rise to selective valence. Here, a *patch* is defined as an attractive region on the surface of the particle which can be described in terms of a conical segment with a solid (opening) angle (2δ) about an axis $\hat{e_\alpha}$. The pair potential is defined as the product of a square-well potential $u_{ij}^{hssw}(r)$ and an angular (orientational) function which takes the anisotropy [246, 248, 250] of the system into account,

$$u_{ij}(r_{ij}; \tilde{\Omega}_i, \tilde{\Omega}_j) = u_{ij}^{hssw}(r_{ij}).f(\tilde{\Omega}_i, \tilde{\Omega}_j) \tag{1.9}$$

where for some reduced range λ,

$$u_{ij}^{hssw}(r) = \begin{cases} \infty & \text{for } r < \sigma \\ -\varepsilon & \text{for } \sigma \leq r < \lambda\sigma \\ 0 & \text{for } \lambda\sigma \leq r \end{cases} \tag{1.10}$$

The angular dependence of the interaction depends on the direction $\hat{r_{ij}}$ of the vector $\vec{r_{ij}}$ and on the particle orientations $\tilde{\Omega}_i$ and $\tilde{\Omega}_j$ as

$$f(\hat{r_{ij}}; \tilde{\Omega}_i, \tilde{\Omega}_j) = \begin{cases} 1 & \text{if } \hat{e_\alpha}.\hat{r_{ij}} \leq \cos\delta \text{ for some patch } \alpha \text{ on } i \\ & \text{and, } \hat{e_\beta}.\hat{r_{ji}} \leq \cos\delta \text{ for some patch } \beta \text{ on } j \\ 0 & \text{otherwise} \end{cases} \tag{1.11}$$

Kern-Frenkel like *patchy particle* models [247, 248, 250] provide robust frameworks for exploring self-assembly through site-specific interactions using computational techniques like Monte Carlo or Molecular Dynamics simulations, such as those used in modeling cellulose nanocrystals [254] (through supra-coarse grained methods) or colloidal clusters functionalized with biotinated-DNA oligomers [176] that form *patches*.

1.7.2 APPLICATION OF WERTHEIM'S THERMODYNAMIC PERTURBATION THEORY TO STUDY EQUILIBRIUM POLYMERIZATION OF LINEAR CHAINS

Generating extended objects with valence 2 (linear chains of polymers) can be quite useful for folding studies to design interesting architectures. A major motivation driving the development of the coarse-grained model discussed in Chapter 2 is to study optimal conditions that can help in generating long linear chains of emulsion droplets [50, 161, 165] called *colloidomers* (this can guide future folding experiments). Wertheim (1987) introduced a thermodynamic perturbation theory (TPT) [174, 255, 256] designed for patchy colloidal particles to elucidate association phenomena [66, 246, 257–260]. The theory operates on the premise that a sticky site on a particle is incapable of binding concurrently to two or more sites on another particle [174, 255, 256, 258, 259, 261]. For M identical (indistinguishable) *patchy* sites (in this case, $M = 2$ for forming chains), the Helmholtz free energy [174, 256, 258] for the patch-patch interaction, A_p is given by

$$\frac{\beta A_p}{N} = M\left(\ln X - \frac{X}{2}\right) + \frac{M}{2} \tag{1.12}$$

where, $\beta = \frac{1}{k_\mathrm{B}T}$ and X is the fraction of sites that are not bonded. X is calculated from the mass-action equation

$$X = \frac{1}{1 + M\rho X\Delta} \tag{1.13}$$

where, $\rho = \frac{N}{V}$ is the particle number density and the patchy interaction strength Δ is defined as

$$\Delta = 4\pi \int g_\mathrm{HS}(r_{12})\langle f(12)\rangle_{\omega_1,\omega_2} r_{12}^2 dr_{12} \tag{1.14}$$

Here, $g_\mathrm{HS}(r_{12})$ is the reference HS fluid pair correlation function, the Mayer-f function is

$$f(12) = \exp\left(-\frac{V(r_{12})}{k_\mathrm{B}T}\right) - 1 \tag{1.15}$$

and, $\langle f(12) \rangle_{\omega_1,\omega_2}$ represents an angle average over all orientations of particles 1 and 2 at a fixed relative distance r_{12}.

Sciortino *et al.* [174, 256–260] performed Grand-Canonical Monte Carlo [204] simulations for a system consisting of hard-sphere particles. These particles were characterized by a surface coated with $M = 2$ identical sites positioned diametrically opposite each other. The simulations were carried out at various temperatures and densities [174, 258, 259]. A critical temperature for a given ρ was observed at which the system undergoes a polymerization transition [174], from a gas of monomers. The average chain length, chain length distribution, average end-to-end distance, the static structure factor and various other thermodynamic properties were quantified for the polymerization and remarkably, the simulation results aligned closely with the predictions of the Wertheim theory [174, 255, 256, 258, 259]. The absence of considerations for interactions between the chains highlights a limitation in the Wertheim theory, particularly evident at very high densities, such as during the isotropic to nematic phase transition [262–265]. This observation opens avenues for future investigations and further exploration in the field.

1.7.3 Models to study interactions of particles with mobile binding moieties

In self-assembling soft matter systems involving functionalized emulsions [38, 160, 161, 163, 266] or lipid bilayers [70, 267–269], linkers capable of unrestricted surface diffusion on particles have been largely employed, inspired by van der Meulen and Leunissen's experiments [270]. The association/dissociation transition is notably more gradual, broadening the temperature range for achieving equilibrium self-assembly [187, 270, 271]. The incorporation of mobile binders effectively addresses concerns related to slow rearrangement kinetics, particularly in cases involving patches with immobile binding groups. Above the DNA melting temperature, the mobile binders (linkers) are evenly dispersed, whereas below this temperature, they visibly accumulate at the inter-particle junctions.

DNA-coated colloids (DNACCs) [160–164, 186, 240, 270, 272–274] stands out as one of the most prominent systems of study involving mobile binders. Various coarse-grained strategies have been developed in the past to calculate the free energy of interaction for a general system of many colloids coated with DNA strands that are capped with reactive sticky-ends [240, 273, 275, 276]. The interaction between two grafted colloids is due to both the attraction (because of decrease in free energy of bond formation) and the repulsion resulting from compression of the DNA strands trapped between the colloids [273]. This theory does not assume that DNA-mediated interactions are pairwise additive – many-body effects play a crucial role in controlling valency in this class of colloids [240].

$$\beta F_{\text{interaction}} = F_{\text{att}} + F_{\text{rep}} \tag{1.16}$$

The effective interaction between DNA-coated colloids is based on the mean-field approach developed in Refs. [275, 276]. At any given time, each linker i can bind at most one other linker j, with a free energy change $\Delta G_{ij}(\vec{r}_i, \vec{r}_j)$ that depends on the linker properties. Mostly, the probability that linker i is unbound is approximately independent of whether or not any other linker is also unbound (which holds true when the density of linkers is low enough such that two linkers not bonded to each other can be thought of as not interacting at all). The attractive part of the effective interaction free-energy is given by the following expression (in this limit):

$$\beta F_{\text{att}} = \sum_i \ln p_i + \sum_{i<j} p_{ij} \tag{1.17}$$

where, p_i is the probability that a linker i is unbound and p_{ij} is the probability that two linkers i and j form a bond. Also, it was shown previously in Ref. [275] that these quantities are given by the unique physical solution to the following set of self-consistent equations:

$$p_{ij} = p_i p_j \exp\left(-\beta \Delta G_{ij}(\vec{r}_i, \vec{r}_j)\right) \tag{1.18}$$

and

$$p_i = 1 - \sum_j p_{ij} \tag{1.19}$$

In standard coarse-grained models for mobile DNA-coated colloids, the hybridising DNA-strand is represented as a *point-like* attractive site, called *sticky end*, tethered to the colloidal surface by a *spacer* [200, 240, 273, 275, 276]. If the spacer does not influence the structure of the sticky end, the free energy of bond formation can be split into the following terms [240, 273, 275, 277]:

$$\beta \Delta G_{ij}(\vec{r}_i, \vec{r}_j) = \beta \Delta G_0 + \beta \Delta G_{\mathrm{cnf}}(\vec{r}_i, \vec{r}_j, \vec{R}_i) \tag{1.20}$$

where, $\beta \Delta G_0$ is the hybridization free-energy for two untethered, complementary DNA strands in solution, and depends on the DNA sequence, temperature and salt concentration [278, 279]. $\beta \Delta G_{\mathrm{cnf}}(\vec{r}_i, \vec{r}_j, \vec{R}_i)$ represents the configurational entropic cost [240, 273, 275, 278] associated with linking two tethered strands i and j, and depends on the positions of the grafting points, and of all nearby colloids. This term can be either calculated analytically for simple models, or computed via *Monte Carlo* simulations.

1.8 THESIS CHAPTERS IN CONTEXT

Now, having established a foundation by introducing crucial concepts, relevant phenomenology, and examples of dynamic binding in soft matter systems, along with an exploration of self-organization processes and the computational techniques employed for simulation, I proceed to provide an overview of the contents within the context of this thesis. It is important to note that all the work presented in this thesis was conducted under the guidance of and in collaboration with Prof. Glen M. Hocky, my dissertation advisor.

Chapter 2 introduces a coarse-grained MD simulation platform to study the self-assembly of colloidal particles [50, 242] featuring *explicit mobile binding molecules*, exemplified by DNA-coated emulsion droplets [38, 160, 162, 163, 280], where binders can freely diffuse on the surface. Our focus involves optimizing experimental control parameters to achieve the highest yield of long linear *colloidomer* (droplet polymer) chains [161, 164]. Through the implementation of temperature-dependent binding/unbinding dynamics, we are able to observe the collapse of a heptamer chain [165] into various rigid structures, aligning well with recent folding experiments. The insights gained from our coarse-grained MD simulation model serve to guide programmable design in experimental setups. Notably, this collaborative effort was conducted with Prof. Jasna Brujic from the Center for Soft Matter Research and the Department of Physics at NYU.

In Chapter 3, we probe the dynamics of adhesion patch formation between two droplets, employing explicit mobile binding moieties [240, 242, 269, 272–275]. The focus is on exploring how the molecular features of the system can be manipulated to tune the growth, shape, and geometry of the adhesion patch [39, 50, 161, 164]. Our investigation extends to the impact of lateral or cis-interactions, a phenomenon crucial in enhancing binder recruitment, particularly observed in cellular junctions where E-cadherin proteins [38, 39, 93] mediate cell-cell adhesion [100]. Therefore, we examine the consequences of introducing lateral binding interactions [281–285] between binders on the same droplet in the context of adhesion patch formation dynamics. Importantly, this collaborative work has been conducted with Prof. Jasna Brujic.

Chapter 4 delves into the creation of a coarse-grained modeling platform, incorporating previously developed dynamic binding and unbinding kinetics. This platform aims to explore the formation of both equilibrium and kinetically arrested gels [189, 190, 286–298] resulting from the interaction of ligated nanoparticles and macromers with discrete functionalities [299–301]—moieties capable of dynamic binding and unbinding. Our investigation encompasses the impact of binding and unbinding kinetics, the utilization of bifunctional linkers [302], and the influence of capping molecules [296, 298, 303] in the design of such assemblies [189, 190, 286–298]. This ongoing work is part of a collaborative effort of our research group with another computational and two experimental research groups at the University of Texas, Austin. The simulation studies are a joint undertaking involving our group and the research group led by Prof. Thomas Truskett.

In Chapter 5, we discuss the development of an *in silico* coarse-grained molecular dynamics (CGMD) simulation platform tailored for a synthetic liquid-liquid phase separation (LLPS) system named *synDrops*. This endeavor aims to investigate how the cellular environment influences the formation of condensates [51, 304, 305]. Our findings indicate that the synergistic effects of crowding and active matter in the cytoplasm favor mesoscale molecular assembly, offering enhanced predictive insights into biomolecular condensate formation *in vivo* [305, 306]. Specifically, we observed that macromolecular crowding fosters condensate nucleation while impeding droplet growth through coalescence. The frustration of growth is overcome by ATP-dependent cellular activities. This work was done in collaboration with Prof. Liam J. Holt from NYU Langone School of Medicine.

In conclusion, Chapter 6 provides a comprehensive summary of the research findings and discusses future prospects within the dynamic and diverse field of self-assembly in soft materials.

Chapter 2

A coarse-grained simulation model for colloidal self-assembly *via* explicit mobile binders

This chapter is adapted from the work published as [50].

2.1 Abstract

Colloidal particles with mobile binding molecules constitute a powerful platform for probing the physics of self-assembly. Binding molecules are free to diffuse and rearrange on the surface, giving rise to spontaneous control over the number of droplet-droplet bonds, i.e., valence, as a function of the concentration of binders. This type of valence control has been realized experimentally by tuning the interaction strength between DNA-coated emulsion droplets. Optimizing for valence two yields droplet polymer chains, termed ‘colloidomers’, which have recently been used to probe the physics of folding. To understand the underlying self-assembly mechanisms,

here we present a coarse-grained molecular dynamics (CGMD) model to study the self-assembly of this class of systems using *explicit representations of mobile binding sites*. We explore how valence of assembled structures can be tuned through kinetic control in the strong binding limit. More specifically, we optimize experimental control parameters to obtain the highest yield of long linear colloidomer chains. Subsequently tuning the dynamics of binding and unbinding *via* a temperature-dependent model allows us to observe a heptamer chain collapse into all possible rigid structures, in good agreement with recent folding experiments. Our CGMD platform and dynamic bonding model (implemented as an open-source custom plugin to HOOMD-blue) reveal the molecular features governing the binding patch size and valence control, and opens the study of pathways in colloidomer folding. This model can therefore guide programmable design in experiments.

2.2 INTRODUCTION

Self-assembly of colloidal materials can create non-trivial and programmable structures with wide-ranging and tunable material properties. The spatio-temporal visualization of colloids renders them as useful model systems for probing the underlying physics behind assembly processes of molecular systems [52, 53, 187, 307]. The synthesis of colloidal particles with chemically or physically patterned solid surfaces—“patches”— has been an active area of research due to the desire to control the bond valence and orientation, going beyond what can be achieved through isotropic interactions [173, 176, 307, 308]. For example, a long-desired target is a diamond lattice, with an open structure that is difficult to achieve without an imposed tetrahedral symmetry [309].

The most common approach to engineering specific interactions between patches is to use complementary strands of DNA, whose interaction strength can be tuned by the length and specific sequence of nucleotides. [177, 178, 187, 310–312]. Each DNA duplex has an associated melting temperature (T_{melt}) and it is possible to employ multiple sets of complementary strands exhibiting different T_{melt} to control the types of bonds present during an annealing protocol [313].

Self-assembly of patchy particles can be studied in simulations using short-range directional non-bonded interactions [246] or using only pairwise interactions in combination with specific geometric constraints that prevent multiple bonding to the same patch [173, 174, 314, 315]. Interactions due to many DNAs on a colloidal surface can also be computed using more detailed MD simulations [316], or through a mean-field approach [275]. An alternative strategy to modeling explicit patches is to develop pair-potentials from inverse design principles, which have been successfully leveraged to produce systems that assemble with low valence, such as dimers or chains [317, 318].

An intriguing alternative to patchy particles of fixed valence is a system of particles coated with mobile adhesion molecules. In this case, it is possible for particles to "choose" their valence based on the number of available neighbors with complementary binding molecules, minimizing the total free energy of the system. Experimentally, using oil droplets in water provides a mobile interface on which the DNA linkers segregate into patches by diffusion to give rise to *e.g.*, dimers when all the DNA is recruited into a single patch or droplet chains at higher concentrations of DNA where two patches per droplet are favored [161]. Colloids with mobile binders can also be formed by coating solid particles with fluid lipid bilayers [160, 270], or by directly functionalizing liposomes or giant unilamellar vesicles [269, 319–321]. The mobility of the linkers broadens the melting temperature window of the DNA, facilitating equilibrium self-assembly [187, 271]. Particles with mobile binders can also serve as a physical mimic for biological adhesion, where cells use a variety of dynamic binding molecules to stick to each other and to surfaces [100]. To this end, biomimetic emulsion droplets have been successfully functionalized with adhesive mobile proteins, such as biotin-streptavidin complexes [38, 266], cadherin ectodomains [93], or other ligand-binder pairs relevant for immunotherapy [322]. Early theoretical work expanding on the model of Ref. [275] predicts that such particles could have an equilibrium valence that depends on the number of available neighboring particles in the system[240].

Our previous work shows that monodisperse PDMS oil droplets functionalized with different flavors of single-stranded DNA on the surface can self-assemble into structures of tunable valence [160–163, 280, 323]. Under conditions where DNA bonds are reversible at room temperature, these systems achieve their equilibrium valence configuration. These results are predicted by a free-energy functional that takes into account the molecular properties of the system, including DNA binding strength, flexibility, steric repulsion, and concentration [164]. Optimizing for valence two, the self-assembly of complementary DNA-coated droplets yields linear *colloidomer* chains [161]. Further programming the secondary interactions along the chains offers a physical model system to probe the energy landscape of biopolymer folding, and for building small 'foldamer' structures that can serve as the basis for larger scale assemblies [165, 324, 325]. A complementary work demonstrated the formation of reconfigurable colloidal molecules using polydisperse droplets surrounded by ligands [326]. It has also been shown previously through both experiments and simulation studies that anisotropic interactions between polymer-grafted nanoparticles (NPs) [327–330] can result in self-assembly of sheets and string-like structures. The graft density of the polymers and the relative size of the graft to the NP can play a crucial role in determining the kind of structures observed during self-assembly, quite analogous to how the density of the mobile DNA binders on the surface of oil droplets can be used to tune the droplet valence.

Motivated by these experimental studies, our work develops a coarse-grained molecular dynamics (CGMD) simulation model and framework to study the self-assembly of these colloidal chains with mobile binders, and their subsequent folding. The crucial feature of our model is the use of *explicit mobile linkers* with bonds between complementary binding partners. Prior work on these types of systems used implicit models of binding between neighboring droplets *via* the formation of adhesion patches, and some models included approximations to account for the dynamics of adhesion[240, 242, 269, 272–274]. The use of explicit mobile binders allows us to test the underlying assumptions in a more realistic model, albeit at the cost of additional complexity. For example, our model explicitly shows how steric repulsion between binders (designed to mimic electrostatic repulsion between DNA strands) affects the adhesion patch size and the concentration of binders therein. These results in turn explain the overall valence distribution that results from the assembly process. To demonstrate the capabilities of our model, we describe the parameters that optimize the formation of colloidal chains under kinetic control, and show that it exhibits the folding behavior of two-dimensional colloidal chains commensurate with what has been recently demonstrated experimentally [165]. Our scheme lays the groundwork for studying the mechano-sensitive effects of mobile binders at interfaces, including the role of catch bonds, lateral interactions, or cooperativity in strengthening adhesions [93, 98].

2.3 Description of the model

2.3.1 Coarse-Grained model for colloidal particles with explicit mobile binders

The central unit of our simulation model is a droplet, as shown in Fig. 2.1a. Each droplet consists of a central spherical particle of radius R (type A) with N_b binders distributed on the surface. Each binder is composed of two particles — the outer particle (type C or D) is responsible for binding complementary partners, while the inner one (type B) is used to modulate excluded volume between binders. The positions of the binders are initialized in a “Fibonacci” arrangement to prevent overlap between any adjacent binders in the initial configurations [331]. This pair of particles mimics the combination of the double-stranded tether and the single-stranded sticky-end DNA used in experiments [161] (Fig. 2.1a). This configuration also allows us to apply an angular term to tune the propensity of the binder to stand vertically from the surface. The binders diffuse on the surface [160] due to a harmonic bond between the center of the droplet and that of the inner binder particle with a spring constant k_{AB} and rest length l^0_{AB}.

The inner and outer particles in the binder are similarly held together by a harmonic bond with spring constant k_{BC} and $l_{\mathrm{BC}} = r_{\mathrm{B}} + r_{\mathrm{C}}$, the sum of their radii. To have the binder stick outward from the droplet, the two binder particles are forced to align along the radial vector from the center of the droplet, by introducing a harmonic angular potential between the triplet of particles with parameters k_{ABC} and rest angle $\theta^0_{\mathrm{ABC}} = 180^\circ$. In each case, the spring constants are chosen such that the thermal standard deviation $\sigma = \sqrt{k_{\mathrm{B}}T/k}$ (where k_{B} is the Boltzmann's constant) is a small fraction of the rest length or angle (see Table 2.5). As a trade-off between enforcing rigid bonds and using an infinitesimal MD time step, we chose to use spring constants where the standard deviation is $1-2\%$.

2.3.2 NON-BONDED INTERACTIONS

To prevent overlap between particles, we use a soft repulsion given by

$$U_{\mathrm{soft}}(r) = \begin{cases} \varepsilon_{\mathrm{soft}}\left[1 - \left(\frac{r}{r_{\mathrm{cut}}}\right)^4\right] & \text{if } r < r_{\mathrm{cut}} \\ 0 & \text{if } r \geq r_{\mathrm{cut}} \end{cases} \tag{2.1}$$

, a smoothed version of which is applied between all particle types except between pairs of outer binder particles of complementary types (otherwise repulsion can prevent binding). Here, $\varepsilon_{\mathrm{soft}}$ is the strength of the interaction potential (in units of $k_{\mathrm{B}}T$) and r_{cut} is the cut-off distance, as shown by the dotted green curve in Fig. 2.2. By tuning the effective diameter of B particles, we tune the steric repulsion between adjacent binders, which corresponds to the case of altering the screening of the electrostatic interactions between DNA strands on the surface [164]. A smoothing function was applied to this potential $U_{\mathrm{soft}}(r)$ that results in both the potential energy and the force going

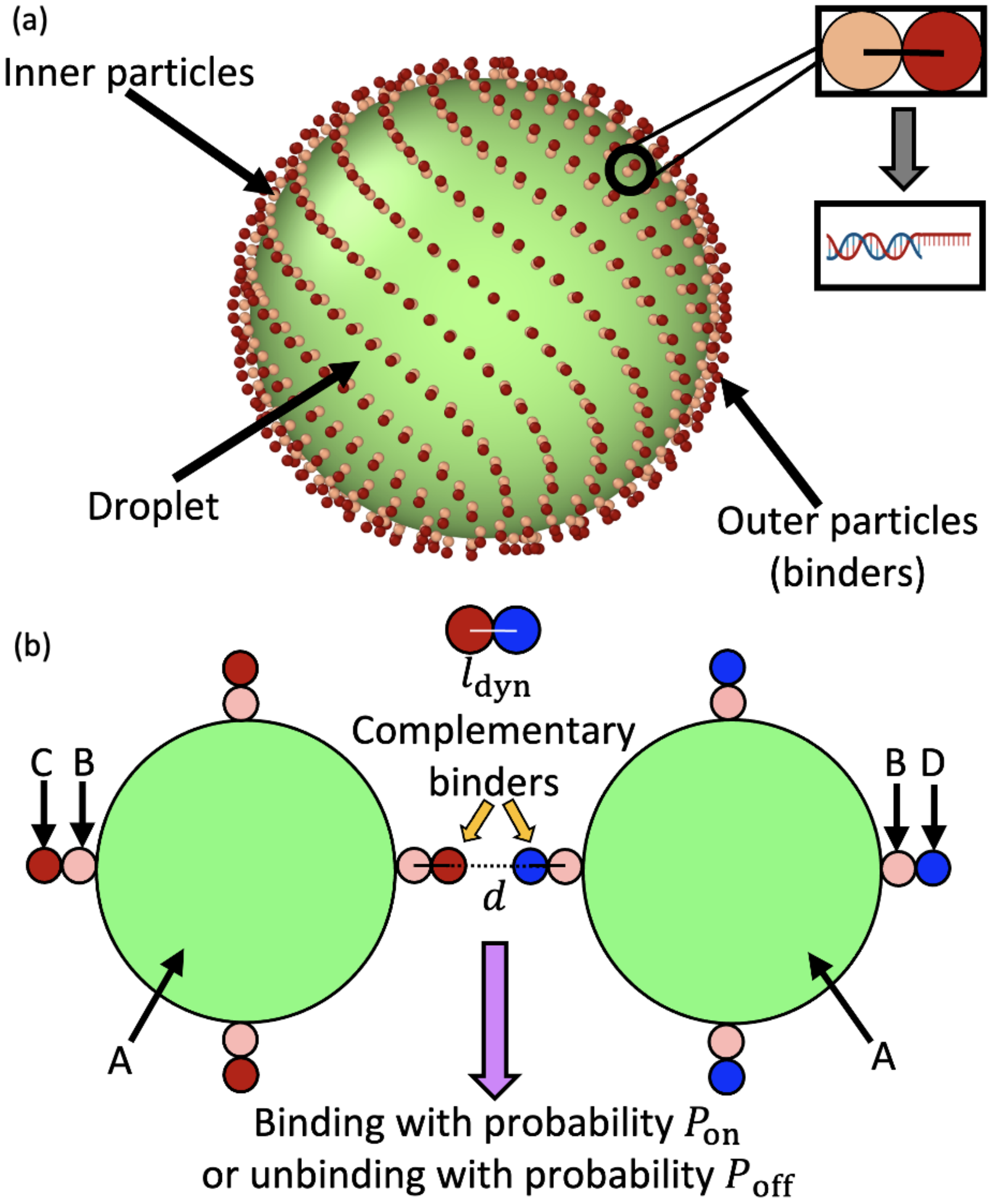

Figure 2.1: (a) The initial configuration of a droplet with binders adhered to its surface, arrayed in their initial "Fibonacci" structure. As shown in the inset, each binder consists of two constituent particles, which in the case of DNA corresponds to a spacer double-stranded sequence and a single stranded sequence which is available to bind to a complementary strand. (b) A schematic showing dynamic binding between the outer binder particles of two droplets. Different particle types used in our python framework are schematically labeled A–D, with C and D representing a pair of complementary binders.

smoothly to 0 at $r = r_{\text{cut}}$, in this case the XLPOR smoothing [332] function $S(r)$, given by

$$S(r) = \begin{cases} 1 & \text{if } r < r_{\text{on}} \\ \frac{(r_{\text{cut}}^2 - r^2)^2 (r_{\text{cut}}^2 + 2r^2 - 3r_{\text{on}}^2)}{(r_{\text{cut}}^2 - r_{\text{on}}^2)^3} & \text{if } r_{\text{on}} \le r \le r_{\text{cut}} \\ 0 & \text{if } r > r_{\text{cut}} \end{cases} \tag{2.2}$$

Here, r_{on} is chosen as the point at which the smoothing starts. We set $r_{\text{on}} = 0.1 r_{\text{cut}}$ for our simulations. The modified potential is shown in Fig. 2.2 and is given by

$$V_{\text{soft}}(r) = \begin{cases} S(r) U_{\text{soft}}(r) & \text{if } r_{\text{on}} < r_{\text{cut}} \\ U_{\text{soft}}(r) - U_{\text{soft}}(r_{\text{cut}}) & \text{if } r_{\text{on}} \ge r_{\text{cut}} \end{cases} \tag{2.3}$$

The soft potential was implemented by using HOOMD-blue's tabulated potential option (with 1000 interpolation points between $r_{\text{min}} = 0$ and $r_{\text{max}} = 1.05\, r_{\text{cut}}$).

Our CGMD model can be used to study droplet interactions in three dimensions, but we add an optional confining potential for comparison with recent experiments where droplets are found in a plane due to the effect of gravity. To replicate a quasi two-dimensional arrangement in our system, we use a force-shifted Lennard-Jones wall potential [333] on each droplet, between a fixed z-position and the center of the droplet A particle. The origins of the walls are given by $(0, 0, 2.5R)$ and $(0, 0, -2.5R)$.

The wall potential is given by a shifted LJ potential with $r_{\text{cut}} = 2^{1/6}(2R)$.

$$V_{\text{wall}}(r) = V_{\text{FLJ}}(r) - V_{\text{FLJ}}(r_{\text{cut}}) \tag{2.4}$$

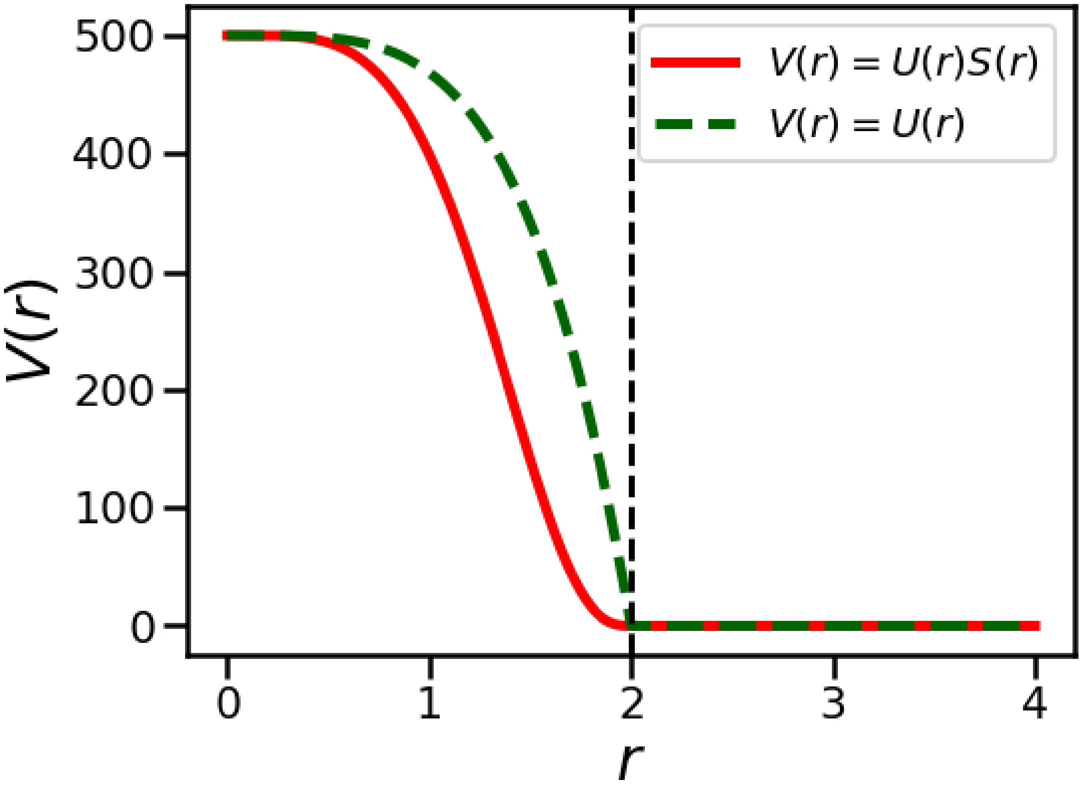

Figure 2.2: The soft repulsive pair potential $V(r)$ as a function of the distance r between two binder particles of radius $r_C = 1$. In this figure, $r_{\text{cut}} = 2$ is indicated by the vertical dotted line. The green dotted curve shows the potential $U(r)$ without any smoothing function applied to it and the red solid curve shows the potential $V(r)$ after it is multiplied by a suitable smoothing function $S(r)$.

where, $V_{\mathrm{FLJ}}(r)$, the force-shifted Lennard-Jones pair potential is given by,

$$V_{\mathrm{FLJ}}(r) = \begin{cases} 4\varepsilon_{\mathrm{wall}}\left[\left(\frac{\sigma}{r}\right)^{12} - \alpha\left(\frac{\sigma}{r}\right)^{6}\right] & \text{if } r < r_{\mathrm{cut}} \\ +\Delta V(r) & \\ & \\ 0 & \text{if } r \geq r_{\mathrm{cut}} \end{cases} \tag{2.5}$$

$$\Delta V(r) = -(r - r_{\mathrm{cut}})\frac{\partial V_{\mathrm{LJ}}}{\partial r}(r_{\mathrm{cut}}) \tag{2.6}$$

where $\alpha = 1$.

2.3.3 Dynamic bonding model

We model interactions between binders through covalent bonds. To do so, we develop a plugin to HOOMD-blue [334] [335] that builds upon a model for epoxy binding developed in Ref. [336]. Adhesive bonds form only between complementary outer binder particles of respective droplets, as shown in Fig. 2.1b. In the simplest case, we have a mixture of droplets containing outer binder particles that are 100% of types C and D, respectively. The model allows for individual droplets to contain mixtures of binder types, and there may be many more than two types, as designated by the user. In this study, harmonic bonds are added with spring constant k_{dyn} and length $l_{\mathrm{dyn}} = r_{\mathrm{C}} + r_{\mathrm{D}}$, the sum of the radii of particles forming a bond. Here, we choose harmonic bonds, but any form of bond implemented in HOOMD-blue could be used, since our algorithm only changes the bond table within the MD simulation, and does not compute or apply forces. [1]

In our approach, we enforce that each binder can only participate in one possible binding reaction at a time, such that all binding events are independent. In this case, each reaction can be

---

[1] The Metropolis criterion employed for binding/unbinding described later requires knowing the energy of adding or removing a bond. At this time only a harmonic interaction is supported, but this can be trivially extended.

characterized as a two-state reaction, where the effective free energy difference between a bound and an unbound state is given by

$$\Delta G = k_\mathrm{B} T \ln \left(\frac{k_\mathrm{on}}{k_\mathrm{off}} \right) \equiv \varepsilon \tag{2.7}$$

Here, k_on and k_off are the rate constants for binding and unbinding, respectively. Below, we tune ε to modulate the affinity between individual binders.

2.3.3.1 ALGORITHM FOR BINDING AND UNBINDING

Here, we describe details of the algorithm for binding and unbinding, satisfying detailed balance.

Every n steps of the MD simulation (run using HOOMD-blue), a Dynamic Bond Updater is called. The Dynamic Bond Updater is an open source C++ plugin (based on previous work on epoxy curing [336]) that stochastically adds or removes dynamic bonds during the course of the MD simulation. If there is more than one dynamic bond type present in the system, the Bond Updater has to be configured for each independently.

Each time the Bond Updater is called, it first iterates over all the existing dynamic bonds to attempt unbinding. The probability of unbinding is calculated, given by

$$P^0_\mathrm{off} = n \, k_\mathrm{off} \, \mathrm{d}t \tag{2.8}$$

where, $\mathrm{d}t$ is the timestep of the MD simulation. For each bond in sequence, a uniform random number $r \in [0, 1)$ is generated, and if $r < P_\mathrm{off}$ the bond is added to a list of bonds to be removed from the bond table. Once all the possible unbinding events are taken into consideration, we iterate over the list of bonds to be removed and perform unbinding.

After performing unbinding, we create a list of proposed bonds to add. We iterate over particles which were unbound at the start of the binding update (but not those freed by unbinding), and find the closest available complementary particle which is also unbound and whose distance from the particle under consideration is between l_{min} and l_{max} (by iterating over HOOMD-blue's neighbor list). If an eligible neighbor exists, and neither particle is already in the proposed bonds list, then this pair is appended. Our binding algorithm is inspired by (but not identical) to the implementations in Refs. [103–105].

We then iterate over the proposed bond list, generating new uniform random numbers and creating a bond if $r < P_{\text{on}}$. By default, $P^0_{\text{on}} = n\, k_{\text{on}}\, \mathrm{d}t$. Here we choose k_{on} such that $k_{\text{on}}(n\, \mathrm{d}t) = 1$, i.e. the fastest possible reaction rate for a specific time discretization because we want to form as many bonds as possible without rejecting too many Monte Carlo [337] moves. We note that as a consequence, this scheme does not intend to match detailed chemical kinetics of the underlying processes, which would require schemes that would be more computationally demanding such as the Gillespie algorithm [338] used in Ref. [274]. To ensure detailed balance for individual binding reactions, the probability of binding is modified [118, 193] such that $P_{\text{on}} = P^0_{\text{on}} e^{-\Delta U(d)/k_{\text{B}}T}$, where ΔU is the additional energy added by creating a bond of length d, possibly away from its rest length. Since we are only using harmonic bonds in this work,

$$P_{\text{on}}(d) = P^0_{\text{on}} e^{-k_{\text{dyn}}(d-l_{\text{dyn}})^2/(2k_{\text{B}}T)}, \tag{2.9}$$

where $k_{\text{B}}T$ is the instantaneous temperature of the system.

As in Ref. [118], we are putting all of the energetic dependence into the binding step and none in the unbinding step, although other choices are possible [193]. The stretch dependent binding rates prevents formation of bonds which are very unlikely, so this helps in preventing non-equilibrium heating of the system. This choice of stretch-dependent on rate and constant off rate does not correspond to our belief about the detailed molecular kinetics of DNA unbinding, but rather is an algorithmic choice that is valid because we are not currently interested in including the detailed effect of stretching on the rates, although we are planning to pursue this direction in the future. [97, 98, 193]

Detailed balance for the overall binding/unbinding reaction is satisfied to the best of our ability when performing a large set of binding/unbinding reactions at once (as compared to only doing one single binding/unbinding per trial) by ensuring that every event is independent such that the probability of the total change in bonded pairs factorizes, and each individually satisfies a Metropolis criterion.[205, 337] We ensure independence by generating a list of possible reactions in a deterministic order and only allowing a particle to possibly bind with one other particle. The only possibly weak breaking of detailed balance comes in the rare situation where upon unbinding, one or both of the particles was assigned a different binding partner since it was not bound to the neighbor from whom its distance is most close to the equilibrium bond length. In practice, because we use a stiff spring this is very unlikely, and moreover, the configuration evolves n steps between binding/unbinding trials, we do not expect this to cause any substantial non-equilibrium effects.

2.3.3.2 TEMPERATURE DEPENDENCE OF BINDING/UNBINDING

Our dynamic bonding model allows us to use non-constant values of k_{off}, k_{on}. As one example, for this work we have incorporated an optional dependence of the rate constants on temperature. Since our binders here might represent double stranded DNA, which dissociates in a cooperative manner, we implemented an optional tunable sigmoidal dependence on temperature for the rate constants. Here, we describe how the binding and unbinding rates are made temperature dependent in such a way that the fraction of bound pairs at the equilibrium distance tends smoothly to zero at high T, with 50% bound pairs at a specified melting temperature T_{melt} (Fig. 2.3).

Without trying to match the behavior of any specific module, we implemented a two parameter sigmoidal dependence on temperature to represent cooperative melting,

$$g(T) = \frac{1}{2}\left[\tanh\left(\alpha\left(T - T_{\text{melt}}\right)\right) + 1\right], \tag{2.10}$$

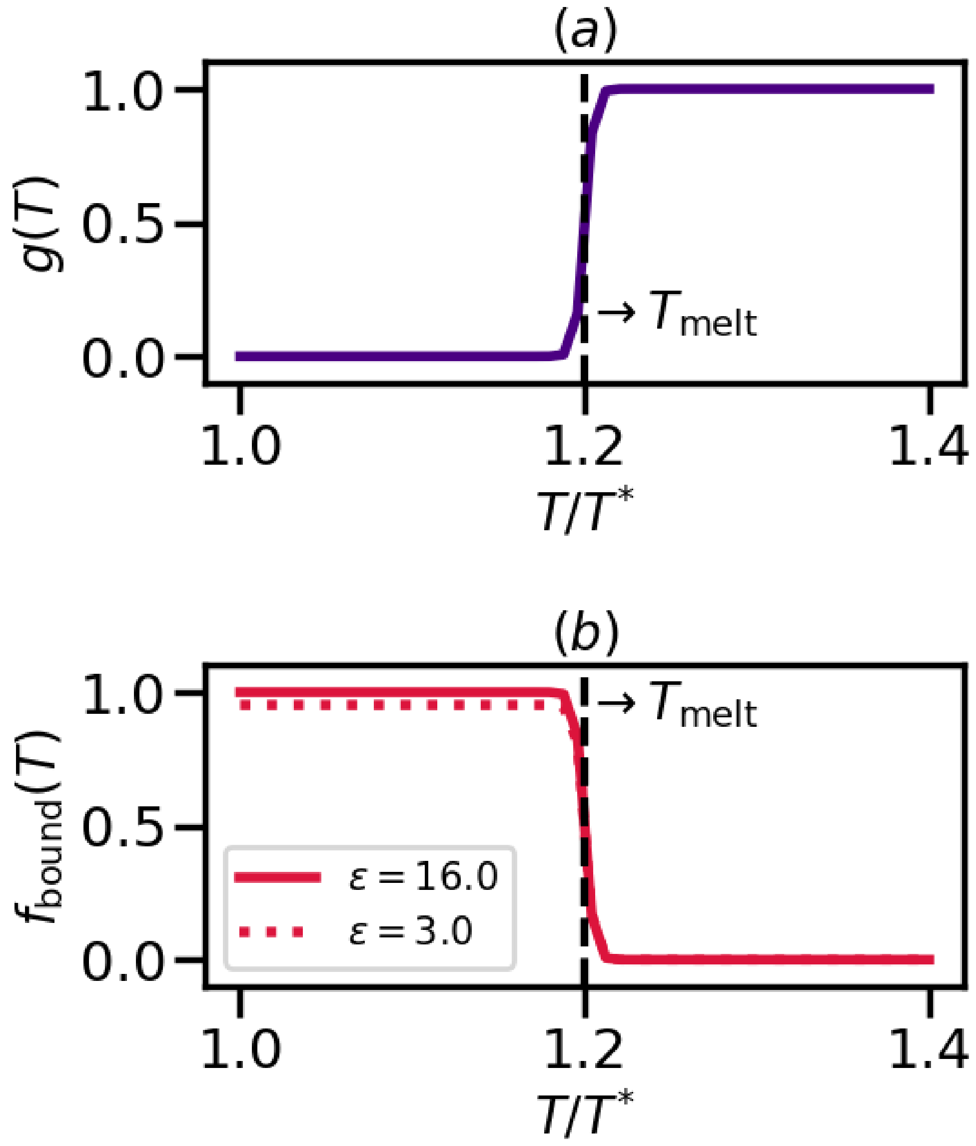

Figure 2.3: (a) $g(T)$ vs. T (b) Fraction $f_{\text{bound}}(T)$ of DNA that is bound for a single DNA pair vs. T for two different binding strengths $\varepsilon = 3.0$ and 16.0. (The temperature is in units of T^*).

$$k_{\mathrm{on/off}}(T) = k^{\mathrm{init}}_{\mathrm{on/off}}\Big(1 - g(T)\Big) + k^{\mathrm{melt}}_{\mathrm{on/off}}\, g(T) \tag{2.11}$$

where, $k^{\mathrm{melt}}_{\mathrm{on/off}}$ is the value of the binding (or unbinding) rate constant after the melting of bonds. The dependence on $T - T_{\mathrm{melt}}$ arises in a two state melting model[339] where ΔH_{melt} and ΔS_{melt} are taken to be constants; in this case $\Delta G = \Delta H_{\mathrm{melt}} - T\Delta S_{\mathrm{melt}} = \Delta H_{\mathrm{melt}} - T\Delta H_{\mathrm{melt}}/T_{\mathrm{melt}} = \frac{\Delta H_{\mathrm{melt}}}{T_{\mathrm{melt}}}(T_{\mathrm{melt}} - T) \propto T - T_{\mathrm{melt}}$; $\Delta S = \Delta H/T_{\mathrm{melt}}$ because $\Delta G(T = T_{\mathrm{melt}}) = 0$.

Combining these results in for either off or on rates and $\Delta T = T - T_{\mathrm{melt}}$,

$$k_{\mathrm{on/off}}(T) = \frac{k^{\mathrm{melt}}_{\mathrm{on/off}} - k^{\mathrm{init}}_{\mathrm{on/off}}}{2}\tanh(\alpha\Delta T) + \frac{k^{\mathrm{melt}}_{\mathrm{on/off}} + k^{\mathrm{init}}_{\mathrm{on/off}}}{2}, \tag{2.12}$$

such that when $\Delta T \gg 0$, $k \longrightarrow k^{\mathrm{melt}}$ and $\Delta T \ll 0$, $k \longrightarrow k^{\mathrm{init}}$. Here, we can set the steepness of the transition with the parameter α (which in experiment could be tuned by changing the DNA sequence and sequence length). T_{melt} should be the temperature where the fraction of bonds formed is 0.5.

For a two-state model, the bound fraction is given by

$$f_{\mathrm{bound}}(T) = \frac{K_{\mathrm{eq}}(T)}{1 + K_{\mathrm{eq}}(T)} \tag{2.13}$$

where, $K_{\mathrm{eq}}(T) = k_{\mathrm{on}}(T)/k_{\mathrm{off}}(T)$. Ensuring $f_{\mathrm{bound}}(T_{\mathrm{melt}}) = 0.5$ requires $k_{\mathrm{on}}(T_{\mathrm{melt}}) = k_{\mathrm{off}}(T_{\mathrm{melt}})$. Therefore

$$k^{\mathrm{init}}_{\mathrm{on}} + k^{\mathrm{melt}}_{\mathrm{on}} = k^{\mathrm{init}}_{\mathrm{off}} + k^{\mathrm{melt}}_{\mathrm{off}} \tag{2.14}$$

since, $g(T_{\mathrm{melt}}) = 0.5$. We choose ${k_{\mathrm{on}}}^{\mathrm{melt}} = 0$, so that there is no binding at $T \gg T_{\mathrm{melt}}$, at which point ${k_{\mathrm{off}}}^{\mathrm{melt}}$ can be determined from Eq. 2.14. Fig. 2.3(b) shows how f_{bound} depends on T_{melt} using this model.

Combining all of these facts together, we get

$$k_{\text{on}}(T) = k_{\text{on}}^{\text{init}} \left(\frac{1 - \tanh(\alpha \Delta T)}{2} \right), \tag{2.15}$$

$$k_{\text{off}}(T) = \frac{k_{\text{on}}^{\text{init}} - 2k_{\text{off}}^{\text{init}}}{2} \tanh(\alpha \Delta T) + \frac{k_{\text{on}}^{\text{init}}}{2}, \tag{2.16}$$

which satisfy all the correct limits for $\Delta T \ll 0$, $\Delta T \gg 0$ and $\Delta T = 0$.

We note that the on rate expression is the commonly used Glauber rule [340] from Monte Carlo simulations [205, 337, 341] assuming a difference in (free) energy between two states proportional to ΔT as explained above, but here the off rate is a modification of this Glauber rule that switches between two finite rates rather than zero and infinity.

2.3.4 Comparison of model and experiment geometry

While this CGMD model is generic, Fig. 2.4 shows how the geometry can be compared to the experimental setup in Ref. [161]. The radius of one binder sphere corresponds to the sticky end of length $\sim$ 5.1nm, which is our reduced unit of length. Therefore, a droplet radius of $R = 300$ corresponds to the droplet size of $\sim$ 1530nm used in Ref. [161]. Smaller particle sizes studied in Section 2.5 are also used in experiments.

Practically, our simulations are computationally limited to hundreds of binders per droplet. Therefore, we equate the scale of the simulations to experiments by matching the excluded volume of all binders to that of DNA surface coverage in the experiment. More specifically, the surface coverage, p is defined as

$$p = \frac{4\pi {r_{\text{B}}}^2 N_{\text{b}}}{4\pi R^2} = N_{\text{b}} \left(\frac{r_{\text{B}}}{R} \right)^2 . \tag{2.17}$$

In the experiment, for droplets of radius $R = 1530$ nm, an effective repulsive radius of DNA

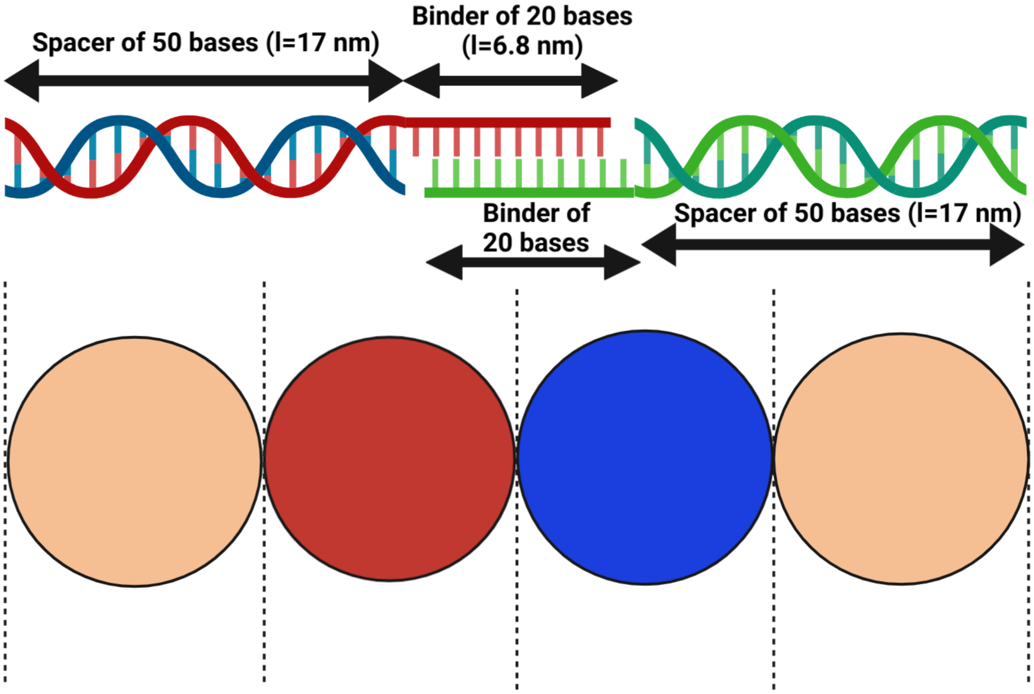

Figure 2.4: Complementary binders in our CG model mapped onto the dsDNA and ssDNA configuration of Ref. [161] for scale. Complementary outer binder particles (red and blue) form a dynamic bond representing the interaction between complementary DNA strands (Figure created with `https://biorender.com/`).

of 1.5nm [164, 342, 343], and an estimated $1{\times}10^3 - 2{\times}10^4$ DNA strands[161, 164], p ranges from $\sim 0.001 - 0.02$ or $0.1 - 2\%$ coverage. For many simulations below, we use $r_\mathrm{B} = 1$, $R = 50$, and $N_\mathrm{b} = 100$, in which case $p = 0.04$. From this perspective, each binder plays the collective role of hundreds of DNA.

2.4 SIMULATION METHODS

MD simulations[205] of droplets coated with mobile binders were performed using HOOMD-blue version 2.9.6 [334, 335, 344]. The Langevin integrator [234, 345] was used to integrate all particles forward in time. Two different values of the drag coefficient γ were used: one for the droplets (γ_A) and the other for the binders (γ_binder).

The equation of motion for each particle i in Langevin dynamics [346] is given by:

$$m_i\ddot{\vec{r}}_i(t) = \vec{F}_i - \gamma_i\dot{\vec{r}}_i(t) + \sqrt{2\gamma_i k_\mathrm{B} T}\vec{\eta}(t) \tag{2.18}$$

where, m_i is the mass of the particle, k_B is the Boltzmann constant, γ_i is the drag coefficient, $\dot{\vec{\boldsymbol{r}}}_{\boldsymbol{i}}(t)$ is the velocity of the particle, $\vec{F}_i = -\nabla U_i$ is the force on particle i derived from the total potential energy function of the system, and $\eta(t)$ is the delta-correlated random white noise, with zero mean and unit variance. We use the tree neighbor list [347, 348] to accelerate non-bonded calculations, and in the construction of our list of possible pairs to bond as described above.

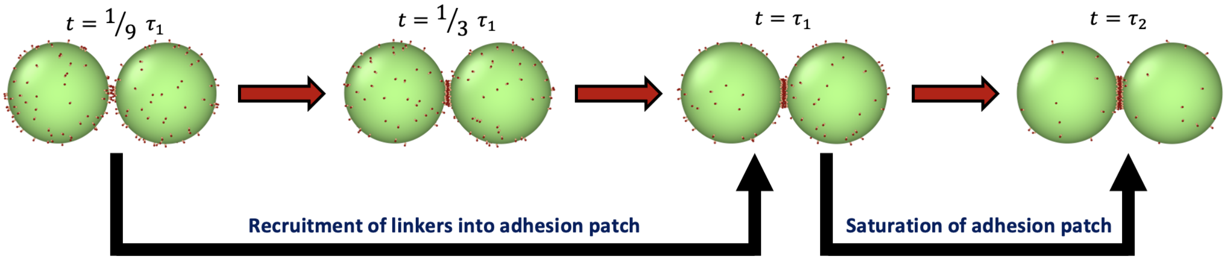

Figure 2.5: Illustration of adhesion patch formation for a dimer of droplets. Patch formation under conditions with high binding affinity occurs *via* a process with two time scales (τ_1 and τ_2), one for recruitment of most linkers into a patch, and a second proceeding to saturation. The conditions for this particular simulation are $R = 50$, $N_b = 100$ and $\varepsilon = 20.7$. See Section 2.5.3 and Table 2.1 for more details.

2.5 RESULTS AND DISCUSSION

2.5.1 MAIN OBJECTIVES

In this section, we optimize simulation conditions to robustly self-assemble long colloidomers, suppressing branched structures. We explore both the molecular properties of the system (droplet radius, binder concentration, and binder interaction strength), and the experimental conditions for assembly (particle concentration and solution viscosity). The detailed parameters used for our MD simulations are listed in Tables 2.5, 2.6, 2.7 and 2.8. Our results indicate that kinetic factors can be rationally employed to target the desired outcome with high yield and fidelity for fixed-time experiments. We subsequently show that our model allows us to study the folding process for colloidomer chains.

2.5.2 ADHESION PATCH FORMATION IS A TWO-STAGE PROCESS FOR HIGH BOND STRENGTHS

The formation of chains requires that each droplet has two contacting neighbors. Monomers first form dimers, after which they either combine with monomers to make trimers, or with other dimers to make tetramers. We therefore first probe the physical processes involved in forming a patch in a dimer or trimer configuration, and then consider *de novo* assembly in Section 2.5.6 .

Simulations of patch formation begin with dimers and trimers in an initial configuration with a single bond already formed between the droplets. Subsequently, the patches progressively grow until they reach steady-state. We find that patch formation (at intermediate and high binding affinities, around $\varepsilon > 13$) happens in two stages, as illustrated in Fig. 2.5 (see Fig. 2.7). Fitting the fraction of unbound binders *versus* time with a double exponential function reveals two time scales, as shown in Section 2.5.3. Initially, the fast time scale of recruitment of binders describes the formation of a stable adhesion patch (τ_1), while the saturation of the patch is captured by a 1–2 orders of magnitude slower timescale (τ_2). Table 2.1 reports values of τ_1 and τ_2 for some of these conditions. Slowing binder motion by increasing γ_{binder} or slowing binding by decreasing k_{on} at fixed bond strength ε increase the recruitment time τ_1, as shown in Fig. 2.6; these changes should increase the yield of higher valences, discussed in Section 2.5.6. Modulation of k_{on} could perhaps be realized in experiment by modifying the length of the spacer molecule, which would change the probability of finding a binding partner. The two-step patch recruitment has important consequences for the kinetically controlled assembly mechanism of colloidal chains at high ε.

2.5.3 Convergence of the fraction of binders not recruited in an adhesion patch with simulation time

The fraction of the total number of binders not present in the adhesion patch is monitored over time for the case of a dimer, the terminal droplet of a trimer and also its central droplet. For low and high ε, we consider different ways of fitting the curves in order to obtain the converged value of the fraction of free binders.

For binding affinity $\varepsilon > 13$, as shown in Fig. 2.7b,d,f for $\varepsilon = 20.7$, we fit the fraction of

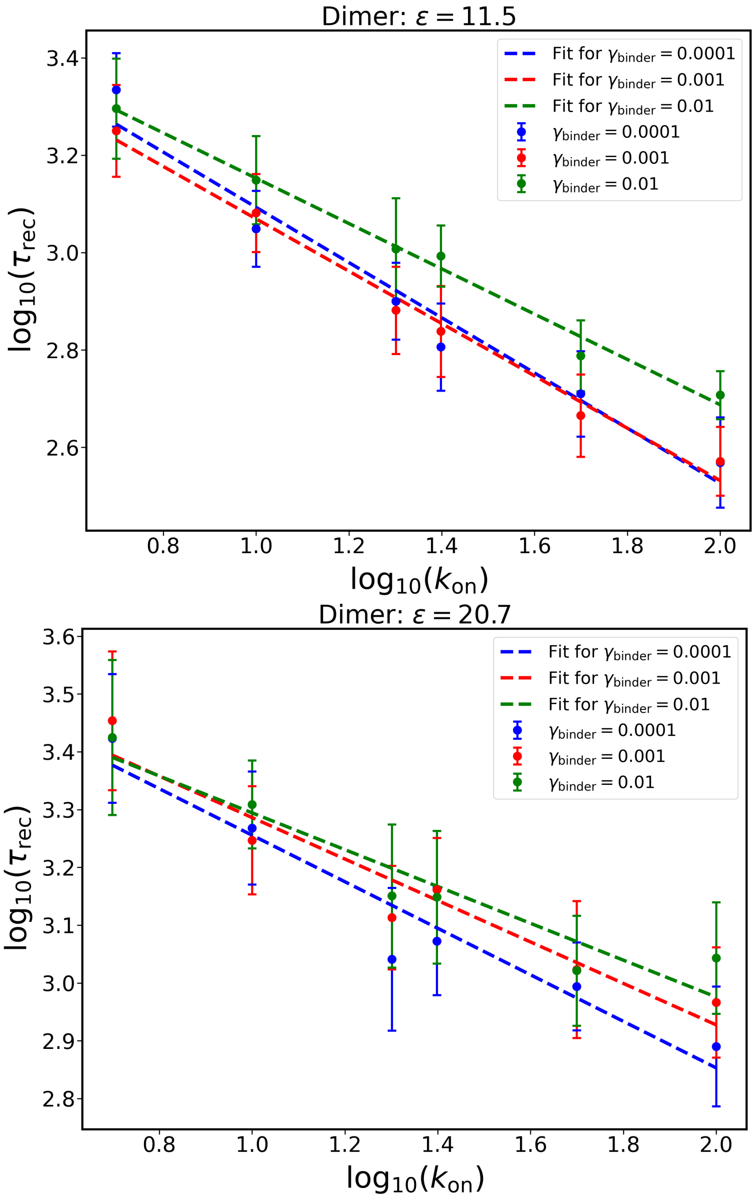

Figure 2.6: Variation of the recruitment timescale $\tau_{\rm rec}$ for the binders into the adhesion patch of a dimer with the binding rate constant $k_{\rm on}$ for the case of R = 50, $N_{\rm b}$ = 100 at low and high binding affinities, (i) ε = 11.5 and (ii) ε = 20.7. The recruitment times were obtained using a single exponential fit done on the data for ε = 11.5 and using a double exponential fit for ε = 20.7, respectively. Plots are shown here for $\log_{10}(\tau_{\rm rec})$ vs $\log_{10}(k_{\rm on})$, scatter points represent the data and the linear fits to the data are indicated by colored dashed lines. Error bars indicate the statistical error (standard deviation) for each of these data points, calculated using a similar bootstrapping procedure as described in Section 2.5.6.4.[349, 350] 2000 bootstrap samples were generated for each of the conditions. The slopes obtained from the linear fits for the different conditions are— (i) ε = 11.5: -0.569 ($\gamma_{\rm binder}$=0.0001), -0.542 ($\gamma_{\rm binder}$=0.001), -0.465 ($\gamma_{\rm binder}$=0.01) and (ii) ε = 20.7: -0.403 ($\gamma_{\rm binder}$=0.0001), -0.359 ($\gamma_{\rm binder}$=0.001), -0.319 ($\gamma_{\rm binder}$=0.01). Note that in each of these cases, the drag on the droplet particle ‘A’ is kept constant ($\gamma_{\rm A}$ = 0.1).

binders not in a patch $f(t)$ to a double exponential function of analytical form $f(t) = (f(0) - a)\exp(-k_1 t) + (a-b)\exp(-k_2 t) + b$, where we interpret k_1 and k_2 to be related to the two different time scales—the recruitment time of the binders and the time taken for the adhesion patch to saturate, explained in Section 2.5.2. The fraction of unrecruited binders at saturation of the patch $f(t)|^{t=\infty} = b$ according to this expression. The fitted values for the parameters a, b, k_1, k_2 are obtained using the curve fitting feature of SciPy [349]. From the fitted values of k_1 and k_2, we can estimate the recruitment time τ_1 and the patch saturation time τ_2, as shown in Table 2.1. At larger values of $R > 100$, we find that the curves for trimers are well fit by a single exponential, and this emerges naturally in our double exponential fit with k_1 and k_2 being identical.

For binding affinity $\varepsilon <= 13$, as shown in Fig. 2.7a,c,e for $\varepsilon = 9.2$, we find that the fraction remains fairly constant over time (for all the droplet radii) with fluctuations characteristic of low ε. For each of these situations, we obtain a mean of this fraction over the last 50% of the simulation time (in this case, between 10^8 steps and 2×10^8 steps) and fit the curve to this constant mean value. For all cases the final value of fraction at the final time (at 2×10^8 steps) has been found to lie within 5% of the fit value.

2.5.4 Optimizing bond strength, droplet size, and binder concentration for colloidomerization

Optimal conditions for colloidomerization require considering both the dimer and the trimer assembly, since we must find a condition where not all binders are exhausted in the dimer, where $\sim$ 50% of binders are available on a terminal droplet of a trimer, and where very few are left on the trimer middle droplet, preventing branching. Fig. 2.8a shows a systematic study of the self-assembly of droplets of varying R and ε, for a fixed total number of binders $N_\mathrm{b} = 100$. The heat maps show the fraction of unbound binders in three configurations: a droplet-droplet dimer, a terminal droplet in a trimer, and a central droplet in a trimer. Conditions for colloidomerization

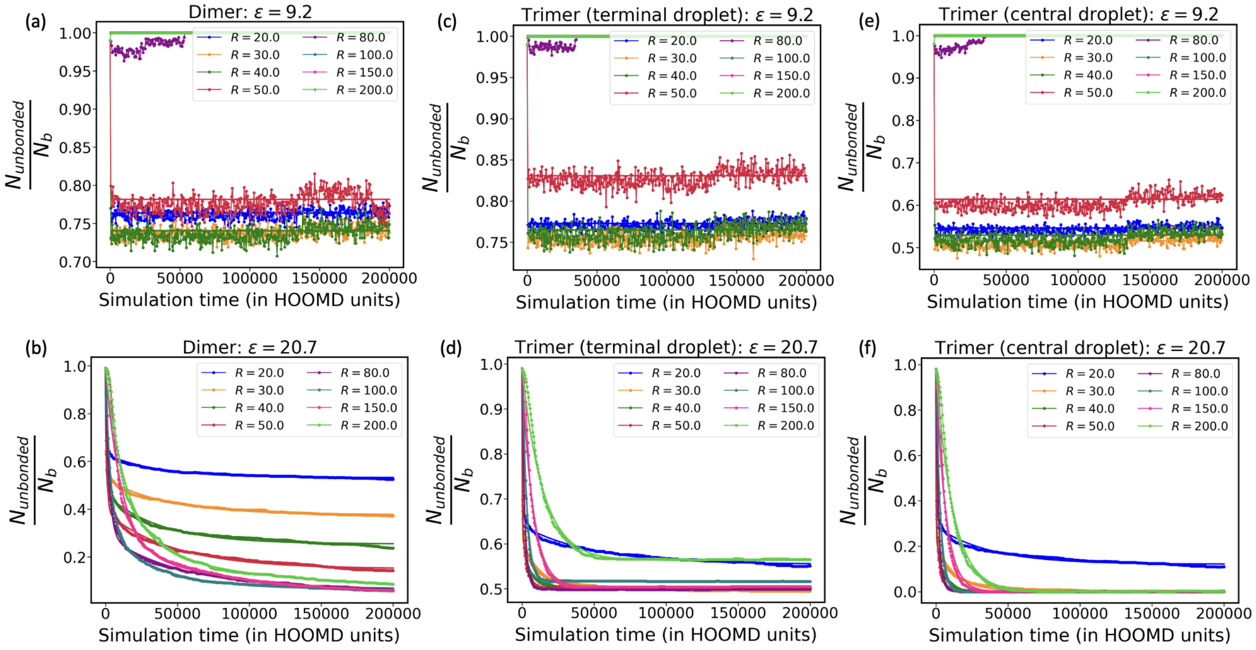

Figure 2.7: Plots showing the convergence of the fraction of the total binders $N_\mathrm{b} = 100$ not in any adhesion patch with the simulation time, for two different binding affinities $\varepsilon = 9.2$ (low)—shown in (a),(c),(e) and $\varepsilon = 20.7$ (high)—shown in (b),(d),(f). (a) and (b) show these cases for the dimer, (c) and (d) for the terminal droplet of a trimer, (e) and (f) for the central droplet of the trimer. Each plot shows the convergence for 8 different droplet radii R ranging from 20 to 200. These simulations are all run for $2{\times}10^8$ HOOMD steps which is sufficient for all the individual curves to attain convergence.

Table 2.1: A table showing the values of the recruitment time (τ_1) and the adhesion patch saturation time (τ_2) obtained from the double exponential fit for $\varepsilon = 20.7$ and $N_\mathbf{b} = 100$

System	$\tau_1 = 1/k_1$	$\tau_2 = 1/k_2$
Dimer		
(i) $R = 20.0$	1.5×10^2	3.7×10^4
(ii) $R = 30.0$	3.2×10^2	4.2×10^4
(iii) $R = 40.0$	5.3×10^2	3.8×10^4
(iv) $R = 50.0$	9.3×10^2	4.7×10^4
(v) $R = 80.0$	2.5×10^3	5.2×10^4
(vi) $R = 100.0$	3.6×10^3	3.6×10^4
(vii) $R = 150.0$	1.1×10^4	1.1×10^5
(viii) $R = 200.0$	1.3×10^4	7.4×10^4
Trimer (terminal droplet)		
(i) $R = 20.0$	1.7×10^2	4.8×10^4
(ii) $R = 30.0$	1.7×10^2	1.3×10^4
(iii) $R = 40.0$	2.1×10^2	4.7×10^3
(iv) $R = 50.0$	2.9×10^2	2.9×10^3
(v) $R = 80.0$	1.8×10^3	1.0×10^4
(vi) $R = 100.0$	4.1×10^3	5.1×10^3
(vii) $R = 150.0$	7.5×10^3	-
(viii) $R = 200.0$	1.5×10^4	-
Trimer (central droplet)		
(i) $R = 20.0$	1.5×10^2	3.8×10^4
(ii) $R = 30.0$	1.7×10^2	1.2×10^4
(iii) $R = 40.0$	2.0×10^2	4.6×10^3
(iv) $R = 50.0$	3.0×10^2	2.7×10^3
(v) $R = 80.0$	1.7×10^3	1.1×10^4
(vi) $R = 100.0$	3.0×10^3	-
(vii) $R = 150.0$	6.6×10^3	-
(viii) $R = 200.0$	1.2×10^4	-

are satisfied in the region where the dashed ovals overlap. Later, we choose $R = 50$, $\varepsilon = 20.7$ and $N_{\mathrm{b}} = 100$ to demonstrate that this condition results in the robust assembly of colloidomers.

The number of binders in a patch at equilibrium is dictated by the free energy of patch formation, which can be considered as the difference in the chemical potential inside and outside the patch [164]. The driving force for a binder to enter the adhesion patch is determined by the energy of forming individual bonds, ε, and opposed by steric repulsion between binders, the stretching of binders at the interface, as well as the loss of entropy as the binder motion is constrained in a patch. As ε increases, the fraction of free binders decreases monotonically in the case of both dimers and trimers until it reaches an asymptotic value that is limited by the steric repulsion between binders.

Similarly, increasing droplet size in the strong binding limit recruits progressively more binders into the patch, since there is more space at the interface between larger droplets (Fig. 2.8a). For large R in both dimers and trimers, we observe that the transition from no binding to all binders in the patch is very sharp as energy gain overtakes entropic losses without a penalty from steric repulsion. In contrast, for small radii, the recruitment of binders into the patch is more gradual with ε due to crowding.

Changing the droplet size not only changes the cost of packing binders into a patch, but also the entropic cost of patch formation, which increases with droplet size. Therefore, at intermediate values of ε we observe a non-monotonic recruitment of binders into the patch as a function of droplet size. While crowding dominates in small droplets, entropic costs dominate in large droplets, giving rise to an optimal size for binder recruitment, *e.g.* $R = 120$ for $\varepsilon = 15$ in the dimer configuration. We thus show that competition between the energy of binding, steric repulsion between binders, and the entropy of free binders can collectively result in non-monotonic patch density when tuning *e.g.* the droplet radius.

We can now consider the transition from dimer to trimer, where two adhesion patches are formed. Competition between the two adhesion patches results in an approximately equal split

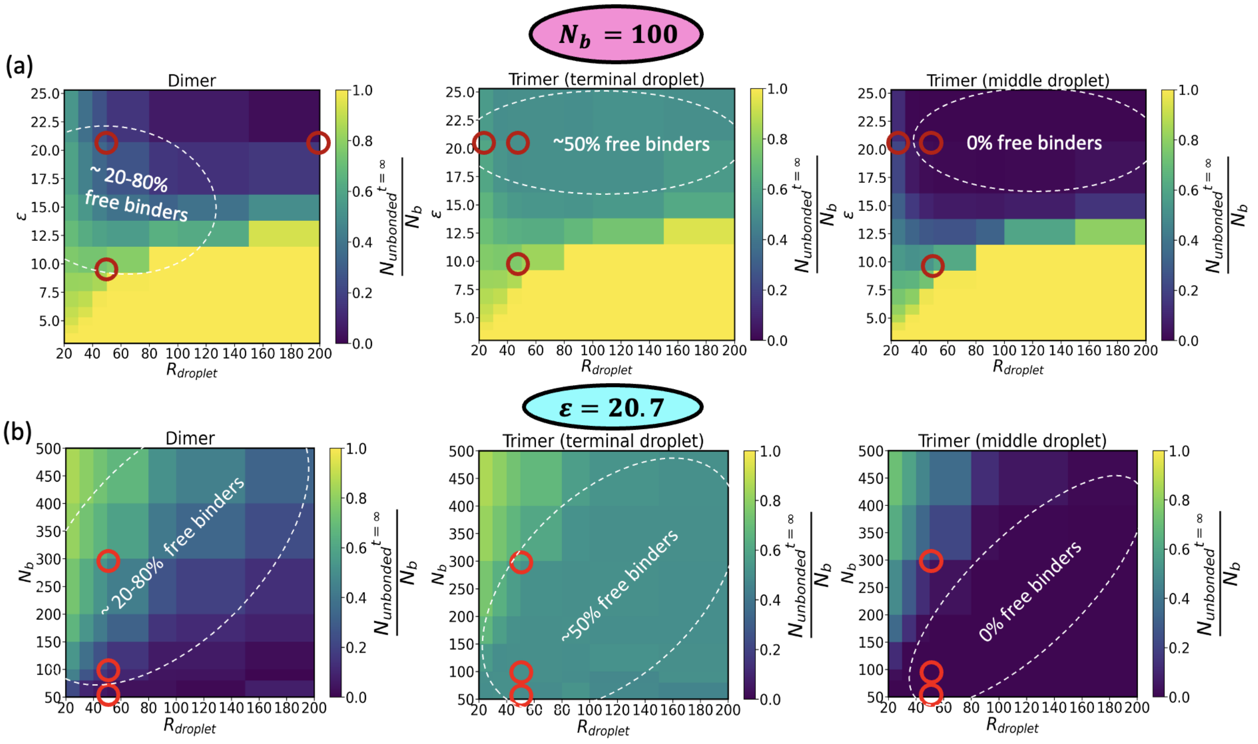

Figure 2.8: Heat maps showing the percentage of binders remaining on the surface of a droplet in a dimer geometry, and on the terminal or central droplets in a trimer geometry. Conditions predicted to be "good" for colloidomer assembly are indicated by dashed ovals, and selected conditions marked by red open circles are illustrated in Fig. 2.11. (a) Fraction of remaining binders at fixed number of binders, varying droplet radius and bond strength. (b) Fraction of remaining binders at fixed high bond strength, varying number of binders and droplet radius.

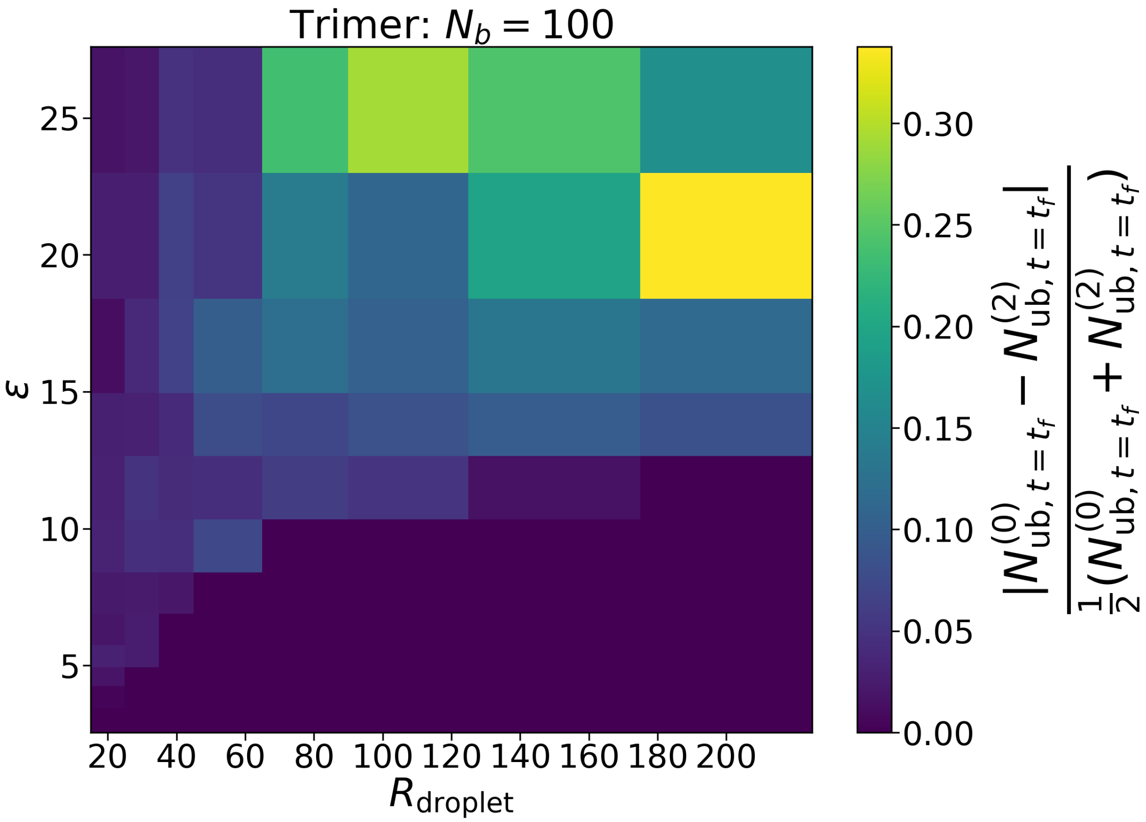

Figure 2.9: Asymmetry in the number of unrecruited binders at saturation $N_{\mathrm{ub},t=t_f}$ (t_f = 2×10^8 HOOMD steps) between the two adhesion patches in a trimer for varying R and ε (N_{b} = 100). $N^{(0)}_{\mathrm{ub},t=t_f}$ represents the number of unrecruited binders on the first terminal droplet at saturation and $N^{(2)}_{\mathrm{ub},t=t_f}$ represents the same for the second terminal droplet.

of binders on the middle droplet; therefore, even in cases where more than half of binders can pack into a patch, only half of the binders on each terminal droplet are exhausted. This situation occurs for higher ε, whereas for weaker binding, entropy dominates and many binders remain outside of the two adhesion patches on both the central and terminal droplets. We note that for high ε, rearrangement of binders between patches is expected to be slow. In Fig. 2.9 we show that there is some asymmetry between patches except at weak binding, and therefore conclude that the onset of effectively irreversible patch formation occurs roughly at $\varepsilon \sim 10$.

In Fig. 2.8b we fix ε = 20.7 at the goldilocks value from Fig. 2.8a, and explore the effect of varying binder surface coverage. In this strong binding regime, we eventually saturate the geometric limit set by the droplet size and binder repulsion (see also Fig. 2.10). If N_b is increased above this limit, it simply results in additional free binders. For small droplets, we quickly reach the situation where not all binders on the middle droplet of a trimer can fit into two patches, but we see that for larger droplets there is a very wide tolerance for binder concentration which might be useful for colloidomerization.

In summary, for certain parameters (including $\varepsilon = 20.7, R = 50, N_\mathrm{b} = 100$) we find that $< 100\%$ of the binders are recruited for dimers, while in trimers patches contain exactly half of the binders due to the competition between neighbors. This is an optimal situation for the self-assembly of colloidomers, and we proceed to study assembly of these droplets in Section 2.5.6.

2.5.4.1 Saturation of adhesion patch

Fig. 2.10 shows that the number of binders in an adhesion patch saturates due to steric repulsion with $N_\mathrm{bonded} < N_\mathrm{b}$.

2.5.5 Illustrating a molecular recipe for colloidomers

Fig. 2.11 illustrates scenarios that are predicted to be good or bad for colloidomer assembly, as described above; full trajectories for these conditions are also shown in Supplementary movies M1 and M2. Considering the dimer, we see that large droplets and high ε allow almost all the binders to fit into a patch, which is detrimental for colloidomer assembly because it terminates the polymerization reaction. Decreasing droplet size to $R = 50$ limits binders due to their steric repulsion in the patch, leaving just enough binders to seed a trimer with no remaining binders on the middle droplet, thus imposing the self-assembly of linear chains. Lowering the droplet size further or decreasing the binding strength leaves too many binders free on the trimer middle droplet at equilibrium, which would eventually lead to the self-assembly of branched colloidomers. Fig. 2.11b illustrates that for a fixed droplet size and bond strength, the number of

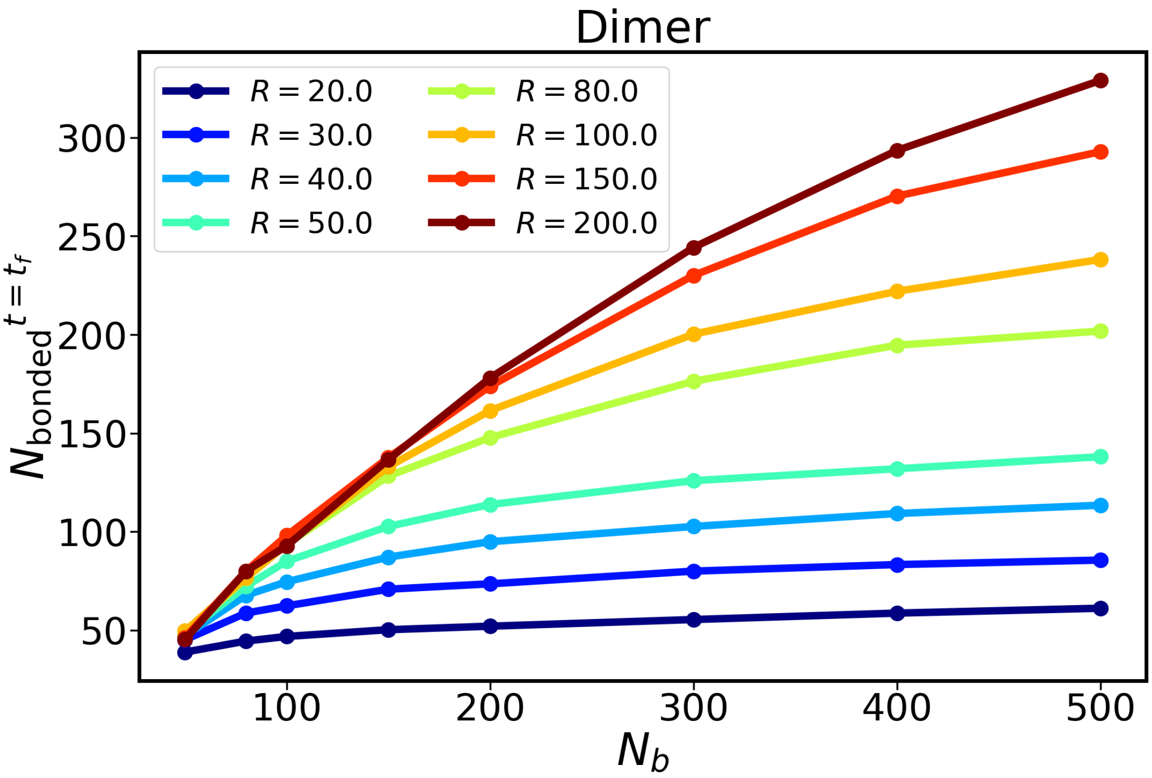

Figure 2.10: Variation of the number of binders in a saturated adhesion patch $N_{\mathrm{bonded}}{}^{t=t_f}$ with N_{b} for different droplet radii at $\varepsilon = 20.7$ for a droplet in a dimer (where $t_f = 2\times10^8$ HOOMD steps).

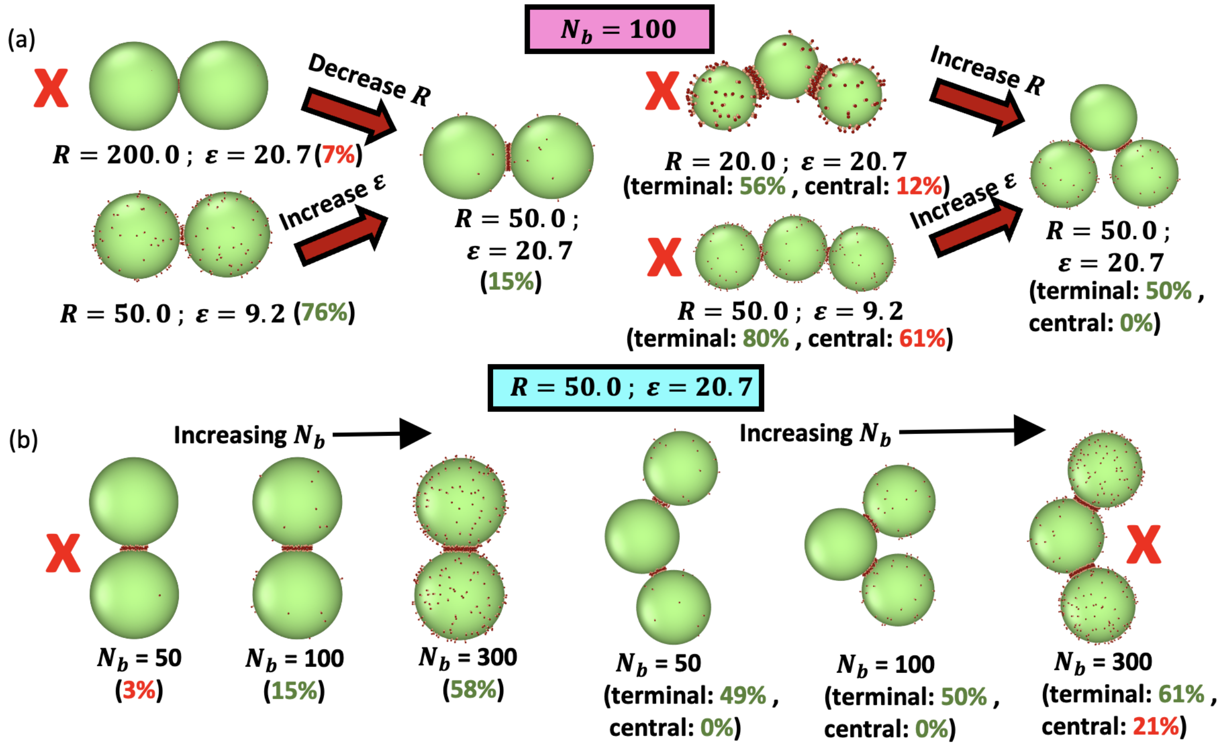

Figure 2.11: Illustrations showing the dimer and trimer geometries simulated in Fig. 2.8, and the "molecular" features of our droplet model that can be tuned to optimize for linear chains. Both results for dimers and trimers must be considered to predict the resulting polymerization reaction. (a) Varying R and ε at fixed number of binders $N_\mathrm{b} = 100$, with dimer on left and trimer on right. (b) Varying the number of binders N_b at fixed $R = 50$ and $\varepsilon = 20.7$. In (a) and (b), the % of free binders available (averaged over 10 independent runs) is indicated in parentheses beside each of these conditions for a droplet in a dimer as well as the terminal and central droplet(s) of a trimer. Based on the values of the percentage of free binders available, the conditions which are not suitable for colloidomer assembly (almost all used up in dimer, too many remaining on central droplet in a trimer) are indicated by a red X.

binders must be chosen such that dimers have free binders to grow the chain, while trimers have no free binders for branching *via* the middle droplet, as is the case for $N_\mathrm{b} = 100$. On the other hand, $N_\mathrm{b} = 50$ has almost all the binders (97%) recruited in the case of the dimer, terminating colloidomer assembly. For $N_\mathrm{b} = 300$, the central droplet of a trimer has 21% binders remaining on the surface, which would result in the branching of colloidomers.

2.5.6 KINETIC OPTIMIZATION OF COLLOIDOMERIZATION

Beyond dimers and trimers, the self-assembly of chains requires further optimization of competing experimental timescales. Combining a 1:1 mixture of droplets containing complementary binders of particles type ‘C’ and ‘D’ mimics the experiments in Ref. [161]. Tuning the density ϕ (area fraction) of droplets modulates the thermodynamic driving force for assembly, but also controls the collision time between droplets and allows us to optimize the formation of long colloidomers out of equilibrium for fixed time of assembly. Given that the droplets are undergoing simple diffusion, the collision time $\tau_{\text{collision}} \sim \langle l^2 \rangle / \mathrm{D}$, where l is the distance between droplets and D is the diffusion constant. In two dimensions, $l^2 \sim \phi^{-1}$, such that the collision time is inversely proportional to the droplet density. The Einstein relation gives $D = k_{\mathrm{B}}T/\gamma$, therefore $\tau_{\text{collision}} \sim \gamma$, the drag on a particle.

In Fig. 2.12, we show that by fixing the previously optimized $R, N_{\mathrm{b}}, \varepsilon$ parameters and varying ϕ and γ_{A}, we can maximize the yield of colloidomers (with results from two lower values of ε shown in Figs. 2.17-2.19). Previous arguments suggest that higher valences would be preferred at equilibrium [272–274], but in this case our goal is to maximize the yield of linear chains. We therefore adopt the strategy of kinetic control, where we predict that chains can be formed whenever adhesion patches form and exhaust approximately half of available binders before subsequent droplet collisions and patch formation, based on the strategies in the previous section. To achieve this control, we first vary the droplet density ϕ. Since droplet collisions are fast in dense suspensions, we observe many droplets with valence three or four at the highest initial density. At lower densities, valence two predominates as predicted based on our dimer or trimer experiments; whenever that does not occur “defects” result, producing branched structures.

A second way to modulate our kinetic yield of chains can be achieved is by increasing γ_{A} for the droplet, which slows down the collision rates without changing the thermodynamic driving force for assembly and increases the yield of linear chains, while also avoiding loop formation

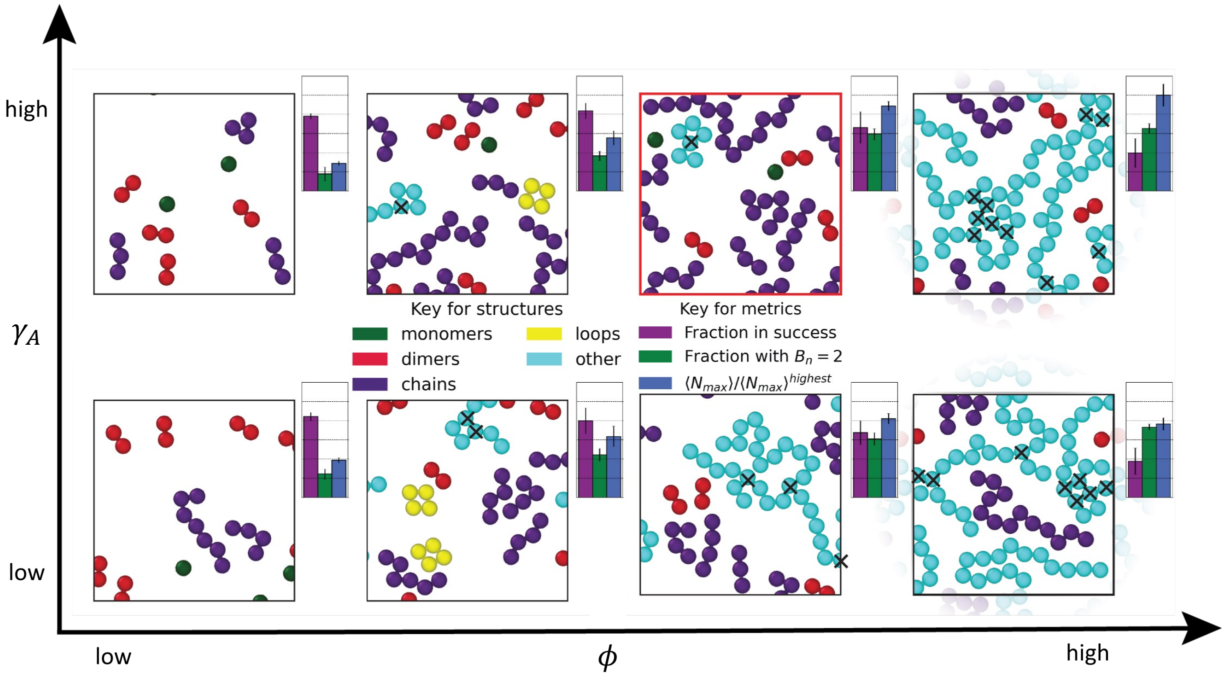

Figure 2.12: Effect of area fraction ϕ and the droplet drag coefficient γ_A on self-assembly in a 1:1 mixture of 81 $R = 50$ droplets containing $N_b = 100$ complementary binders of type C and D (with one surplus droplet of C/D). $\varepsilon = 20.7$. Here, $\phi = 0.1, 0.2, 0.3, 0.4$ (increasing from left to right) and $\gamma_A = 0.01, 1.0$ (bottom and top). Every system is the same size, but each snapshot has identically sized field of view by area, meaning droplets are cropped at $\phi < 0.4$. Droplets are colored according to structure as shown in the key. Each condition is accompanied with bar charts representing quantities computed over 10 independent runs that can quantitatively help in collectively deciding the 'winning condition' for colloidomer formation. These quantities are labeled in the second key, and described in detail in the main text, and for each quantity, optimal would be a larger bar. The few droplets that have valence 3 or higher are also marked with a 'cross' in the representative configurations to reinforce that even the branched structures which are considered part of 'errors' have long segments of droplets with valence=2. The condition we consider optimal, $\phi = 0.3, \gamma_A = 1.0$ is highlighted with a red box. Snapshots at $\phi = 0.4$ show periodic images to emphasize that structures are extended across the periodic boundaries. The distributions of structures obtained, particle valences, and of colloidomer chain lengths for each of these 8 conditions are provided in Fig. 2.14-2.16 respectively. Timing data for these simulations as well as larger systems are given in Tables 2.2, 2.3.

(Fig. 2.12–upper row); full trajectories for the upper row are also provided in Supplementary movie M3. As described in the simulation methods (Section 2.4), it is important to note that we control drag on the central droplet and binders separately; here we only varied the drag on the droplet particle 'A' (γ_A) and kept γ_{binder} at a very small constant value, because increasing γ for each of the binder particles can also slow down the diffusion of the droplet as a whole. We also predict that decreasing the binding rate k_{on} at fixed bond strength ε would be detrimental to our goal of assembling chains, since as described earlier it would take longer to assemble a patch as compared to the collision time of droplets (See Fig. 2.6). The relative speeds of the two competing processes of patch recruitment and droplet-droplet collision can thus be tuned to dictate the kind of structures observed in self-assembly and provide more insights on kinetic control.

More quantitatively, we compute the distribution of structures produced at the end of 10^8 steps, averaging over 10 independent simulations. We partition every interconnected assembly using an algorithm described in Section 2.5.6.2, and then classify these structures as monomers, dimers, linear chains ($N \geq 3$), loops, and 'other' (at least one droplet has valence ≥ 3). To define the best conditions for chain assembly, we sought to maximize three quantities that are shown in bar charts next to each condition in Fig. 2.12: (1) fraction of droplets present in structures that are not monomers or branched—which we call "success" (purple bar), (2) fraction of droplets with valence 2 (green bar), and (3) the average maximum chain length (blue bar, which we scale by the highest value $\langle N_{\max}\rangle^{\text{highest}} = 20$ observed for the condition $\phi = 0.4$, $\gamma_A = 1.0$).

While conditions at $\phi = 0.4$ have the longest chains and a high fraction of particles with valence 2, there are also many 'errors' due to chain branching, and so we eliminate high density. Conditions at lower ϕ have fewer errors but also shorter chains. Based on maximizing these three metrics, we choose the condition ($\phi = 0.3, \gamma_A = 1.0$) as our best, and we provide more details about the structures observed at this condition in Fig. 2.13.

In Fig. 2.13a, we show the evolution of bond valence *versus* time, which reflects on average, colloidomers are formed by conversion of monomers to dimers, followed by the conversion of

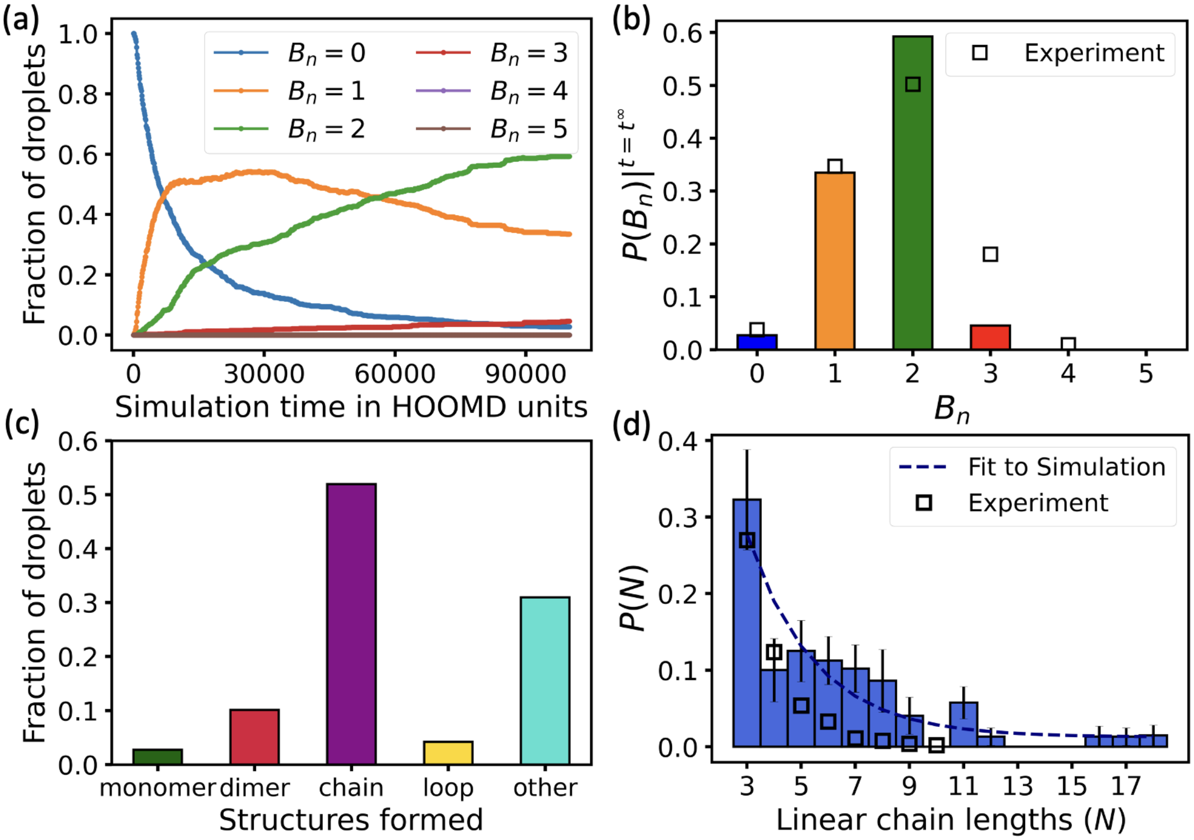

Figure 2.13: Best choice of parameters for obtaining maximum quality of colloidomer chains: $N_\mathrm{b} = 100$, $R = 50$, $\phi = 0.3$, $\varepsilon = 20.7$, $\gamma_\mathrm{A} = 1.0$. (a) Fraction of droplets in each possible valence *versus* time. (b) Final valence distribution obtained across the 10 simulations. Open squares show optimal valence distribution from Fig. 2g in Ref. [161]. (c) A combined histogram showing the fraction of the total number of droplets present as a particular kind of structure from 10 different final configurations for this condition. (d) Distribution of linear chain lengths $P(N)$ obtained for this condition, with the errorbars computed using a bootstrapping procedure described in Section 2.5.6.4. [349, 350] Open squares show experimental length distribution from Fig. 3a in Ref. [161].

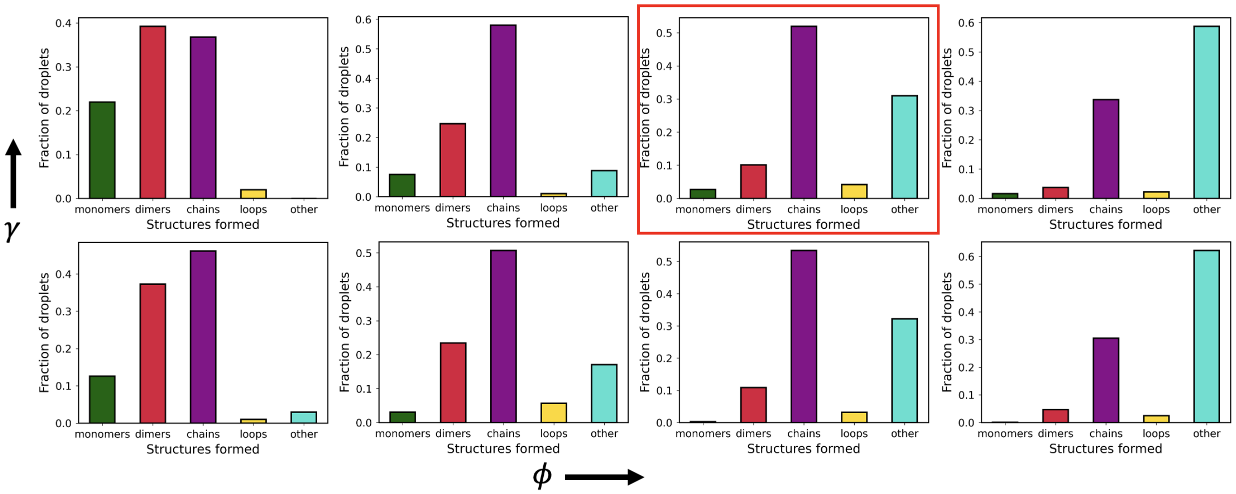

Figure 2.14: Distributions of structures obtained from all final configurations for each of the $(\phi, \gamma_{\mathrm{A}})$ pairs, illustrated in Fig. 2.12. $\phi = 0.1, 0.2, 0.3, 0.4$ (increasing from left to right) and $\gamma_{\mathrm{A}} = 0.01, 1.0$ (bottom and top).

dimers to trimers. Fig. 2.13b shows the distribution of valence, and for this condition, we observe that only $\approx 5\%$ of droplets had valence higher than 2, which is indicative of a small number of branching points in chains. This result actually has a higher yield of linear chains than the best condition found experimentally in Ref. [161]. However, even a small fraction of droplets with valence 3 can prevent extremely high quality assembly of only chains, as shown in Fig. 2.13c, where we observe that $\approx 30\%$ of droplets are present in structures that contain at least one particle of valence 3 (cyan bar), and hence are considered as errors. Finally, Fig. 2.13d shows that the distribution of chain lengths seems to follow an exponential distribution, with an average length longer than in the optimal conditions in Ref. [161]. An exponential distribution implies that it will be challenging to obtain a large median chain length *via* a simple self-assembly strategy. This comports with experimental findings, where for efficiency, a new methodology was developed to engineer longer chains using magnetic fields applied to a dispersion in a ferrofluid [165].

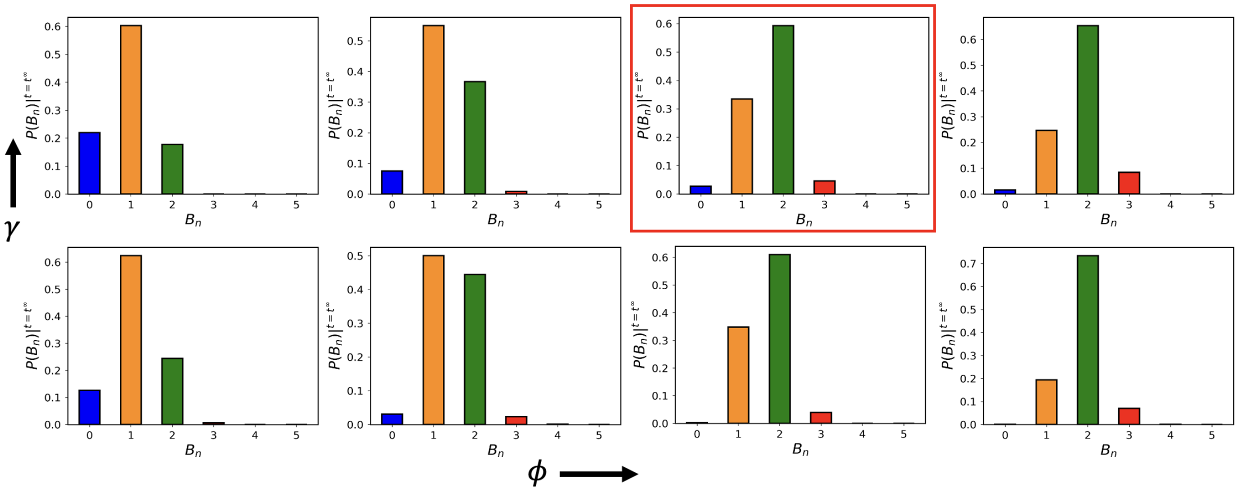

Figure 2.15: Distributions of droplet valences obtained from all final configurations for each of the (ϕ, γ_A) pairs, illustrated in Fig. 2.12. $\phi = 0.1, 0.2, 0.3, 0.4$ (increasing from left to right) and $\gamma_A = 0.01, 1.0$ (bottom and top).

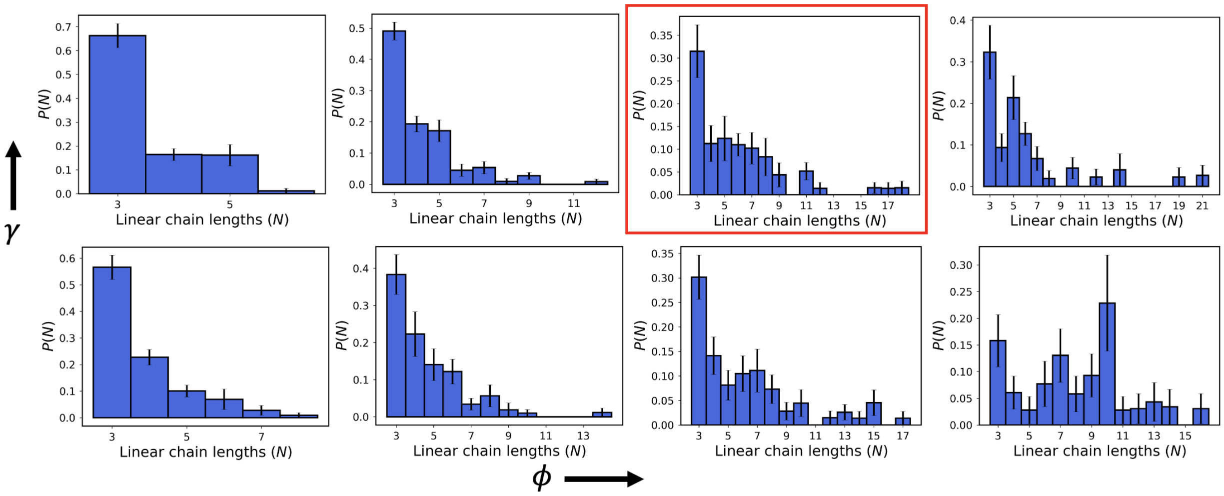

Figure 2.16: Distributions of colloidomer chain lengths from all final configurations for each of the (ϕ, γ_A) pairs, illustrated in Fig. 2.12. $\phi = 0.1, 0.2, 0.3, 0.4$ (increasing from left to right) and $\gamma_A = 0.01, 1.0$ (bottom and top).

2.5.6.1 Effect of kinetic factors on self-assembly in reversible regimes (low and intermediate ε)

In Section 2.5.6 we described how kinetic factors such as ϕ and γ_A can dictate the structures formed in self-assembly for a high ε. In this regime, once an adhesion patch forms, binders are very unlikely to redistribute into bonds with other droplets. However, for reversible binding in case of lower ϵ, we find that this kinetic trapping effect is not observed because redistribution of binders between droplets is allowed here, allowing droplets to potentially achieve their equilibrium valence. We show a case of lower ($\varepsilon = 9.2$) and intermediate ($\varepsilon = 13.8$) binding affinity here to demonstrate the effect of ϕ and γ_A for reversible binding scenarios (final configurations shown in Figures 2.17 and 2.18 respectively.). The distribution of bond valences over time for $\phi = 0.3$ and $\gamma_A = 1.0$ is shown in Fig. 2.19 for lower and intermediate ε. The difference between the two cases is the most profound for lower densities such as $\phi = 0.2$, where for $\varepsilon = 9.2$, we already obtain aggregates whereas for $\varepsilon = 13.8$, we end up mostly in chains, with and without branching. For $\varepsilon = 9.2$ and high densities such as $\phi = 0.4$, it is almost impossible to differentiate the effect that low and high γ_A have, because of system-spanning gels forming in both situations.

2.5.6.2 Clustering *via* a segmentation algorithm to identify unconnected assemblies and classification of the structures

For every frame in our simulation, we identify the unconnected assemblies of droplets bonded to each other *via* a simple segmentation algorithm, using the bond table of droplet pairs. The bond table is a list of unique pairs of droplets that have at least one dynamic bond between them.

From this list of bonded droplet pairs, we want to find the components which have common elements between them. We follow an algorithm to continuously merge sets of pairs that have common elements[2]to perform the clustering: (i) We take the first set, say ‘A’ from the list and

---

[2] https://stackoverflow.com/questions/4842613/merge-lists-that-share-common-elements

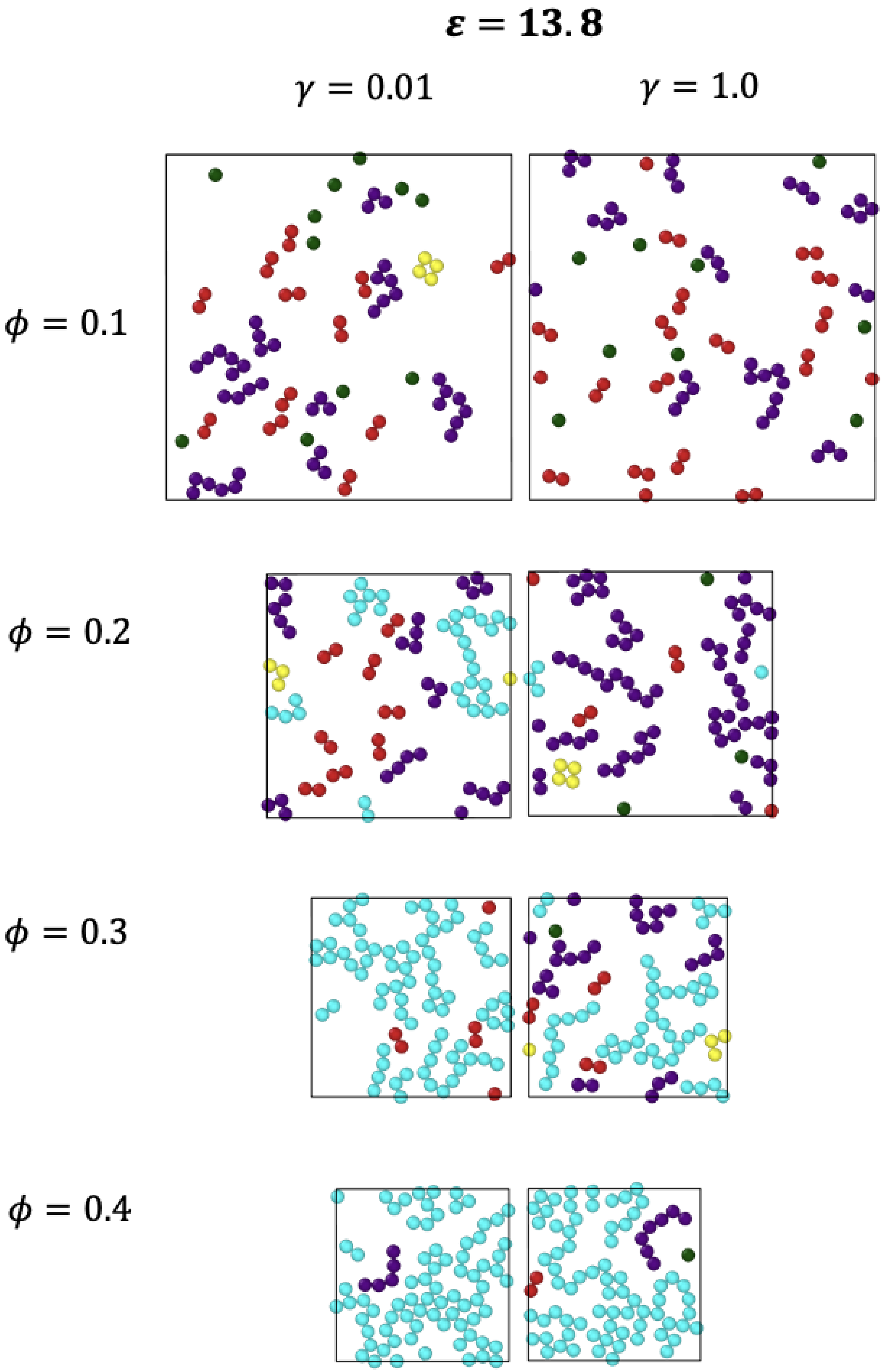

Figure 2.17: Effect of ϕ and γ_A on the kind of self-assembled structures for our system of 81 droplets with $N_b = 100$, $R = 50$ for intermediate binding affinity $\varepsilon = 13.8$. The droplets are colored according to the type of structure to which they belong, as explained in Fig. 2.12

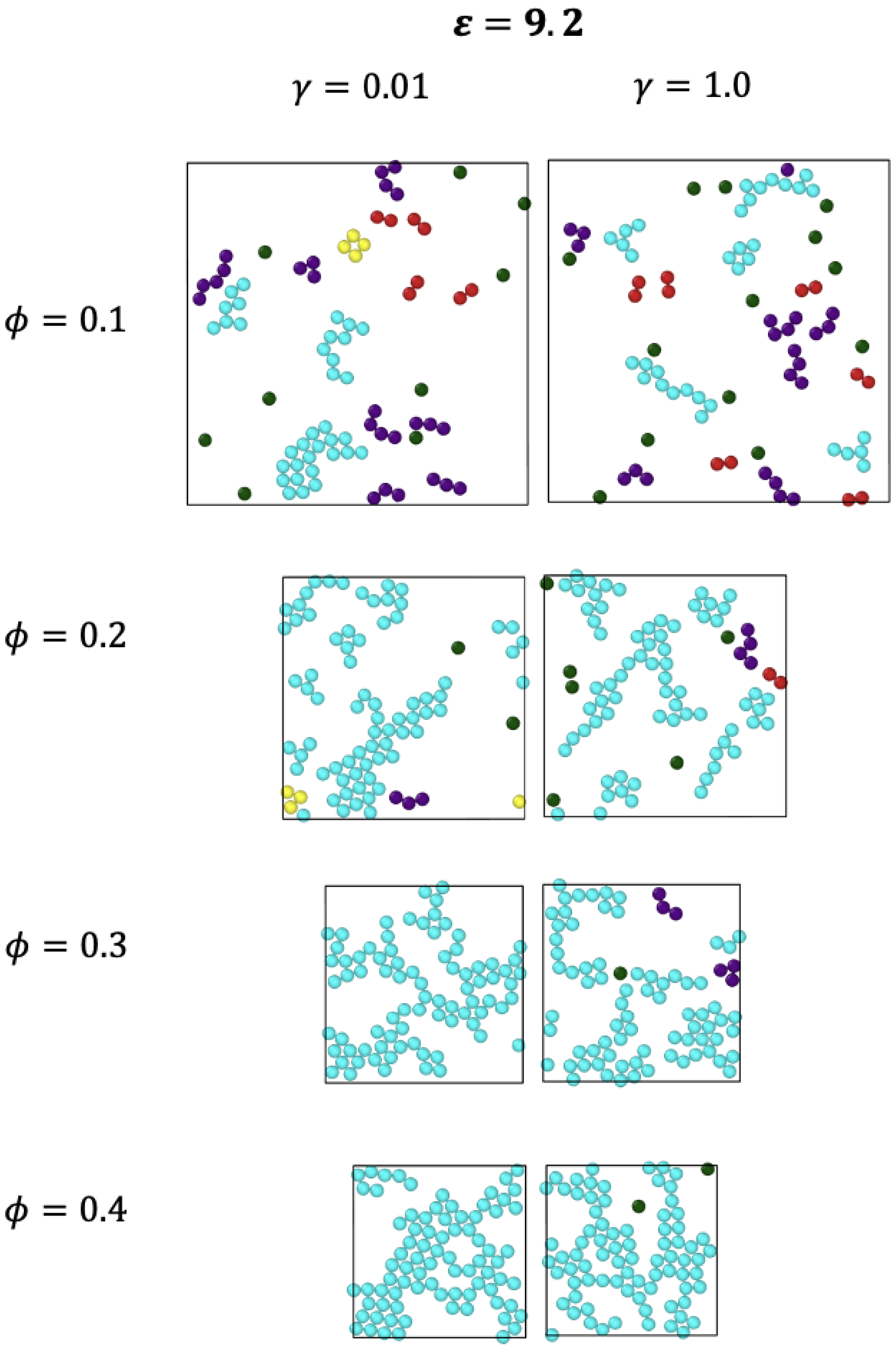

Figure 2.18: Effect of ϕ and γ_A on the kind of self-assembled structures for our system of 81 droplets with $N_b = 100$, $R = 50$ for lower binding affinity $\varepsilon = 9.2$. The droplets are colored according to the type of structure to which they belong, as explained in Fig. 2.12

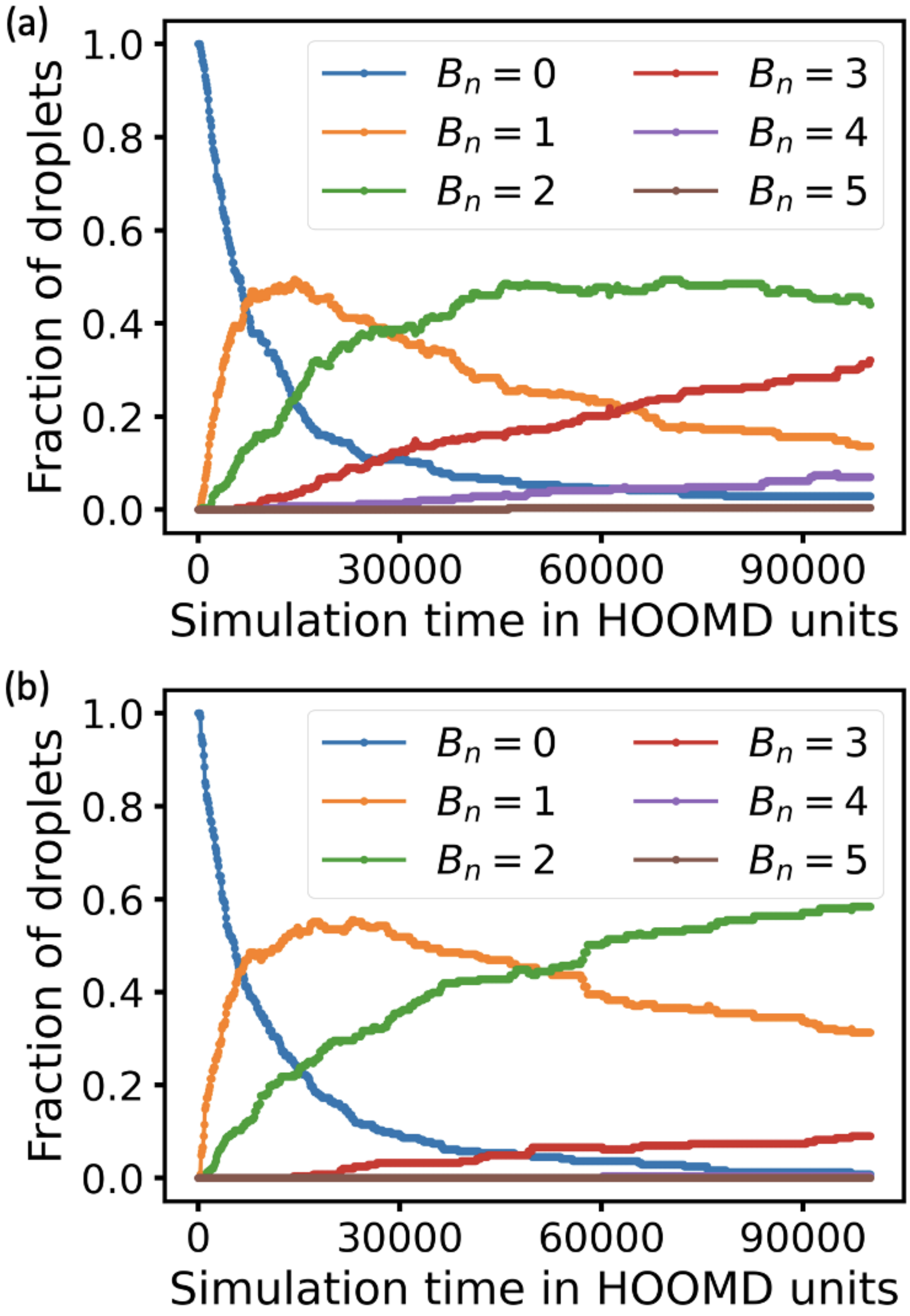

Figure 2.19: Fraction of droplets with a given bond valence (B_n) as a function of the simulation time (in HOOMD units) for the optimized condition which gives maximum quality of colloidomer chains at high binding energy: $N_b = 100$, $R = 50$, $\phi = 0.3$, $\gamma_A = 1.0$ but for (a) lower binding affinity $\varepsilon = 9.2$ and (b) intermediate binding affinity $\varepsilon = 13.8$. The corresponding plot for $\varepsilon = 20.7$ is shown in Fig. 2.13a.

separate the rest of the list from it. (ii) Next, for every other set B in the list, if B has common element(s) with A then we merge sets A and B and remove B from the list. (iii) This step is repeated until none of the other sets have any overlap with A. (iv) The set A is then added to the output of the clustering. (v) Step (i) is repeated, but now with the rest of the list (excluding 'A'). In this way, we ultimately end up with a list of lists where each sub-list consists of droplets which are 'bonded' to each other.

Once the set of unconnected assemblies (or 'clusters') is obtained, the next step is to classify them into structures—monomers, dimers, linear chains ($N \geq 3$), loops and 'other' (which includes any branched colloidomer chains or gels/aggregates with higher droplet valences). Monomers are identified as those that do not appear in the bond table. Next, in order to classify the remaining droplets into the other structures, for every cluster we obtained, we first calculate the valence of each droplet in that cluster from the bond table of droplets, and then count the number of droplets with valence 1 and 2 respectively. If the size of the cluster is 2, then both of the droplets belong to a 'dimer'. However, if the size of the cluster list is greater than 2, then the valence information will help us to further identify if it is a linear chain, a loop, or 'other'. If the number of droplets in the given cluster with valence 1 is 0 and the number of droplets with valence 2 is equal to the total size of the cluster, then the structure is a 'loop'. If the number of droplets with valence 1 is 2 and the number of droplets with valence 2 is equal to the (size of the cluster)-2, then the structure is a 'linear colloidomer chain' (for which only the 2 terminal droplets have valence 1 and the rest have valence 2). Else, the cluster is classified as 'other'.

2.5.6.3 Execution times for MD simulations of assembly of 1:1 mixtures of C and D droplets for different simulation conditions

2.5.6.4 Bootstrapping procedure

From the original data set of chain lengths for 10 final configurations, we create 100 new resampled sets of data with replacements (each resampled set is of the same size as the original

Table 2.2: A table showing the speed of MD simulations (in timesteps per second) and the approximate time (in GPU hours) taken to run 10^8 steps for $N = 81$ droplets for various system sizes (variable $N_\mathbf{b}$), with $R = 50$, $\phi = 0.3$ and $\varepsilon = 20.7$.

Number of binders on a droplet ($N_\mathbf{b}$)	Total number of particles in the system = $N(2N_\mathbf{b} + 1)$	TPS	Number of GPU hours for each run of 10^8 steps
50	8181	2350	11.8
100	16281	1010	27.5
150	24381	800	34.7
200	32481	570	48.7
300	48681	360	77.2
500	81081	207	134.2

Table 2.3: A table showing the speed of MD simulations (in timesteps per second) and the approximate time (in GPU hours) taken to run 10^8 steps using HOOMD-blue for various system densities (variable ϕ) with $R = 50$, $N_\mathbf{b} = 100$ and $\varepsilon = 20.7$. The total number of droplets N is 81 and the number of particles in the system is 16281.

Area fraction (ϕ)	TPS	Number of GPU hours for each run of 10^8 steps
0.1	1070	26
0.2	1020	27.2
0.3	1010	27.5
0.4	1000	27.8

data set). To create a bootstrap sample, the resampling is done randomly, by choosing a random integer between 0 and (the size of the original data set)-1. The element from the original data set with this random index is then added to the bootstrap sample and this process is repeated for as many times as the size of the original data set. Ultimately from the 100 bootstrap samples obtained, we can calculate the mean fraction of all chain sizes and also the standard deviation. By bootstrapping, we obtain an estimate of the error resulting from having a small number of samples [350].

2.5.7 Application of the model to colloidomer folding

Folding of colloidomer chains and the study of their pathways towards stable structures is an area of active research [165]. Here, we demonstrate that our CG model can capture experimentally relevant folding behavior of colloidomer chains and use this to highlight additional features of our CG framework.

Our CG framework allows the user to generate an initial linear colloidomer chain of any length and an arbitrary sequence of binder types. Moreover, there can be multiple types of binders on the same droplet. To study colloidomer folding, we mimic the experimental setup of having two types of binders on the same droplet, C and D, *each of which is self-complementary*. Here, C-C bonds are intended to make up the backbone of the chain, while D-D bonds are the ones driving folding. As described earlier, our dynamic bonding model can also have temperature dependent binding/unbinding (see Section 2.3.3.2 for full details). We therefore choose different melting temperatures such that D-D bonds melt at a lower temperature, while C-C bonds stay in place.

Here, we generate folded structures using a square wave heating and cooling cycle. During the first segment at higher temperature, the backbone adhesion patches form and the chain explores unfolded configurations. After that, repeated cooling and heating are used to generate low energy structures.

In contrast to our work in Section 2.5.4 on optimizing colloidomer assembly, here we do want to produce higher valences. This is achieved through the use of smaller $R = 20$ and lower $\varepsilon_{\mathrm{DD}} = 4.6$, where reversible bonding allows for rearrangements such that equilibrated structures form. Low R has the additional benefit of faster folding times, allowing us to generate many structures in relatively little computational time.

As a benchmark case to confirm that our model would be applicable in future studies of colloidomer chain folding, we investigate the heptamer case consisting of $N = 7$ droplets that has been experimentally realized in Ref. [165]. There are four possible rigid structures which are the

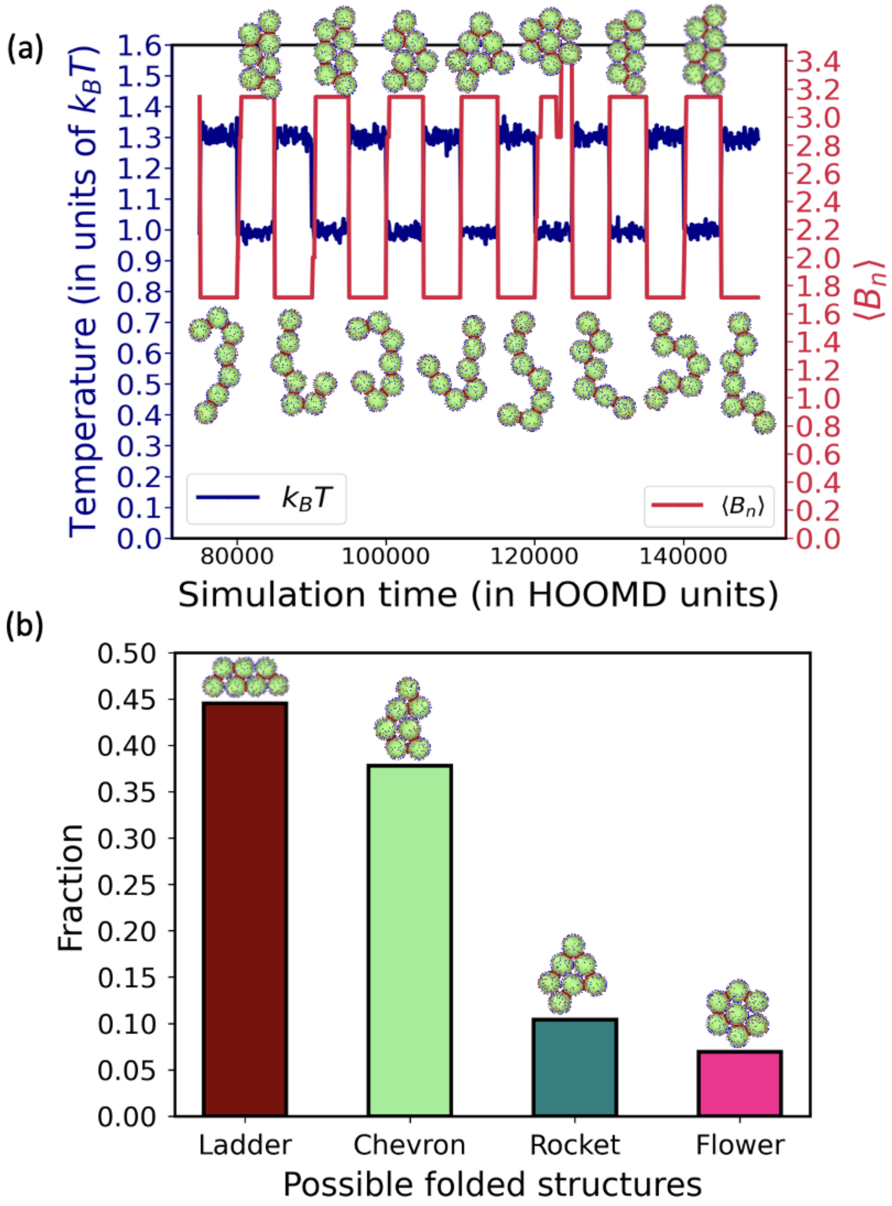

Figure 2.20: (a) Folding and unfolding cycles shown for a heptamer of droplets with 100 'C' binders and 100 'D' binders on each droplet, $R = 20$, $\varepsilon_{\mathrm{DD}} = 4.6$, $\varepsilon_{\mathrm{CC}} = \infty$, and $\gamma_{\mathrm{A}} = 0.1$. $T_{\mathrm{melt}} = 1.2$ for D-D bonds and temperature is cycled between 1.0 and 1.3. The variation of the average bond valence $\langle B_n \rangle$ (red) with simulation time is shown, as the temperature (navy blue) is alternately raised and lowered. An expected $\langle B_n \rangle = 1.7$ is obtained when the structures unfold back to chains. (b) Histogram showing the yield of each of the four possible folded rigid structures (ladder, chevron, rocket and flower)[165] from a total of 1500 folded structures obtained from 300 independent simulations each consisting of 5 folding and unfolding cycles. (only 5/1500 did not reach one of these structures, and are not shown in this histogram).

low energy states of the heptamer. Scanning a small range of R and $\varepsilon_{\mathrm{DD}}$ over 15 heating-cooling cycles we uncover the aforementioned condition ($R = 20, \varepsilon_{\mathrm{DD}} = 4.6$) where all four possible structures are observed in a single simulation, as shown in Fig. 2.20a, and Supplementary movie M4.

Having obtained all structures in a single long simulation, we wished to quantify the population of each stable folded state. We ran 300 independent simulations each consisting of 5 folding/unfolding cycles and show in Fig. 2.20b the yields of each structure; the ladder and the chevron structures are kinetically accessible and have a higher yield than the rocket and flower geometries, in good agreement with Ref [165].

From these preliminary studies of folding within our model, we have learned several key principles. Firstly, we only observe the flower structure—which has the highest bond count—when $\varepsilon_{\mathrm{DD}}$ is very low; this is because folding to this structure is not fully downhill, and requires the breaking of a droplet-droplet bond (dissolving an entire adhesion patch) to reach the final state. Second, every droplet contains both C and D binders, and so it could be a concern that the D's become exhausted in forming backbone bonds, which would tend to form faster than bonds farther away in sequence space. In our simulation, this is prevented by choosing R and N_{b} where the patch is fully saturated by C's (see Fig. 2.10 and 2.21), meaning that there is no opportunity for D's to enter the backbone.

Moreover, the exclusion of D's from the adhesion patches means there is a smaller area for them to occupy, which results in faster formation of bonds during the folding process. The factors which contribute to the speed of folding are also important to our results, since both in simulations and in experiments we do not want to wait arbitrarily long times in the cooling phase when generating low energy structures.

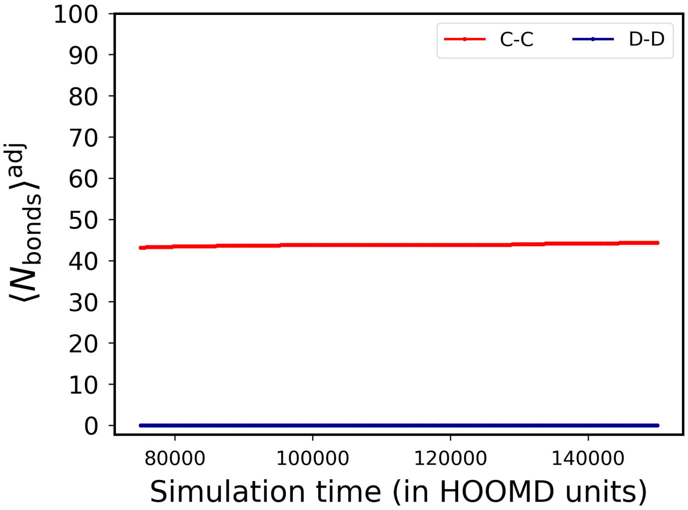

Figure 2.21: Plot showing the average number of bonds of C-C (backbone) and D-D (secondary) types per adhesion patch between adjacent droplets, as a function of the simulation time for the square wave heating and cooling cycle described in Section 2.5.7. The conditions for this simulation are: $N_\mathrm{b} = 200$ (100 binders of types C and D respectively on every droplet), $R = 20$, $\gamma_\mathrm{A} = 0.1$. The choice of R and N_b used here ensures that on an average, $\sim 44\%$ of the C binders get recruited whereas $\sim 0\%$ D binders are able to go into an adhesion patch between any two adjacent droplets. As a result, the adhesion patches between adjacent droplets are always fully saturated by C's (See Section 2.5.7)

2.5.7.1 IDENTIFICATION OF THE FOLDED STRUCTURES FOR THE HEPTAMER

The folded structures obtained in our 300 independent simulations for the heptamer can be classified as either a ladder, a chevron, a rocket or a flower (see Section 2.5.7, and Ref. [165]). These structures can be differentiated from one another on the basis of the valence of the droplets present in the structure. A valence list of all the 7 droplets is obtained for every folded structure. The number of droplets with valence 2,3,4,5 and 6 is calculated for each of these structures from the list of valences. We assign the structure based on the counts for each of these valences (see Table 2.4). We found that only 5 of the 1500 folded structures obtained could not be assigned to any of the four folded states mentioned above.

Table 2.4: A table showing the counts of the droplet valences for the different folded geometries for N=7 in two dimensions

Valence	Ladder	Chevron	Rocket	Flower
2	2	2	3	0
3	2	3	1	6
4	3	1	2	0
5	0	1	1	0
6	0	0	0	1

2.6 CONCLUSIONS

In this work, we report a CG model and simulation framework for colloidal liquid droplets with explicit mobile binders. The core of this model is a dynamic bonding protocol that satisfies detailed balance, that is very flexible in allowing one to control separately binding and unbinding rate constants, as well as implementing a tunable temperature dependence. Both the dynamic bonding code and the pyColloidomer framework are easy to use and freely available with examples from `https://github.com/hocky-research-group/pyColloidomer_2023`.

Previous modeling works have studied colloidal liquid droplets with implicit mobile linkers, such that bonds are formed or removed based on a statistical mechanical model that predicts the strength of a patch and which can include timescales for bonding. Our model with explicit binders complements these studies—while having many explicit binders makes the model higher resolution, and hence slower, it also allows us to build insight into the adhesion patch formation process. For example, the use of explicit binders allowed us to see the effects of excluding particles from patches once they are formed, which had major consequences for ensuring valence=2 structures in optimizing colloidomer assembly, and in preventing binders from being used up in colloidomer backbones in our folding studies. We also observe that above a certain binding strength (around $\varepsilon > 13$), the growth of a patch can follow a process characterized by two timescales, where saturation can take much longer than initial formation and recruitment. This could have an important effect at higher densities and lower viscosities, where droplet collisions can take place before patches are fully recruited; this effect could be incorporated into simulation models that use a parameterized equation for the recruitment process, such as recently done in Ref. [242]. The separation of the timescales for the motion of the droplet and for the binders in our CGMD model can also be applied in the case of systems such as polymer-grafted nanoparticles (NPs) [327–330] which can help in kinetically controlling the interactions and hence the formation of non-equilibrium structures such as sheets and strings.

In ongoing work, we are now using these explicit binders to test the contributions to the free energy of patch formation and patch shape predicted experimentally in Ref. [164]. We are also expanding our dynamic bonding model to include the effect of force on unbinding rates [97, 98, 193] to probe its effect on adhesion patch formation [161, 164], a dependence which is known to play an important role in the behavior of biomimetic assemblies of cellular adhesion proteins [38]. Preliminary data shows that our model captures observed behavior for folding of two dimensional colloidomer homopolymer chains; in future work we can use our model to compare the structures and pathways generated through the use of explicit binders with those using very reduced models [165, 351]. We can also trivially expand our folding studies to three dimensions by removing confinement, which will allow us to detail folding pathways in ways that are difficult to quantify in experiment.

Our CG model is quite versatile and can also be adapted to represent the behavior of analogous systems of lipid bilayers mentioned earlier [160, 269, 270, 319–321]; it can also be used to explore the assembly of colloidal nanoparticles coated with ligands that bond *via* formation of reversible dynamic bonds with secondary linker molecules [294, 296]. Linker-mediated colloidal assembly is a ripe area for exploration because the mobility of the secondary linkers and the reversibility in bonding can lead to formation of kinetically controlled structures such as string-like gels. Tuning the ratio of the linker to the colloid concentration [294, 296] can appropriately control the phase behavior. It would be fascinating to explore the consequences of assembling our particles with mobile binders using explicit free linkers with complementary binding sites rather than using direct binding.

Although our model captures what we believe to be the most crucial features of systems with mobile binding sites, there are simplifications whose effects we would like to investigate in the future. For example, the presence of a spring between the center of the droplet and binders allows the binders' vertical position to vary, and by tuning this parameter we can explore the tendency to form a planar adhesion patch — however, we are missing the lateral coupling between binders that could be important in the case of deformable droplets. Our work also currently employs harmonic springs, and we plan to investigate the differences where more complex stretching behavior is taken into account [164]. Our powerful and flexible framework is freely available and simple to use, and so we hope others will build upon our work and take these studies in new directions.

2.7 Detailed simulation parameters

All important simulation parameters are enumerated in the tables 2.5, 2.6, 2.7 and 2.8.

Table 2.5: A table containing all the general simulation parameters

Description (Symbol)	Value in HOOMD units
MD timestep (dt)	0.0005-0.001
Dimensionality (d)	2
Temperature (T)	1.0-1.6
Number of simulation steps run (n_{steps})	10^8 - 2×10^8
Radius of droplet (R)	20.0-200.0
Radius of inner binder particle (r_{B})	1.0
Radius of outer binder particle ($r_{\text{C/D}}$)	1.0
Number of binders in a droplet (N_{b})	50-500
Mass of droplet (m_{A})	1.0
Mass of inner binder particle (m_{B})	0.001
Mass of outer binder particle ($m_{\text{C/D}}$)	0.001
Drag coefficient of droplet (γ_{A})	0.01-1.0
Drag coefficient of binder (γ_{binder})	0.0001
Harmonic bond spring constants:	
(i) k_{AB}	200.0
(ii) $k_{\text{BC/BD}}$	500.0
(iii) $k_{\text{ABC/ABD}}$	10.14
Harmonic bond rest lengths:	
(i) l^0_{AB}	50.0 (R = 50.0)
(ii) $l^0_{\text{BC/BD}}$	2.0 (r_{C} = 1.0)
(iii) $\theta^0_{\text{ABC/ABD}}$	3.141593
Epsilon for soft repulsive potential ($\varepsilon_{\text{soft}}$)	200.0-5000.0
Cut-off distance for soft potential:	
(i) $r_{\text{cut,AA}}$	110.0 (R = 50.0)
(ii) $r_{\text{cut,AC/AD}}$	53.0 (R = 50.0, r_{C}=1.0)
(iii) $r_{\text{cut,BB}}$	2.0 (r_{B}=1.0)
(iv) $r_{\text{cut,CC/DD}}$	2.0 (r_{C}=1.0)
Epsilon for Wall Potential ($\varepsilon_{\text{wall}}$)	10.0 (d = 2)
Cut-off distance for Wall Potential ($r_{\text{cut,wall}}$)	112.25 (R = 50.0)
z-coordinate of upper wall plane origin	125.0 (R = 50.0)
z-coordinate of lower wall plane origin	-125.0 (R = 50.0)
Initial rate constant for binding ($k^{\text{init}}_{\text{on}}$)	100.0-200.0
Initial rate constant for unbinding ($k^{\text{init}}_{\text{off}}$)	10^{-9}-5.0
Rate constant for binding after melting ($k^{\text{melt}}_{\text{on}}$)	0
Melting Temperature (T_{melt})	1.2-1.6
Inflexion steepness parameter (α)	200.0
Dynamic bond rest length (l_{dyn})	2.0
Dynamic bond spring constant (k_{dyn})	10.0
Dynamic bonding minimum distance (l_{min})	1.368 ($l_{\text{dyn}} - 2\sigma$)
Dynamic bonding maximum distance (l_{max})	2.632 ($l_{\text{dyn}} + 2\sigma$)
Dynamic bond checksteps (n)	10

Table 2.6: A table containing important parameters specific to the simulations for a dimer/trimer of droplets

Description (Symbol)	Value in HOOMD units
MD timestep (dt)	0.001
Temperature (T)	1.0
Number of simulation steps run (n_{steps})	2×10^8
Radius of droplet (R)	20.0-200.0
Number of droplets (N)	2,3
Number of binders on each droplet (N_{b})	50-500
Drag coefficient of droplet (γ_{A})	0.1
Initial rate constant of binding for CC ($k_{\text{on}}^{\text{init,CC}}$)	100.0
Initial rate constant of unbinding for CC ($k_{\text{off}}^{\text{init,CC}}$)	10^{-9} - 5.0

Table 2.7: A table containing important parameters specific to the self-assembly simulations for a 1:1 mixture of 81 droplets

Description (Symbol)	Value in HOOMD units
MD timestep (dt)	0.001
Temperature (T)	1.0
Number of simulation steps run (n_{steps})	10^8
Radius of droplet (R)	50.0
Number of droplets (N)	81 (9×9 lattice)
Number of binders on each droplet (N_{b})	100
Drag coefficient of droplet (γ_{A})	0.01,1.0
Initial rate constant of binding for CD ($k_{\text{on}}^{\text{init,CD}}$)	100.0
Initial rate constant of unbinding for CD ($k_{\text{off}}^{\text{init,CD}}$)	10^{-9} - 5.0

Table 2.8: A table containing important parameters specific to the folding/unfolding simulations for 300 independent simulations with 5 folding/unfolding cycles in each

Description (Symbol)	**Value in HOOMD units**
MD timestep ($\mathrm{d}t$)	0.0005
Temperature (T)	1.0 (quench), 1.3 (heating)
Number of simulation steps run (n_{steps})	10^8 (for 5 folding/unfolding cycles)
Radius of droplet (R)	20.0
Number of droplets (N)	7
Number of 'C' type binders on each droplet ($N_{\mathrm{b}}^{\mathrm{C}}$)	100
Number of 'D' type binders on each droplet ($N_{\mathrm{b}}^{\mathrm{D}}$)	100
Drag coefficient of droplet (γ_{A})	0.1
Initial rate constant of binding for CC/DD ($k_{\mathrm{on}}^{\mathrm{init,CC/DD}}$)	200.0
Initial rate constant of unbinding for CC ($k_{\mathrm{off}}^{\mathrm{init,CC}}$)	0
Initial rate constant of unbinding for DD ($k_{\mathrm{off}}^{\mathrm{init,DD}}$)	2.0
Melting Temperature for DD ($T_{\mathrm{melt,DD}}$)	1.2

CHAPTER 3

PROBING THE MOLECULAR PROPERTIES OF DROPLETS FEATURING MOBILE BINDERS THAT GOVERN THE SHAPE AND SIZE OF THE ADHESION PATCH AND THE EFFECT OF ADDING LATERAL INTERACTIONS

3.1 ABSTRACT

Expanding upon our prior research on the self-assembly of colloidal droplets with mobile binders [50, 240, 242, 269, 272–275], our current emphasis is on a comprehensive exploration of the dynamics involved in adhesion patch formation between two droplets. Our objective is to manipulate molecular features, such as droplet size, binding strength, excluded binder volume, binder concentration, and the flexibility of harmonic springs, to tune the growth, shape,

and geometry of the adhesion patch [39, 50, 161, 164]. This investigation extends to the crucial impact of lateral or *cis*-interactions, particularly relevant in cellular junctions where E-cadherin proteins [38, 39, 93, 284, 352] mediate cell-cell adhesion [100]. Consequently, we examine the consequences of introducing lateral binding interactions [39, 281, 282, 284, 285, 353–355] between binders on the same droplet in the context of adhesion patch formation dynamics. In our coarse-grained model, we introduced Lennard Jones attractions [356–359] between inner binder particles with varying interaction strengths. Our simulations demonstrate that, in the presence of lateral binding (or *cis*-interactions), binders exhibit a more ordered packing [39, 284, 285] into the adhesion patch, with a significantly higher recruitment compared to scenarios without *cis* interactions, thereby reinforcing the phenomenon of 'cis-trans cooperativity' [39, 93, 281, 282] observed in experiments. Recent experiments to study homophilic droplet assembly also indicate an accelerated decay rate of the fraction of droplet monomers over time in the presence of lateral interactions. In our ongoing coarse-grained simulations of droplet assembly with lateral interactions, we are actively investigating the parameter regime that aligns with this observed phenomenon.

3.2 INTRODUCTION

Adhesion phenomena in biological systems include processes by which cells and other biological structures adhere or stick together [360], playing vital roles in physiological processes like development, immune responses, and tissue repair. Cell-cell adhesion is crucial for tissue structure, supporting dynamic processes such as morphogenesis, cell locomotion, and signaling [100, 361]. A distinctive feature that sets apart cell-cell adhesion from adhesion or aggregation in colloidal systems is the specific binding that occurs between receptors on the surface of cells and counter-adhesion molecules [362, 363]. Receptor-ligand binding is considered to typically take place *via* a lock-and-key mechanism [141–143, 364].

Cellular adhesion relies on achieving a balance between nonspecific, long-range interactions encountered in the surroundings and the more specific chemical bonds formed by complementary receptors at cell junctions [100, 362, 363, 365]. The interplay between mechanical forces and lateral interactions [366] significantly influences adhesion in biological and biomimetic systems [367].

Adhesion is subject to modulation by external mechanical forces [362, 368, 369], including shear or tensile forces, which can enhance or diminish its strength. In processes like cell migration and tissue morphogenesis [370], cells or tissues utilize mechanical forces to shape their architecture. In many cases, the kinetics of force-dependent dynamic adhesion [38, 93, 97–99] plays a crucial role in either promoting stronger adhesion of cells under applied force (catch bonds [371–374]), or providing a mechanism for cells to detach (slip bonds [101, 375]) or reorganize in response to external forces, thus allowing for adaptability to mechanical cues in their environment. Several theoretical models have been proposed in the past to describe the kinetics of mechano-sensitive biological adhesion, including the Bell model [99] for slip bond kinetics.

Cadherins, acting as transmembrane proteins, facilitate calcium-dependent [376] cell adhesion [39, 281, 282, 284, 285, 353]. Cadherins predominantly participate in homophilic binding [377, 378], where cadherins of identical types on neighboring cells interact. Cadherin interactions can manifest in both *cis* (on the same cell) and *trans* (between cadherins on adjacent cells) configurations. The latter is crucial for creating 'adherens' junctions [39, 93, 282, 285, 352, 354, 355, 378], large protein complexes that maintain cellular integrity by bridging cells. The *cis* or lateral interactions contribute to the formation of clusters on the cell membrane, strengthening cell-cell adhesions. The interplay and cooperativity between *cis* and *trans* interactions [39, 93, 281, 282, 284, 285] play a central role in the mediation of cadherin-driven cell-cell adhesion. The adhesive interface is formed by multiple cadherin repeats within the extracellular domains during the binding process [39, 93, 281, 284, 355, 378].

Experimentally designed biomimetic systems, such as emulsion droplets coated with adhesive ligand moieties (e.g., streptavidin/biotin) [38, 39, 93, 280] or 3D hydrogels [379–381] derived from natural polymers, serve as versatile platforms for the study of cell adhesion. These systems offer the capability to replicate various facets of the intricate cellular microenvironment [382–385]. They often incorporate substrates designed to mimic the extracellular matrix (ECM) of tissues, featuring adhesion-promoting molecules like integrin ligands [383, 384, 386, 387] or cadherin mimetics [38, 39, 93, 388]. In addition, to emulate the physiological forces experienced by cells, these biomimetic systems allow for probing the cellular responses and adaptations in adhesion under realistic conditions by incorporating dynamic stimuli.

Building upon our previous investigations into the self-assembly of colloidal droplets utilizing explicit mobile binders [50, 240, 242, 269, 272–275], our current focus involves a thorough exploration of the dynamic processes inherent in the formation of adhesion patches between these biomimetic droplets functionalized with binders that can mimic cadherin-mediated adhesion [38, 39, 93, 281, 282, 284, 285, 352–355] in cells. Biological cells allow sticky mobile binders to diffuse freely and form adhesions at the interface. Several theoretical models for cellular adhesion [389–393] have been developed in the past that combine the interfacial elasticity of the cell membrane [390, 392, 393] with the adhesive forces from the E-cadherin and N-cadherin binders, to determine the optimized parameters for the shape and size of the ‘adherens’ junction [390–393] (by minimizing the global interfacial energy functional). More recently, McMullen and co-workers have derived the free energy functional of adhesion for a circular patch to determine the equilibrium patch size and binder density profiles within the adhesion patch [164]. Our primary goal in these coarse-grained simulations is to manipulate molecular characteristics, including droplet size, binding strength, excluded binder volume, binder concentration, and the flexibility of harmonic springs, with the aim of finely tuning the growth, shape, and geometry of the resulting adhesion patch [39, 50, 161, 164].

The ectodomains of naturally occurring cadherins create a crystalline-like two-dimensional lattice at cell junctions [39, 281], facilitated by both *trans* (between adjacent cells) and *cis* (within the same cell) interactions. Recent experiments have delved into the study of cadherin-mediated assembly using a biomimetic emulsion system of homophilic droplets. The goal of this investigation was to understand the impact of cis and trans cooperativity on the kinetics of cadherin binding, with a comparative analysis of cluster formation rates among three cadherin types: WT E, WT N, and the cis E-cadherin mutant [39, 281, 284, 352, 355]. The studies revealed that the rates of cluster formation are notably higher for the wild-type (WT) cadherins when compared to the *cis* mutant. In our coarse-grained simulations, we have introduced Lennard Jones attractions [356–359] between inner binder particles on the same droplet (with varying interaction strengths), to model the lateral interactions in cadherin binding. Our simulations additionally illustrate that, when lateral binding is present, binders demonstrate a more organized packing [39, 284, 285] within the adhesion patch, showcasing a significantly higher patch recruitment compared to cases where *cis* interactions are absent. This observation reinforces the phenomenon of cis-trans cooperativity [39, 93, 281, 282, 353] observed experimentally.

3.3 Model description and incorporating Lateral Interactions

The droplets featuring explicit mobile binders have been designed according to the coarse-grained model described in Section 2.3.1 of Chapter 2.

3.3.1 Non-bonded interactions

To prevent overlap between particles, a soft repulsion of the form described in Section 2.3.2 of Chapter 2 has been used here as well, but now in addition, we also have presence of lateral interactions between the inner binder particles present on the same droplet. To model the lateral interactions between the inner binder particles, a Lennard-Jones [356–359] potential of the form

$$V_{\mathrm{LJ}}(r) = \begin{cases} 4\varepsilon_{\mathrm{LJ}}\left[\left(\frac{\sigma}{r}\right)^{12} - \alpha\left(\frac{\sigma}{r}\right)^{6}\right] & \text{if } r < r_{\mathrm{cut}} \\ 0 & \text{if } r \geq r_{\mathrm{cut}} \end{cases} \tag{3.1}$$

is used. Here, $\alpha = 1$. The strength of the lateral interactions can be varied by tuning $\varepsilon_{\mathrm{LJ}}$.

In order to study droplet assembly in presence and absence of lateral interactions between binders in a quasi two-dimensional arrangement, we implement a force-shifted Lennard-Jones wall potential [333] on each droplet, as described in Section 2.3.2 of Chapter 2.

3.3.2 Dynamic bonding model

Dynamic binding and unbinding between the binders from adjacent droplets is implemented in exactly the same way as described in Section 2.3.3 of Chapter 2. In this chapter, we are mostly going to consider adhesion of 'homophilic' droplets — in this case, adhesive bonds can form between outer binder particles of respective droplets which are *self-complementary*.

3.4 Simulation Methods

MD simulations [205] for the assembly of droplets (with explicit mobile binders) were performed using HOOMD-blue version 2.9.6 [334, 335, 344], in a similar manner as discussed in Section 2.4 of Chapter 2, using the tree neighbor list [347, 348] to accelerate non-bonded calculations, and the Langevin integrator [234, 345] was used to integrate the particle motions over time.

In case of simulations involving a dimer or trimer of droplets featuring explicit mobile binders, since we are only interested in monitoring the growth of the adhesion patch [50, 161, 164, 242] as a consequence of the diffusion of the mobile binders on the surface of the droplets, we have constrained the droplets to move only along the x-direction, while performing the Langevin dynamics [234, 345] on the droplets.

In specifically the simulations where we study the microscopic parameters that control the formation of the adhesion ring in a droplet dimer, we set the rest length (l_{dyn}) for the dynamic bonds equal to 0, as opposed to the sum of the radii of the bonding particles. Since the binders are typically believed to represent DNA, which are known to stand up from the surface of the droplet, it is imperative that we make the two outer bonding particles overlap so that no dihedral interactions arise (between the two inner and two outer particles from each of the adhering droplets).

Simulation parameters are all indicated in Tables 3.1 and 3.2.

3.5 Results and Discussion

The results are organized as follows: initially, we investigate the primary parameters influencing binder recruitment and adhesion patch size and shape. Subsequently, we examine the impact of introducing lateral (Lennard-Jones) interactions among inner binder particles to enhance recruitment in homophilic droplet self-assembly [39]. Finally, we aim to compare the rates of decay in the fraction of monomers present in the system across different scenarios, with varying strengths of lateral interactions.

3.5.1 Exploration of microscopic parameters governing the size and shape of the adhesion patch

Fig. 3.1 shows a zoomed-in snapshot of the interface between two droplets that can adhere to form a dimer, *via* dynamic bonds formed by explicit mobile binders. The choice of $N_b = 2000$ and a droplet radius $R = 500.0$ correspond to a more realistic scale of parameters, closer to what has been realized in experiments (as compared to the smaller droplet sizes and binder concentrations discussed in Chapter 2).

The formation of the adhesion patch [164] involves various contributions to the free energy

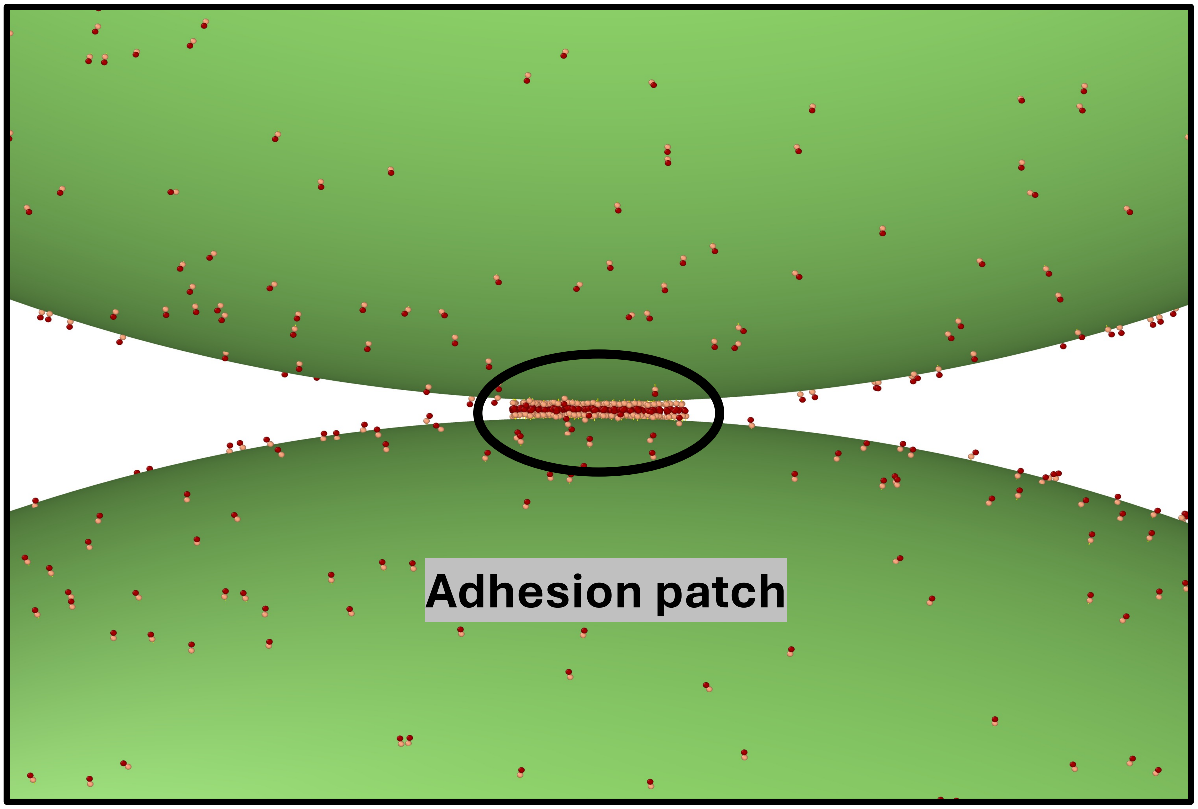

Figure 3.1: Snapshot showing the adhesion patch formed at the interface between two droplets that bind using explicit mobile binders ($N_b = 2000$, $R = 500.0$ and bond strength $\beta\varepsilon = 25.1$)

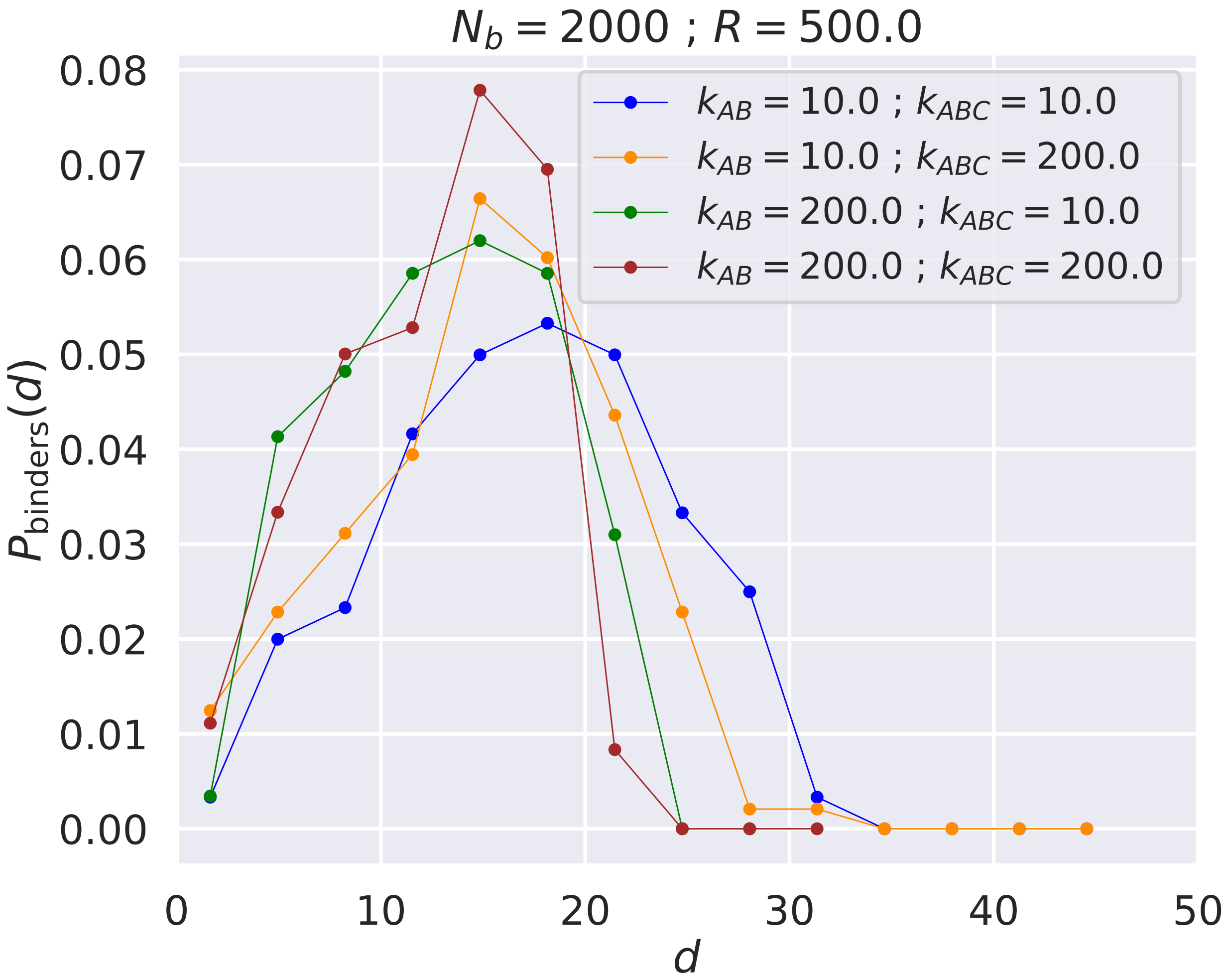

Figure 3.2: Histograms showing the probability $P(d)$ of finding the binders in the adhesion patch at a given radial distance d from the center, for fixed binder concentration $N_b = 2000$ and the droplet radius $R = 500.0$, for various choices of the spring constant for the droplet-binder harmonic bond (k_{AB}) and the bending (angular) spring constant (k_{ABC}). Bond strength $\beta\varepsilon$ for these simulations was 25.1.

(A_p), including the stretching and bending energies of the binder springs and the repulsion between the binders, stemming from factors like electrostatic interactions, steric hindrance, or excluded volume effects. Additionally, the formation of the patch typically reduces the configurational entropy of the system, as binders lose some freedom of movement when constrained within the patch.

In particular, the stretching and bending energies of binder springs govern the deformations required for adhesion, ultimately shaping the size and geometry of these adhesion patches. In our simulations, the stiffness of the harmonic springs is controlled by the droplet-binder stretching spring constant k_{AB} and the bending rigidity of the binders is governed by the angular spring constant k_{ABC}. We have studied these effects in our simulations.

A higher stretching constant (high k_{AB}) limits deformation, potentially resulting in a smaller adhesion patch size, while a lower stretching constant allows greater deformation, leading to a larger patch. With high k_{AB}, binders form a *circular ring* due to reduced deformation, resulting in a symmetrical distribution. Conversely, low k_{AB} promotes more deformation, allowing irregularities in patch shape, resembling a *pancake*.

The angular spring constant (k_{ABC}) determines how binders resist bending deformations, affecting their orientation on the droplet surface. High bending constant promotes flat conformations, yielding uniform adhesion patches with reduced bending energy. Conversely, low bending constant allows greater flexibility, resulting in irregular patch shapes. A high bending constant ensures rigidity and compact patches, while a low one permits more deformations, potentially leading to larger or dispersed patches.

Fig. 3.2 shows histograms of the probability of finding binders at a radial distance d from the center (binder concentration $N_b = 2000$ and droplet radius $R = 500.0$), for various choices of the stretching and bending spring constants. The blue curve corresponding to the lowest k_{AB} and k_{ABC} is representative of the most dispersed patch (wider distribution), whereas the brown curve (for the highest k_{AB} and k_{ABC}) shows a more compact distribution of the binders (narrower

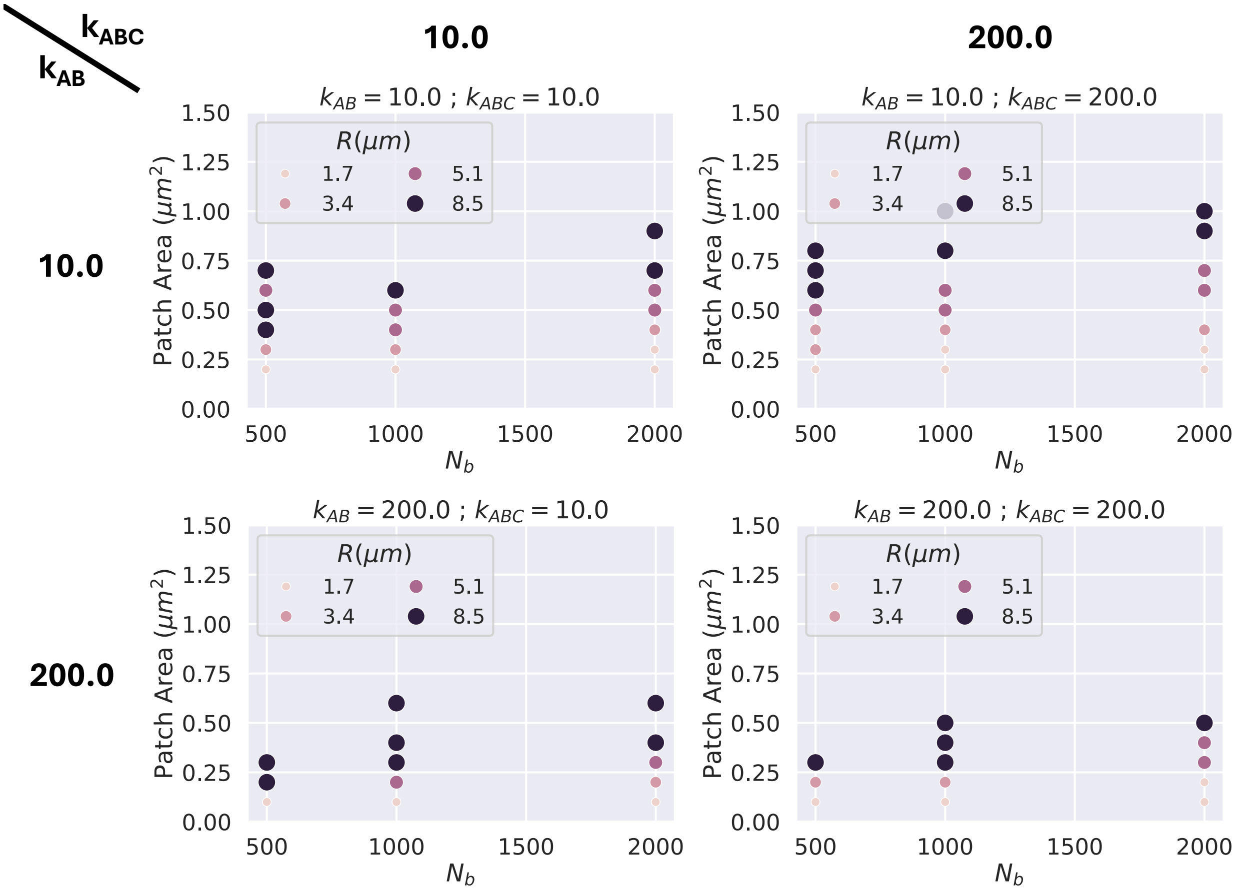

Figure 3.3: Plots showing how the area of the adhesion patch varies with the binder concentration N_b and the droplet radius R, for various choices of the spring constant for the droplet-binder harmonic bond (k_{AB}) and the bending (angular) spring constant (k_{ABC}). Bond strength $\beta\varepsilon$ for these simulations was 25.1.

distribution).

The area of the adhesion patch (in μm^2) and the number of binders recruited ($N_{b,\text{patch}}$) are important quantitative metrics for monitoring the growth of the adhesion patch. Fig. 3.3 and Fig. 3.4 show respectively how the area of the ring and the number of recruited binders ($N_{b,\text{patch}}$) vary with the binder concentration N_b, for various droplet radii R, indicated in units of μm (data points corresponding to different R are indicated by colored circles of increasing size scaled according to the R value). These analyses have been shown for various choices of (k_{AB}, k_{ABC}). On an average, the patch area and the number of recruited binders both increase with an increase in the binder

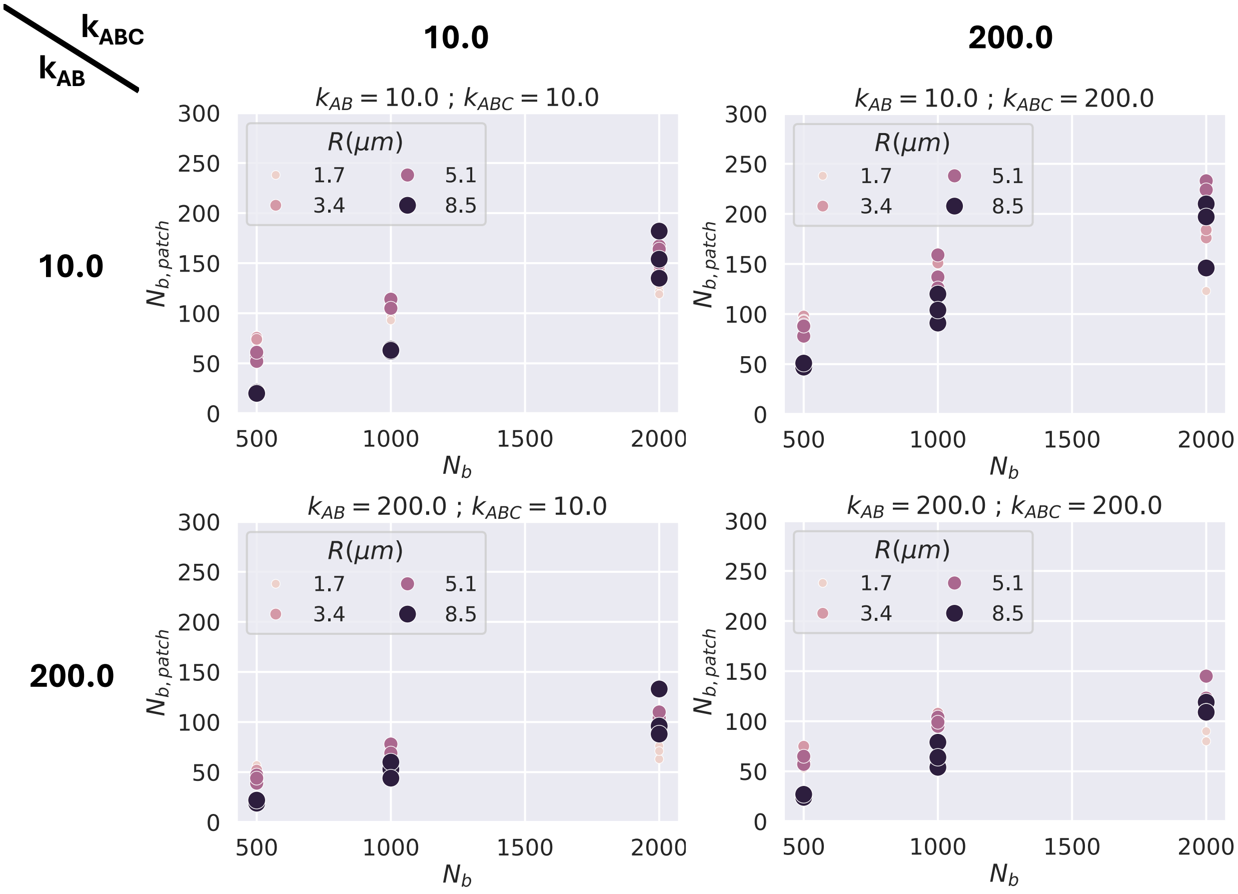

Figure 3.4: Plots showing how the number of binders recruited into the patch ($N_{b,\text{patch}}$) varies with the binder concentration N_b and the droplet radius R, for various choices of the spring constant for the droplet-binder harmonic bond (k_{AB}) and the bending (angular) spring constant (k_{ABC}). Bond strength $\beta\varepsilon$ for these simulations was 25.1.

concentration N_b.

On increasing k_{AB} from 10.0 to 200.0 (at a fixed k_{ABC}), we find the patch area and the number of binders both decrease (since higher stretch energies promote compact patches by limiting deformation). This trend remains the same for both low ($k_{ABC} = 10.0$) and high ($k_{ABC} = 200.0$) bending spring constants.

Conversely, when k_{ABC} is increased from 10.0 to 200.0 (at a fixed low stretch spring constant $k_{AB} = 10.0$), we observe that both the patch area and the number of recruited binders undergo an increase, which is typically counter-intuitive to the idea that a higher bending spring constant should promote a decrease in binder density, because of the resistance to bending deformations. This can be attributed to the fact that in case of a low stretch spring constant ($k_{AB} = 10.0$), the binders are more susceptible to deformation under bending forces. This increased flexibility allows binders to accommodate bending deformations more easily. Despite their resistance to bending (at high k_{ABC}), the binders can adjust their conformations to fit within the patch, potentially leading to a higher density of binders, when the bending spring constant k_{ABC} is increased. The increased flexibility provided by the combination of low stretch and high bending constants can also promote the expansion of the adhesion patch area. Binders can spread out more easily over the surface due to their ability to deform under bending forces.

Fig. 3.5 shows the inner and outer rings of the adhesion patch for $N_b = 2000$ and $R = 500.0$, for the choices of k_{AB} and k_{ABC} discussed above. Typically, for the case of high k_{AB}, we should obtain a non-uniform distribution of binders, due to the limited ability of binders to spread out (leading to a more uniform donut-shaped ring). However, in cases of both low and high k_{AB}, we obtain a *pancake*-like irregular ring shape. The only noticeable difference is that in case of low k_{AB}, the rings appear more concentrated with binders, because the binders are able to pack tightly due to increased flexibility and deformability. This consistent pattern of observing *pancake*-shaped irregular rings (across all choices of k_{AB}, k_{ABC}) can be attributed to the presence of the Boltzmann-like exponential (metropolis) term in the binding probability P_{on}, preventing the formation of a large number of bonds with high stretch energies, and thereby limiting the recruitment of binders into the patch to form clearly defined rings.

3.5.2 Effect of lateral interactions on binder recruitment and kinetics of droplet assembly

Now, we will investigate the effect of incorporating lateral interactions between our binders in coarse-grained MD simulations. We first ran simulations for the assembly of three droplets

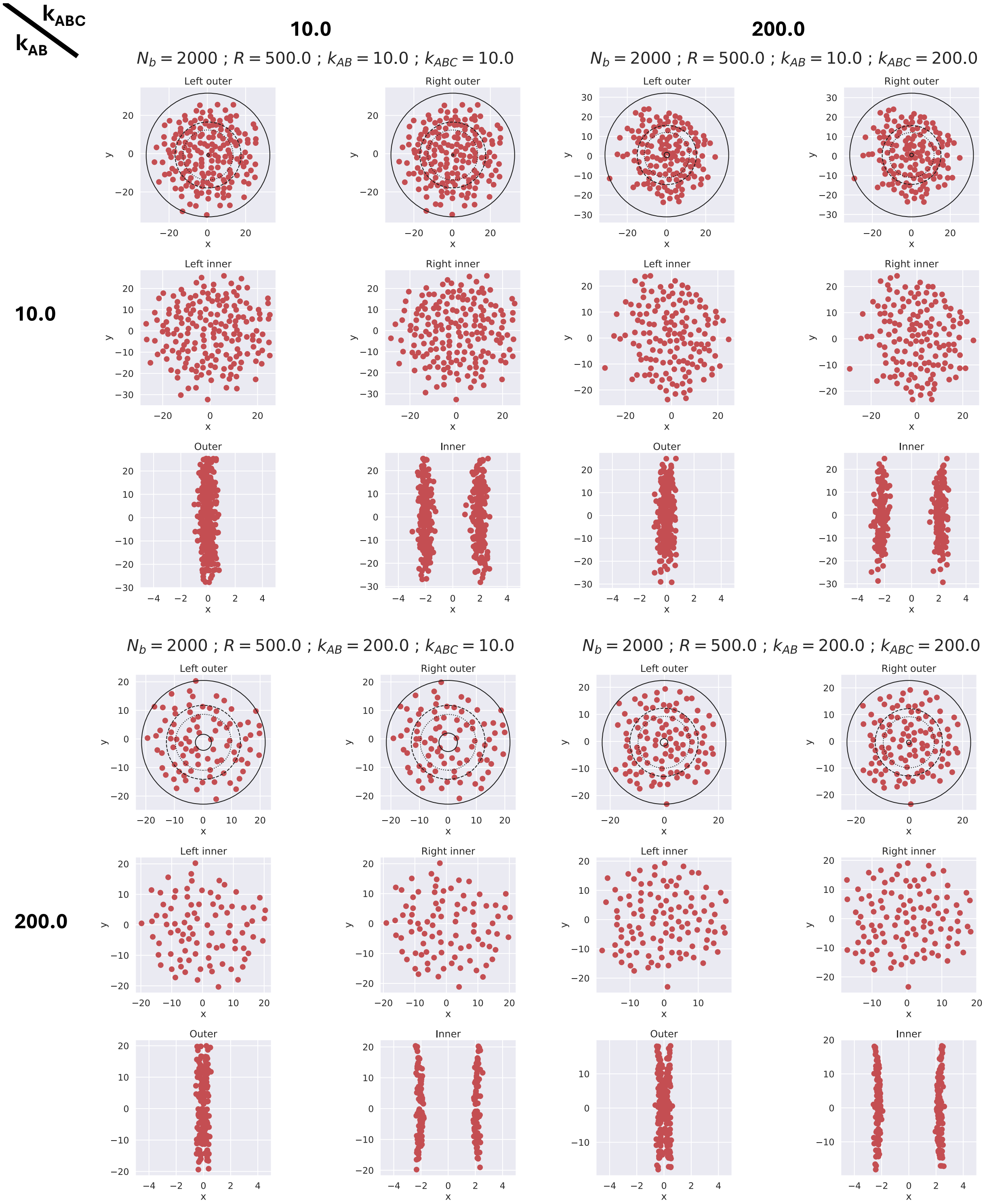

Figure 3.5: Plots showing the inner and outer rings of the adhesion patch for fixed binder concentration $N_b = 2000$ and the droplet radius $R = 500.0$, for various choices of the spring constant for the droplet-binder harmonic bond (k_{AB}) and the bending (angular) spring constant (k_{ABC}). Bond strength $\beta\varepsilon$ for these simulations was 25.1.

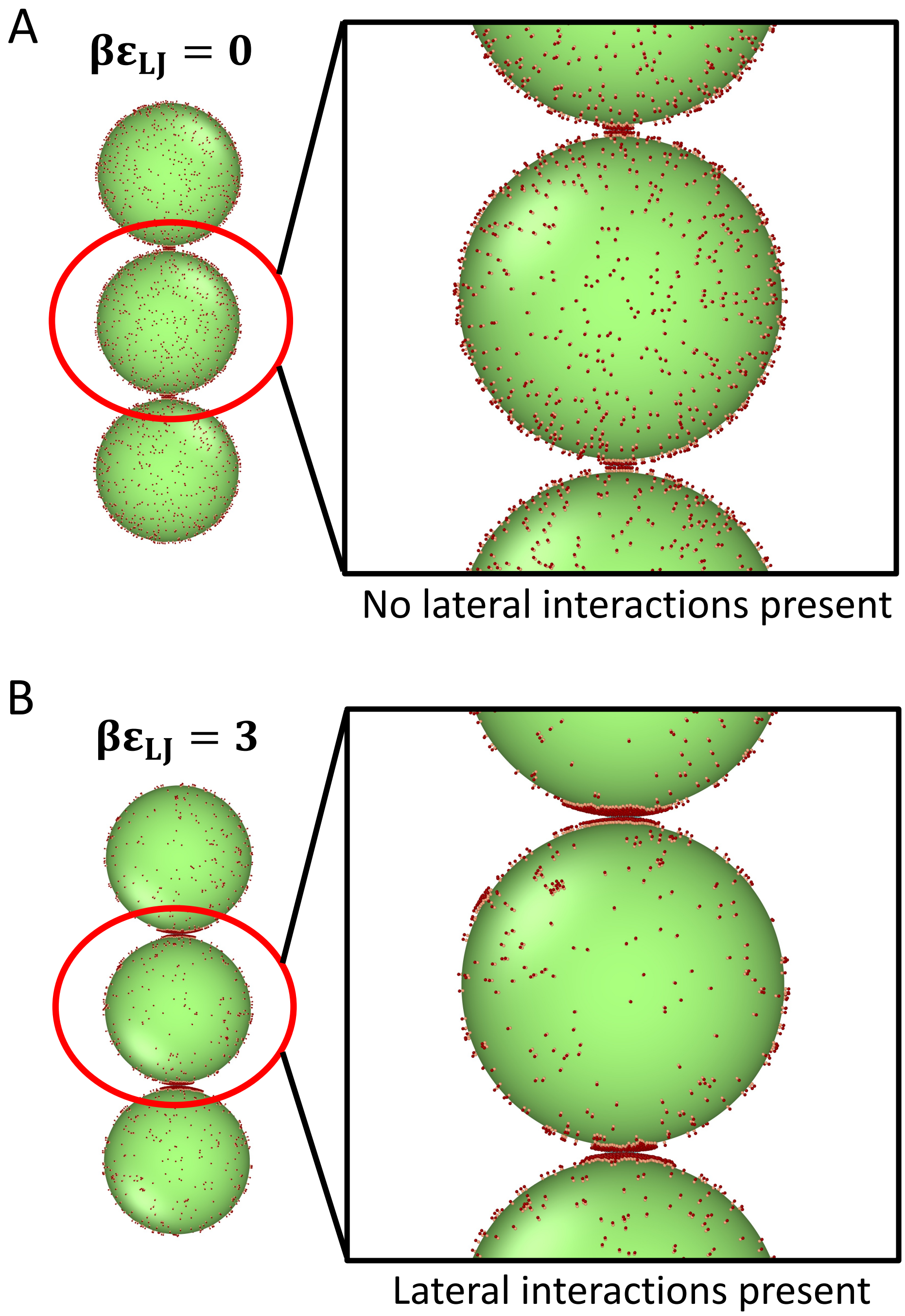

Figure 3.6: Snapshots showing the adhesion patches (from the final time point of simulation) between three droplets with explicit mobile binders ($N_b = 1000$, $R = 100.0$ and *trans* bond strength $\beta\varepsilon = 11$), with the inset(s) showing zoomed-in images of the adhesive patches at the droplet interfaces, (A) when no lateral (*cis*) LJ interactions are present ($\beta\varepsilon_{\mathrm{LJ}} = 0$) and (B) when lateral (*cis*) LJ interactions are present ($\beta\varepsilon_{\mathrm{LJ}} = 3$).

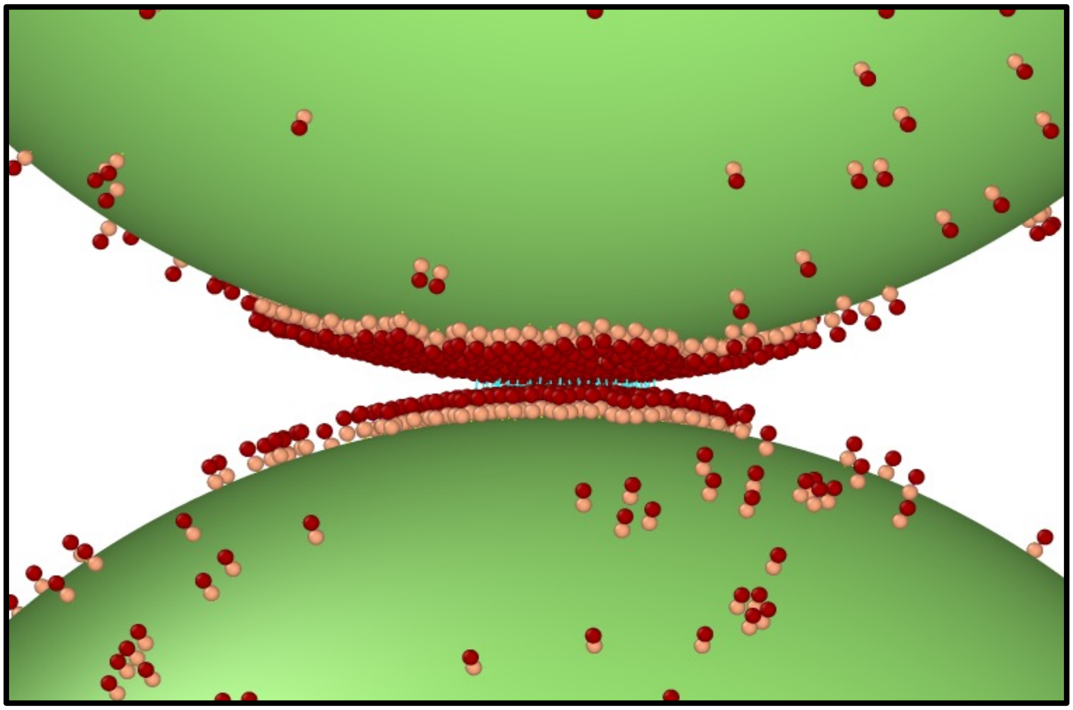

Figure 3.7: Snapshot showing a further zoomed-in image of the adhesion patch formed at the interface between two droplets (in a trimer) with $N_b = 1000$, $R = 100.0$ and *trans* bond strength $\beta\varepsilon = 11$, and in presence of lateral (*cis*) Lennard-Jones interactions between the binders, with an attraction strength $\beta\varepsilon_{\mathrm{LJ}} = 3$. The binders pack themselves in an ordered arrangement near the interface due to the presence of lateral interactions which further reinforces the formation of more *trans* bonds, thus strengthening the adhesion.

with mobile binders ($N_b = 1000$, $R = 100.0$) to form a trimer, for different conditions, where lateral interaction strengths were varied. As shown in Fig. 3.6 (see the zoomed-in images), for the case where the strength of the lateral Lennard-Jones attraction is $\beta\varepsilon_{\mathrm{LJ}} = 0$ (no lateral interactions present), we find only a very small recruitment of binders into the patch. On the other hand, when the interaction strength is increased to $\beta\varepsilon_{\mathrm{LJ}} = 3$, the number of binders recruited increased by more than 2 fold (as shown in Fig. 3.8). The phenomenon arises from the more ordered arrangement of binders at the interface when lateral interactions are present (as evident from the zoomed-in snapshot of the adhesion patch in Fig. 3.7). This organized arrangement strengthens the adhesive bonds between binders from neighboring droplets, demonstrating the observed cis-trans cooperativity [39, 93, 281, 282, 353] in previous experiments. Once a few binders are recruited into the patch, they create a favorable local environment that promotes the recruitment of additional binders, in a cascade.

Recent experiments have explored cadherin-mediated assembly using a biomimetic emulsion system comprised of homophilic droplets. The aim was to investigate the influence of cis and trans cooperativity on cadherin binding kinetics, analyzing cluster formation rates across three cadherin variants: WT E, WT N, and the cis E-cadherin mutant [39, 281, 284, 352, 355]. These studies revealed significantly higher rates of cluster formation for the wild-type (WT) cadherins compared to the cis mutant. We wanted to determine if our coarse-grained simulations with lateral LJ interactions between the inner binder particles could at least qualitatively match the experimental observations about the kinetic rates.

We ran droplet assembly [39, 161] simulations for 49 homophilic droplets for a fixed amount of simulation time ($N_b = 250$, $R = 50.0$) initially arranged in a quasi-2D lattice arrangement (with area fraction $\phi = 0.1$). We observed that for the condition with *trans* bond strength $\beta\varepsilon_{\mathrm{dyn}} = 5.0$, the fraction of monomers in the system decays much sooner in simulation time, for the case where the strength of the lateral interaction is high ($\beta\varepsilon_{\mathrm{LJ}} = 1.5 - 2.0$), as compared to the smaller lateral interaction strengths $\beta\varepsilon_{\mathrm{LJ}} = 0.0 - 1.0$ (see Fig. 3.10A, top left). The simulation snapshots for all

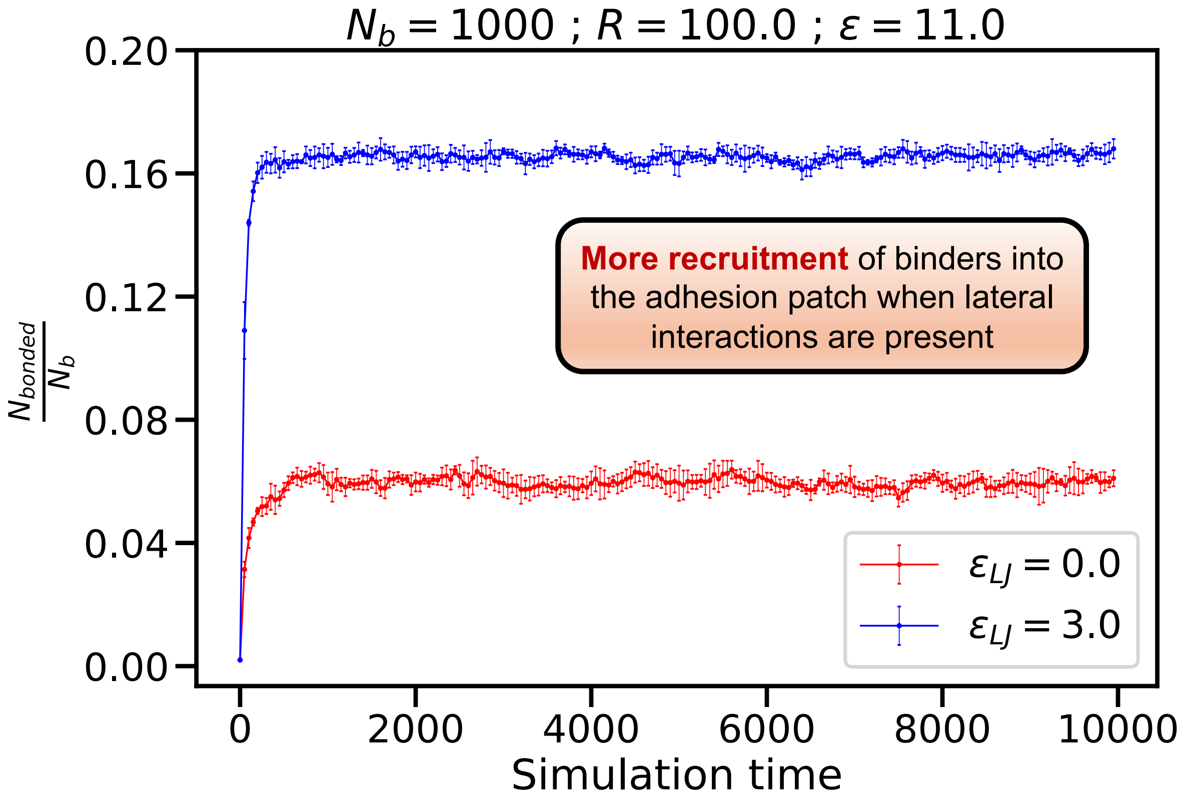

Figure 3.8: Plot of the fraction of binders recruited in the adhesion patch vs. simulation time ($N_b = 1000$, $R = 100.0$ and bond strength $\beta\varepsilon = 11$) for the two distinct cases, (1) when no lateral interactions are present ($\beta\varepsilon_{\mathrm{LJ}} = 0$) and, (2) when strong lateral interactions are present ($\beta\varepsilon_{\mathrm{LJ}} = 3$). The presence of lateral interactions enhances the number of binders that can be recruited into the adhesion patch. Error bars indicate standard deviations computed from simulations across 3 repeats.

these conditions indicating the self-assembly of these droplets for a *trans* bond strength $\beta\varepsilon_{\mathrm{dyn}} = 5.0$ are shown in Fig. 3.9 (upper row). The extent of clustering is clearly the maximum for $\beta\varepsilon_{\mathrm{LJ}} = 2.0$ (when $\beta\varepsilon_{\mathrm{dyn}} = 5.0$). For the slightly higher *trans* bond strength ($\beta\varepsilon_{\mathrm{dyn}} = 5.5$), we find that there is considerable difference in the extent of decay of the fraction of monomers (see Fig. 3.10A, top right) between the case where $\beta\varepsilon_{\mathrm{LJ}} = 0.0$ and the higher lateral interaction strengths ($\beta\varepsilon_{\mathrm{LJ}} = 1.0 - 2.0$). As also evident from the simulation snapshots shown in Fig. 3.9 (lower row), it appears that for this particular *trans* bond strength ($\beta\varepsilon_{\mathrm{dyn}} = 5.5$), the 3 higher lateral interaction strengths almost result in similar extent of aggregation (within the fixed simulation time). This shows that the *trans* binding strength ($\varepsilon_{\mathrm{dyn}}$) is important in determining the effect of *cis*-interactions on the self-assembly kinetics when the interaction strengths are varied. The distinction in aggregation kinetics between the various lateral interaction strengths arises because of the presence of 'cis-trans cooperativity', where the presence of one binder in the patch increases the likelihood of neighboring binders to be recruited as well. High lateral interaction strength between binders also reduces the overall free energy of the system when binders are in close proximity within an adhesion patch.

Next, we will calculate the rates of monomer fraction decay for these conditions and compare them to the rates determined from experimental findings.

3.6 CONCLUSIONS

Extending our previous work on colloidal droplet self-assembly with mobile binders [240, 242, 269, 272–275] further, our current research delves into a comprehensive exploration of adhesion patch dynamics between two droplets. In this study, we have examined how specific molecular features, including droplet size, bond strength, binder concentration, and the flexibility of harmonic springs, influence the growth, shape, and geometry of the adhesion patch [39, 50, 161, 164].

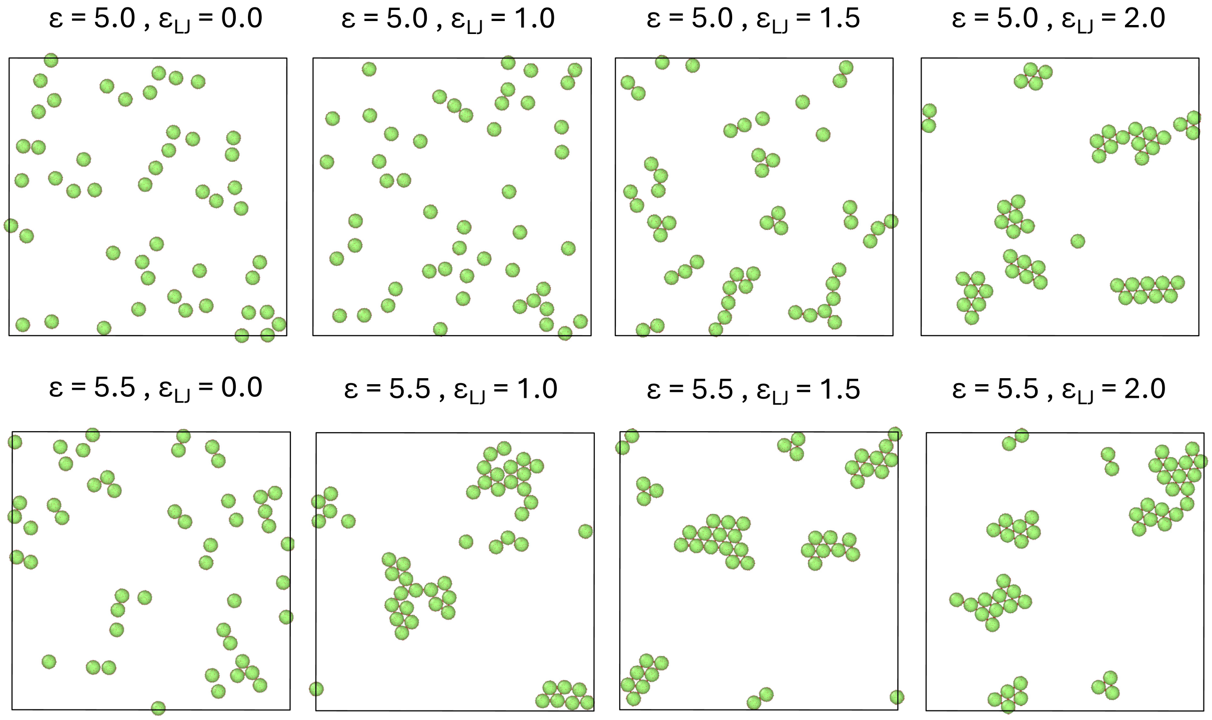

Figure 3.9: Snapshots showing the assembly of 49 homophilic droplets (from the final time point of simulation), where $N_b = 250$ and $R = 50.0$ and a 2D area fraction $\phi = 0.1$. The scenarios shown here correspond to two different *trans* bond strengths: $\beta\varepsilon_{\text{dyn}} = 5$ and $\beta\varepsilon_{\text{dyn}} = 5.5$ and four different lateral (*cis*) interaction strengths for each: $\beta\varepsilon_{\text{LJ}} = 0$, $\beta\varepsilon_{\text{LJ}} = 1$, $\beta\varepsilon_{\text{LJ}} = 1.5$ and $\beta\varepsilon_{\text{LJ}} = 2$.

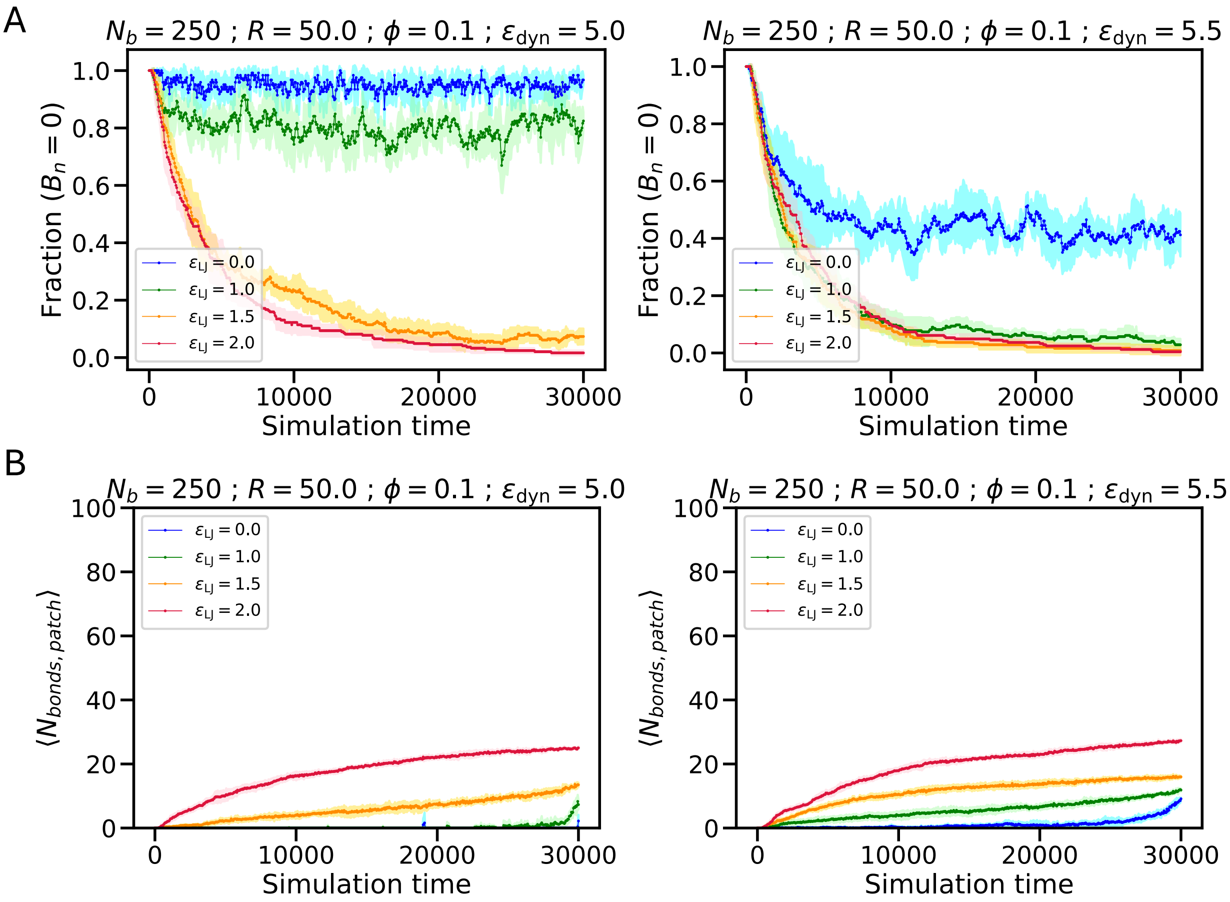

Figure 3.10: Plots showing (A) the fraction of monomers in the system (as the assembly progresses) as a function of the simulation time and, (B) the time evolution of the average number of bonds present in an adhesion patch — for the system of 49 homophilic droplets, where $N_b = 250$ and $R = 50.0$ and a quasi-2D area fraction $\phi = 0.1$, and corresponding to two different bond strengths: $\beta\varepsilon_{\mathrm{dyn}} = 5$ and $\beta\varepsilon_{\mathrm{dyn}} = 5.5$. Within each plot, four different lateral interaction strengths are shown: $\beta\varepsilon_{\mathrm{LJ}} = 0$ (blue), $\beta\varepsilon_{\mathrm{LJ}} = 1$ (green), $\beta\varepsilon_{\mathrm{LJ}} = 1.5$ (orange) and $\beta\varepsilon_{\mathrm{LJ}} = 2$ (red). The colored shaded regions represent the errors computed from five repeat simulations for every condition.

This study also investigates the impact of lateral or cis-interactions on binder recruitment, crucial in cellular junctions like E-cadherin-mediated adhesion [38, 39, 93, 100, 284]. We explore the consequences of introducing lateral binding interactions between binders on the same droplet in adhesion patch formation. Using a coarse-grained model with Lennard Jones attractions, our simulations show that lateral binding leads to a more ordered packing of binders in the adhesion patch, significantly increasing binder recruitment compared to scenarios without cis-interactions [39, 284, 285]. This supports the observed 'cis-trans cooperativity', emphasizing the accelerated decay rate of droplet monomers with lateral interactions. Our focus is on identifying the parameter regime validating this phenomenon in coarse-grained simulations of droplet assembly with lateral interactions [93, 281, 282].

In our upcoming research, we aim to analyze the experimental contributions to free energy [394], focusing on patch formation and shape [164]. We plan to employ advanced sampling techniques, such as umbrella sampling [395], to quantitatively measure the free energy of droplet adhesion facilitated by mobile binders.

A crucial direction for our project involves incorporating forces in unbinding kinetics [97, 98, 193] for cellular adhesion proteins, like cadherins [38, 39, 93, 284], to model slip and catch bonds [97, 98, 101, 396] observed in various mechano-sensitive systems [38, 39, 93, 99, 100]. Through molecular dynamics simulations, including steered MD [397] or constant-force MD, we aim to determine the threshold force for rupture when pulling apart droplets with mobile binders, initially utilizing standard unbinding kinetics. Additionally, we are intrigued by variations in the threshold rupture force when applying slip [99] and catch [101, 371, 375, 398] bond unbinding kinetics.

3.7 DETAILED SIMULATION PARAMETERS

All important simulation parameters are enumerated in the table 3.1, and parameters specific to the homophilic droplet assembly simulations are listed in the table 3.2.

Table 3.1: A table containing all the general simulation parameters

Description (Symbol)	Value in HOOMD units
MD timestep ($\mathrm{d}t$)	0.001
Dimensionality (d)	2
Temperature (T)	1.0
Number of simulation steps run (n_{steps})	10^7 - 5×10^7
Radius of droplet (R)	50.0-500.0
Radius of inner binder particle (r_{B})	1.0
Radius of outer binder particle (r_{C})	1.0
Number of binders in a droplet (N_{b})	200-2000
Mass of droplet (m_{A})	1.0
Mass of inner binder particle (m_{B})	0.001
Mass of outer binder particle (m_{C})	0.001
Drag coefficient of droplet (γ_{A})	0.1
Drag coefficient of binder (γ_{binder})	0.0001
Harmonic bond spring constants:	
(i) k_{AB}	10.0-200.0
(ii) k_{BC}	500.0
(iii) k_{ABC}	10.0-200.0
Harmonic bond rest lengths:	
(i) l^0_{AB}	51.0 (R = 50.0)
(ii) l^0_{BC}	2.0 (r_{C} = 1.0)
(iii) θ^0_{ABC}	3.141593
Epsilon for soft repulsive potential ($\varepsilon_{\text{soft}}$)	200.0-5000.0
Cut-off distance for soft potential:	
(i) $r_{\text{cut,AA}}$	110.0 (R = 50.0)
(ii) $r_{\text{cut,AC}}$	53.0 (R = 50.0, r_{C}=1.0)
(iv) $r_{\text{cut,CC}}$, $r_{\text{cut,BC}}$	2.0 (r_{C}=1.0)
Epsilon for LJ potential for lateral interactions (ε_{LJ})	0.0-3.0
Cut-off distance for LJ potential ($r_{\text{cut,LJ}}$)	5.0
Epsilon for Wall Potential ($\varepsilon_{\text{wall}}$)	20.0 (d = 2)
Cut-off distance for Wall Potential ($r_{\text{cut,wall}}$)	112.25 (R = 50.0)
z-coordinate of upper wall plane origin	125.0 (R = 50.0)
z-coordinate of lower wall plane origin	-125.0 (R = 50.0)
Initial rate constant for binding ($k^{\text{init}}_{\text{on}}$)	200.0
Initial rate constant for unbinding ($k^{\text{init}}_{\text{off}}$)	2.5×10^{-9}-10.0
Rate constant for binding after melting ($k^{\text{melt}}_{\text{on}}$)	0
Melting Temperature (T_{melt})	1.6
Inflexion steepness parameter (α)	200.0
Dynamic bond rest length (l_{dyn})	2.0 or 0.0 (for the dimer adhesion runs)
Dynamic bond spring constant (k_{dyn})	10.0
Dynamic bonding minimum distance (l_{min})	1.368 ($l_{\text{dyn}} - 2\sigma$) or 0.0
Dynamic bonding maximum distance (l_{max})	2.632 ($l_{\text{dyn}} + 2\sigma$) or 2.0
Dynamic bond checksteps (n)	5

Table 3.2: A table containing important parameters specific to the homophilic self-assembly simulations for 49 droplets in the presence or absence of lateral LJ interactions

Description (Symbol)	**Value in HOOMD units**
MD timestep ($\mathrm{d}t$)	0.001
Temperature (T)	1.0
Number of simulation steps run (n_{steps})	3×10^7
Radius of droplet (R)	50.0
Number of droplets (N)	49 (7×7 lattice)
Number of binders on each droplet (N_{b})	250
2D Area fraction (ϕ)	0.1
Drag coefficient of droplet (γ_{A})	0.1
Epsilon for LJ potential for lateral interactions ($\varepsilon_{\mathrm{LJ}}$)	0.0-2.0
Cut-off distance for LJ potential ($r_{\mathrm{cut,LJ}}$)	5.0
Initial rate constant of binding ($k_{\mathrm{on}}^{\mathrm{init}}$)	200.0
Initial rate constant of unbinding ($k_{\mathrm{off}}^{\mathrm{init}}$)	0.81 - 1.3
Dynamic bond rest length (l_{dyn})	2.0

CHAPTER 4

STUDY OF THE STRUCTURE AND DYNAMICS OF LINKER-MEDIATED COLLOIDAL GELS AND THE EFFECTS OF INTRODUCING ‘CAPPING’ MOLECULES

4.1 ABSTRACT

The dynamic connectivity and organization in gel networks inspire the development of structural design principles [399, 400] for gels assembled from multi-functional nanocrystals [189, 190, 286–298] and macromers with discrete functional groups, such as tetraPEG [299–301]. In collaboration with the Truskett Research Group at UT Austin, we have established an integrated coarse-grained modeling platform treating the building blocks as ‘patchy’ colloids with discrete binding sites [189, 190, 292, 293] that can bind or unbind dynamically [50]. Employing dynamic bonding among the components offers kinetic tunability, and specificity, enabling the design

of novel responsive materials [28, 58, 77]. These colloids can form networks through a linker-mediated strategy [189, 286, 296, 298], where macromers or nanocrystals are reversibly connected by bifunctional molecules [302], or by implicitly modeling them as bonds between binding sites with the properties of a semiflexible polymer [401] chain. Our approach aims to derive design principles for controlling the mechanical and optical properties of these gels by studying the phase behavior through modulating the linker-to-colloid ratio, binding affinities, system densities, and linker flexibilities. We also investigate the impact of capping molecules [296, 298, 303] (that can dynamically inhibit the binding of linkers to colloids) on the structure and dynamics of the gel networks [402–404]. Statistical control over network valence can be achieved through the ratios of colloidal building blocks to linkers and capping molecules. Additionally, incorporating our existing dynamic binding and unbinding model [50] provides kinetic leverage on the binding/unbinding reaction rates with important consequences on the relative timescales of the colloid diffusion processes and the binding/unbinding events.

4.2 Introduction

Colloidal gels are intriguing systems for study both from a scientific perspective and also for their practical applications. What makes colloidal gels fascinating is their diverse components, the attractive forces that stabilize their networks, and the different pathways through which gelation happens [290, 404, 405]. This combination grants them distinct properties such as targeted elastic modulus, strain hardening or softening characteristics, and optical response to deformation [287, 290, 406, 407]. These gels display a hierarchical organization at different length scales, with building blocks varying in shape and size, ranging from nanometers to micrometers.

Most gels exhibit non-uniform structure and dynamics due to their non-equilibrium preparation protocols, such as when attractive colloids undergo kinetically arrested spinodal decomposition [189, 257, 287, 292, 404, 408, 409]. Gels formed through these processes typically exhibit uneven local density variations and undergo aging as time progresses. On the other hand, equilibrium gels resistant to aging are formed when the arrested structure truly represents a stable state [405, 410–414]. Gelation occurs when the effective bonds between colloids in this state persist much longer [190, 415] than the observation time, resulting in the assembly of porous, percolating networks with visco-elastic properties [416] similar to biomolecular condensates in the cellular cytoplasm [51, 417].

Designing equilibrium gels from colloidal particles can be achieved by limiting the number of effective bonds formed between colloids [405, 410]. By microscopically limiting the valence of these patchy colloids [258, 259, 314], the spinodal boundary for spontaneous phase separation can be suppressed to low colloid volume fractions, as shown by computational studies. This has motivated several attempts to synthesize equilibrium gels in experiments, including gels at low particle density formed from patchy colloidal clay particles [418], DNA nanostars [419–429] (with typically three or four double-stranded arms that reversibly bind to one another via sticky, self-complementary single-stranded ends), and dipeptides in which π-π stacking interactions [430] of the side chains are present to mediate gelation.

Valence-restricted patchy particles are conventional examples of this approach, but a more robust method for macroscopically generating equilibrium gels involves introducing a secondary linker [287], like a small bifunctional molecule, to mediate the bonds between the colloids. The extent of bonding among the colloids can be controlled by adjusting the amount of added linker appropriately [189, 287], as well as the specific design of the linker [189, 291, 292, 296, 298, 302]. When using short-chain linkers, networks are anticipated to exhibit behavior similar to patchy colloidal gels [66, 174, 259, 314, 405]. Conversely, when employing high molecular-weight linkers, the resulting networks may resemble cross-linked polymeric gels [28, 77, 84–86, 189, 302]. The concept of bridging via secondary molecules has been used extensively in several systems spanning from mixtures of polymers and colloids [34, 431–434] to combinations of inorganic nanocrystals linked by ions [435–438].

Employing dynamic covalent bonding to link gel network components allows for customizable bond strength and kinetics through synthetic variations in chemical substituents and environmental factors like pH and temperature [439–442]. This approach is foundational for creating reversible hydrogels (such as and polymer networks, utilizing bonds such as disulfide, boronic ester, imine, and thiol-ene reactions [28, 58, 59, 77, 84–86, 167, 168]. These bonds possess the unique ability to break and reform (at ambient conditions), facilitating continuous rearrangement within the polymer network. This results in materials (such as hydrogels assembled from tetra-PEG macromers) that exhibit self-healing and pH-responsive stress relaxation [299, 300]. DCB ligands and linkers have also been used to induce controlled reversible assembly of tin-doped indium oxide (ITO) colloidal nanocrystals [288, 289, 294, 296–298, 443] into gels. The NCs were modified with ligands containing one element of a dynamic covalent bonding pair, such as benzaldehyde [291, 296, 298]. Gels, having distinctive mechano-optical response, were subsequently formed by introducing a bifunctional hydrazide linker [288, 291, 296, 298, 444, 445].

Computational modeling and simulations have demonstrated that the concentration of linkers serves as a macroscopic control parameter in linked-colloidal gels [287, 446–448], enabling the tuning of network connectivity and visco-elastic dynamics. By adjusting the length and concentration of the linker, one can alter the spinodal boundary of the mixture [189]. This boundary determines the colloid volume fractions at which equilibrium gelation becomes possible. Simulation results suggest that, especially at low colloid density, numerous linkers either attach both ends to the same particle or form double bonds between particles, impeding the percolation of the gel network [189, 287]. Previous simulations have also demonstrated that a significant fraction of large loops, under constant colloid and linker concentrations, inhibits phase separation (gelation) [287, 293]. Additionally, the flexibility of the linker systematically influences the structure of the gel [292], providing further avenues for tailoring linker-mediated nanocrystal gelation. In mixtures with a constant linker concentration, the presence of flexible or rigid linkers display phase separation at low colloid volume fractions, in contrast to semiflexible-linker mixtures [292], which do not exhibit this behavior.

Previous simulation studies also have probed the dynamics associated with the formation of equilibrium gels [190, 422, 425, 428], highlighting that the persistence time of colloid–colloid bonds dictates the characteristic slow relaxation of the self-intermediate scattering function. Reentrant characteristics [433, 434] emerge when adjusting the linker concentration away from the stoichiometric ratio, where the number of linker ends aligns with the number of colloidal binding sites. A decrease in linker concentration diminishes the network's connectivity by depriving the system of linkers that connect sites on adjacent colloids.

In our present work, we have built a robust and simplified workflow building upon our previous 'Poly-Patch' model [189, 190, 287, 292]), integrating it with our recently developed dynamic binding and unbinding protocol [50] (serving as a substitute for the non-bonded pair potential interactions used earlier). This unified coarse-grained platform is designed to be applicable for describing both multi-functional NCs [288, 289, 291, 294, 296–298, 302, 443] and macromers exhibiting discrete functionality (such as tetraPEG [299, 300]). This approach, employing dynamic bonding among the components, facilitates the design of responsive materials, involving the reversible connection of macromers or NCs by bifunctional molecules. Alternatively, they can be implicitly modeled as bonds between binding sites, exhibiting the properties of a semi-flexible polymer chain [401]. In this ongoing work, we are currently modifying the simulation setup to model both explicit and implicit linkers. We are also exploring the influence of capping linker molecules [291, 296, 298, 436, 449] (that can dynamically compete with binding of linker ends to colloids), on the structure and dynamics of these gel networks. Controlling the ratios between colloidal building blocks, linkers, and competing capping molecules can enable statistical regulation of network valence. Furthermore, incorporating our existing dynamic binding and unbinding model grants kinetic leverage over the reaction rates of binding/unbinding, which can influence the dynamics and phase behavior of gels.

4.3 COARSE-GRAINED *POLY-PATCH* MODEL COUPLED WITH OUR DYNAMIC BINDING AND UNBINDING PROTOCOL

In this study, we employed a modified version of the 'Poly-Patch' (Polymer linked, Patchy colloid) model, a simple coarse-grained model extensively utilized in prior research on colloidal gelation with bifunctional polymeric linker molecules [189, 190, 292]. However, our approach in this investigation involves the integration of our recently developed dynamic binding and unbinding scheme [50] with the existing Poly-Patch model.

This adaptation enables us to investigate the structures and dynamics involved in gel formation through bonded interactions. Unlike previous studies that utilized a non-bonded (Gaussian) attraction between colloidal interaction sites and linker ends, our model now incorporates kinetically controlled binding and unbinding rates. This modification offers a more nuanced exploration of the processes underlying gel formation.

Similar to the Poly-Patch model, the linkers are modeled as short linear polymer chains [189, 190, 292] of diameter σ and mass m, and chain length M (typically, M=8). The linkers are *bi-functional* polymers of M beads with two ends which are capable of binding to the colloids. The colloids are represented by larger spheres (diameter = 5σ and mass = $125m$), and their surface is decorated with $n_c = 6$ patches with diameter σ and mass m in an octahedral arrangement. In the current version of the model, angle potentials are present between adjacent pairs of patches and the colloid center to introduce a level of rigidity (as opposed to modeling the patches as rigid bodies in previous versions of the model). The system composition is described in terms of colloid volume fraction η_c, the number ratio of the polymeric linkers to the colloids, $\Gamma_{\text{lc}} = N_p/N_c$ and the number ratio of the cap molecules to the linkers, $\Gamma_{\text{cal}} = N_{\text{cap}}/N_p$ (where N_p is the total number of linkers, N_{cap} is the total number of caps, and N_c is the total number of colloids in the system).

Fig. 4.1 shows a snapshot of the initial configuration (with colloids and linkers present), at a

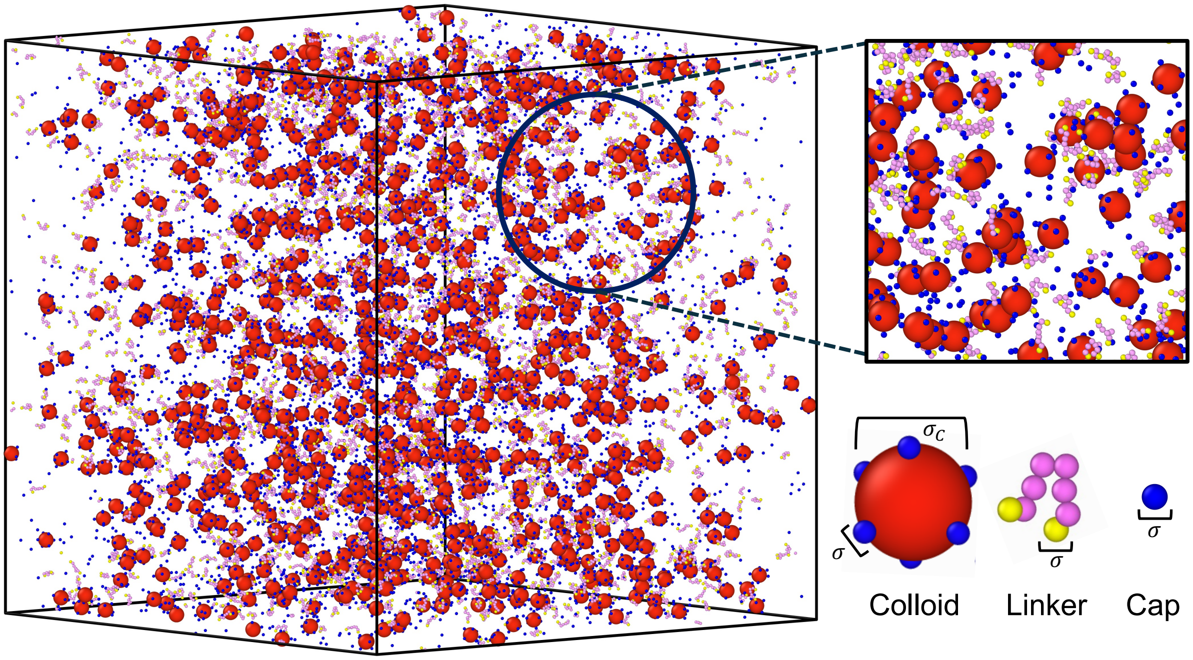

Figure 4.1: The initial snapshot for a system of colloids, capping molecules and polymers (linkers with bifunctional ends) of length $M = 8$ at $\Gamma_{\mathrm{lc}} = 1.5$, $\Gamma_{\mathrm{cal}} = 1.0$, $\eta_c = 0.01$, and bond strength $\beta\varepsilon = 20.0$. The inset shows a small region of the snapshot with zoomed-in images of the colloid, linker and cap molecules. The diameter of a polymer-segment and colloid patch (σ), and the colloid diameter $\sigma_c = 5\sigma$ are indicated as well.

colloid volume fraction $\eta_c = 0.01$ and linker-to-colloid ratio $\Gamma_{\mathrm{lc}} = 1.5$.

The detailed parameters used for running these simulations are listed in Table 4.4.

4.3.1 PARTICLE INTERACTIONS

Non-bonded interactions between particles were modeled using a repulsive shifted WCA potential [450, 451] given by

$$U_{\mathrm{WCA}}(r) = \begin{cases} 4\varepsilon_{\mathrm{WCA}}\left[\left(\frac{\sigma}{r-\delta}\right)^{12} - \left(\frac{\sigma}{r-\delta}\right)^{6}\right] + \varepsilon_{\mathrm{WCA}} & \text{if } r \leq r^* \\ 0 & \text{if } r > r^* \end{cases} \tag{4.1}$$

where, r is the distance between the centers of two particles i and j, and $\delta = \frac{\sigma_i+\sigma_j}{2} - \sigma$. The point at which the potential is truncated is given by $r^* = 2^{1/6}\sigma$.

Bonds between the successive beads constituting a linker were modeled using finitely extensible nonlinear elastic springs [452] with the standard 'Kremer–Grest' [453] parameters for the spring constant k_p and maximum bond extension $r_0 = 1.5\sigma$, ensuring that there is no chain crossing. The bonds between the patches and the colloid center were also modeled similarly.

$$U_p(r) = \begin{cases} -\frac{k_p r_0^2}{2} \ln\left[1 - \left(\frac{r}{r_0}\right)^2\right] & \text{if } r \leq r_0 \\ \infty & \text{if } r > r_0 \end{cases} \tag{4.2}$$

In the earlier version of the model, the polymer ends were attracted to the colloid patches *via* a short-ranged Gaussian attraction, but now the formation of covalent bonds between a patch and a linker end is modeled using dynamic bonds discussed in Chapter 2 (which are harmonic springs in this case, with a rest length $l_{\mathrm{dyn}} = 0$), with a bond strength ε.

In addition, we have cosine-squared bending (angle) potentials between sets of three consecutively bonded beads in a linker [454, 455], with the bending stiffness constant κ serving as a parameter to control the flexibility of the linker.

$$u_\theta(\theta) = \frac{1}{2}\kappa(\cos\theta - \cos\theta_0)^2 \tag{4.3}$$

Here, θ is the angle between the beads and $\theta_0 = \pi$ is the rest angle. Mostly, simulations have been run for fully flexible linkers ($\kappa = 0$).

In the current model, as described earlier, cosine-squared angle potentials have also been defined for adjacent pairs of patches ($\theta_0 = \frac{\pi}{2}$ for octahedral arrangement of patches) and the colloid center, and the bending constant κ can be tuned to change the rigidity of the patches on the colloid surface.

The 'cap' molecules which are currently of the same particle type as the colloid patches, have the same non-bonded interactions as the latter do.

4.4 SIMULATION METHODS

MD simulations [205] of the mixture of colloids with patchy binding sites and polymeric linker molecules or caps (in a cubic, periodic simulation box) were performed using HOOMD-blue version 4.3.0 [334, 335, 344]. Simulation parameters are all indicated in Table 4.4. The Langevin integrator [234, 345, 456, 457] was used to integrate all particles forward in time.

The equation of motion for each particle i in Langevin dynamics [234, 346, 457] is given by:

$$m_i\ddot{\vec{r}}_i(t) = \vec{F}_i - \gamma_i\dot{\vec{r}}_i(t) + \sqrt{2\gamma_i k_\mathrm{B}T}\vec{\eta}(t) \tag{4.4}$$

where, m_i is the mass of the particle, k_B is the Boltzmann constant, γ_i is the drag coefficient, $\dot{\boldsymbol{r}}_{\boldsymbol{i}}(t)$ is the velocity of the particle, $\vec{F}_i = -\nabla U_i$ is the force on particle i derived from the total potential energy function of the system, and $\eta(t)$ is the delta-correlated random white noise, with zero mean and unit variance. We use the cell neighbor list [347] to accelerate non-bonded calculations, and in the construction of our list of possible pairs to bond as described above.

The simulations were conducted using a streamlined and robust workflow module implemented in a Python 3.8.6 environment. The process includes initializing the workflow, incorporating the Poly-Patch model and the dynamic bonding plugin. Two distinct stages define the system's progression: (i) initialization of the system and (ii) setup of the Molecular Dynamics (MD) run with activated particle interactions. Critical parameters are assigned values for variation during simulations. Additionally, simulation parameters from separate .json files, containing default settings, are linked. The final step involves submitting simulation jobs to High-Performance Computing (HPC) resources.

4.5 RESULTS AND DISCUSSION

Using our workflow, we performed MD simulations of (i) a mixture of colloids and linker molecules in a periodic box (ii) a mixture of colloids, linker molecules and free capping molecules (of the same particle type as the patches on the colloids), which can bind to the linker ends and render them ineffective for bridging colloids together (to form gels).

In these simulations, we have varied the colloid volume fraction η_c, the linker-to-colloid ratio Γ_{lc} and the cap-to-linker ratio Γ_{cal}. The binding affinity was maintained at a constant value of $\beta\varepsilon = 20.0$, although we plan to probe the effects of varying the bond strength and the rates of binding and unbinding, in the future.

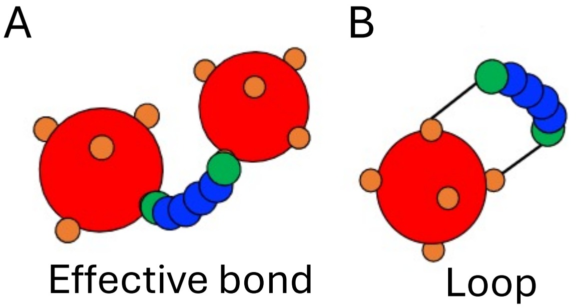

Figure 4.2: Motifs formed by the linkers when their ends bind to the colloid patches — (A) an Effective bond is one that bridges two colloids *via* the ends of a single bifunctional linker (B) a Loop is formed when the ends of a linker are bonded to patches on the same colloid, thus hindering colloidal gelation (this figure has been adapted from [189]).

4.5.1 COLLOID VOLUME FRACTION AND THE LINKER-COLLOID RATIO CAN CONTROL THE NUMBER OF LOOPS AND EFFECTIVE BONDS FORMED IN SIMULATIONS

From our simulations (run for the systems where no caps are present), we quantified the various kinds of motifs formed by the linker molecules for our choices of $(\eta_c, \Gamma_{\mathrm{lc}})$. The formation of loops are known to hinder the gel network formation [189, 287], whereas the formation of effective bonds serve as bridges to join two colloid moieties together (as shown in Fig. 4.2).

Here, we observe that the number of loops (intra-colloidal bridges) formed decreases as the colloid volume fraction increases (or the system becomes more dense), and correspondingly the number of effective bonds (inter-colloidal bridges) increases. This trend is consistent across all the choices of the linker-to-colloid ratio Γ_{lc}. This can be explained in terms of the effect of combinatorial entropy (S_{comb}) in driving aggregation in such colloidal gels [458]. With increase in colloidal volume fraction, the distance (d) between the colloidal particles decreases, and as the particles come closer, there is an increase in the number of possible inter-particle bonding patterns (microstates), and this entropy difference ($\Delta S_{\mathrm{comb}}(d)$) leads to a greater number of effective bonds between colloids.

For higher Γ_{lc}, more number of loops and the effective bonds per colloid are formed at a given η_c, as compared to the corresponding values at a lower Γ_{lc}.

We also observe in all these plots for varying Γ_{lc}, for a certain critical value of the colloid volume fraction ($\eta_c^{\mathrm{cr}} \approx 0.012$), a cross-over occurs between the number of loops and effective bonds relative to each other, thereby indicating an onset of the formation of network gels (since for $\eta_c > \eta_c^{\mathrm{cr}}$, the number of effective bonds predominates over the number of loops).

4.5.2 EFFECTS OF ADDING CAPPING MOLECULES THAT BIND TO LINKERS ON THE FORMATION OF PHASE SEPARATED GELS

Now, we want to study the effects of introducing 'capping' molecules into our simulations, where only colloids and linkers were present. Because the caps are supposed to bind to the linkers (according to our system design), we expect significant reduction in the number of colloid-colloid bridges formed by linkers. The effect on gelation would be more predominant as the concentration of the cap molecules are increased.

Phase separation in these gels is quantified by the partial static structure factor $S(q)$ for the colloids [189, 287, 292, 459], given by

$$S(\mathbf{q}) = \frac{1}{N_c}\left\langle \sum_{j,k}^{N_c} \exp\Big(-i\mathbf{q}\cdot(\mathbf{r}_j - \mathbf{r}_k)\Big)\right\rangle \tag{4.5}$$

where, $\mathbf{q} = \frac{2\pi\mathbf{n}}{L}$ is the wave-vector, L is the edge length of the periodic simulation box, and $\mathbf{n}$ is a vector of integers. $\mathbf{r}_j$ is the position of the j^{th} colloid. The structure factor was then extrapolated to the zero-wavevector, $S(0)$, by fitting $S(q)$ to a Lorentzian form [189, 460],

$$S(q) = \frac{S(0)}{1 + (q\xi)^2} \tag{4.6}$$

where, ξ is the correlation length. From qualitative inspections, it was hypothesized that $S(0) >$

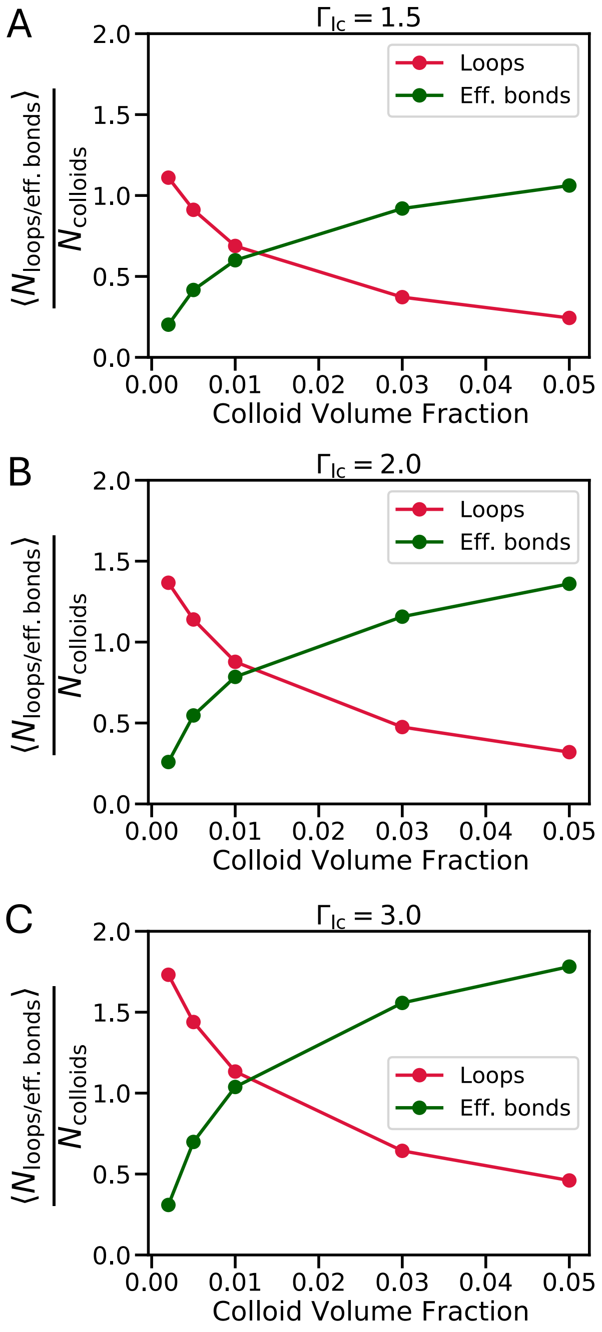

Figure 4.3: Variation of the number of loops and effective bonds formed per colloid (at the final time point of simulation) with the colloid volume fraction (η_c) for three different linker-colloid ratios (A) $\Gamma_{\mathrm{lc}} = 1.5$, (B) $\Gamma_{\mathrm{lc}} = 2.0$ and (C) $\Gamma_{\mathrm{lc}} = 3.0$. These simulations correspond to the $\Gamma_{\mathrm{cal}} = 0.0$ case (no cap molecules present).

10 [189, 287, 410] is usually considered to be phase-separated in simulations.

Table 4.1: A table showing the $S(0)$ values for different combinations of η_c and Γ_{lc} when no capping molecules are present ($\Gamma_{\text{cal}} = 0.0$)

η_c	$\Gamma_{\text{lc}} = 1.5$	$\Gamma_{\text{lc}} = 2.0$	$\Gamma_{\text{lc}} = 3.0$
0.002	1.4439	1.5554	1.7247
0.005	2.0949	2.9572	4.4588
0.01	3.1124	5.4857	11.1778
0.03	5.2226	14.0285	205.6339
0.05	2.3804	8.1032	15.7871

Table 4.2: A table showing the $S(0)$ values for different combinations of η_c and Γ_{lc}, in presence of low concentration of cap molecules (cap-to-linker ratio $\Gamma_{\text{cal}} = 1.0$)

η_c	$\Gamma_{\text{lc}} = 1.5$	$\Gamma_{\text{lc}} = 2.0$	$\Gamma_{\text{lc}} = 3.0$
0.002	1.1738	1.1933	1.3142
0.005	1.3262	1.4757	1.4638
0.01	1.4065	1.4843	1.6938
0.03	1.1449	1.1883	1.3102
0.05	0.8017	0.8204	0.8155

Table 4.3: A table showing the $S(0)$ values for different combinations of η_c and Γ_{lc}, when the concentration of cap molecules is increased further (cap-to-linker ratio $\Gamma_{\text{cal}} = 2.0$)

η_c	$\Gamma_{\text{lc}} = 1.5$	$\Gamma_{\text{lc}} = 2.0$	$\Gamma_{\text{lc}} = 3.0$
0.002	1.1092	1.1266	1.0902
0.005	1.1148	1.2078	1.0941
0.01	1.0409	1.0496	1.0980
0.03	0.8552	0.8765	0.8658
0.05	0.7577	0.7548	0.7385

Fig. 4.4 shows a phase diagram of final simulation snapshots for $\eta_c = 0.03$ and $\beta\varepsilon = 20.0$ where Γ_{lc} and Γ_{cal} are varied. With increasing Γ_{lc}, the gels seem to be more phase-separated, as also corroborated by the high $S(0)$ values (see Table 4.1). On moving from left to right across the phase diagram, the gels become less phase-separated as the cap concentration is increased further (the $S(0)$ values also decrease, see Tables 4.2 and 4.3). This behavior is also indicated by the trends in the $S(q)$ vs q plots, shown in Fig. 4.7, where, for $\Gamma_{\text{cal}} = 0.0$ (no caps present), $S(q)$

diverges more at $q = 0$, with the maximum divergence observed for $\Gamma_{\text{lc}} = 3.0, \Gamma_{\text{cal}} = 0.0$. This is the case for which we observe maximum amount of phase-separation ($S(0) \approx 206$) in the gel (at $\eta_c = 0.03$).

Fig. 4.5 show the total number of colloid-linker and cap-linker bonds formed separately, for each of the cases described above. Presence of caps reduces the number of effective colloid-linker bonds, by binding to the linker ends. As the cap-to-linker ratio is increased to $\Gamma_{\text{cal}} = 1.0$, as compared to the case of no caps, the number of linker-colloid bonds falls down drastically, and on further increasing the cap concentration ($\Gamma_{\text{cal}} = 2.0$), the linkers get almost completely exhausted by the caps, thus rendering them ineffective to form many bridging bonds between colloids. For $\Gamma_{\text{cal}} = 2.0$, we also find that on increasing Γ_{lc} from 1.5 to 3.0, the difference between the number of cap-linker and colloid-linker bonds steadily increases. These observations are also concomitant with the histograms showing the distribution of the number of free colloid patches (at the final time point of simulation), for all these cases (Fig. 4.6). For $\Gamma_{\text{lc}} = 3.0$, the clearest differences are observed, on moving from left to right, we find that the distribution with most number of colloids having 0 free patches left (indicating all patches are bound to linkers, when no caps are present) changes to a distribution where colloids with 4 and 5 free patches are the most in number (for $\Gamma_{\text{cal}} = 2.0$).

Lastly, we construct phase diagrams (Figs. 4.8 and 4.9) in the $(\eta_c, \Gamma_{\text{lc}})$ plane, for the 3 different cases of cap concentration ($\Gamma_{\text{cal}} = 0.0, 1.0, 2.0$), to quantify the phase separation in these gels. The color-map in these phase diagrams represents the value of $S(0)$ obtained for the given choice(s) of $(\eta_c, \Gamma_{\text{lc}})$. These values are also indicated in Tables 4.1, 4.2 and 4.3. In Fig. 4.8, the yellow region in the top right hand corner of the diagram indicates phase-separation in the gels ($S(0) > 10$), whereas dark blue regions as the bottom left do not ($S(0) < 5$). For both the phase diagrams shown in Fig. 4.9, neither of the conditions demonstrate any phase separation (since the maximum $S(0)$ out of all these cases is only ≈ 1.7).

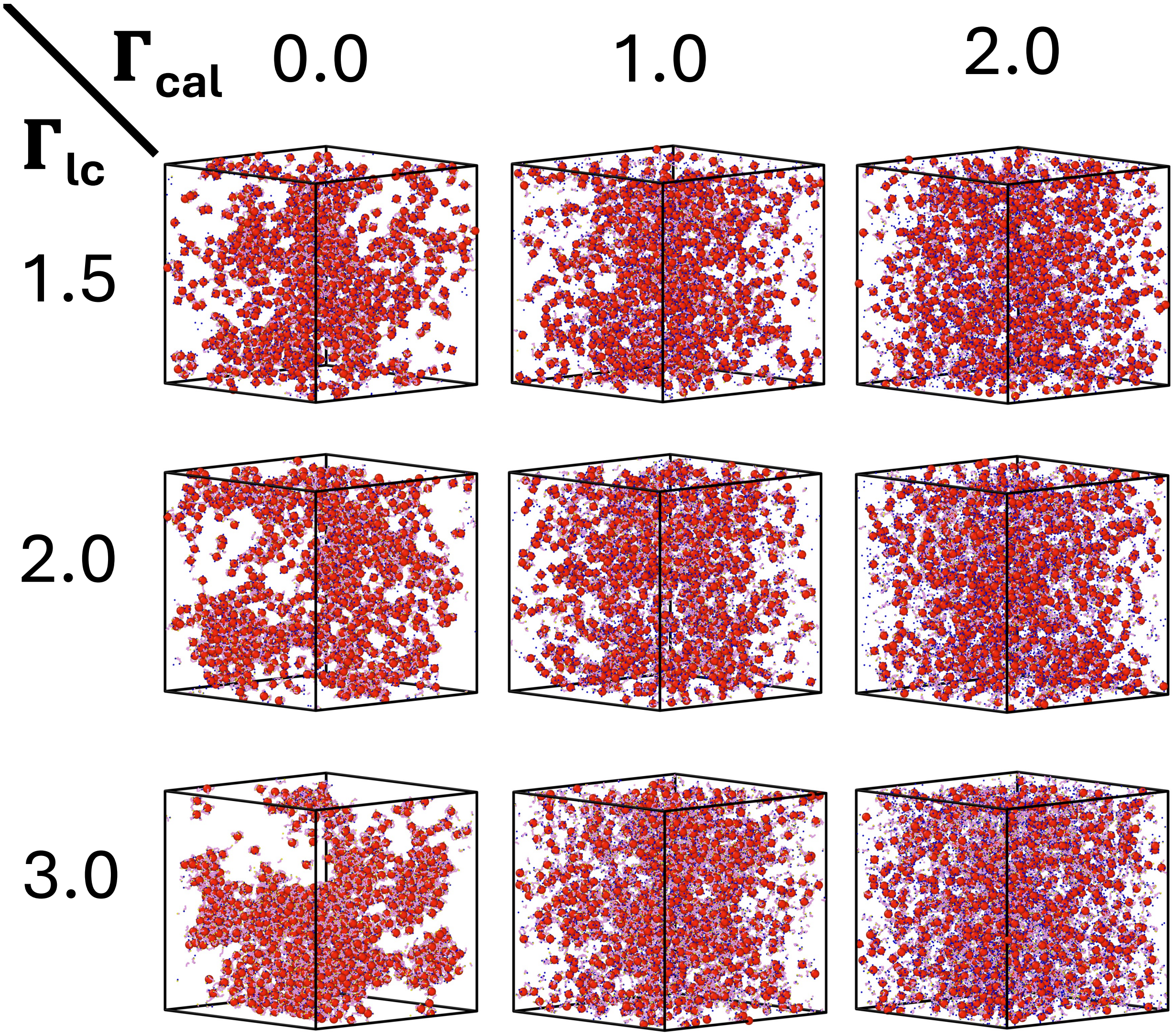

Figure 4.4: Phase diagram of simulation snapshots for a system of colloids mixed with linkers (in presence or absence of cap molecules) at the final time point of the simulation in the (Γ_{lc},Γ_{cal}) plane for $\beta\varepsilon = 20.0$ and $\eta_c = 0.03$. $\Gamma_{cal} = 0.0$ indicates the presence of no cap molecules (only linkers present). The system sizes in all these cases are different, due to variable number of linkers and cap molecules being present.

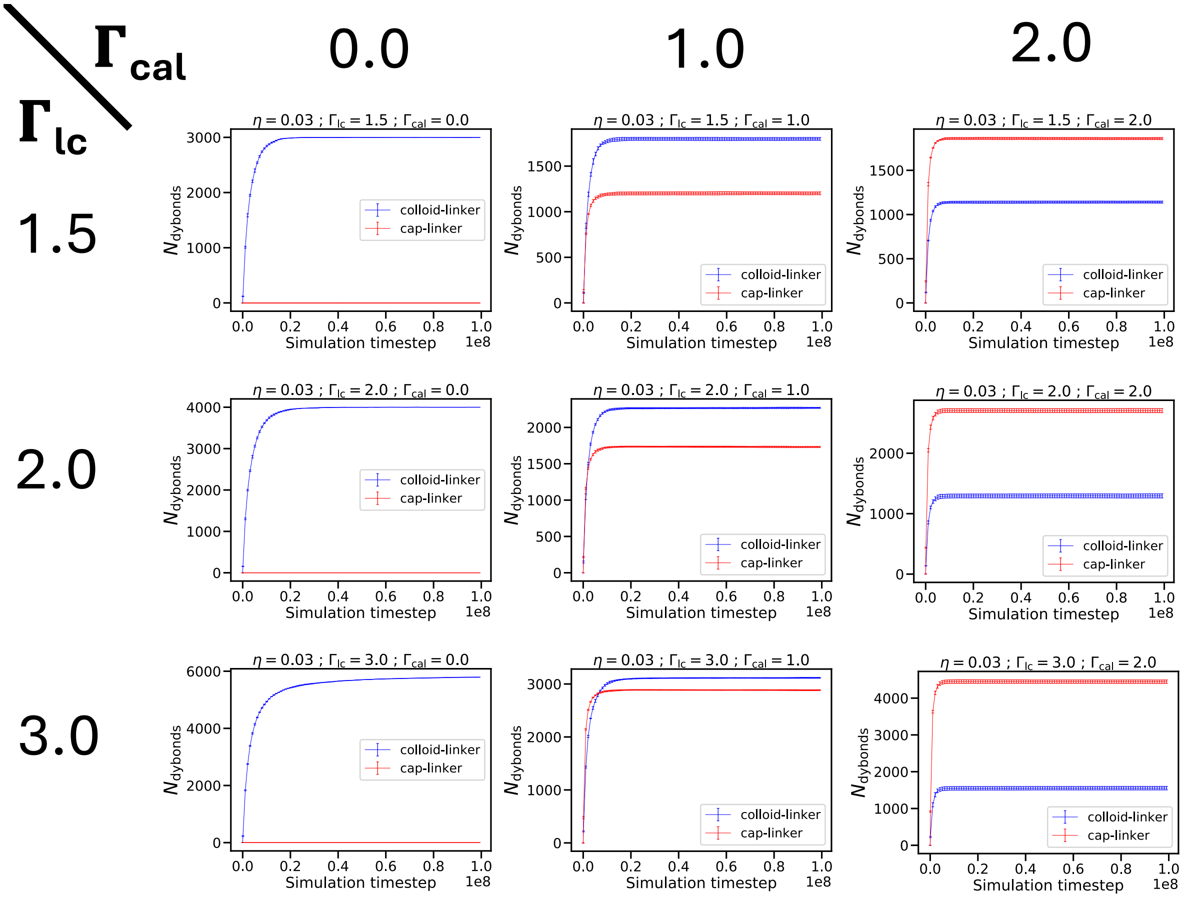

Figure 4.5: Total number of dynamic bonds formed as a function of the simulation time, with the number of colloid-linker and cap-linker bonds plotted separately — for a system of colloids mixed with linkers (in presence or absence of cap molecules). All plots shown here correspond to varying linker-colloid and cap-linker ratios (Γ_{lc},Γ_{cal}), for a fixed $\beta\varepsilon = 20.0$ and $\eta_c = 0.03$. $\Gamma_{\text{cal}} = 0.0$ indicates the presence of no cap molecules (only linkers present). The maximum possible number of dynamic bonds (the upper limit of the y-axes) are different when Γ_{lc} varies, due to variable number of linker molecules. Error bar(s) correspond to standard deviation(s) computed from three repeat simulations for each condition.

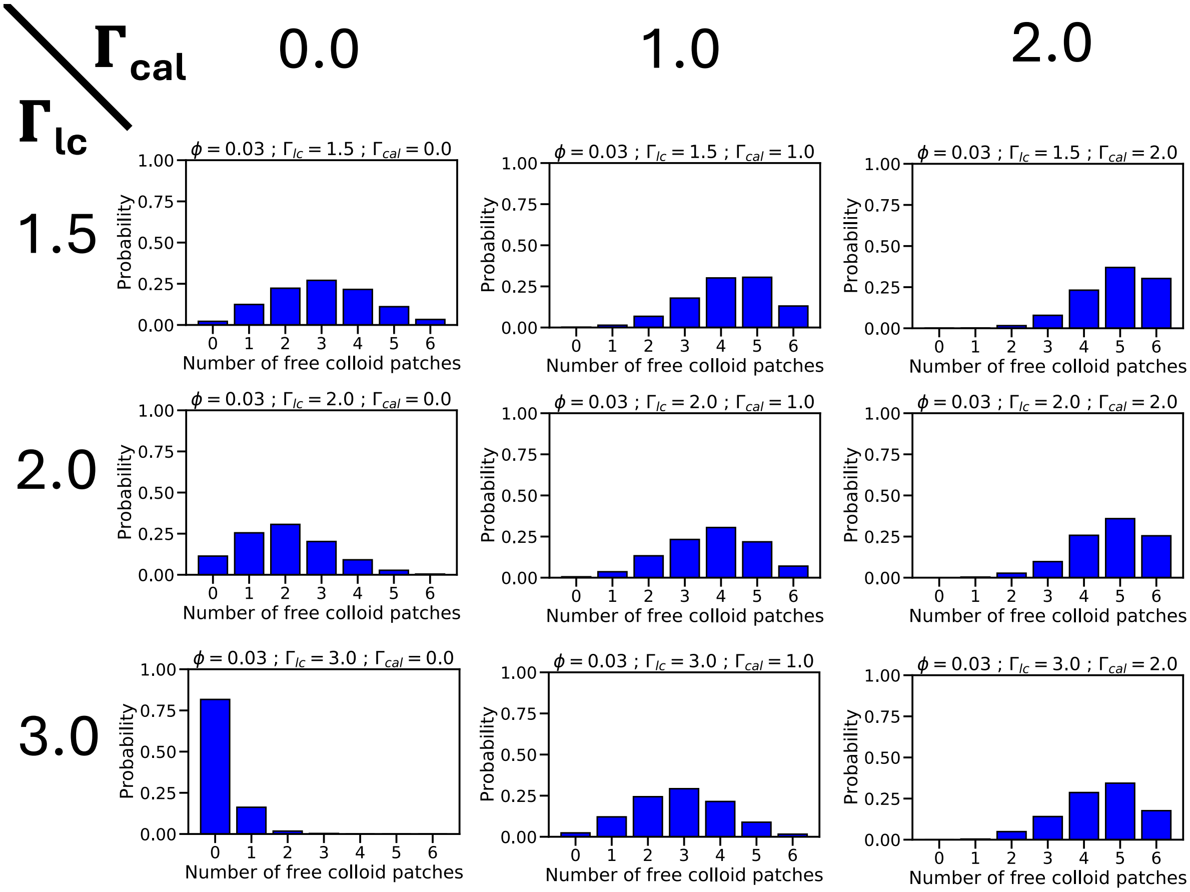

Figure 4.6: Histograms showing the distribution of number of free colloid patches at the final time point of the simulation — for a system of colloids mixed with linkers (in presence or absence of cap molecules). All histograms shown here correspond to varying linker-colloid and cap-linker ratios (Γ_{lc},Γ_{cal}), for a fixed $\beta\varepsilon = 20.0$ and $\eta_c = 0.03$. $\Gamma_{\text{cal}} = 0.0$ indicates the presence of no cap molecules (only linkers present). The histograms were generated from the combined data of three repeat simulations for each condition, respectively.

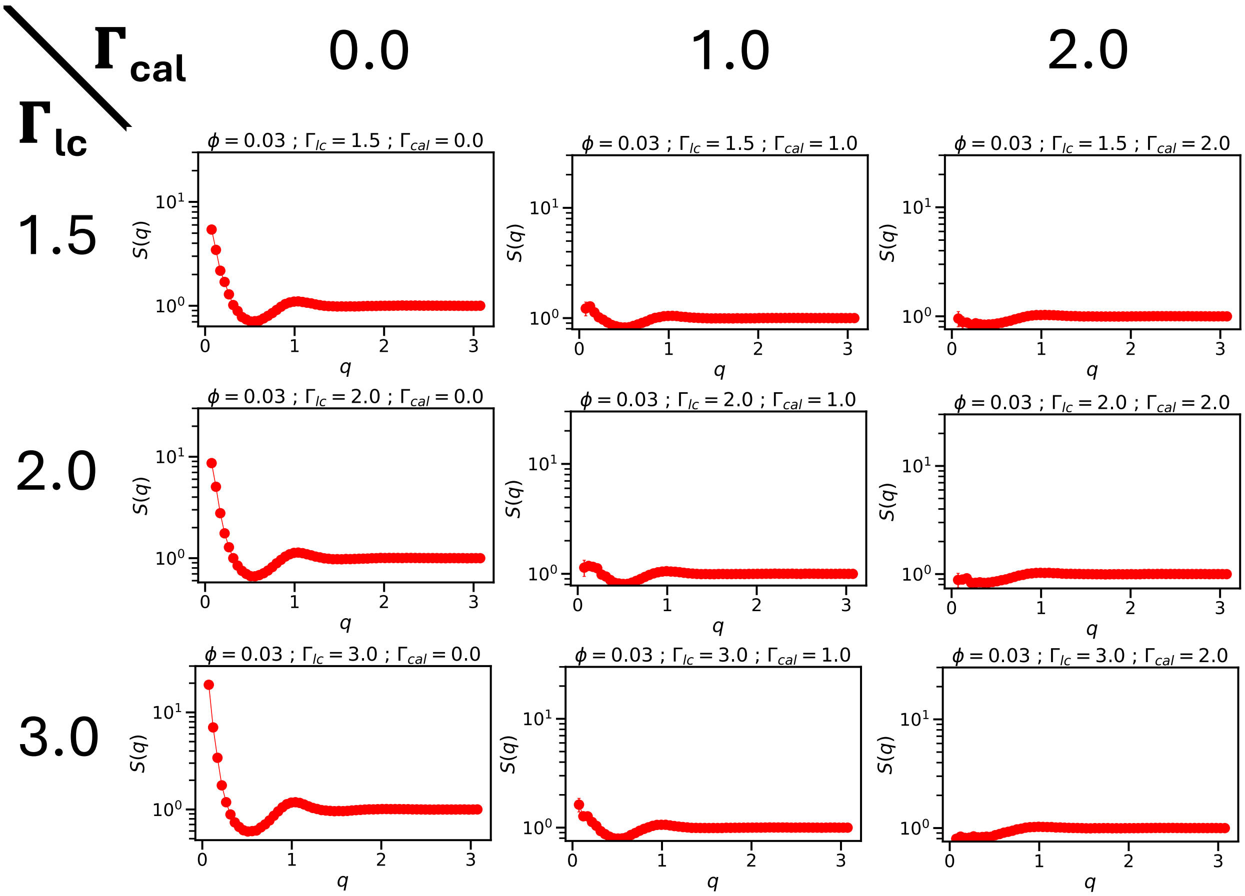

Figure 4.7: The colloid partial static structure factor $S(q)$ (averaged over the final 20 frames of simulation) plotted against the wave-vector q — for a system of colloids mixed with linkers (in presence or absence of cap molecules). All the plots shown here correspond to varying linker-colloid and cap-linker ratios (Γ_{lc},Γ_{cal}), for a fixed $\beta\varepsilon = 20.0$ and $\eta_c = 0.03$. $\Gamma_{\text{cal}} = 0.0$ indicates the presence of no cap molecules (only linkers present). Error bar(s) correspond to standard deviation(s) in the $S(q)$ values computed from three repeat simulations for each condition. A diverging $S(q)$ value at zero wave-vector is indicative of prominent phase separation (> the threshold of $S(0) = 10$).

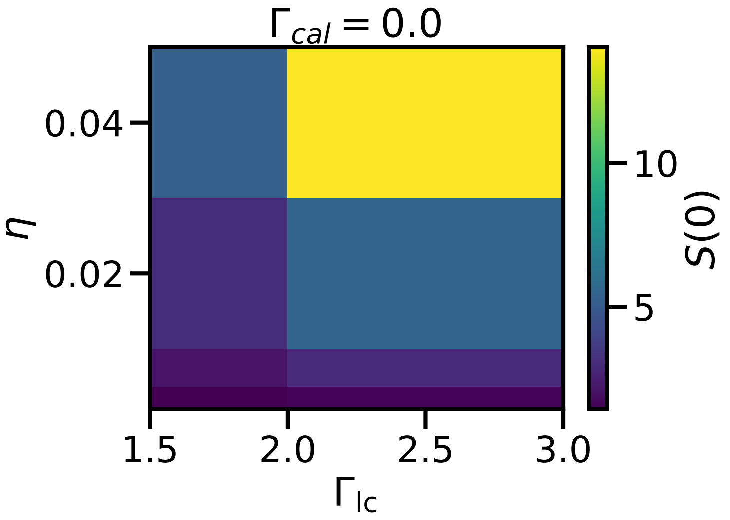

Figure 4.8: Phase diagram for colloids mixed with linkers (no capping molecules present) at the final time point of the simulation in the (η_c,$\Gamma_{\rm lc}$) plane for $\beta\varepsilon$ = 20.0 and $\Gamma_{\rm cal}$ = 0.0. The 'viridis' color-map illustrates the extrapolated colloid partial structure factor to zero wave-vector, denoted as $S(0)$, derived from the simulations. Large values of $S(0)$, typically above a threshold value of 10, indicate phase separation in the gels (in this case, the yellow region in the top right corner of the diagram).

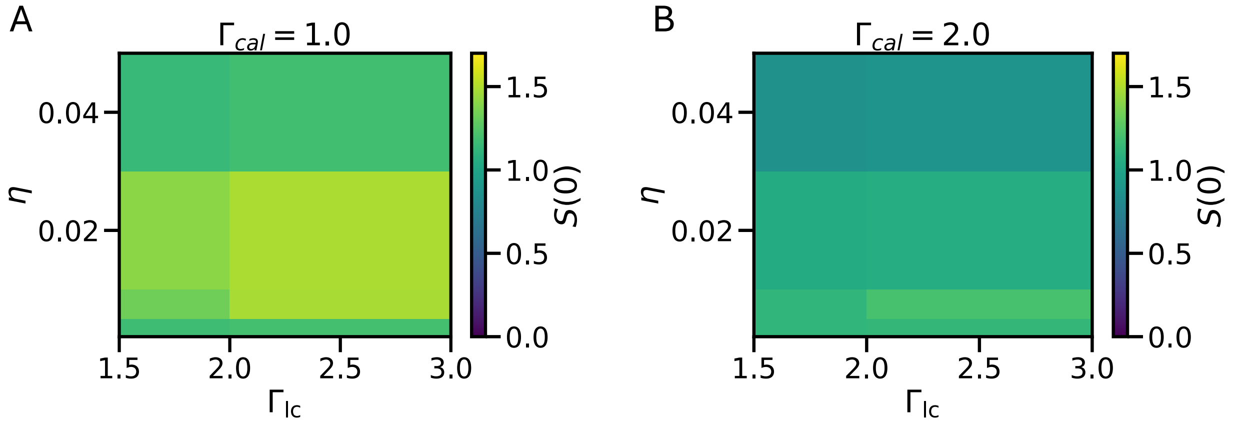

Figure 4.9: Phase diagram for colloids mixed with linkers and free capping molecules at the final time point of the simulation in the (η_c,$\Gamma_{\rm lc}$) plane for $\beta\varepsilon$ = 20.0 and for (A) a cap-to-linker ratio $\Gamma_{\rm cal}$ = 1.0 and (B) a cap-to-linker ratio $\Gamma_{\rm cal}$ = 2.0, with the color map indicating the $S(0)$. In presence of the capping molecules, no phase separation is typically observed since in both the cases (A) and (B), the highest values of $S(0)$ are always < 10.

4.6 CONCLUSIONS

In an integrated coarse-grained modeling platform developed in this work to study colloidal gelation, we treat the building blocks as patchy colloids with discrete binding sites [189, 190, 292, 293] capable of dynamic binding or unbinding [50]. This approach, employing dynamic bonding among the components, facilitates the design of responsive materials [28, 58, 77]. These colloids can form networks through a linker-mediated strategy [189, 286, 296, 298], involving the reversible connection of functionalized macromers or nanocrystals by bifunctional molecules [302]. Alternatively, they can be implicitly modeled as bonds between binding sites, exhibiting the properties of a semiflexible polymer [401] chain. The dynamic rates of binding and unbinding also confer kinetic leverage, thereby impacting the dynamics and structure of these gels. [402–404].

The current simulation setup involves explicit bifunctional linkers that facilitate the bonding of colloids through patchy binding sites [189, 190, 292, 293, 298]. However, our goal is to develop an implicit linker representation similar to our mobile binder coarse-grained model. One major objective is to generate theoretical and experimentally validate phase diagrams for linker-mediated functionalized macromer [299–301, 461, 462] and nanocrystal [189, 190, 286–298] networks with both symmetric and asymmetric linkers.

These phase diagrams will highlight regions of the parameter space conducive to forming arrested-phase-separation [402–404] and equilibrium gels. We want to study how tuning the ratio of active to inactive ligands (represented in simulations by the patches on the colloids), as well as altering the concentration of caps [296, 298, 303], can affect the phase behavior. The control of exchange kinetics for caps and linkers will lead to gel networks with diverse structures, depending on whether they are under thermodynamic or kinetic control regimes. Additionally, we aim to control the structure and dynamics of gels by leveraging the linker length and rigidity [292]. Effect of using asymmetric linkers, that can inhibit any linker self-looping, can also be tested next in our simulation model.

Currently, in our simulation model, we have the cap molecules of the same particle type as the colloid patches and so it is hard to investigate the effects of varying the kinetic rates of cap-linker binding and patch-linker binding separately. This can be rectified once we make certain changes to our dynamic binding / unbinding plugin. This is one of the major drawbacks of the current model.

4.7 Detailed simulation parameters

All important simulation parameters are enumerated in the table 4.4.

Table 4.4: **A table containing all the general simulation parameters**

Description (Symbol)	**Value in HOOMD units**
MD timestep (dt)	0.0005
Dimensionality (d)	3
Temperature (T)	1.0
Number of simulation steps run (n_{steps})	1×10^8
Diameter of colloid (σ_c)	2.5
Diameter of patch (σ)	0.5
Diameter of each linker segment (σ)	0.5
Number of patches in a colloid (N_{patch})	6
Number of colloids (N_c)	1000
Linker-to-colloid ratio (Γ_{lc})	1.5-3.0
Cap-to-linker ratio (Γ_{cal})	1.0-2.0
Colloid volume fraction (η_c)	0.002-0.1
Mass of colloid	125.0
Mass of patch	1.0
Mass of each linker segment	1.0
Drag coefficient (γ)	0.1
FENE-WCA bond parameters:	
(i) r_0	1.5
(ii) ε_{WCA}	1.0
(iii) σ_{WCA}	1.0
(iv) Spring constant k_p	30.0
Cosine-squared angle potential parameters:	
(a) Rest angles-	
(i) θ_0^{linker} for linker angles	3.1415
(ii) θ_0^{patch} for patch angles	1.5708
(b) Angle spring constants-	
(i) Linker angle flexibility κ	0.0
(ii) k_{patch}	300.0
Shifted WCA potential parameters:	
(i) ε_{WCA}	1.0
(ii) σ_{WCA}	1.0
Binding affinity (ε) for dynamic binding	20.0
Initial rate constant for binding ($k_{\text{on}}^{\text{init}}$)	200.0
Rate constant for binding after melting ($k_{\text{on}}^{\text{melt}}$)	0
Melting Temperature (T_{melt})	2.0
Inflexion steepness parameter (α)	200.0
Dynamic bond rest length (l_{dyn})	0.0
Dynamic bond spring constant (k_{dyn})	20.0
Dynamic bonding minimum distance (l_{min})	0.0
Dynamic bonding maximum distance (l_{max})	0.4472
Dynamic bond checksteps (n)	10

Chapter 5

Molecular dynamics simulations to study mesoscale molecular assembly in the active, crowded cytoplasm

This chapter is adapted from the work published as [51].

5.1 Abstract

The mesoscale organization of molecules into membraneless biomolecular condensates is emerging as a key mechanism of rapid spatiotemporal control in cells [463]. Principles of biomolecular condensation have been revealed through *in vitro* reconstitution [306]. However, intracellular environments are much more complex than test-tube environments: They are viscoelastic, highly crowded at the mesoscale, and are far from thermodynamic equilibrium due to the constant action of energy-consuming processes [305]. We developed *synDrops*, a synthetic phase separation system, to study how the cellular environment affects condensate formation. Three key

features enable physical analysis: synDrops are inducible, bioorthogonal, and have well-defined geometry. This design allows kinetic analysis of synDrop assembly and facilitates computational simulation of the process. We compared experiments and simulations to determine that macromolecular crowding promotes condensate nucleation but inhibits droplet growth through coalescence. ATP-dependent cellular activities help overcome the frustration of growth. In particular, stirring of the cytoplasm by actomyosin dynamics is the dominant mechanism that potentiates droplet growth in the mammalian cytoplasm, by reducing confinement and elasticity . Our results demonstrate that mesoscale molecular assembly is favored by the combined effects of crowding and active matter in the cytoplasm. These results move toward a better predictive understanding of condensate formation *in vivo*.

5.2 INTRODUCTION

Liquid-liquid phase separation (LLPS), has emerged as a ubiquitous mechanism for driving formation of biomolecular condensates inside the cell that are dynamic and can form and dissolve on relatively short timescales; for example, stress granules [464] transiently form in response to potentially detrimental changes in the environment such as temperature shock. Phase separation occurs when molecules exceed their solubility limit and condense into a new phase [306]. LLPS inside the cell is strongly affected by the environment - crowded environments can both drive nucleation and frustrate the growth (coalescence) of droplets, while active environments can help overcome this frustration.

Cells are highly crowded, with macromolecules excluding 20% - 30% of cellular volume in eukaryotic cells and 30% - 40% in prokaryotic cells [304, 465]. This high excluded volume can inhibit molecular motion (and thus disfavor diffusion-limited reactions), but on the other hand can entropically favor assembly through depletion-attraction forces[466, 467]. Binding reactions are entropically unfavorable, because the reactants become more ordered. However, when two or more components bind one another, they take up less space. In crowded environments, this gives more space for the crowders to move, thus increasing their entropy.

The majority of cytoplasmic volume is taken up by mesoscale (10 - 1000 nm diameter) particles [304]. Mesoscale systems are too small to "coarse grain" without losing crucial features, and too large to completely understand the massive complexity of every component. The effects of crowding strongly affect the behavior of mesoscale particles and assemblies, while having less impact on nanoscale processes because nanoscale particles can move relatively freely between mesoscale crowders, but mesoscale particles cannot. Studies have shown that the decreased motion due to macromolecular crowding can change biochemical reaction kinetics, protein conformations, and motor functions[467–469].

The cell also contains elastic networks that constrain and organize the cell interior. These include the actomyosin cytoskeleton in the cytoplasm [470] and chromatin in the nucleus[471]. The presence of these networks and the high concentration of particles together make the intracellular environment viscoelastic. This contrasts with simple buffer solutions, which are only viscous.

Finally, cells are non-equilibrium open systems, and use adenosine triphosphate (ATP)-dependent cellular activities to maintain a non-equilibrium steady state by exchanging energy, information and material with the extracellular environment, thereby locally reducing entropy [472]. Overall, the intracellular environment is highly complex, and its impact on the assembly of membraneless biomolecular condensates remains largely unexplored.

The assembly of membraneless biomolecular condensates bridges length scales between the nanoscale and mesoscale, where nanometer diameter molecules come together to form higher-order structures of tens to thousands of nanometers in diameter [473]. This wide range of length- and time-scales makes it difficult to predict how the crowded, active cellular environment will affect biomolecular condensate formation. Several studies have focused on the impact of elastic mechanical properties on condensate growth [474–477]. For example, elastic chromatin mechanics has been shown to frustrate the growth of nuclear condensates [476, 477]. However, the combined impacts of macromolecular crowding, elastic networks, and non-equilibrium cellular activities on condensate formation are less well understood.

It is difficult to derive general physical principles from the study of endogenous condensates because these systems are formed through complex coacervation of many molecules. Furthermore, these components are often dynamically altered by posttranslational regulation, the details of which are typically unknown. Thus, when perturbing intracellular environments, it is difficult to fully attribute structural changes in endogenous condensates to only biophysical cues, since biological functional changes associated with perturbations can also lead to structural changes in endogenous condensates. To overcome these issues, an orthogonal synthetic intracellular condensate system called *synDrops* was developed experimentally. synDrops adapted a previous approach to create a molecular condensate of well-defined geometry [478], but adds the ability to chemically induce the interaction of components.

synDrop formation was successfully induced experimentally in both budding yeast S. *cerevisiae* cells and mammalian cervical cancer HeLa cells. Complementary to the experimental system, we also developed two independent agent-based coarse-grained molecular dynamics models to simulate synDrops within cellular environments from first principles. Combining experiments and simulations, we show that macromolecular crowding facilitates the nucleation process while inhibiting the growth phase of condensate dynamics. However, ATP-dependent active processes in the cytoplasm prevent kinetic trapping of larger assemblies and thus promote coarsening and fusion of individual droplets. In conclusion, we found that the assembly of mesoscale biomolecular condensates is favored by the crowded and active cellular environment. Our hypothesis is that translation and motion of ribosomes increase local effective temperature and thereby cellular activity, while actomyosin contractility overcomes kinetic trapping at longer length- and time-scales.

5.3 DESCRIPTION OF THE EXPERIMENTAL *SYNDROP* SYSTEM

In collaboration with Emmanuel Levy, the Holt Lab (NYU Langone Health) designed an *in vivo* synthetic droplet (*synDrop*) system to study the biophysical properties of LLPS. SynDrops are composed of two protein components, each of which has three modular domains. The design was based on the Flory-Stockmeyer theory [479], which governs polymer network growth. Multivalency is essential for the formation of mesoscale condensates through phase separation [480–484]. Homomultimerizing domains were used to create multivalency in the system (Fig. 5.1). The first component contains a hexamerization domain to create multivalency (PDB: 3BEY), an inducible interaction domain and a blue fluorescent protein (BFP). The second component contains a long coiled-coil dimerization domain for multivalency (PDB: 4LTB), an inducible interaction domain, and a green fluorescent protein (GFP). The two components interact in trans through two halves of an inducible heterodimeric binding interaction, enabling kinetic analysis. Importantly, the dimerization domain is a 19 nm long, stiff, antiparallel coiled-coil. Due to the structural rigidity and the length of the coiled-coil in the dimer, and because the distance between interaction surfaces on the hexamer is approximately 6 nm, self-closed structures are prohibited (i.e. both dimer domains cannot bind to a single hexamer). Thus, geometric constraints strongly favor the expansion of synDrop molecular networks that form by spanning alternatively between the two components (as shown in Fig. 5.1 (bottom)). This greatly simplifies simulation and physical analysis compared to other synthetic systems [482–484].

The inducible binding domains are the plant GAI (Gibberellin insensitive DELLA proteins) and GID (Gibberellin Insensitive Dwarf 1) domains. These domains undergo a heterotypic interaction that is potentiated in the presence of the plant hormone Gibberellin (GA) [485] (Fig. 5.1). GAI is truncated to a minimum dimerization domain [486]. Adding GA increases the affinity between the two synDrop components and triggers synDrop formation.

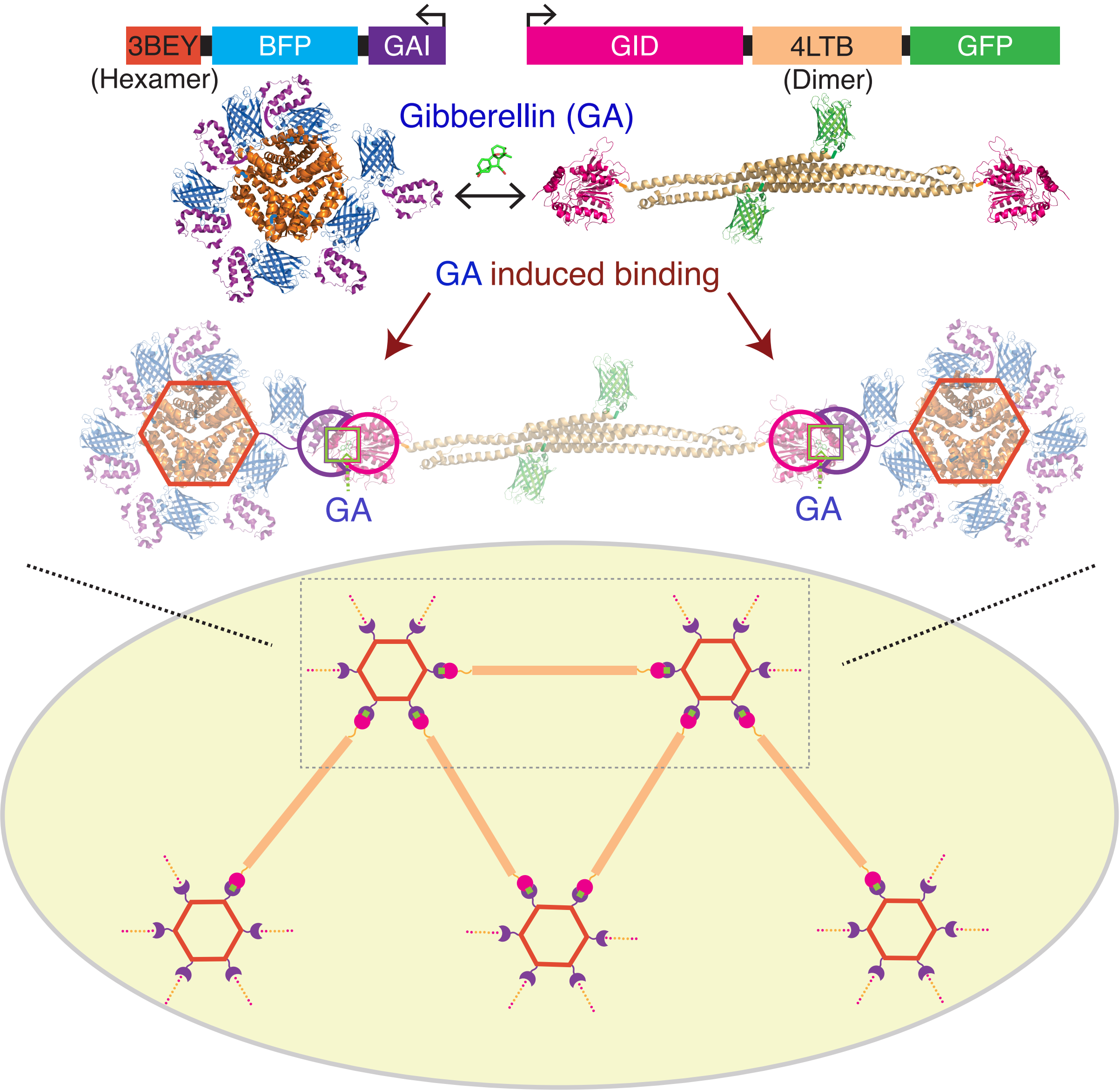

Figure 5.1: synDrops, composed of two proteins, is a synthetic system designed *in vivo* via experiments, and enables the analysis of condensate formation kinetics. It is amenable to modeling via coarse-grained simulations. The top part of the figure shows the gene and crystal structures of the two components. Each protein has three domains: an oligomerization domain (3BEY: Hexamer or 4LTB: Dimer), an inducible interaction domain (GAI or GID) and a fluorescent protein (BFP or GFP). Gibberellin (GA) induces binding between GAI and GID favoring the formation of a mesoscale molecular network (bottom schematic).

5.4 COARSE-GRAINED SIMULATION MODEL TO STUDY MESOSCALE ASSEMBLY IN THE *SYNDROP* SYSTEM

Our *in vivo* system enables detailed analysis of mesoscale assembly, but cannot easily report on the microscopic protein interactions that underpin this process. Therefore, we developed an independent agent-based molecular dynamics (MD) platform and also developed a new graph-theory network to provide complementary information *in silico* and also quantitatively describe LLPS. The simulation setup used a HOOMD-blue engine [334, 335] combined with a dynamic bonding plugin that we previously developed [50] (Fig. 5.2 and 5.3). In MD simulations with HOOMD-blue, we modeled the hexamer as a single sphere of diameter 12.6 nm with six uniformly distributed binding sites, and the dimer as a rod-like structure formed from three spheres with two binding sites positioned on opposing sites of the two outer spheres (Fig. 5.2). The inner sphere has a diameter of 11.7 nm and the two outer spheres are slightly bigger in size, each having a diameter of 13.45 nm. The binding sites on the ends of the hexamers and the rods have a diameter of 2 nm each. The sizes of these simulated structures were chosen based on crystal structure data from the Protein Data Bank (PDB) for the individual protein components within each protein complex. In addition, we included a third agent to mimic ribosomes, which are the dominant macromolecular crowders in the cytoplasm. This agent was a 30 nm diameter sphere with no binding interactions. Binding occurs between a hexamer and a dimer through complementary interaction points at the end of these objects. The formation of synDrops was simulated with or without crowders under equilibrium conditions (Fig. 5.3). There is a discrepancy in the time scales of synDrops formation between simulations and experiments. This could be due to various factors, such as the significantly smaller droplet sizes in simulations – approximately one-tenth the radius of those in the experimental system – and the simplified assumptions inherent in coarse-grained models representing cellular systems.In summary, we have developed the synDrop system both in cells and *in silico*, allowing us to address how the intracellular environment affects the assembly of mesoscale condensates.

5.5 Simulation Methods

An agent-based molecular dynamics (MD) simulation approach has been developed to study the synDrops system. MD Simulations were performed using HOOMD-blue v2.9.6 [334, 335]. The HOOMD-blue model uses GPU acceleration to increase simulation speeds, enabling us to investigate cluster formation dynamics over much longer timescales (>10x), especially at high molecular density. We use coarse-grained (CG) representations of each synDrops component—(i) a sphere with six rigid evenly distributed binding sites to represent the hexamer and (ii) 3 spheres in a rod-like arrangement with two complementary binding sites at two ends to represent the rigid coiled-coil dimer. We have 1170 dimers and 390 hexamers within a cubic box with 860 nm sides (maintaining a 3:1 stoichiometric ratio of dimers and hexamers to have 1:1 ratio of complementary binding sites). This results in concentrations of 3 μm for dimers and 1 μm for hexamers, similar to our estimated values in experiment. Finally, 20 spheres of diameter 40 nm are added to mimic the trace presence of GEMs (Genetically Encoded Multimeric nanoparticles) [304] in the experiment (to enable rapid characterization of the mesoscale physical properties of the cytoplasm).

For the simulations used to determine the dissociation constant (K_d), we set up a monomeric system (where the dimers and hexamers are in a 1:1 stoichiometric ratio), we reduced the available (active) binding sites of two components from 6 and 2 to 1 and 1 each. The number of hexamers and dimers used are 200 each for these simulations (enclosed inside a cubic box with 400 nm sides), as opposed to 390 and 1170 respectively for the synDrop MD simulations described above. Here, each hexamer has only 1 *active* binding site and 5 *inactive* binding sites. Similarly, each dimer has 1 *active* and 1 *inactive* binding site (as shown in Fig. 5.4). Dynamic bonding is only allowed between active binding sites on the hexamer and dimer.

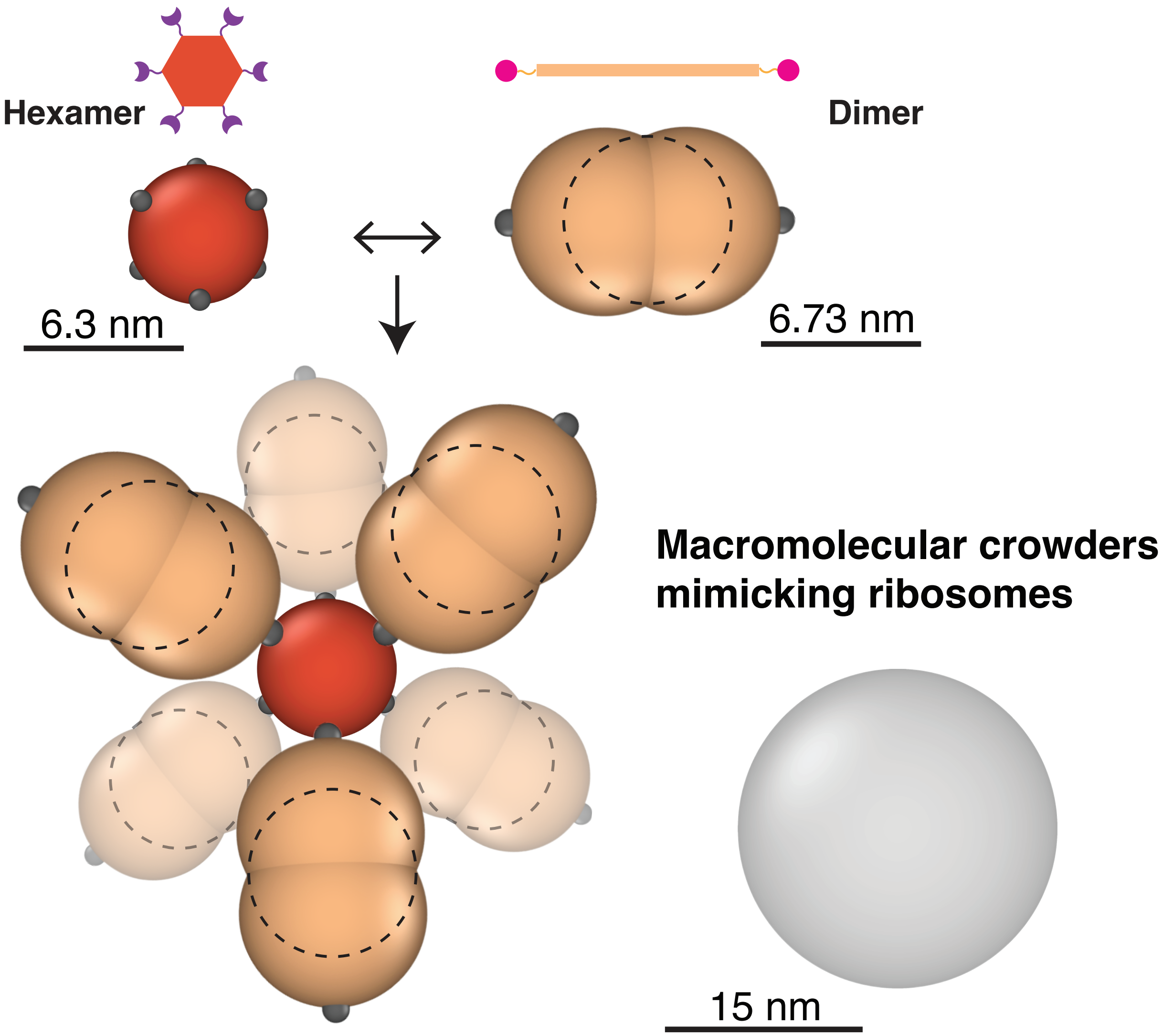

Figure 5.2: Schematic of coarse-grained molecular dynamics model for synDrop assembly. The hexamer component is represented by a sphere with six uniformly distributed binding sites; the dimer component is represented as a rod-like structure formed from three overlapping spheres with two binding sites positioned on opposite ends. A third component with no binding sites mimics ribosomes as macromolecular crowders.

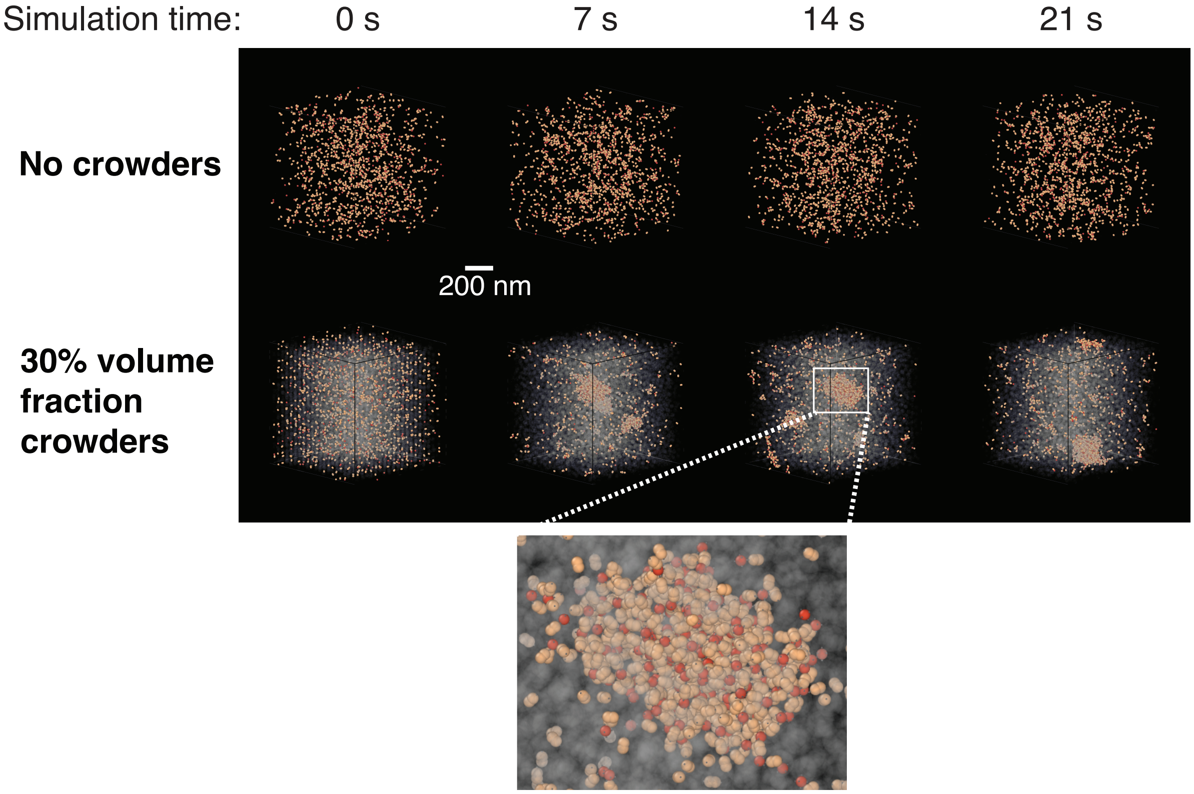

Figure 5.3: Representative images (snapshots) from HOOMD-blue MD simulations of synDrops system over time without crowders (top) and with 30% volume fraction of crowders (bottom). The zoomed-in image under 30% volume fraction condition shows the formation of a large cluster.

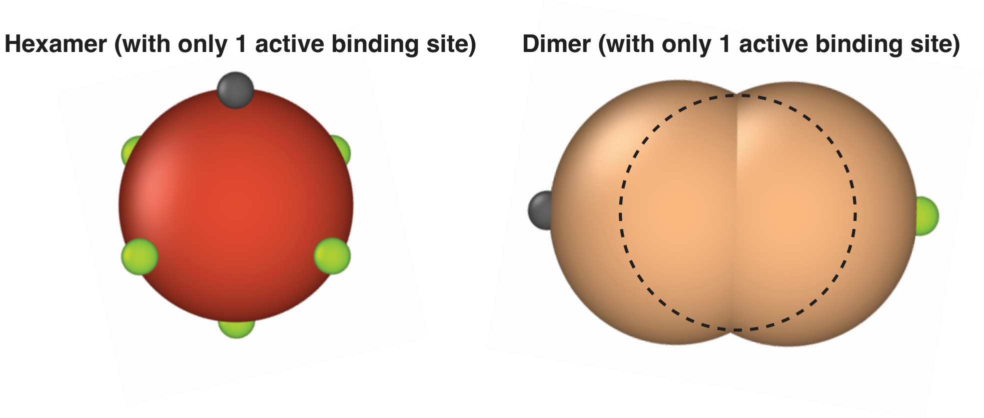

Figure 5.4: For the simulations run to determine K_d, the hexamer component has only 1 *active* binding site (grey) and 5 *inactive* sites (light green); the dimer component similarly has only 1 *active* binding site (grey) and 1 *inactive* site on the opposite end (light green).

In addition, spherical components of various sizes without any binding site are added in the system to mimic the crowded cellular environment (Fig. 5.2). For the initial configuration, the CG components are arranged in a lattice whose positions are generated from a CsCl-type lattice generator using the 'lattice' module from the ASE (Atomic Simulation Environment) [487] package. We ran MD simulations with varying volume fractions of ribosomes to study the effect of crowding in synDrops assembly. We also varied the effective temperatures that only govern the ribosome movements to study how cellular activities affect synDrops assembly.

Binding occurs through complementary interaction sites between dimers and hexamers. We modeled such covalent interactions by developing an open-source C++ plugin, called the Dynamic Bond Updater [50] in HOOMD-blue that builds upon a model for epoxy binding developed in [336]. The Bond Updater, for every n steps during the MD simulation, stochastically adds or removes dynamic bonds. Binding events occur with a fixed probability P_{on} at a critical distance d_{bind} between interaction sites, while unbinding events occur with a probability P_{off}. Using our dynamic bonding framework, we thus have controls over our binding and unbinding rate constants k_{on} and k_{off} respectively; the bond affinity ε is defined by

$$\Delta G = k_B T \ln\left(\frac{k_{\mathrm{on}}}{k_{\mathrm{off}}}\right) \equiv \varepsilon \tag{5.1}$$

and can be increased by lowering the unbinding rate constant k_{off}. We ensure that the dynamic bonding model satisfies detailed balance using a particular Metropolis-like criterion [118, 193, 337], so that the system moves towards an equilibrium ensemble as bonds form and dissolve dynamically. An important point to note here is that for the synDrop MD simulations, we have explicit dependence of the binding/unbinding rates on temperature turned off. The only dependence on temperature arises in the Metropolis factor. We use the cell neighbor list [347] to accelerate nonbonded agents' calculations and possible bonding pairs' constructions.

Interactions between crowders and synDrops proteins occur via a soft repulsion potential [50] defined by

$$U_{\mathrm{soft}}(r) = \begin{cases} \varepsilon_{\mathrm{soft}}\left[1 - \left(\frac{r}{r_{\mathrm{cut}}}\right)^4\right] & \text{if } r < r_{\mathrm{cut}} \\ 0 & \text{if } r \geq r_{\mathrm{cut}} \end{cases} \tag{5.2}$$

, where smoothing was applied using HOOMD-blue's XPLOR [335] smoothing function. The soft potential was implemented by using HOOMD-blue's tabulated potential option (with 1000 interpolation points between $r_{\mathrm{min}} = 0$ and $r_{\mathrm{max}} = 1.5\sigma$, where σ is the sum of the radii of the particles). Here, r_{on} is chosen as the point at which the smoothing starts. We set $r_{\mathrm{on}} = 0.95 r_{\mathrm{cut}}$ for our simulations, and $r_{\mathrm{cut}} = \sigma$. There is no soft repulsion between complementary binding interaction sites on hexamers and dimers, where we implemented a Lennard-Jones (LJ) [356–359] attraction between the hexamer and dimer rigid bodies, with a cut-off distance equal to 2.5σ.

All objects in the system undergo thermal fluctuations using Langevin [345] dynamics, with drag forces proportional to the diameter. The dimensions of every CG component approximate their respective crystal structures. Within our MD simulations, we typically use periodic boundary conditions (PBC). However, we also have the option of adding Lennard-Jones 'walls' to confine our system in a 'closed box'. For volume fractions up to 35%, we are able to place ribosomes in the box without overlaps through random sequential insertion. For higher concentrations, we first set up the initial simulation box size using lengths of 1400 nm on a side (4.3x the target volume) and the appropriate number of ribosomes, and then compress the system to the target size of 860 nm linearly over 5×10^5 simulation steps (using the *hoomd.variant* module of HOOMD-blue), and finally turn on dynamic bonding in the system to record synDrops dynamics.

To study how non-thermal cellular activity [488, 489] impacts formation of synDrops via MD simulations, we assign the crowders a different effective temperature T_c from the rest of the system, which can be achieved through separate Langevin 'thermostats' in HOOMD-blue. We ran a different set of MD simulations at a fixed volume fraction of ribosomes (= 30%) but varying the crowder effective temperatures T_c.

All important simulation parameters are enumerated in the table 5.1.

5.6 RESULTS

5.6.1 MACROMOLECULAR CROWDING PROMOTES NUCLEATION BUT INHIBITS DROPLET GROWTH

From experiments, it was observed that droplets initially nucleate locally but do not grow substantially, followed by a growth phase where droplet sizes become larger, mainly through droplet coalescence. Thus, the synDrops system forms droplets by nucleation and growth, which has been suggested as the most common mechanism of endogenous condensate formation [490, 491]. Also, it has been established through experiments that macromolecular crowding promotes synDrop nucleation but inhibits growth, in both human and yeast cells. The mechanisms underlying the inhibition of droplet growth by macromolecular crowding are important to understand

Table 5.1: Table of parameters for the MD Simulations using HOOMD-blue

Parameter (with description)	**Value used in simulations**
Simulation timestep (dt)	0.002
Crowder Temperature (T_c) relative to $T_{\text{room}} = 298.15K$	0.5-2.0
Simulation box length (in nm)	860 (for the actual system) 400 (for the monomeric system)
Volume fraction of ribosomes (ϕ_{crowder})	0.0-0.5
Initial box length (in nm) for compression ($\phi_{\text{crowder}} > 0.35$)	1400
Number of rod proteins	1170 (for the actual system) 200 (for the monomeric system)
Number of hexamers	390 (for the actual system) 200 (for the monomeric system)
Number of GEMs	20
Number of binders on each hexamer	6
Number of binders on each rod	2
Diameter of inner rod particle (in nm)	11.7
Diameter of the two outer rod particles (in nm)	13.45
Diameter of hexamer (in nm)	12.6
Diameter of ribosome (in nm)	30.0
Diameter of GEM (in nm)	40.0
Diameter of binder on rods and hexamers (in nm)	2.0
Friction coeff. to multiply by particle diameter	0.001
Maximum binding distance (d_{bind}) (in nm)	1.0
Repulsion strength for soft quartic potential (in $k_{\text{B}}T$)	500
ε for Lennard-Jones potential (in $k_{\text{B}}T$)	0
Rate constant for dynamic binding k_{on} (in units of $1/\tau$)	50.0
Rate constant for dynamic unbinding k_{off} (in units of $1/\tau$)	**0.001** (also 0.015, 0.006, 0.0003, 0.0001, 0.000015, 0.000002, 0.0000001, 0.0000000007)
Binding affinity ε (in $k_{\text{B}}T$)	**10.8** (also 8.1, 9.0, 12.0, 13.1, 15.0, 17.0, 20.0, 25.0)
Dynamic bond rest length (l_{dyn})	2.0
Dynamic bond spring constant (k_{dyn})	20.0
Dynamic bond check steps (n)	10

in this context. Droplets can grow in two ways: the first is through droplet coalescence [492] and the other is through Ostwald ripening [493]. However, droplet coalescence has been suggested as the dominant mechanism for droplet growth in biological systems [476]. In this mechanism, the rate of droplet growth depends on the collision rate between two smaller droplets, which in turn depends on the diffusivities of these droplets [476, 492]. A hypothesis was therefore made

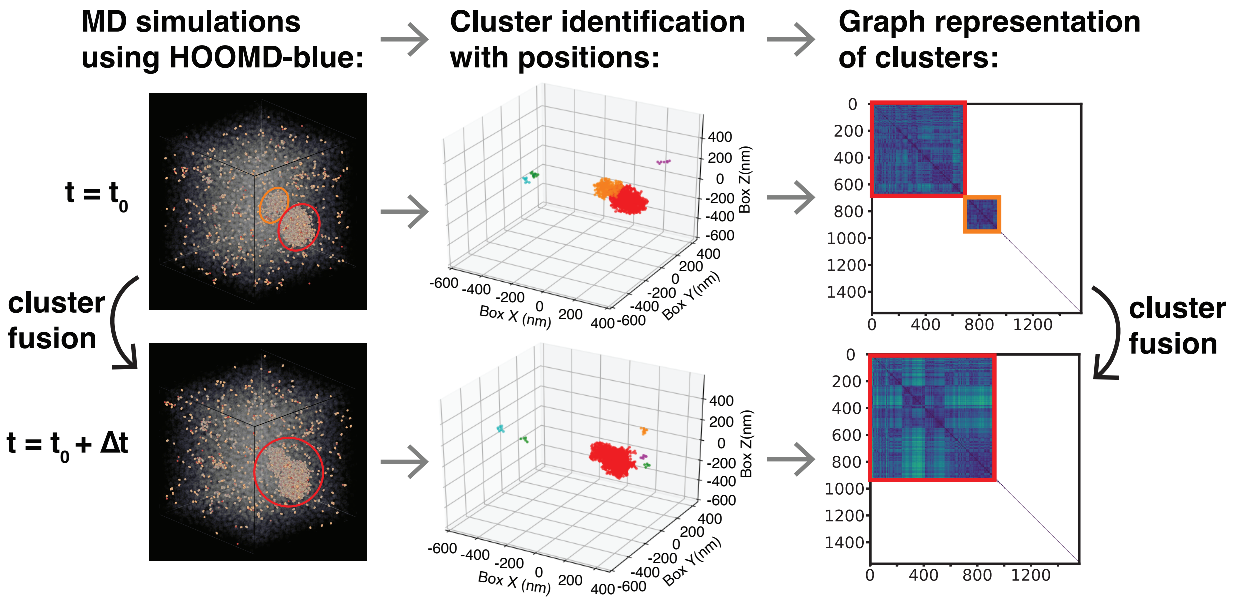

Figure 5.5: Illustration of graph-theory based analyses on cluster formations, showing the cluster fusion process as an example. Extracted from MD simulation data, the positions and binding information of synDrop components are utilized to generate a distance matrix reflecting the topological shortest distances between each component pair. Through clustering this matrix, the clusters are identified both spatially and represented in a clustergram (graph representation of the clusters).

that macromolecular crowding inhibits droplet growth by reducing droplet diffusivities.

To validate this hypothesis further and also to investigate molecular details that are not easily accessible from experimental data, an agent-based coarse-grained Molecular Dynamics simulation model was employed to simulate synDrops. The well-defined structures and binding interactions between the two synDrop components enabled us to quantify droplet network structures with graph theory based analyses (Fig. 5.5). Unless otherwise specified, the concentrations of dimer and hexamer synDrop components remain at $3\mu M$ and $1\mu M$, respectively, in the following simulations. Here, we defined each synDrop component as a node and the bond between two components as an edge. We calculated the topological shortest distances between each pair of components and mapped out bond connectivity to define each molecular cluster. The distance matrix from this analysis was then used for hierarchical clustering [349]. In the initial step, each data point is treated as an individual cluster, and the process iteratively merges the closest clusters until a predefined stopping criterion is met. Within the resulting *clustergram*, squares along the diagonal correspond to clusters of interacting molecules. Each pixel on the x and y axes represents an interaction between two individual molecules in the simulation system and is colored according to the topological distance between them (e.g., molecules that are directly connected are dark blue, while molecules that are indirectly connected through a chain of interactions are a lighter hue). Blank pixels indicate that there is no path connecting the two corresponding molecules (Fig. 5.5, 5.6). Fig. 5.5 shows the process of cluster fusion between two different time points in a simulation as an example to demonstrate how graph theory based analyses can be used to show the cluster formation. Squares on the diagonal correspond to condensates: The red and orange clusters circled in the simulation snapshot (Fig. 5.5, left) and in the 3D graph (Fig. 5.5, middle) were identified from the blocks of interactions highlighted by red and orange in the *clustergram* (Fig. 5.5, right)

When there were no crowders in the system, there was very limited cluster formation (Fig. 5.6 - top). In contrast, large clusters formed when a 30% volume fraction of crowder was added to mimic the excluded volume typically present in the cytoplasm, suggesting that macromolecular crowding can be crucial to nucleate and stabilize synDrop mesoscale networks (Fig. 5.6 - middle). However, when we further increased the crowder volume fraction to 50% (mimicking crowder concentrations in osmotically compressed cells), we observed a larger number of smaller droplets (Fig. 5.6 - bottom). Similar results were also obtained by tracking the number of molecules within the largest cluster (Fig. 5.7 - left). The initial growth rate of average cluster size increased with crowder volume fraction (Fig. 5.7 - right), suggesting that nucleation was promoted by macromolecular crowding, as indicated by the increasing values of the exponent α obtained from a power law fit of the initial growth rate (from 0% to 30% to 50%). However, under high crowding conditions (e.g., 50% volume fraction) cluster size was limited at late time points. These results are consistent with our experimental data that physiological crowding ($\sim$ 30%) appears to be op-

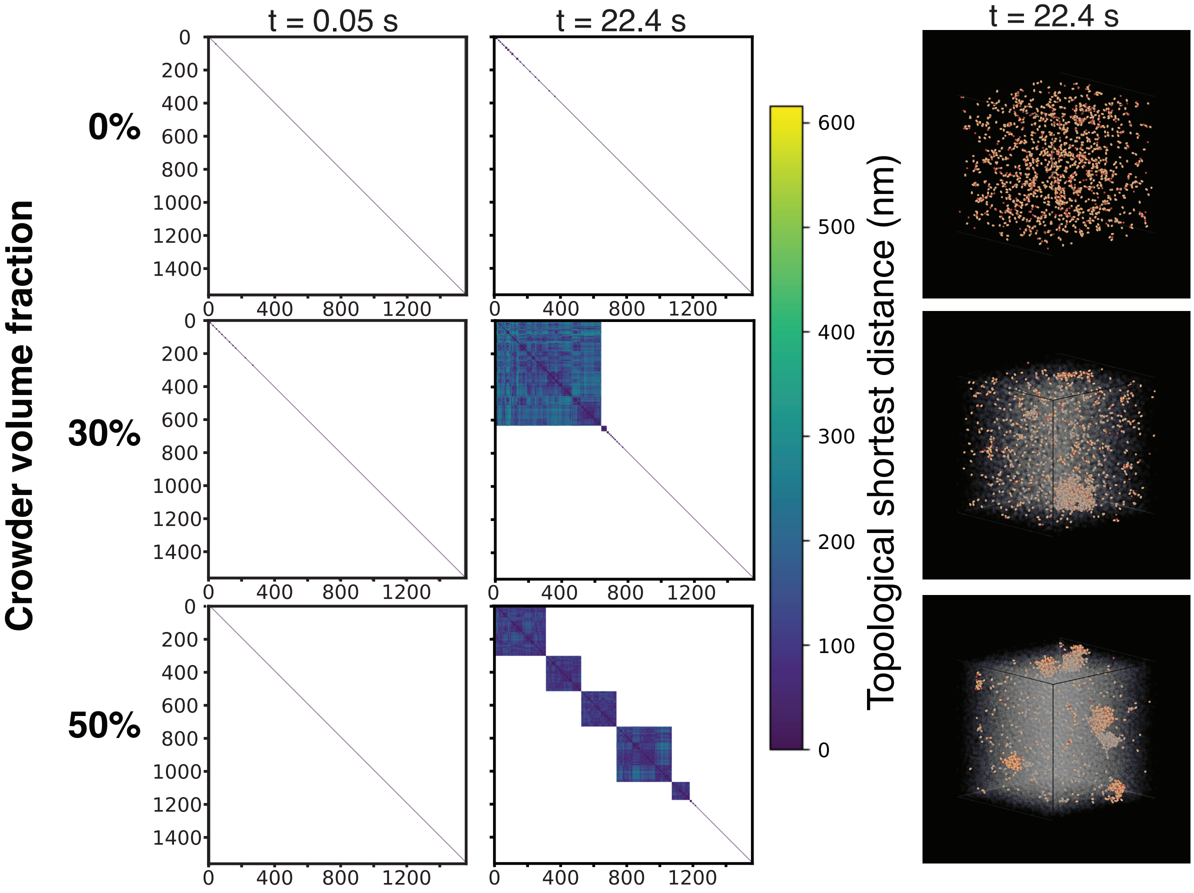

Figure 5.6: Graph theory network analyses (left) of cluster formation at early and later times with corresponding simulation renderings at later times (right), for three different crowder fractions (0%, 30% and 50%, from top to bottom)

timal for the formation of large synDrops. Molecular crowding plays contrasting roles in droplet nucleation and growth. While it is crucial for droplet nucleation, it also inhibits droplet growth.

To further investigate the molecular basis of frustrated synDrop growth in the presence of excessive macromolecular crowding, we plotted the average diffusivity for each cluster as a function of the cluster size. We found that diffusivities decreased as a function of cluster size as expected, and were reduced overall when crowder volume fractions were increased (Fig. 5.8), consistent with our hypothesis that crowding frustrates coalescence by reducing cluster diffusivities. This effect is particularly pronounced under conditions of excess macromolecular crowding.

Finally, we investigated the molecular basis of the promotion of droplet nucleation by macromolecular crowding. We hypothesized that increased macromolecular crowding could favor binding interactions, as previously reported [468]. To assess this idea, we performed MD simulations on a simplified monomeric system where the two synDrop components (hexamers and rods) each had only a single available (*active*) binding site (1,1), as opposed to (6,2). The rationale of using a monovalent system here rather than the full synDrop system was to exclude other factors that affect calculations of chemical bond properties, such as changes in coordination numbers for hexamers and dimers, which increase with crowding. We then extracted the effective dissociation constant (K_d) under different volume fractions of crowders by quantifying the number of bonds formation at equilibrium. The effective K_d was indeed reduced (affinity was increased) in simulations with increased crowder volume fractions, performed for an intermediate binding affinity case ($\varepsilon = 10.8 k_{\mathrm{B}}T$) (Fig. 5.9). Calculation of effective K_d and k_{off} can help in determining the effective binding rate (k_{on}), which is k_{off} divided by K_d.

In conclusion, a combination of *in vivo* experiments and simulations helped in jointly supporting the model that macromolecular crowding promotes droplet nucleation by reducing the effective K_d for chemical bond formation, but also inhibits droplet growth by reducing droplet diffusivity, therefore kinetically frustrating coalescence of small droplets into larger structures.

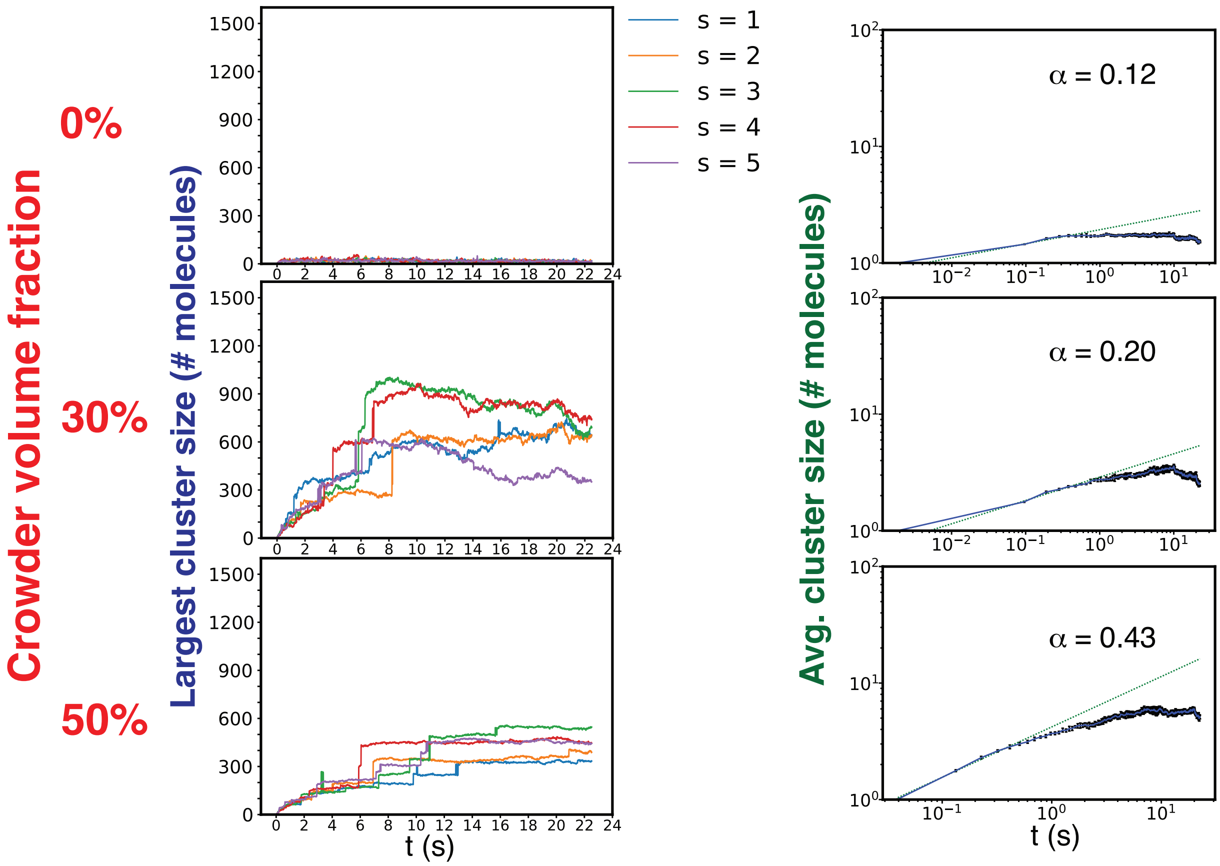

Figure 5.7: Increasing macromolecular crowding promotes synDrop nucleation but inhibits growth or coalescence, shown here for three different crowder fractions (0%, 30% and 50%, from top to bottom). (Left): Number of molecules within the largest cluster over time from five replicate simulations, denoted by different colors, and (Right): Averaged cluster size (number of molecules) over time from five replicate simulations. The dashed line represents the power law fit for the initial 0.5 s, exponent denoted as α. Error bars are standard deviation (SD) of the averaged values of the five repeats.

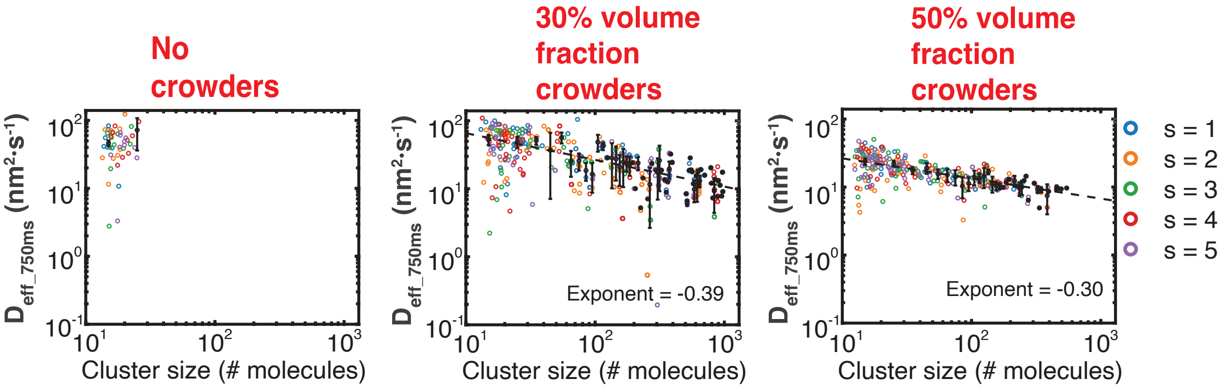

Figure 5.8: Increasing macromolecular crowding promotes synDrop nucleation but inhibits growth or coalescence. Cluster diffusivity versus cluster size (number of molecules) shown here on the log-log scale, for three different crowder fractions (0%, 30% and 50%, from left to right) . The black data points represent the mean of averaged values from five repeats, and the error bars correspond to the SD among these averaged values. The dashed black line represents the linear fit on the log-log scale and the fitted slope is labeled as the exponent.

5.6.2 NON-THERMAL ACTIVITY INSIDE THE CELLS PROMOTES DROPLET GROWTH

We wondered if features of the cytoplasmic environment other than macromolecular crowding could impact synDrop assembly. In addition to being crowded, the cytoplasm is also far from equilibrium due to ATP-dependent activities. Cellular metabolism was previously shown to strongly affect the motion of mesoscale particles [494]. We therefore hypothesized that ATP-dependent cellular activities might affect synDrop formation by promoting their motion and therefore driving coalescence of small droplets into larger structures.

It was observed in experiments that cellular active matter is crucial for both synDrop diffusivity and growth in both yeast and HeLa cells. The dynamics of the actomyosin cytoskeleton are an important source of cellular motion [495]. It was therefore hypothesized that actomyosin contractility might agitate the cytoplasm and increase synDrop motion. It was eventually found that actomyosin dynamics is the dominant mechanism that increases mesoscale diffusivity in the cytoplasm of mammalian cells and is required for the formation of large synDrops.

An important point to understand in this context is whether reduced diffusivity of synDrops is

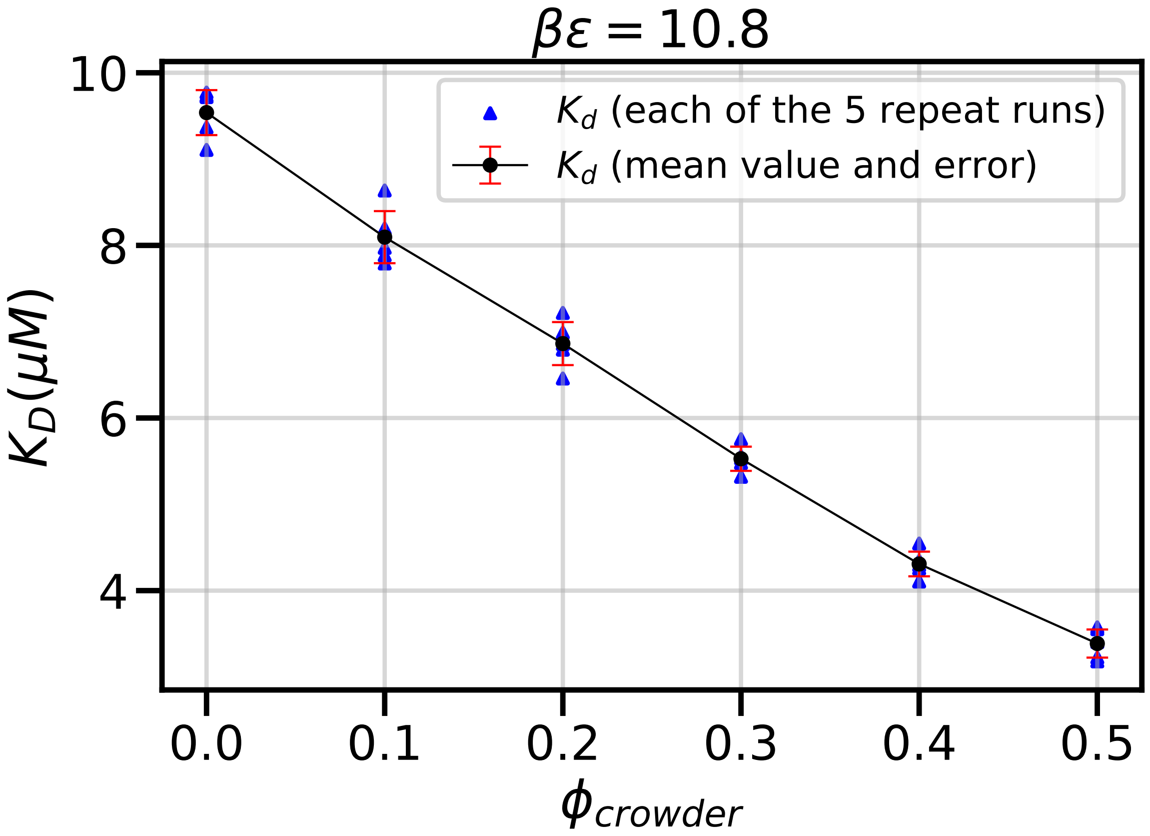

Figure 5.9: Effective dissociation constants (K_d) of a simplified monovalent system as a function of crowder volume fraction ϕ_{crowder}, for a binding affinity of $\varepsilon = 10.8 k_{\text{B}}T$. Error bars are standard deviations calculated from five repeats for a given crowded volume fraction.

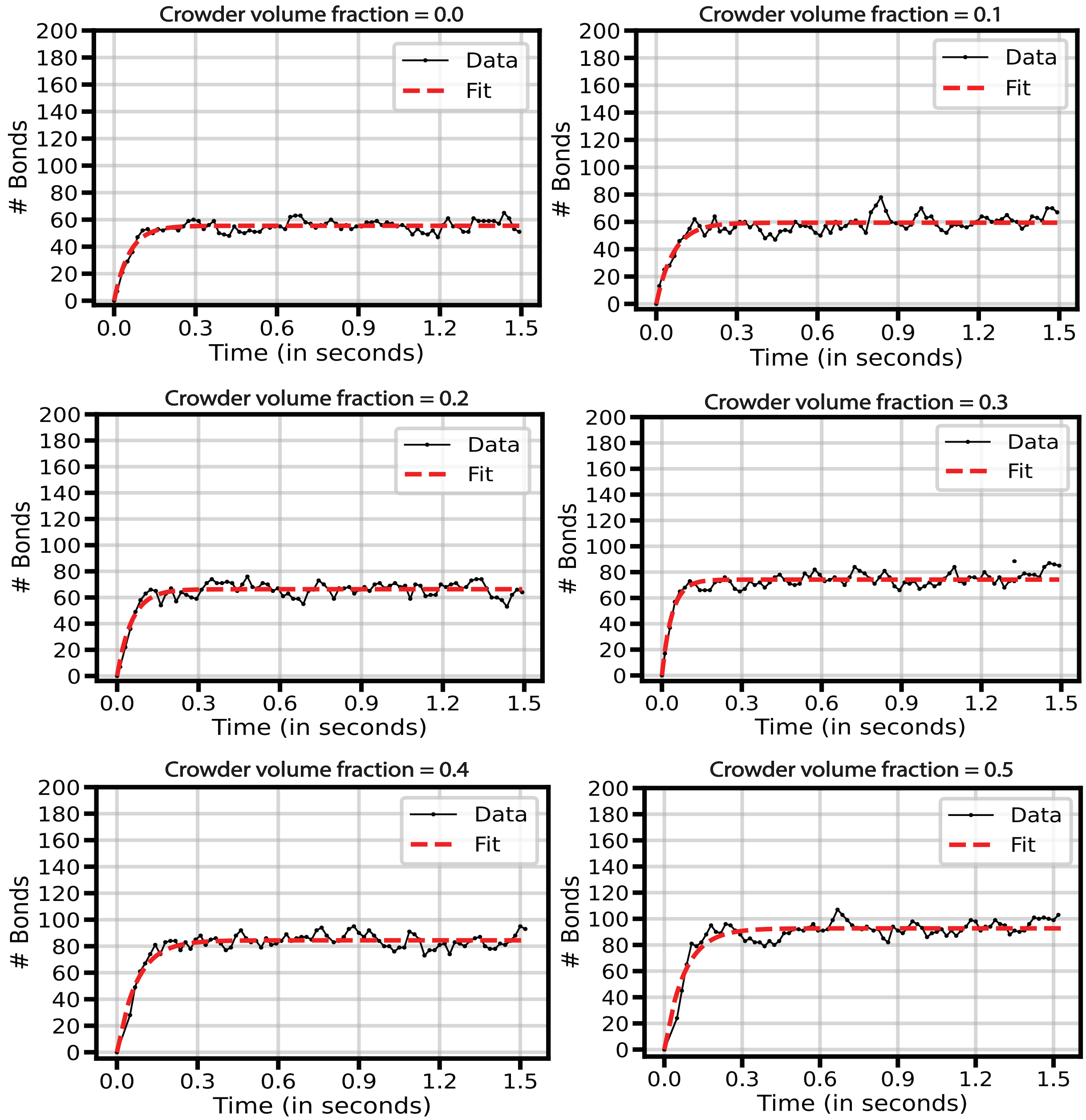
Crowder volume fraction = 0.0

Crowder volume fraction = 0.1

Crowder volume fraction = 0.2

Crowder volume fraction = 0.3

Crowder volume fraction = 0.4

Crowder volume fraction = 0.5

Figure 5.10: Number of dynamic bonds formed plotted against time (in seconds) for the simplified monovalent system MD simulations (binding affinity of $\varepsilon = 10.8 k_{\mathrm{B}}T$), for 6 different crowder volume fractions (0.0-0.5). The bond count at equilibrium B_{eq} was extracted from the fit performed on the data (to an exponential growth function) for each of the cases (fits are shown by the red dotted curves).

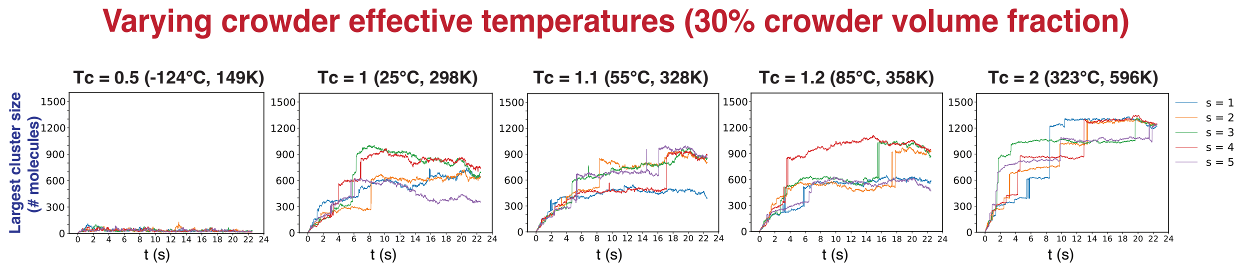

Figure 5.11: Analyses for MD simulations performed using HOOMD-blue keeping a constant 30% crowder volume fraction but varying crowder effective temperatures are shown here. Values of effective crowder temperatures are shown relative to room temperature in units of Kelvin: 0.5, 1, 1.1, 1.2, 2: Number of molecules within the largest synDrop cluster over time from five replicate simulations, denoted by different colors.

the main cause of growth inhibition upon ATP depletion, and from the experiments performed to test this, it was concluded that increasing droplet local diffusivity was insufficient to rescue synDrop growth. Additional ATP-dependent cellular activities are therefore, necessary to promote synDrop growth.

We attempted to model the role of cellular active matter using our MD simulations. To achieve this, we used a simple approximation of altered environmental motion by adding frequency-independent isotropic noise to vary the effective temperature of crowders [488, 489], while keeping the temperature of the synDrop components constant. We observed a positive correlation between the largest cluster size and the effective temperature of the crowders (Fig. 5.11). When we plotted cluster diffusivity versus cluster size on a log-log scale, we observed individual cluster diffusivities were slightly higher with higher effective crowder temperatures (Fig. 5.12). Furthermore, cluster diffusivity roughly decreased with cluster size as a power law: Diffusivity related to temperature with a negative exponent (Fig. 5.12). This exponent was slightly less negative at higher effective crowder temperatures (Fig. 5.13). However, this increase in cluster diffusivity was relatively modest, implying that other factors may contribute more significantly to the increased mesoscale assembly at higher crowder effective temperature, supporting the experimental results within cells. In particular, we found the initial growth rate of average cluster size increased with

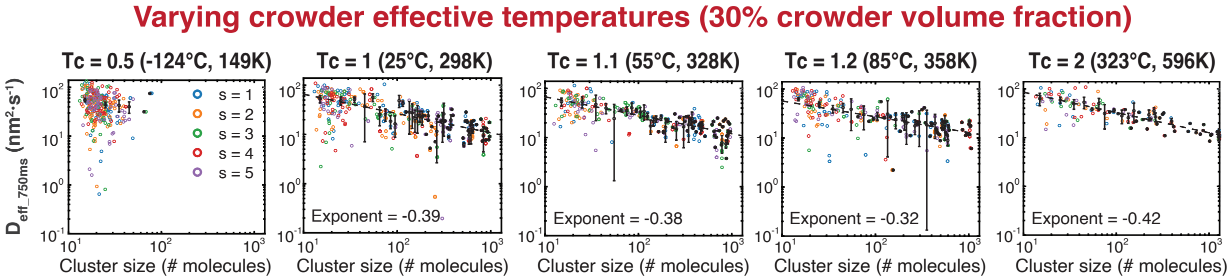

Figure 5.12: Cluster diffusivity versus cluster size (number of molecules). The black data points are the mean of five replicate simulations, error bars are SD, dashed black line is the linear fit in log space with exponent (slope) labeled.

the effective temperature of crowders (Fig. 5.14, Fig. 5.15), which could potentially contribute to the larger cluster sizes at higher crowder effective temperatures in MD simulations.

Given that coalescence dominates synDrop growth, the growth process is intrinsically linked to droplet motion. Multiple intracellular factors can influence droplet motion, including macromolecular crowding, viscoelasticity, and poroelasticity [496]. Non-equilibrium ATP-dependent cellular activities can modify all of these factors. At small length-scales (< 100 nm), ATP-dependent cellular activities may change the spatial distribution and dynamics of macromolecular crowders. At larger length-scales (> 100 nm), cellular structures including membranes and the actomyosin cytoskeleton, both of which undergo dynamic ATP-dependent fluctuations, have strong impacts on mesoscale confinement and elasticity [495, 497]. Droplet trajectories were therefore examined more closely in experiments to gain an insight into how longer-range confinement and elasticity relate to synDrop growth. It was found that ATP-dependent activities reduce confinement in the cytoplasm.

The experimental results are consistent with a model where the diffusivity of droplets is influenced not only by macromolecular crowding [304] but also by additional factors that define longer-range confinement. The actomyosin cytoskeleton dynamics is the dominant ATP-dependent activity that reduces confinement in mammalian cells. In addition to driving ATP-dependent motion, the cytoskeleton also plays a critical role in determining cellular elasticity.

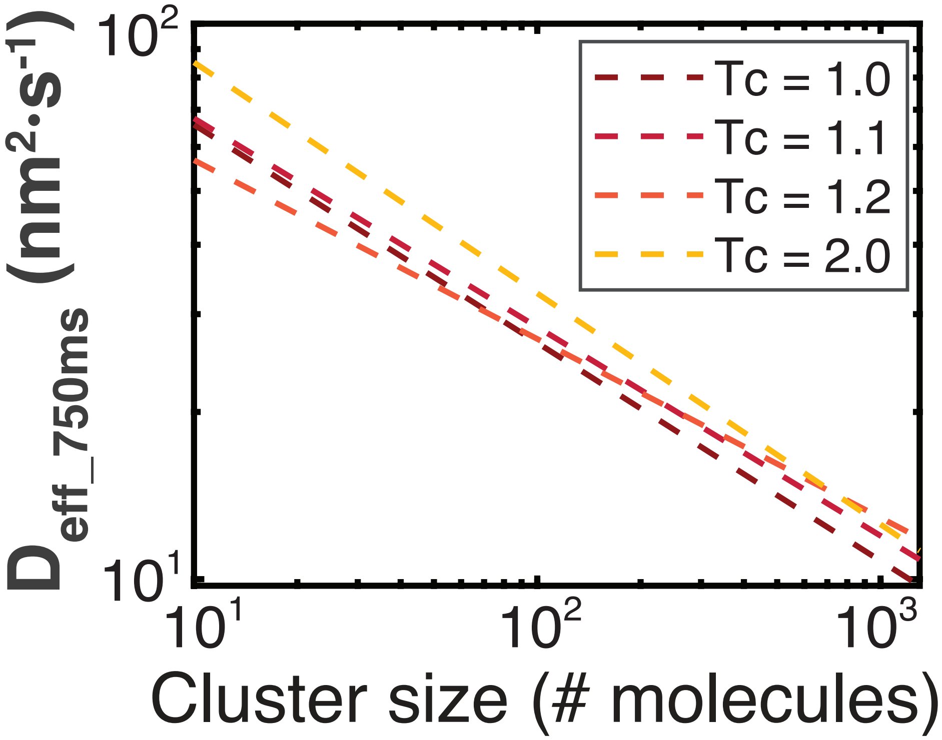

Figure 5.13: Cluster diffusivity versus cluster size (number of molecules). Plot showing an overlay of linear fitted lines in log space for four different effective temperature conditions.

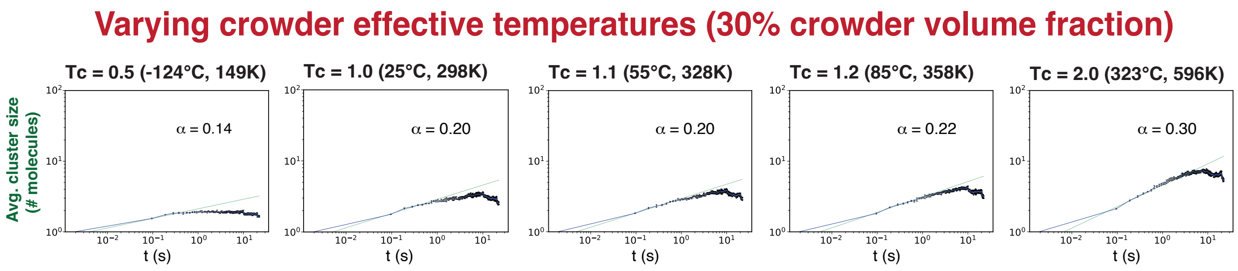

Figure 5.14: Analyses for MD simulations performed using HOOMD-blue keeping a constant 30% crowder volume fraction but varying crowder effective temperatures are shown here. Values of effective crowder temperatures are shown relative to room temperature in units of Kelvin: 0.5, 1, 1.1, 1.2, 2: Averaged cluster size (number of molecules) over time from five replicate simulations. The dashed line represents the power law fit for the initial 0.5 s, with the value of the exponent α indicated. Error bars are standard deviation (SD) of the averaged values of the five repeats.

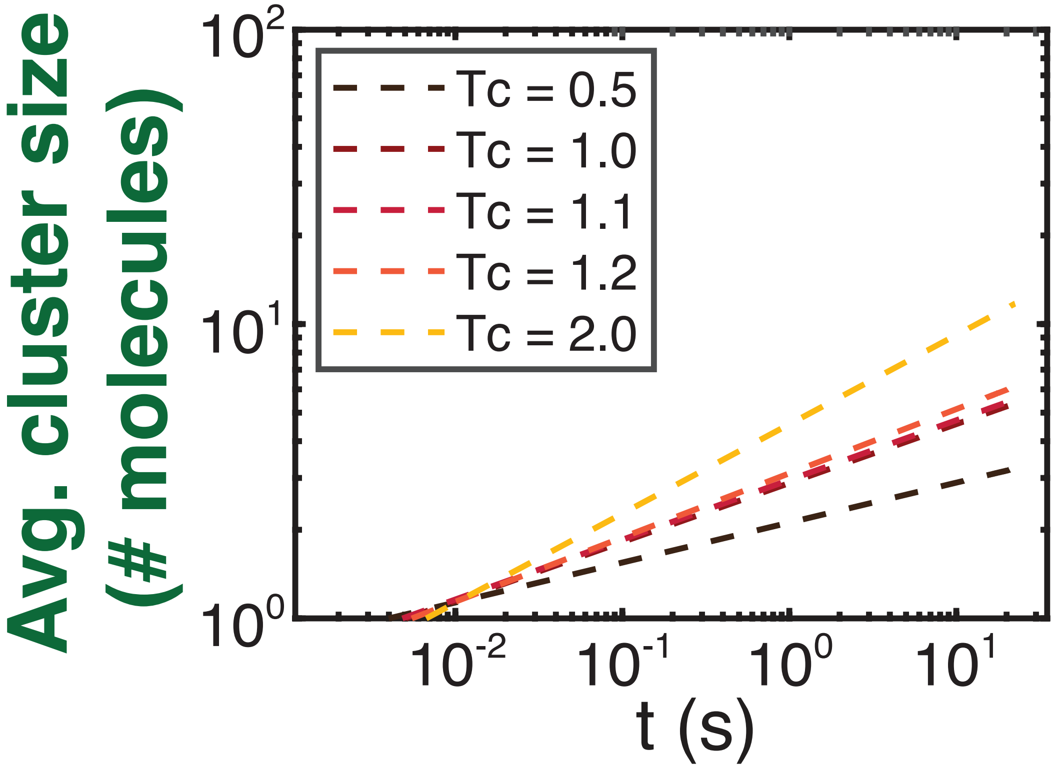

Figure 5.15: Averaged cluster size (number of molecules) over time from five replicate simulations. Plot showing an overlay of power law fitted lines for all five effective temperature conditions.

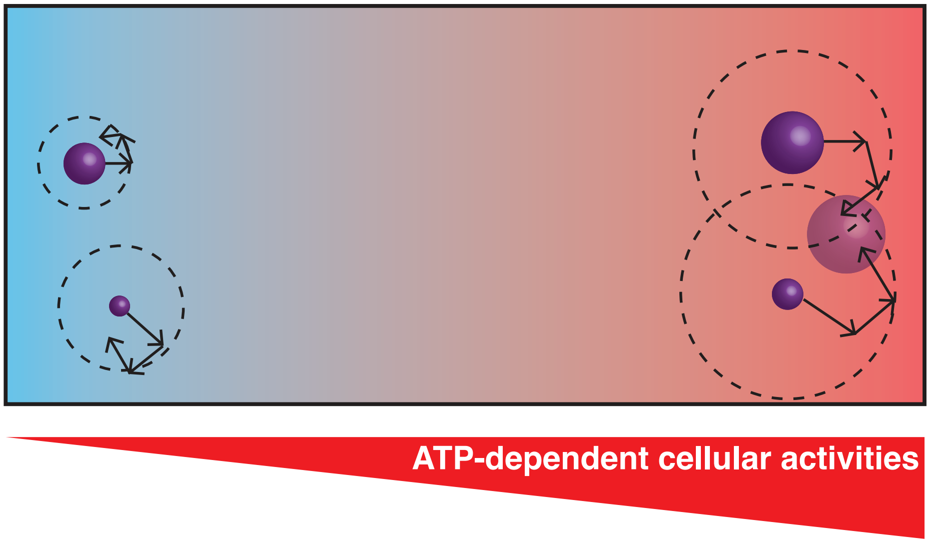

Figure 5.16: Schematic of a model that can explain how ATP-dependent cellular activities may influence droplet growth.

[470]. It was observed that either loss of ATP or inhibition of actomyosin dynamics increases the elasticity of the mammalian cytoplasm. These results support a model in which the actin cytoskeleton promotes long-range structural rearrangements and thereby reduces elasticity and confinement in the cytoplasm. The consequent increase in synDrop motion would promote droplet growth through coalescence (Fig. 5.16).

5.6.3 Effect of binding affinity on the coalescence of droplets

We explored the impact of binding affinities on cluster formation in both no-crowder conditions (Fig. 5.17) and conditions with a 30% volume fraction of crowders (Fig. 5.18). By quantifying the median largest cluster sizes at various binding affinities, we identified the phase transition behaviors in both conditions, with slightly different transition binding affinities. Notably, in the presence of crowders at 30% volume fraction, the phase transition occurred at a lower binding affinity (around 9 - 10 $k_{\mathrm{B}}T$), as compared to the no-crowders condition (for which the transition

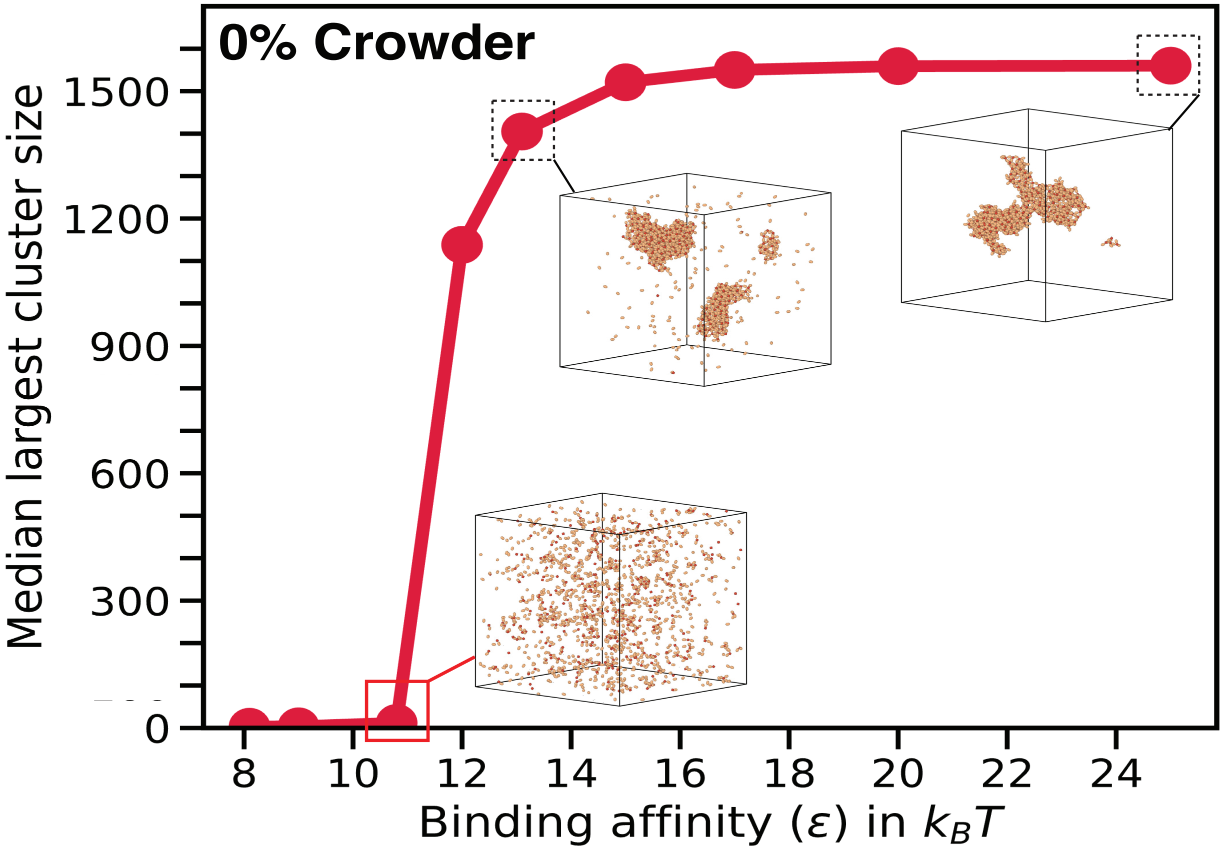

Figure 5.17: Median largest cluster sizes among five repeats plotted as a function of the binding affinity (ε) at 0% volume fraction of crowders and for a crowder temperature $T_c = 1.0$. Representative snapshots are shown for binding affinities 10.8, 13.1 and 25.0 $k_\mathrm{B}T$, indicative of a phase transition observed between binding affinities 11 and 12 $k_\mathrm{B}T$, beyond which the cluster sizes increase dramatically because of lesser unbinding probabilities. The binding affinity ε is varied here by changing the unbinding rate constant k_off, keeping k_on fixed. The binding affinity of 10.8 $k_\mathrm{B}T$ has been used for all subsequent analyses.

occured around 11 - 12 $k_{\mathrm{B}}T$ binding affinities).

It is important to mention that the drop in the largest cluster size at the highest binding affinity (ε = 25.0 $k_{\mathrm{B}}T$) under the 30% crowder volume fraction condition is due to the slower dynamics in cluster formation within the same simulation times, leading to kinetic trapping and slower fusion in forming large clusters. This is a point of difference from the case of no crowders where, for ε = 25.0 $k_{\mathrm{B}}T$, almost all of the synDrop components were present in one giant cluster.

Furthermore, when we quantified the differences in the largest cluster sizes between these two conditions and plotted them as a function of binding affinity (Fig. 5.19), a peak emerged at ε = 10.8 $k_{\mathrm{B}}T$. This observation suggests that at this binding affinity, the crowder volume fraction has the most significant effect on cluster formation. To capture the full dynamic range of the system, we chose this binding affinity (ε = 10.8 $k_{\mathrm{B}}T$), for all other MD simulation analyses to study the effects of macromolecular crowding and non-equilbrium activity in the cytoplasm.

5.7 MD SIMULATION ANALYSES

We used graph-theory based methods for analyzing MD simulations. Each molecule within MD simulations had a unique number identifier and was treated as the node for the graph. Bonds formed at each time point were recorded based on molecule pairs that formed each bond, and were treated as the edges for the graph. The graph at each time point was then constructed by providing both node and edge information inputs using the *igraph* [498] package in python. To identify clusters, a distance matrix was first calculated based on the topological shortest path that links each pair of molecules. Subsequently, a hierarchical clustering algorithm was employed on the distance matrix. This led to the reordering of molecule sequences, with molecules within each cluster being grouped together. Cluster size was then determined based on the number of molecules that were within each cluster. Locations of each molecule were also recorded at each time point.

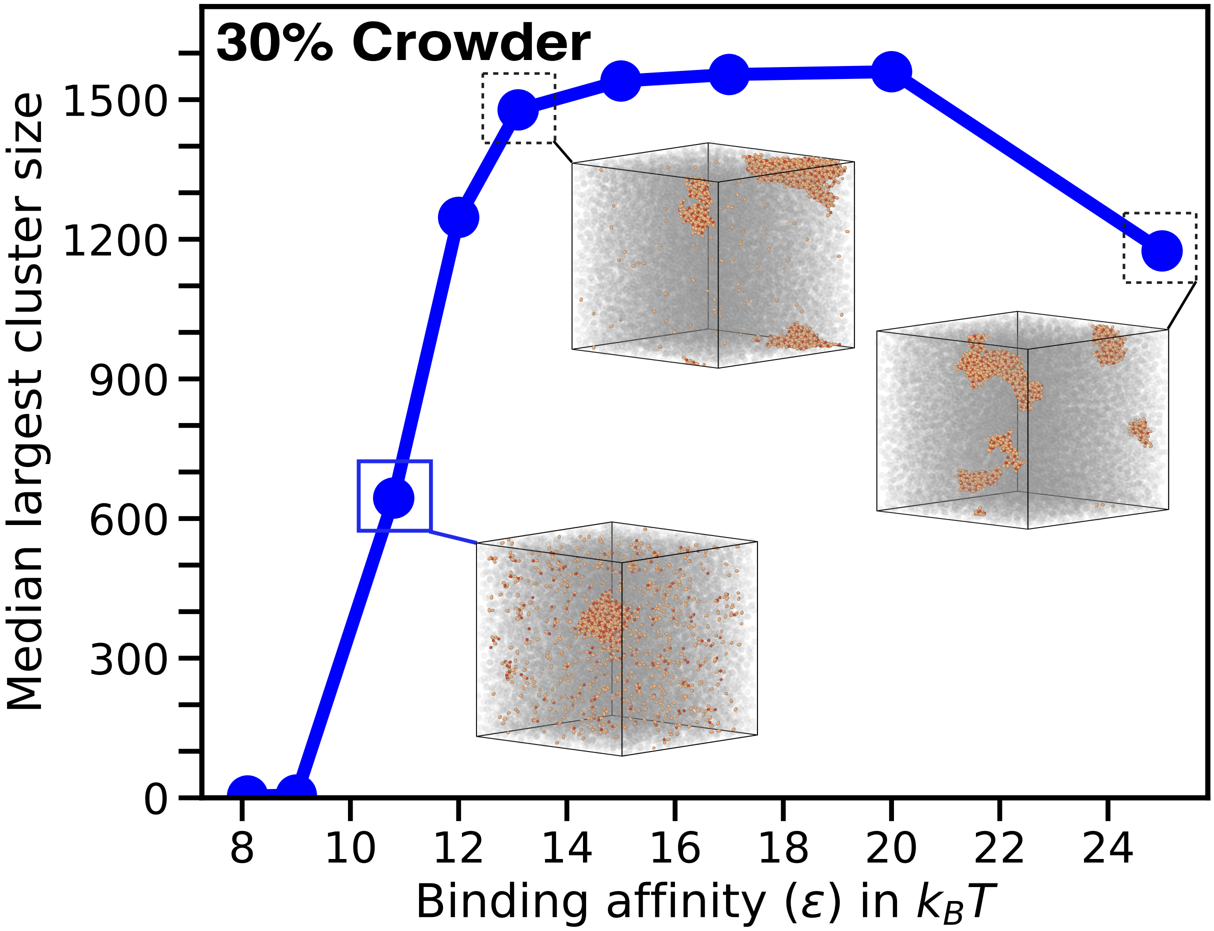

Figure 5.18: Median largest cluster sizes among five repeats plotted as a function of the binding affinity (ε) at 30% volume fraction of crowders and for a crowder temperature $T_c = 1.0$. Representative snapshots are shown for binding affinities 10.8, 13.1 and 25.0 $k_\mathrm{B}T$. A phase transition is observed between binding affinities 9 and 10 $k_\mathrm{B}T$.

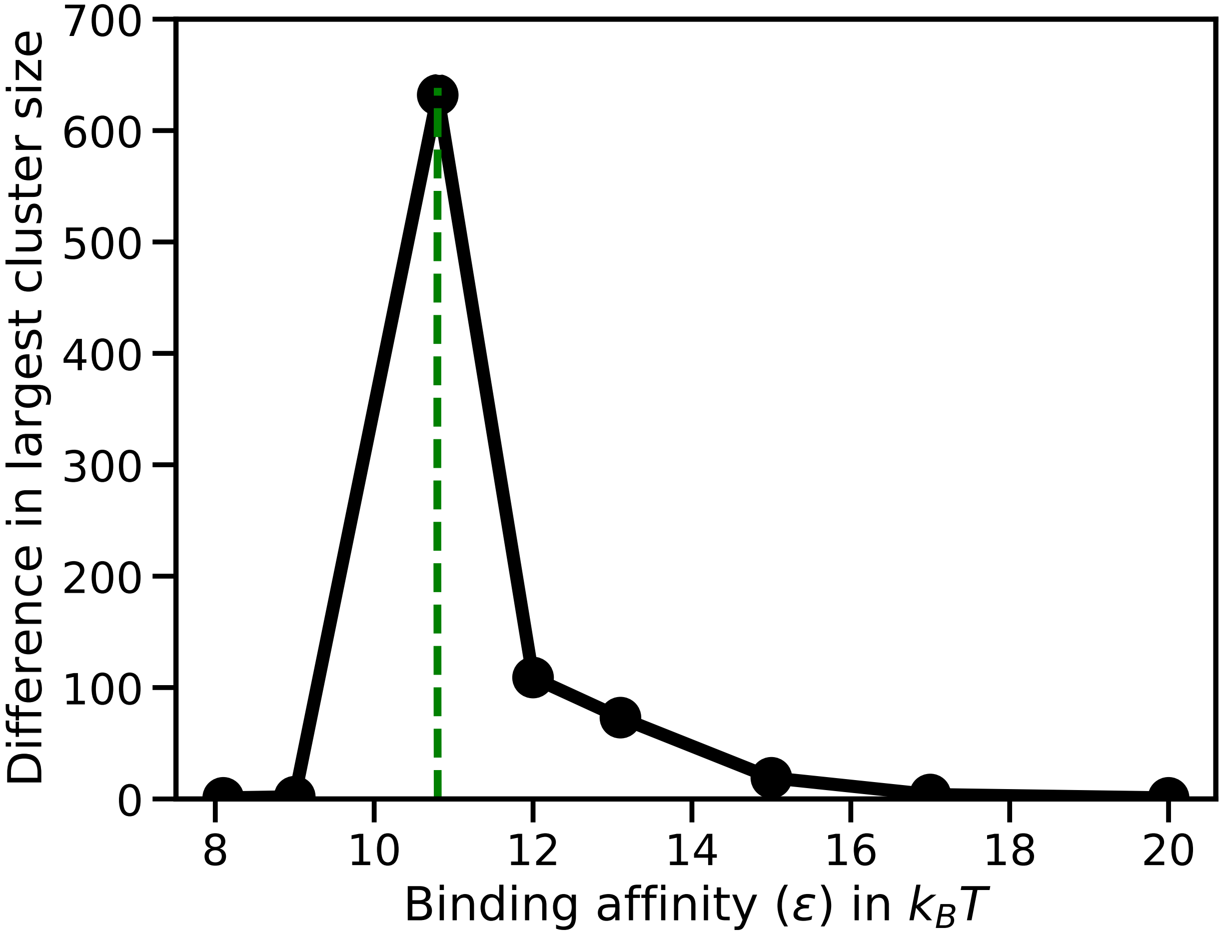

Figure 5.19: Differences in the median largest cluster sizes between the 2 crowder volume fraction conditions (0% and 30%) plotted as a function of the binding affinity (ε) and for a crowder temperature $T_c = 1.0$. A peak emerged at $\varepsilon = 10.8\ k_\mathrm{B}T$, suggesting that at this binding affinity, the crowder volume fraction has the most significant effect on cluster formation.

To calculate cluster diffusivity, clusters with size larger than 10 molecules were first identified at each time point. Pairwise clusters from consecutive time points were connected from the last time point by determining the largest number of same nodes, thus forming trajectories. If a cluster's size changed by 20 within a time interval, it was considered as a new cluster and tracked as a distinct trajectory. Only trajectories with more than 10 time points were selected for calculating cluster diffusivities, where mean squared displacement of the cluster's center of mass for each trajectory was fitted over the first 10 time intervals. All analyses were performed using in-house Python3 code.

To determine the effective dissociation constants (K_d) of the chemical bonds, we analyzed the kinetics of bond formation in monomeric MD simulations until equilibrium was achieved. In the monomeric system (where the dimers and hexamers are in a 1:1 stoichiometric ratio), we reduced the available binding sites of two components from 6 and 2 to 1 and 1 each. By fitting the data to an exponential growth function $B(t) = B_{\text{eq}}(1 - \exp(-kt))$, we extracted the number of bonds formed at equilibrium B_{eq}. Subsequently, K_d was calculated based on the concentration of all species at equilibrium, using the formula for a dimerization reaction

$$D + H \Leftrightarrow DH \tag{5.3}$$

$$K_d = \frac{[D][H]}{[DH]} = \frac{N_D N_H}{N_{DH} V} \tag{5.4}$$

, where V is the volume of the simulation box. 'D' and 'H' correspond to the dimer and hexamer species respectively.

To roughly match simulation time scales to experimental ones, the mean-squared displacement of 40 nm GEM particles in simulation were fit to the Einstein diffusion relation in 3D $MSD(t) = 6Dt$ for long times, and D was obtained in the units of $\mu m^2/\tau$. The unit of time $\tau = 7.5 \times 10^{-8}$ seconds was then obtained by matching this D to an approximate cellular value of

$\mu m^2/s$.

5.8 Discussion

Membraneless organelles carry out many essential cellular functions within cells [463]. Therefore, it is important to understand the spatial and temporal information associated with membraneless organelles formation and dissolution – how cells regulate and coordinate this information. Many studies have focused on specific chemical signals [499]; however, few studies have looked at physical cues, which are indispensable but often neglected. Here, we demonstrated that intracellular macromolecular crowding promotes droplet nucleation by reducing effective dissociation constants of binding reactions but inhibits droplet growth by reducing droplet diffusivities, while ATP-dependent cellular activity promotes droplet growth by fluidizing cellular environment through promoting long-range structural rearrangements.

Macromolecular crowding has several effects on molecular assembly. First, it increases the local concentrations of molecules due to excluded volume occupied by macromolecular crowders [467]. Second, it imposes depletion-attraction forces that increase the propensity of molecular assembly [466]. The cytoplasmic excluded volume is dominated by mesoscale particles, in particular ribosomes, therefore this entropic effect is most prominent at the mesoscale. Both effects can affect binding interactions, leading to reduced effective dissociation constants [468]. Crowding agents have been shown to lower the critical concentrations for several in vitro reconstituted phase separation systems [464, 500]. However, the inhibition of the kinetics of droplet growth by excess macromolecular crowding is less studied due to the limited availability of controlled in vivo phase separation systems.

ATP-dependent cellular activities impart a dynamic and non-equilibrium nature to the intracellular environment, introducing non-thermal forces that amplify random fluctuating motion beyond thermal effects [501]. The cytoskeleton, a key contributor to ATP-dependent activities, exhibits unique time-dependent material properties [495, 502]. On shorter timescales, it behaves as semiflexible polymers primarily influenced by thermal fluctuations, resulting in subdiffusive motion of attached beads. However, on longer timescales, the cytoskeleton transitions into a soft glass-like material, leading to the superdiffusive movement of attached beads through structural rearrangement driven by ATP-dependent activities. These time-dependent material properties, influenced by ATP-dependent cellular activities, extend beyond the cytoskeleton and have also been observed in the mammalian cytoplasm [503] and the membrane of red blood cells [497]. While existing studies on condensates have focused on biochemical aspects of ATP molecules [504] or ATP-consuming processes within condensates [505–507], limited research has investigated the impact of physical properties emerging from environmental ATP-dependent cellular activities on condensate formation.

synDrops have a unique combination of features that make them an ideal platform to investigate how intracellular biophysical environments affect condensates assembly. Droplet nucleation and growth dynamics can be studied on a reasonable time scale (minutes - 1 hour). In contrast to endogenous condensates, the synDrops components were designed to minimize non-specific interactions with endogenous molecules within cells, including ATP-consuming enzymes. Moreover, the well-defined protein structures and network geometry make synDrops highly amenable to simulation and analysis with graph-theoretical approaches.

Our study highlights how the intracellular environment modulates mesoscale molecular assembly through a combination of macromolecular crowding and cellular active-matter. Notably, the intracellular environment is highly heterogeneous in mesoscale diffusivity [508], reflecting local heterogeneity in macromolecular crowding and cellular activity. These physical variations may underlie the distinct behavior of droplet formation within cells compared to the theoretical prediction that droplets should thermodynamically fuse into a single entity. By actively modulating local macromolecular crowding and cellular activity levels, cells could potentially control the formation of endogenous condensates at different locations via biophysical signals. For example, increased cellular activity, such as actin dynamics near the cell cortex, could facilitate endogenous condensate formation, which might in turn contribute to the nucleation and growth of the cytoskeleton network.

We speculate that changes in the biophysical properties of cells could be sensed by their impacts on condensate assembly. Indeed, a synthetic droplet can modulate the rates of kinase reaction in response to changes in macromolecular crowding, demonstrating the feasibility of this idea in cells [509]. On the other hand, the biophysical properties of the cell interior may also change during disease progression, leading to aberrant phase separation of endogenous condensates. Our study provides a framework to guide future investigations into the effects of intracellular biophysical properties on endogenous condensate formation and dissolution and their relevance to normal biology and disease pathology.

CHAPTER 6

CONCLUSIONS AND FUTURE OUTLOOK

6.1 BRIEF SUMMARY OF THE THESIS

Soft materials, known for their flexibility and deformability [8–11], include polymers, colloids, foams, and biological materials [15–21]. Their unique properties make them essential in a wide range of applications, from materials science to biology and medicine. This thesis aims to understand the physics of self-organization in diverse soft matter systems, including materials and biological entities. Focusing on dynamic binders and utilizing Coarse-Grained Molecular Dynamics simulations with a custom HOOMD-blue plugin to enable stochastic binding and unbinding [50, 51], our research aims to elucidate the self-aggregation mechanisms in soft matter, connecting the realms of materials and biological sciences.

Before delving into detailed discussions of concluding remarks and future prospects for the thesis projects, I will present a concise summary of the key findings from the main projects.

6.2 Detailed outline of work and key findings

The prevalent method for engineering specific interactions between *patches* in colloidal materials to design programmable structures [52, 53, 187, 307] with high fidelity involves employing complementary DNA strands, whose interaction strength can be adjusted by the nucleotide sequence and length [177, 178, 187, 310–312]. The first thesis project entails the design of a coarse-grained molecular dynamics (CGMD) simulation model [50] using a simulation framework in Python, named *pyColloidomer*, designed to explore the self-assembly of colloidal liquid droplets with explicit mobile binders [240, 242, 269, 272–275], such as DNA. Central to this model is a dynamic binding and unbinding protocol ensuring detailed balance [50, 118, 193, 337], offering flexibility in controlling binding and unbinding rate constants with a tunable temperature dependence (implemented as an open-source custom plugin in C++ [336]). The simulation framework is accessible and freely available on GitHub, providing a realistic simulation of the adhesion patch formation process [161, 164, 242] using explicit mobile binders. This approach enables insights into the consequences of excluding particles from formed patches, critical for optimizing colloidomer assembly [161], and in preventing binders from being used up in colloidomer backbones in our folding studies [165, 324, 325].

The model, based on droplets with a central particle (type A) and binders, each constituting a pair of particles (types B and C) on its surface [50], mimics double-stranded tether and single-stranded sticky-end DNA used in experiments [160–163, 280, 323]. The simulation incorporates harmonic bonds and angular potentials to facilitate binder diffusion [160] and alignment along the radial vector from the droplet center, providing a comprehensive understanding of the self-assembly process. This *versatile* CG model is not only applicable to the study of mobile colloidal self-assembly, but also to liposomes [269, 319–321], cell-cell interactions at biological interfaces [38, 39, 93, 98, 100, 266], and nanoparticle gels [189, 190, 292–297, 327–330].

We investigate the tuning of the valence of assembled structures through kinetic control in the strong binding limit. The model not only effectively replicates the average behavior observed in experiments, but also we can optimize experimental control parameters to achieve the highest yield of long linear colloidomer chains [50, 161, 317, 318, 326], surpassing previous experimental conditions. We anticipate that chains can be obtained when adhesion patches form and deplete approximately half of the available binders before subsequent droplet collisions and patch formation. The relative speeds of the two competing processes, patch recruitment [242] and droplet-droplet collision, can be adjusted to influence the types of structures observed in self-assembly, thereby offering insights into kinetic control.

The temperature-controlled binding and unbinding rates allows us to setup an alternate heating and cooling protocol (with backbone and secondary interactions) that let us observe a heptamer chain collapse into all possible rigid structures, in agreement with recent folding experiments [50, 165]. In contrast to the experimental approach that aimed to design specific droplet interactions for selecting a unique folded geometry, our model demonstrates that tuning DNA interaction energy allows for the realization of all possible geometric configurations in simulations. Thus, the model is not only validated by experiments but also exhibits predictive capabilities.

Additionally, we also observed that above a certain binding strength (around $\varepsilon > 13$), the growth of a patch can follow a process characterized by two timescales, where saturation can take much longer than initial recruitment [50, 242], thus offering insights that can be leveraged to guide the assembly process in future studies. We also discovered that slowing binder motion by increasing the drag on the binders (γ_{binder}) or slowing down the binding by decreasing k_{on} at fixed bond strength ε can increase the patch recruitment time, which in turn can increase the yield of higher valences in droplet assembly. The use of *explicit* binders in our model also shows how steric repulsion between binders (designed to mimic electrostatic repulsion between DNA strands [164, 342, 343]) affects the adhesion patch size and the concentration of binders therein. The explicit binder model allows testing contributions to the free energy of patch formation [164] and patch shape, aligning with experimental predictions.

Building upon our prior work investigating the self-assembly of colloidal droplets with *mobile* binders [240, 242, 269, 272–275], our current focus involves a detailed exploration of the dynamics of adhesion patch formation between two droplets. Specifically, we aim to understand how the molecular features of the system (such as the droplet size, binding strength, excluded binder volume, binder concentration, flexibility of the harmonic springs) can be manipulated to tune the growth, shape, and geometry of the adhesion patch [39, 50, 161, 164].

This investigation extends to the impact of lateral or cis-interactions, a phenomenon crucial for enhancing binder recruitment, particularly observed in cellular junctions where E-cadherin [38, 39, 93, 284] proteins mediate cell-cell adhesion [100]. Hence, we examine the consequences of introducing lateral binding interactions [39, 281, 282, 284, 285] between binders on the same droplet in the context of adhesion patch formation dynamics. In our coarse-grained model, we introduced Lennard Jones attractions [356–359] between the inner binder particles on the same droplet with varying interaction strengths. Our simulations reveal that in the presence of lateral binding (or *cis*-interactions), the binders exhibit a more ordered packing into the adhesion patch [39, 284, 285]. Moreover, a significantly higher number of binders can be recruited into the adhesion patch compared to scenarios where no *cis* interactions are present. This observation reinforces the phenomenon of *cis-trans* cooperativity [39, 93, 281, 282], which has also been noted in experimental studies. Recent experiments report that the decay rate of the fraction of droplet monomers over time is accelerated in the presence of lateral interactions. In our coarse-grained simulations of droplet assembly with lateral interactions, our current focus is on investigating the parameter regime that substantiates this observed phenomenon. All of the above mentioned directions constitute ongoing work in progress.

Our dynamic binding and unbinding protocol found an interesting application in a recent collaboration with the Truskett, Rosales, and Milliron research groups (University of Texas at Austin). This ongoing work involves the development of structural design principles [399, 400] for gels assembled from multi-functional nanocrystals [189, 190, 286–298] and macromers featuring discrete functional groups, such as tetraPEG [299–301]. In an integrated coarse-grained modeling platform established in collaboration with the Truskett group, we treat the building blocks as *patchy* colloids with discrete binding sites [189, 190, 292, 293] capable of dynamic binding or unbinding [50]. This approach, employing dynamic bonding among the components, facilitates the design of responsive materials [28, 58, 77]. These colloids can form networks through a linker-mediated strategy [189, 286, 296, 298], involving the reversible connection of macromers or nanocrystals by bifunctional molecules [302]. Alternatively, they can be implicitly modeled as bonds between binding sites, exhibiting the properties of a semiflexible polymer [401] chain. Currently, we are working on building the simulation setup for modeling both explicit and implicit linkers. We are also exploring the influence of capping molecules [296, 298, 303] (that dynamically compete with linkers for binding to colloids) on the structure and dynamics of the gel networks. Furthermore, the integration of our existing dynamic binding and unbinding model grants kinetic leverage over the reaction rates of binding/unbinding, which can influence the dynamics and morphology of kinetically arrested gels [402–404].

Intracellular environments are characterized as viscoelastic, highly crowded at the mesoscale [304, 465, 473], and far from thermodynamic equilibrium. These distinctions arise from the complexity of intracellular conditions, including the constant action of energy-consuming processes [305, 306, 472]. As a versatile application of our dynamic binding and unbinding model to an intriguing biological problem of interest, we also developed an *in silico* coarse-grained molecular dynamics (CGMD) simulation platform tailored for a synthetic liquid-liquid phase separation (LLPS) system named *synDrops* [478, 480–484], consisting of 2 protein components, a hexamerization and a dimerization domain [482–484], respectively. This endeavor aims to investigate how the cellular environment influences the formation of condensates. In our CGMD model (simulations run using HOOMD-blue [50, 51, 334, 335]), binding occurs between a hexamer and a dimer [51, 485, 486] through complementary interaction points at the end of these objects. In addition, we included a third agent to mimic ribosomes (represented by spheres with no binding interactions), which are the dominant macromolecular crowders [304, 467] in the cytoplasm. The well-defined structures and binding interactions between the two synDrop components enabled us to quantify droplet network structures with graph theory based analyses [498].

Our results suggest that the combined influences of crowding and active matter [474–477] in the cytoplasm promote mesoscale molecular assembly, providing improved predictive understanding of biomolecular condensate formation *in vivo.* More specifically, we observed that macromolecular crowding facilitates condensate nucleation while hindering droplet growth through coalescence [476, 490–493]. In the absence of crowders in the system, cluster formation was highly limited. However, upon introducing a 30% volume fraction of crowders to simulate the excluded volume effect typical in the cytoplasm, substantial cluster formation occurred, indicating the crucial role of macromolecular crowding in nucleating and stabilizing synDrop networks. Interestingly, with a further increase in crowder volume fraction to 50%, we observed a higher number of smaller droplets. Our simulation findings align with experimental data, suggesting that physiological crowding at approximately 30% is optimal [51] for the formation of large synDrops. We also observed that crowding frustrates coalescence (growth) by reducing cluster diffusivities. This effect is particularly pronounced under conditions of excess macromolecular crowding. We also determined the effective dissociation rate (K_d) under various crowder volume fractions by quantifying the equilibrium number of bond formations in a monomeric system. The simulations showed a reduction in effective K_d (increased affinity) with higher crowder volume fractions, suggesting that increased macromolecular crowding may enhance binding interactions [468].

The inhibition of growth is overcome by ATP-dependent cellular activities. Actomyosin dynamics [495, 497] emerged as the primary mechanism [470] driving increased mesoscale diffusivity in mammalian cell cytoplasm, essential for the formation of large synDrops. To investigate the influence of non-thermal cellular activity [488, 489, 494] on the formation of synDrops through molecular dynamics simulations, we introduce a distinct effective temperature T_c for the crowders, achieved by employing separate Langevin [345] thermostats in HOOMD-blue. A positive correlation between the effective temperature of the crowders and the size of the largest cluster was found, and also the individual cluster diffusivities were slightly higher with higher effective crowder temperatures. The observed rise in cluster diffusivity was relatively modest, suggesting that other factors may play a more significant role in the enhanced mesoscale assembly at higher crowder effective temperatures (supporting experimental observations).

We also investigated the impact of binding affinities on cluster formation under both no-crowder conditions and conditions with a 30% volume fraction of crowders. We identified phase transition behaviors in both conditions, with slightly different transition binding affinities [51]. Notably, in the presence of crowders at a 30% volume fraction, the phase transition occurred at a lower binding affinity, compared to the no-crowders condition.

6.3 Future Research Directions

Our advanced coarse-grained simulation platform, incorporating Monte Carlo moves [118, 193, 337] to explicitly model binding/unbinding [50, 336] kinetics with mobile binders [240, 242, 269, 272–275], presents a methodological breakthrough that can be expanded to simulate a variety of related phenomena in soft matter physics. Preliminary data suggests that our coarse-grained (CG) model for colloidal droplets with explicit mobile binders adeptly reproduces the observed behavior in the folding [162, 163, 165] of two-dimensional colloidomer homopolymer chains. In future work, we intend to utilize our model for comparative analysis, contrasting the structures and pathways generated through the use of explicit binders with those produced using highly simplified models [161, 351]. Additionally, we plan to extend our folding studies to three dimensions by removing confinement, providing a detailed exploration of folding pathways [165, 510, 511] that may be challenging to quantify experimentally.

While our model captures what we consider to be the most crucial features of systems with mobile binding sites, there are simplifications that we intend to investigate in future research.

For instance, the inclusion of a spring between the center of the droplet and binders allows for variation in the binders' vertical position. By tuning this parameter, we can explore the tendency to form a planar adhesion patch — an aspect important in the case of deformable droplets [512], a regime yet to be explored in our simulations. Our current work employs harmonic springs, and we plan to investigate the differences that arise when more complex stretching behavior is taken into account (such as use of FENE bond potentials).

In future work, our aim is to employ the coarse-grained (CG) model with explicit binders to assess the contributions to the free energy [394] of patch formation and patch shape [164], as predicted experimentally. We intend to utilize advanced enhanced sampling techniques, such as umbrella sampling [395], to quantitatively measure the free energy of the adhesion process for droplets that bind through these mobile binders on the surface.

A pivotal future direction for this project involves attempting to incorporate the effect of forces [97, 98, 193] in the unbinding kinetics for cellular adhesion proteins, such as cadherins [38, 39, 93, 284]. This exploration is motivated by the desire to model *slip* and *catch* bonds [97, 98, 101, 396] commonly observed in various mechanosensitive biophysical systems [38, 39, 93, 99, 100]. Cadherins are recognized for their ability to undergo force-dependent tuning of adhesion [39, 281, 282, 284, 285], functioning as catch-bonds under tensile stress [101, 396] — rigorously defined as an increase in lifetime with increasing force. Using molecular dynamics (MD) simulation techniques like steered MD [397] or constant-force MD, our aim is to quantitatively ascertain the *threshold* force for rupture when two droplets with mobile binders are pulled apart, initially implementing standard unbinding kinetics. Subsequently, we are also intrigued by understanding how this threshold rupture force varies when employing *slip* [99] and *catch* [101, 371, 375, 398] bond unbinding kinetics.

The exploration of structural design principles [399, 400] for colloidal gelation using our integrated coarse-grained simulation approach (employing a *patchy* particle treatment of colloids with fixed binding sites [189, 190, 292, 293, 298] coupled with our dynamic binding/unbinding protocol [50]) opens up numerous avenues for future research. Currently, our simulation setup involves explicit bifunctional linkers [189, 286, 296, 298, 302] facilitating the bonding of colloids. However, our goal is to develop an implicit linker representation akin to our mobile binder coarse-grained model. A significant future objective is to theoretically generate and experimentally validate phase diagrams for linker-mediated star polymer [299–301, 461, 462] and nanocrystal [189, 190, 286–298] networks with both symmetric and asymmetric linkers. These phase diagrams will emphasize regions of the parameter space suitable for forming arrested-phase-separation [402–404] and single-phase equilibrium gels. Furthermore, the results will elucidate various pathways available to form these gel networks. We will assess the effects of altering the ratio of functional to inert surface ligands compared to adjusting the concentration of caps [296, 298, 303] on the phase behavior. The current dynamic binding and unbinding code needs to be adjusted to accommodate the probabilistic switching of ligands between uncapped (available for bonding) and capped (unavailable) states.

The tunability of exchange kinetics [300, 513] for caps and linkers can enable the formation of networks with qualitatively different morphologies, contingent on whether they are under thermodynamic (chains or stringy gels) or kinetic control (trapped structures with branching [50, 297, 327]). We want to employ coarse-grained simulations to determine parameter ranges where these behaviors should be accessible for networks of linked nanocrystals with caps [296, 298, 303]. Ultimately, this can serve as a guide for designing suitable control experiments. We also want to establish design rules governing how linker length and flexibility [190, 292] can affect the network bond correlation, bond persistence time [190], structure factor [189], elastic modulus [514, 515], structural relaxation time, and optical properties (such as absorption spectra [288, 294, 296, 302, 399]) of these gels. Previous experimental work has demonstrated that tuning the bond exchange kinetics and thermodynamics can alter the shear relaxation time and plateau modulus for dynamic covalent tetraPEG hydrogels [299, 300]. It will be interesting to examine whether simulations incorporating these kinetic effects at varying stoichiometries can provide insights into achieving behaviors, such as strain stiffening [514–516]. These proposed future goals could facilitate the design of materials with phase behavior and mechanical properties suitable for a diverse range of applications.

Exploring liquid-liquid phase separation in the mesoscale [304, 465, 473] organization of macromolecules within the crowded and active cellular cytoplasm, utilizing a coarse-grained simulation approach, opens up numerous potential future directions for investigation. In our current model, as described above, we simplify by assuming that the majority of crowding arises from a single agent [304, 517, 518], ribosomes, which serves as a reasonable initial approximation to the cytoplasm. We have the ability to enhance polydispersity by incorporating various crowding proteins of different sizes, potentially derived from experimental data on cytoplasmic content. For our preliminary investigation, we will explore the role of polysomes [519–521](in addition to ribosomes), which are assemblies of individual ribosomes on a single mRNA strand. The polysomes can be modeled in CG simulations as bonded chains of ribosomes with a spacing.

Currently, in our simulations, periodic boundary conditions [205] are employed. Nevertheless, we can introduce *walls* to encapsulate the contents of our system. This leads to apparent subdiffusive behavior [522] as particle motion becomes restricted after an intermediate timescale. We will further investigate the impact of explicit confinement [523] on modulating the effect of crowders on critical condensate concentration. We are also exploring the impact of altering protein concentrations (rods and hexamers) in our MD simulations while maintaining a fixed stoichiometry of 3:1 (for a given crowder volume fraction and binding affinity). This investigation aims to elucidate whether our coarse-grained MD simulations replicate phase separation phenomena [524], where a critical concentration and a well-defined phase transition exist concerning a specific property of the system, such as the size of the largest condensate.

In the current model, we account for non-equilibrium activity [488, 489, 494] in the cell by assigning a different effective temperature to the crowders (mimicking them as *active* enzymes) compared to the rest of the system, achieved through separate MD 'thermostats' in HOOMD-

Blue [334, 335]. In future work, we aim to explore the integration of a colored noise thermostat scheme [525, 526] into the MD engine. This enhancement would enable us to simulate dynamics arising from various types of active processes beyond the current temperature-based approach.

6.4 Concluding remarks

This thesis has leveraged a dynamic binding and unbinding protocol to investigate the physics of self-organization phenomena in a spectrum of diverse soft and biological materials [8–11] featuring binders, ranging from colloidal liquid droplets [50, 160–163, 242, 280, 323, 326] to biomimetic adhesive emulsions [38, 39, 93, 266], nano-particles forming gels [189, 190, 286, 287, 292–298] and even the active, crowded cytoplasm of mammalian cells [51, 304, 468, 488, 489, 492]. The study delves into the effects of crowding, kinetic rates, binder concentration, binding affinities and non-equilibrium activity to obtain a comprehensive understanding of self-aggregation mechanisms in these materials. Our framework, characterized by its strength and flexibility, is readily accessible and user-friendly. We encourage and hope that researchers will build upon our work, exploring new directions and expanding the scope of these studies.

BIBLIOGRAPHY

[1] Anthony Stone. *The theory of intermolecular forces.* oUP oxford, 2013.

[2] Th Zeegers-Huyskens and P Huyskens. "Intermolecular forces". In: *Intermolecular forces: An introduction to modern methods and results.* Springer, 1991, pp. 1–30.

[3] JA Barker and D Henderson. "Theories of liquids". In: *Annual review of physical chemistry* 23.1 (1972), pp. 439–484.

[4] Charles Kittel. *Introduction to solid state physics.* John Wiley & sons, inc, 2005.

[5] Alexander Y Malkin and Avraam I Isayev. *Rheology: concepts, methods, and applications.* Elsevier, 2022.

[6] Michael P Marder. *Condensed matter physics.* John Wiley & Sons, 2010.

[7] Nhan Phan-Thien and Nam Mai-Duy. *Understanding viscoelasticity: an introduction to rheology.* Springer, 2013.

[8] Pierre-Gilles De Gennes. "Soft matter". In: *Science* 256.5056 (1992), pp. 495–497.

[9] PA Hassan, Gunjan Verma, and R Ganguly. "Soft materials-properties and applications". In: *Functional Materials: Preparation, Processing and Applications; Elsevier: London, UK* (2011), p. 1.

[10] Dominique Langevin. "An Adventure into the World of Soft Matter". In: *Annual Review of Condensed Matter Physics* 14 (2023), pp. 21–33.

[11] Ian W Hamley. *Introduction to soft matter: synthetic and biological self-assembling materials*. John Wiley & Sons, 2007.

[12] Heinrich M Jaeger, Sidney R Nagel, and Robert P Behringer. “Granular solids, liquids, and gases”. In: *Reviews of modern physics* 68.4 (1996), p. 1259.

[13] Ronald Midgley Nedderman et al. *Statics and kinematics of granular materials*. Vol. 352. Cambridge University Press Cambridge, 1992.

[14] Peter J Collings and John W Goodby. *Introduction to liquid crystals: chemistry and physics*. Crc Press, 2019.

[15] E Ben Jacob, Yakir Aharonov, and Yoash Shapira. “Bacteria harnessing complexity”. In: *Biofilms* 1.4 (2004), pp. 239–263.

[16] Matthew F Copeland and Douglas B Weibel. “Bacterial swarming: a model system for studying dynamic self-assembly”. In: *Soft matter* 5.6 (2009), pp. 1174–1187.

[17] Clemens Bechinger et al. “Active particles in complex and crowded environments”. In: *Reviews of Modern Physics* 88.4 (2016), p. 045006.

[18] Megan S Davies Wykes et al. “Dynamic self-assembly of microscale rotors and swimmers”. In: *Soft matter* 12.20 (2016), pp. 4584–4589.

[19] Ramin Golestanian. “Collective behavior of thermally active colloids”. In: *Physical review letters* 108.3 (2012), p. 038303.

[20] Arshad Desai and Timothy J Mitchison. “Microtubule polymerization dynamics”. In: *Annual review of cell and developmental biology* 13.1 (1997), pp. 83–117.

[21] Anna Akhmanova and Michel O Steinmetz. “Control of microtubule organization and dynamics: two ends in the limelight”. In: *Nature reviews Molecular cell biology* 16.12 (2015), pp. 711–726.

[22] RM Christensen. *Introduction to viscoelasticity*. 1990.

[23] T Ando. “Length Scales Characterizing Mesoscopic Systems”. In: *Mesoscopic Physics and Electronics* (1998), pp. 3–10.

[24] David S Dean et al. *Electrostatics of Soft and Disordered Matter.* CRC Press, 2014.

[25] Fritz London. “The general theory of molecular forces”. In: *Transactions of the Faraday Society* 33 (1937), 8b–26.

[26] Michel Grandbois et al. “How strong is a covalent bond?” In: *Science* 283.5408 (1999), pp. 1727–1730.

[27] Yongfei Zeng et al. “Covalent organic frameworks formed with two types of covalent bonds based on orthogonal reactions”. In: *Journal of the American Chemical Society* 137.3 (2015), pp. 1020–1023.

[28] Progyateg Chakma and Dominik Konkolewicz. “Dynamic covalent bonds in polymeric materials”. In: *Angewandte Chemie International Edition* 58.29 (2019), pp. 9682–9695.

[29] Kenneth M Harmon. “Hydrogen Bonding in Biological Structures”. In: *Science* 257.5077 (1992), pp. 1774–1776.

[30] George A Jeffrey and Wolfram Saenger. *Hydrogen bonding in biological structures.* Springer Science & Business Media, 2012.

[31] Young Ho Ko et al. “Supramolecular assemblies built with host-stabilized charge-transfer interactions”. In: *Chemical Communications* 13 (2007), pp. 1305–1315.

[32] Jennifer Galanis, Ralph Nossal, and Daniel Harries. “Depletion forces drive polymer-like self-assembly in vibrofluidized granular materials”. In: *Soft Matter* 6.5 (2010), pp. 1026–1034.

[33] Stefano Sacanna et al. “Lock and key colloids”. In: *Nature* 464.7288 (2010), pp. 575–578.

[34] Lang Feng et al. “Re-entrant solidification in polymer–colloid mixtures as a consequence of competing entropic and enthalpic attractions”. In: *Nature materials* 14.1 (2015), pp. 61–65.

[35] Joost Groen et al. “Associative interactions in crowded solutions of biopolymers counteract depletion effects”. In: *Journal of the American Chemical Society* 137.40 (2015), pp. 13041–13048.

[36] Emily E Meyer, Kenneth J Rosenberg, and Jacob Israelachvili. “Recent progress in understanding hydrophobic interactions”. In: *Proceedings of the National Academy of Sciences* 103.43 (2006), pp. 15739–15746.

[37] Ilya Levental, Penelope C Georges, and Paul A Janmey. “Soft biological materials and their impact on cell function”. In: *Soft Matter* 3.3 (2007), pp. 299–306.

[38] Lea-Laetitia Pontani et al. “Biomimetic emulsions reveal the effect of mechanical forces on cell–cell adhesion”. In: *Proceedings of the National Academy of Sciences* 109.25 (2012), pp. 9839–9844.

[39] Kartikeya Nagendra et al. “Push-pull mechanics of E-cadherin ectodomains in biomimetic adhesions”. In: *Biophysical journal* 122.17 (2023), pp. 3506–3515.

[40] Andrea E Rawlings, Jonathan P Bramble, and Sarah S Staniland. “Innovation through imitation: biomimetic, bioinspired and biokleptic research”. In: *Soft Matter* 8.25 (2012), pp. 6675–6679.

[41] Ali Miserez, James C Weaver, and Ovijit Chaudhuri. “Biological materials and molecular biomimetics–filling up the empty soft materials space for tissue engineering applications”. In: *Journal of Materials Chemistry B* 3.1 (2015), pp. 13–24.

[42] George M Whitesides. “Soft robotics”. In: *Angewandte Chemie International Edition* 57.16 (2018), pp. 4258–4273.

[43] Carmel Majidi. “Soft-matter engineering for soft robotics”. In: *Advanced Materials Technologies* 4.2 (2019), p. 1800477.

[44] Ying Dan Liu and Hyoung Jin Choi. “Electrorheological fluids: smart soft matter and characteristics”. In: *Soft Matter* 8.48 (2012), pp. 11961–11978.

[45] Quan Li, Albert PHJ Schenning, and Timothy J Bunning. *Light-Responsive Smart Soft Matter Technologies.* 2019.

[46] Maya Pishvar and Ryan L Harne. “Foundations for soft, smart matter by active mechanical metamaterials”. In: *Advanced science* 7.18 (2020), p. 2001384.

[47] Hyunhyub Ko and Ali Javey. “Smart actuators and adhesives for reconfigurable matter”. In: *Accounts of chemical research* 50.4 (2017), pp. 691–702.

[48] Pulat K Khabibullaev and Abdulla Saidov. *Phase separation in soft matter physics: micellar solutions, microemulsions, critical phenomena.* Vol. 138. Springer Science & Business Media, 2003.

[49] Leo Radzihovsky. “Critical Soft Matter”. In: (2015).

[50] Gaurav Mitra et al. “A coarse-grained simulation model for colloidal self-assembly via explicit mobile binders”. In: *Soft Matter* (2023).

[51] Tong Shu et al. “Mesoscale molecular assembly is favored by the active, crowded cytoplasm”. In: *PRX Life* 2 (3 July 2024), p. 033001.

[52] George M Whitesides and Bartosz Grzybowski. “Self-assembly at all scales”. In: *Science* 295.5564 (2002), pp. 2418–2421.

[53] Ludovico Cademartiri and Kyle JM Bishop. “Programmable self-assembly”. In: *Nat. Mater.* 14.1 (2015), pp. 2–9.

[54] Kyle JM Bishop. “Self-assembly across scales”. In: *Nature Materials* 21.5 (2022), pp. 501–502.

[55] Santosh Yadav, Ashwani Kumar Sharma, and Pradeep Kumar. "Nanoscale self-assembly for therapeutic delivery". In: *Frontiers in Bioengineering and Biotechnology* 8 (2020), p. 127.

[56] Marek Grzelczak et al. "Directed self-assembly of nanoparticles". In: *ACS nano* 4.7 (2010), pp. 3591–3605.

[57] Stephen Whitelam and Robert L Jack. "The statistical mechanics of dynamic pathways to self-assembly". In: *Annual review of physical chemistry* 66 (2015), pp. 143–163.

[58] Ying Yang and Marek W Urban. "Self-healing polymeric materials". In: *Chemical Society Reviews* 42.17 (2013), pp. 7446–7467.

[59] Siyang Wang and Marek W Urban. "Self-healing polymers". In: *Nature Reviews Materials* 5.8 (2020), pp. 562–583.

[60] Mireille MJPE Sthijns, Vanessa LS LaPointe, and Clemens A van Blitterswijk. "Building complex life through self-organization". In: *Tissue Engineering Part A* 25.19-20 (2019), pp. 1341–1346.

[61] Isha Bhorkar and Abhishek S Dhoble. "Advances in the synthesis and application of self-assembling biomaterials". In: *Progress in Biophysics and Molecular Biology* 167 (2021), pp. 46–62.

[62] Nicholas Stephanopoulos, Julia H Ortony, and Samuel I Stupp. "Self-assembly for the synthesis of functional biomaterials". In: *Acta materialia* 61.3 (2013), pp. 912–930.

[63] Michael D Ward. "Directing the assembly of molecular crystals". In: *MRS bulletin* 30.10 (2005), pp. 705–712.

[64] Mérina K Corpinot and Dejan-Kresimir Bucar. "A practical guide to the design of molecular crystals". In: *Crystal Growth & Design* 19.2 (2018), pp. 1426–1453.

[65] Vuk Uskoković. "Theoretical and practical aspects of colloid science and self-assembly phenomena revisited". In: *Reviews in Chemical Engineering* 23.5 (2007), pp. 301–372.

[66] Emanuela Bianchi, Ronald Blaak, and Christos N Likos. “Patchy colloids: state of the art and perspectives”. In: *Physical Chemistry Chemical Physics* 13.14 (2011), pp. 6397–6410.

[67] Anthony J Kim, Paul L Biancaniello, and John C Crocker. “Engineering DNA-mediated colloidal crystallization”. In: *Langmuir* 22.5 (2006), pp. 1991–2001.

[68] Erich SACKMANN. “Structure and dynamics of membranes”. In: *Handbook of Biological Physics* 1 (1995), p. 213.

[69] Alexander P Lyubartsev and Alexander L Rabinovich. “Recent development in computer simulations of lipid bilayers”. In: *Soft Matter* 7.1 (2011), pp. 25–39.

[70] SF Shimobayashi et al. “Direct measurement of DNA-mediated adhesion between lipid bilayers”. In: *Physical Chemistry Chemical Physics* 17.24 (2015), pp. 15615–15628.

[71] Yuri S Lipatov and Tatiana T Alekseeva. *Phase-separated interpenetrating polymer networks*. Springer, 2007.

[72] Michael Nguyen and Suriyanarayanan Vaikuntanathan. “Design principles for nonequilibrium self-assembly”. In: *Proceedings of the National Academy of Sciences* 113.50 (2016), pp. 14231–14236.

[73] Ben Wang et al. “Self-assembly of nanoparticles: Static and dynamic”. In: *Materials Today* 25 (2019), pp. 112–113.

[74] Jaakko VI Timonen et al. “Switchable static and dynamic self-assembly of magnetic droplets on superhydrophobic surfaces”. In: *Science* 341.6143 (2013), pp. 253–257.

[75] Anna V Davis, Robert M Yeh, and Kenneth N Raymond. “Supramolecular assembly dynamics”. In: *Proceedings of the National Academy of Sciences* 99.8 (2002), pp. 4793–4796.

[76] Matthew J Webber and Mark W Tibbitt. “Dynamic and reconfigurable materials from reversible network interactions”. In: *Nature Reviews Materials* 7.7 (2022), pp. 541–556.

[77] Shiwanka V Wanasinghe, Obed J Dodo, and Dominik Konkolewicz. "Dynamic Bonds: Adaptable Timescales for Responsive Materials". In: *Angewandte Chemie International Edition* 61.50 (2022), e202206938.

[78] Chunbai He, Demin Liu, and Wenbin Lin. "Nanomedicine applications of hybrid nanomaterials built from metal–ligand coordination bonds: nanoscale metal–organic frameworks and nanoscale coordination polymers". In: *Chemical reviews* 115.19 (2015), pp. 11079–11108.

[79] M Das, S Pal, and K Naskar. "Exploring various metal-ligand coordination bond formation in elastomers: Mechanical performance and self-healing behavior". In: *Express Polymer Letters* 14.9 (2020), pp. 860–880.

[80] Christopher A Hunter and Jeremy KM Sanders. "The nature of. pi.-. pi. interactions". In: *Journal of the American Chemical Society* 112.14 (1990), pp. 5525–5534.

[81] Yi Liu et al. "Effect of pi–pi stacking on the self-assembly of azomethine-type rod–coil liquid crystals". In: *Liquid Crystals* 38.8 (2011), pp. 995–1006.

[82] Garry Sinawang et al. "Biofunctional hydrogels based on host–guest interactions". In: *Polymer Journal* 52.8 (2020), pp. 839–859.

[83] Xing Ma and Yanli Zhao. "Biomedical applications of supramolecular systems based on host–guest interactions". In: *Chemical reviews* 115.15 (2015), pp. 7794–7839.

[84] Laura Porath et al. "Vitrimers: using dynamic associative bonds to control viscoelasticity, assembly, and functionality in polymer networks". In: *ACS Macro Letters* 11.4 (2022), pp. 475–483.

[85] Yong Xu et al. "Conductive hydrogels with dynamic reversible networks for biomedical applications". In: *Advanced Healthcare Materials* 10.11 (2021), p. 2100012.

[86] Guohua Deng et al. “Dynamic hydrogels with an environmental adaptive self-healing ability and dual responsive sol–gel transitions”. In: *ACS Macro Letters* 1.2 (2012), pp. 275–279.

[87] Yan Zhang et al. “Dynamic covalent polymers for biomedical applications”. In: *Materials chemistry frontiers* 4.2 (2020), pp. 489–506.

[88] Alperen N Ketene et al. “Actin filaments play a primary role for structural integrity and viscoelastic response in cells”. In: *Integrative Biology* 4.5 (2012), pp. 540–549.

[89] Yong Wang, Joao Miguel Martins, and Kresten Lindorff-Larsen. “Biomolecular conformational changes and ligand binding: from kinetics to thermodynamics”. In: *Chemical science* 8.9 (2017), pp. 6466–6473.

[90] Andre EX Brown and Dennis E Discher. “Conformational changes and signaling in cell and matrix physics”. In: *Current Biology* 19.17 (2009), R781–R789.

[91] Masatoshi Takeichi. “The cadherins: cell-cell adhesion molecules controlling animal morphogenesis”. In: *Development* 102.4 (1988), pp. 639–655.

[92] Lawrence Shapiro et al. “Structural basis of cell-cell adhesion by cadherins”. In: *Nature* 374.6520 (1995), pp. 327–337.

[93] Lea-Laetitia Pontani, Ivane Jorjadze, and Jasna Brujic. “Cis and trans cooperativity of e-cadherin mediates adhesion in biomimetic lipid droplets”. In: *Biophys. J* 110.2 (2016), pp. 391–399.

[94] Daniel A Fletcher and R Dyche Mullins. “Cell mechanics and the cytoskeleton”. In: *Nature* 463.7280 (2010), pp. 485–492.

[95] Shigenobu Yonemura. “Cadherin–actin interactions at adherens junctions”. In: *Current opinion in cell biology* 23.5 (2011), pp. 515–522.

[96] Jean-Léon Maıtre and Carl-Philipp Heisenberg. “Three functions of cadherins in cell adhesion”. In: *Current Biology* 23.14 (2013), R626–R633.

[97] Willmor J Peña Ccoa and Glen M Hocky. “Assessing models of force-dependent unbinding rates via infrequent metadynamics”. In: *J. Chem. Phys.* 156.12 (2022), p. 125102.

[98] David Gomez et al. “Molecular paradigms for biological mechanosensing”. In: *J. Phys. Chem. B* 125.44 (2021), pp. 12115–12124.

[99] George I Bell. “Models for the specific adhesion of cells to cells: a theoretical framework for adhesion mediated by reversible bonds between cell surface molecules.” In: *Science* 200.4342 (1978), pp. 618–627.

[100] George I Bell, MICAH Dembo, and PIERRE Bongrand. “Cell adhesion. Competition between nonspecific repulsion and specific bonding.” In: *Biophys. J.* 45.6 (1984), p. 1051.

[101] Sabyasachi Rakshit et al. “Ideal, catch, and slip bonds in cadherin adhesion”. In: *Proceedings of the National Academy of Sciences* 109.46 (2012), pp. 18815–18820.

[102] Carien M Niessen, Deborah Leckband, and Alpha S Yap. “Tissue organization by cadherin adhesion molecules: dynamic molecular and cellular mechanisms of morphogenetic regulation”. In: *Physiological reviews* 91.2 (2011), pp. 691–731.

[103] Simon L Freedman et al. “A versatile framework for simulating the dynamic mechanical structure of cytoskeletal networks”. In: *Biophysical journal* 113.2 (2017), pp. 448–460.

[104] Simon L Freedman et al. “Nonequilibrium phase diagrams for actomyosin networks”. In: *Soft matter* 14.37 (2018), pp. 7740–7747.

[105] Simon L Freedman et al. “Mechanical and kinetic factors drive sorting of F-actin crosslinkers on bundles”. In: *Proceedings of the National Academy of Sciences* 116.33 (2019), pp. 16192–16197.

[106] Glen M Hocky et al. “Structural basis of fast-and slow-severing actin–cofilactin boundaries”. In: *Journal of Biological Chemistry* 296 (2021).

[107] Anthony C Schramm et al. “Actin filament strain promotes severing and cofilin dissociation”. In: *Biophysical journal* 112.12 (2017), pp. 2624–2633.

[108] Karen E Kasza and Jennifer A Zallen. “Dynamics and regulation of contractile actin–myosin networks in morphogenesis”. In: *Current opinion in cell biology* 23.1 (2011), pp. 30–38.

[109] Michael A Geeves. “The dynamics of actin and myosin association and the crossbridge model of muscle contraction.” In: *Biochemical journal* 274.Pt 1 (1991), p. 1.

[110] Michael Lorenz and Kenneth C Holmes. “The actin-myosin interface”. In: *Proceedings of the National Academy of Sciences* 107.28 (2010), pp. 12529–12534.

[111] Paola Llinas et al. “How actin initiates the motor activity of Myosin”. In: *Developmental cell* 33.4 (2015), pp. 401–412.

[112] Elizabeth M Reichl et al. “Interactions between myosin and actin crosslinkers control cytokinesis contractility dynamics and mechanics”. In: *Current Biology* 18.7 (2008), pp. 471–480.

[113] Oliver Lieleg, Mireille MAE Claessens, and Andreas R Bausch. “Structure and dynamics of cross-linked actin networks”. In: *Soft Matter* 6.2 (2010), pp. 218–225.

[114] Björn Sjöblom, A Salmazo, and K Djinović-Carugo. “α-Actinin structure and regulation”. In: *Cellular and molecular life sciences* 65 (2008), pp. 2688–2701.

[115] Asier Jayo and Maddy Parsons. “Fascin: a key regulator of cytoskeletal dynamics”. In: *The international journal of biochemistry & cell biology* 42.10 (2010), pp. 1614–1617.

[116] Daniel H Wachsstock, WH Schwarz, and TD Pollard. “Cross-linker dynamics determine the mechanical properties of actin gels”. In: *Biophysical journal* 66.3 (1994), pp. 801–809.

[117] Maral Adeli Koudehi, David M Rutkowski, and Dimitrios Vavylonis. “Organization of associating or crosslinked actin filaments in confinement”. In: *Cytoskeleton* 76.11-12 (2019), pp. 532–548.

[118] Ondrej Maxian, Aleksandar Donev, and Alex Mogilner. “Interplay between Brownian motion and cross-linking controls bundling dynamics in actin networks”. In: *Biophys. J.* 121.7 (2022), pp. 1230–1245.

[119] Yossi Eliaz et al. “Insights from graph theory on the morphologies of actomyosin networks with multilinkers”. In: *Physical Review E* 102.6 (2020), p. 062420.

[120] Haosu Tang, Damien Laporte, and Dimitrios Vavylonis. “Actin cable distribution and dynamics arising from cross-linking, motor pulling, and filament turnover”. In: *Molecular biology of the cell* 25.19 (2014), pp. 3006–3016.

[121] Elena Kudryashova et al. “Actin cross-linking toxin is a universal inhibitor of tandem-organized and oligomeric G-actin binding proteins”. In: *Current biology* 28.10 (2018), pp. 1536–1547.

[122] Olivier M Rossier et al. “Force generated by actomyosin contraction builds bridges between adhesive contacts”. In: *The EMBO journal* 29.6 (2010), pp. 1055–1068.

[123] Francois Nedelec and Dietrich Foethke. “Collective Langevin dynamics of flexible cytoskeletal fibers”. In: *New Journal of Physics* 9.11 (2007), p. 427.

[124] Hajer Ennomani et al. “Architecture and connectivity govern actin network contractility”. In: *Current Biology* 26.5 (2016), pp. 616–626.

[125] James D Watson and Francis HC Crick. “Molecular structure of nucleic acids: a structure for deoxyribose nucleic acid”. In: *Nature* 171.4356 (1953), pp. 737–738.

[126] Yirong Mo. “Probing the nature of hydrogen bonds in DNA base pairs”. In: *Journal of molecular modeling* 12 (2006), pp. 665–672.

[127] Célia Fonseca Guerra et al. “Hydrogen bonding in DNA base pairs: reconciliation of theory and experiment”. In: *Journal of the American Chemical Society* 122.17 (2000), pp. 4117–4128.

[128] Aaron Klug. “The discovery of the DNA double helix”. In: *Journal of molecular biology* 335.1 (2004), pp. 3–26.

[129] Stephen P Bell and Anindya Dutta. “DNA replication in eukaryotic cells”. In: *Annual review of biochemistry* 71.1 (2002), pp. 333–374.

[130] Arthur Kornberg, Tania A Baker, et al. *DNA replication*. Vol. 3. Wh Freeman New York, 1992.

[131] Thomas A Kunkel. “DNA replication fidelity”. In: *Journal of Biological Chemistry* 279.17 (2004), pp. 16895–16898.

[132] Carl O Pabo and Robert T Sauer. “Transcription factors: structural families and principles of DNA recognition”. In: *Annual review of biochemistry* 61.1 (1992), pp. 1053–1095.

[133] Peter McGlynn, Nigel J Savery, and Mark S Dillingham. “The conflict between DNA replication and transcription”. In: *Molecular microbiology* 85.1 (2012), pp. 12–20.

[134] David A Clayton. “Transcription and replication of mitochondrial DNA”. In: *Human reproduction* 15.suppl_2 (2000), pp. 11–17.

[135] Thomas Garel, Cécile Monthus, and Henri Orland. “A simple model for DNA denaturation”. In: *Europhysics Letters* 55.1 (2001), p. 132.

[136] René Thomas. “The denaturation of DNA”. In: *Gene* 135.1-2 (1993), pp. 77–79.

[137] Julianne M Gibbs-Davis, George C Schatz, and SonBinh T Nguyen. “Sharp melting transitions in DNA hybrids without aggregate dissolution: Proof of neighboring-duplex cooperativity”. In: *Journal of the American Chemical Society* 129.50 (2007), pp. 15535–15540.

[138] GW Lehman and JP McTague. “Melting of DNA”. In: *The Journal of Chemical Physics* 49.7 (1968), pp. 3170–3179.

[139] Yariv Kafri, David Mukamel, and Luca Peliti. “Melting and unzipping of DNA”. In: *The European Physical Journal B-Condensed Matter and Complex Systems* 27 (2002), pp. 135–146.

[140] Pierre Bongrand. “Ligand-receptor interactions”. In: *Reports on progress in Physics* 62.6 (1999), p. 921.

[141] Irving M Klotz. “Ligand-receptor complexes: origin and development of the concept”. In: *Journal of Biological Chemistry* 279.1 (2004), pp. 1–12.

[142] Mark A Murcko. “Computational methods to predict binding free energy in ligand-receptor complexes”. In: *Journal of medicinal chemistry* 38.26 (1995), pp. 4953–4967.

[143] Neil J Bruce et al. “New approaches for computing ligand–receptor binding kinetics”. In: *Current opinion in structural biology* 49 (2018), pp. 1–10.

[144] RFW Bader and WH Henneker. “The ionic bond”. In: *Journal of the American Chemical Society* 87.14 (1965), pp. 3063–3068.

[145] Moshuqi Zhu et al. “Long-lasting sustainable self-healing ion gel with triple-network by trigger-free dynamic hydrogen bonds and ion bonds”. In: *ACS Sustainable Chemistry & Engineering* 6.12 (2018), pp. 17087–17098.

[146] Yan Peng et al. “Strong and tough self-healing elastomers enabled by dual reversible networks formed by ionic interactions and dynamic covalent bonds”. In: *Polymer* 157 (2018), pp. 172–179.

[147] H Margenau. “Van der Waals forces”. In: *Reviews of Modern Physics* 11.1 (1939), p. 1.

[148] Igor Ekhiel’evich Dzyaloshinskii, Efrat M Lifshitz, and Lev P Pitaevskii. “The general theory of van der Waals forces”. In: *Advances in Physics* 10.38 (1961), pp. 165–209.

[149] David M Webster, Andrew H Henry, and Anthony R Rees. “Antibody-antigen interactions”. In: *Current opinion in structural biology* 4.1 (1994), pp. 123–129.

[150] Stephen A Kuby. *A Study of Enzymes: Enzyme Catalysts, Kinetics, and Substrate Binding.* CRC Press, 2019.

[151] Alan Roy Fersht. “Catalysis, binding and enzyme-substrate complementarity”. In: *Proceedings of the Royal Society of London. Series B. Biological Sciences* 187.1089 (1974), pp. 397–407.

[152] Alex Gutteridge and Janet Thornton. “Conformational changes observed in enzyme crystal structures upon substrate binding”. In: *Journal of molecular biology* 346.1 (2005), pp. 21–28.

[153] Ron O Dror et al. “Pathway and mechanism of drug binding to G-protein-coupled receptors”. In: *Proceedings of the National Academy of Sciences* 108.32 (2011), pp. 13118–13123.

[154] Stuart Maudsley, Bronwen Martin, and Louis M Luttrell. “The origins of diversity and specificity in G protein-coupled receptor signaling”. In: *Journal of Pharmacology and Experimental Therapeutics* 314.2 (2005), pp. 485–494.

[155] Daniel M Rosenbaum, Søren GF Rasmussen, and Brian K Kobilka. “The structure and function of G-protein-coupled receptors”. In: *Nature* 459.7245 (2009), pp. 356–363.

[156] JAMES A WELLS et al. “The molecular basis for growth hormone–receptor interactions”. In: *Recent Progress in Hormone Research* (1993), pp. 253–275.

[157] James A Wells. “Binding in the growth hormone receptor complex.” In: *Proceedings of the National Academy of Sciences* 93.1 (1996), pp. 1–6.

[158] Christine Helsen et al. “Structural basis for nuclear hormone receptor DNA binding”. In: *Molecular and cellular endocrinology* 348.2 (2012), pp. 411–417.

[159] Roy M Daniel et al. “The role of dynamics in enzyme activity”. In: *Annual review of biophysics and biomolecular structure* 32.1 (2003), pp. 69–92.

[160] Lang Feng et al. “Specificity, flexibility and valence of DNA bonds guide emulsion architecture”. In: *Soft Matter* 9.41 (2013), pp. 9816–9823.

[161] Angus McMullen et al. “Freely jointed polymers made of droplets”. In: *Phys. Rev. Lett.* 121.13 (2018), p. 138002.

[162] Yin Zhang et al. “Multivalent, multiflavored droplets by design”. In: *Proc. Natl. Acad. Sci.* 115.37 (2018), pp. 9086–9091.

[163] Yin Zhang et al. “Sequential self-assembly of DNA functionalized droplets”. In: *Nature Comm.* 8.1 (2017), pp. 1–7.

[164] Angus McMullen, Sascha Hilgenfeldt, and Jasna Brujic. “DNA self-organization controls valence in programmable colloid design”. In: *Proc. Natl. Acad. Sci.* 118.46 (2021), e2112604118.

[165] Angus McMullen et al. “Self-assembly of emulsion droplets through programmable folding”. In: *Nature* 610.7932 (2022), pp. 502–506.

[166] Patrick S Stayton et al. “Streptavidin–biotin binding energetics”. In: *Biomolecular engineering* 16.1-4 (1999), pp. 39–44.

[167] Sudipto K De et al. “Equilibrium swelling and kinetics of pH-responsive hydrogels: Models, experiments, and simulations”. In: *Journal of Microelectromechanical systems* 11.5 (2002), pp. 544–555.

[168] Xiao Zheng Shu et al. “Disulfide cross-linked hyaluronan hydrogels”. In: *Biomacromolecules* 3.6 (2002), pp. 1304–1311.

[169] George M Whitesides and Mila Boncheva. “Beyond molecules: Self-assembly of mesoscopic and macroscopic components”. In: *Proceedings of the National Academy of Sciences* 99.8 (2002), pp. 4769–4774.

[170] Marcin Fialkowski et al. *Principles and implementations of dissipative (dynamic) self-assembly.* 2006.

[171] Raj Rajagopalan. “Simulations of self-assembling systems”. In: *Current opinion in colloid & interface science* 6.4 (2001), pp. 357–365.

[172] Bartosz A Grzybowski et al. “From dynamic self-assembly to networked chemical systems”. In: *Chemical Society Reviews* 46.18 (2017), pp. 5647–5678.

[173] Zhenli Zhang and Sharon C Glotzer. “Self-assembly of patchy particles”. In: *Nano Lett.* 4.8 (2004), pp. 1407–1413.

[174] Francesco Sciortino et al. “Self-assembly of patchy particles into polymer chains: A parameter-free comparison between Wertheim theory and Monte Carlo simulation”. In: *J. Chem. Phys.* 126.19 (2007), p. 194903.

[175] Amar B Pawar and Ilona Kretzschmar. “Fabrication, assembly, and application of patchy particles”. In: *Macromol. Rapid. Comm.* 31.2 (2010), pp. 150–168.

[176] Yufeng Wang et al. “Colloids with valence and specific directional bonding”. In: *Nature* 491.7422 (2012), pp. 51–55.

[177] Dmytro Nykypanchuk et al. “DNA-guided crystallization of colloidal nanoparticles”. In: *Nature* 451.7178 (2008), pp. 549–552.

[178] Chad A Mirkin et al. “A DNA-based method for rationally assembling nanoparticles into macroscopic materials”. In: *Nature* 382.6592 (1996), pp. 607–609.

[179] Sung Young Park et al. “DNA-programmable nanoparticle crystallization”. In: *Spherical Nucleic Acids.* Jenny Stanford Publishing, 2020, pp. 515–525.

[180] Younjin Min et al. “The role of interparticle and external forces in nanoparticle assembly”. In: *Nature materials* 7.7 (2008), pp. 527–538.

[181] Michael F Hagan, Oren M Elrad, and Robert L Jack. “Mechanisms of kinetic trapping in self-assembly and phase transformation”. In: *The Journal of chemical physics* 135.10 (2011).

[182] Brigitte AK Kriebisch et al. “Tuning the Kinetic Trapping in Chemically Fueled Self-Assembly”. In: *ChemSystemsChem* 5.1 (2023), e202200035.

[183] Yun Yan, Jianbin Huang, and Ben Zhong Tang. “Kinetic trapping–a strategy for directing the self-assembly of unique functional nanostructures”. In: *Chemical Communications* 52.80 (2016), pp. 11870–11884.

[184] James Grant, Robert L Jack, and Stephen Whitelam. “Analyzing mechanisms and microscopic reversibility of self-assembly”. In: *The Journal of chemical physics* 135.21 (2011).

[185] Michael F Hagan and Gregory M Grason. “Equilibrium mechanisms of self-limiting assembly”. In: *Reviews of modern physics* 93.2 (2021), p. 025008.

[186] Kun-Ta Wu et al. “Kinetics of DNA-coated sticky particles”. In: *Phys. Rev. E* 88.2 (2013), p. 022304.

[187] W Benjamin Rogers, William M Shih, and Vinothan N Manoharan. “Using DNA to program the self-assembly of colloidal nanoparticles and microparticles”. In: *Nat. Rev. Mat.* 1.3 (2016), pp. 1–14.

[188] Stephanie Vial et al. “Linear mesostructures in DNA–nanorod self-assembly”. In: *Acs Nano* 7.6 (2013), pp. 5437–5445.

[189] Michael P Howard et al. “Structure and phase behavior of polymer-linked colloidal gels”. In: *The Journal of Chemical Physics* 151.12 (2019).

[190] Taejin Kwon et al. “Dynamics of equilibrium-linked colloidal networks”. In: *The Journal of Chemical Physics* 157.18 (2022).

[191] Martin J Klein. “Principle of detailed balance”. In: *Physical Review* 97.6 (1955), p. 1446.

[192] Ying Zhang and Samuel A Isaacson. “Detailed balance for particle models of reversible reactions in bounded domains”. In: *The Journal of Chemical Physics* 156.20 (2022).

[193] Sophie Marbach and Christopher E Miles. “Coarse-grained dynamics of transiently-bound fast linkers”. In: *arXiv preprint arXiv:2212.08777* (2022).

[194] Richard C Tolman. “The principle of microscopic reversibility”. In: *Proceedings of the National Academy of Sciences* 11.7 (1925), pp. 436–439.

[195] Pritam Kumar Jana and Bortolo Matteo Mognetti. “Translational and rotational dynamics of colloidal particles interacting through reacting linkers”. In: *Physical Review E* 100.6 (2019), p. 060601.

[196] Micah Dembo et al. “The reaction-limited kinetics of membrane-to-surface adhesion and detachment”. In: *Proceedings of the Royal Society of London. Series B. Biological Sciences* 234.1274 (1988), pp. 55–83.

[197] Florian Berger, Stefan Klumpp, and Reinhard Lipowsky. “Force-dependent unbinding rate of molecular motors from stationary optical trap data”. In: *Nano letters* 19.4 (2019), pp. 2598–2602.

[198] Joseph J Klobusicky, John Fricks, and Peter R Kramer. “Effective behavior of cooperative and nonidentical molecular motors”. In: *Research in the mathematical sciences* 7 (2020), pp. 1–49.

[199] Teemu Murtola et al. “Multiscale modeling of emergent materials: biological and soft matter”. In: *Physical Chemistry Chemical Physics* 11.12 (2009), pp. 1869–1892.

[200] Stefano Angioletti-Uberti. “Theory, simulations and the design of functionalized nanoparticles for biomedical applications: A Soft Matter Perspective”. In: *npj Computational Materials* 3.1 (2017), p. 48.

[201] Raffaello Potestio, Christine Peter, and Kurt Kremer. “Computer simulations of soft matter: Linking the scales”. In: *Entropy* 16.8 (2014), pp. 4199–4245.

[202] M Reza Shaebani et al. “Computational models for active matter”. In: *Nature Reviews Physics* 2.4 (2020), pp. 181–199.

[203] Andrea J Liu et al. “Opportunities in theoretical and computational polymeric materials and soft matter”. In: *Soft Matter* 11.12 (2015), pp. 2326–2332.

[204] Kurt Kremer. “Computer simulations in soft matter science”. In: *Soft and Fragile Matter: Non Equilibrium Dynamics, Metastability And Flow; IOP Publishing Ltd.: Bristol, UK* (2000), pp. 145–184.

[205] Daan Frenkel, Berend Smit, and Mark A Ratner. *Understanding molecular simulation: from algorithms to applications*. Vol. 2. Academic press San Diego, 1996.

[206] Martin Karplus and Gregory A Petsko. “Molecular dynamics simulations in biology”. In: *Nature* 347.6294 (1990), pp. 631–639.

[207] Martin Oliver Steinhauser. “Introduction to molecular dynamics simulations: Applications in hard and soft condensed matter physics”. In: *Molecular dynamics-Studies of synthetic and biological macromolecules* (2012), pp. 3–28.

[208] Michael P Allen et al. “Introduction to molecular dynamics simulation”. In: *Computational soft matter: from synthetic polymers to proteins* 23.1 (2004), pp. 1–28.

[209] David J Earl and Michael W Deem. “Monte carlo simulations”. In: *Molecular modeling of proteins* (2008), pp. 25–36.

[210] Andreas Vitalis and Rohit V Pappu. “Methods for Monte Carlo simulations of biomacromolecules”. In: *Annual reports in computational chemistry* 5 (2009), pp. 49–76.

[211] David C Joy. “An introduction to Monte Carlo simulations”. In: *Scanning microscopy* 5.2 (1991), p. 4.

[212] Dirk P Kroese et al. “Why the Monte Carlo method is so important today”. In: *Wiley Interdisciplinary Reviews: Computational Statistics* 6.6 (2014), pp. 386–392.

[213] Christian P Robert et al. “The metropolis—hastings algorithm”. In: *Monte Carlo statistical methods* (2004), pp. 267–320.

[214] Siddhartha Chib and Edward Greenberg. “Understanding the metropolis-hastings algorithm”. In: *The american statistician* 49.4 (1995), pp. 327–335.

[215] Gary S Ayton, Will G Noid, and Gregory A Voth. “Systematic coarse graining of biomolecular and soft-matter systems”. In: *Mrs Bulletin* 32.11 (2007), pp. 929–934.

[216] Emiliano Brini et al. “Systematic coarse-graining methods for soft matter simulations–a review”. In: *Soft Matter* 9.7 (2013), pp. 2108–2119.

[217] Christine Peter and Kurt Kremer. “Multiscale simulation of soft matter systems–from the atomistic to the coarse-grained level and back”. In: *Soft Matter* 5.22 (2009), pp. 4357–4366.

[218] Radek Erban, Jonathan Chapman, and Philip Maini. “A practical guide to stochastic simulations of reaction-diffusion processes”. In: *arXiv preprint arXiv:0704.1908* (2007).

[219] David Fange et al. “Stochastic reaction-diffusion kinetics in the microscopic limit”. In: *Proceedings of the National Academy of Sciences* 107.46 (2010), pp. 19820–19825.

[220] Ikemefuna C Agbanusi and Samuel A Isaacson. “A comparison of bimolecular reaction models for stochastic reaction–diffusion systems”. In: *Bulletin of mathematical biology* 76.4 (2014), pp. 922–946.

[221] David Strang and Nancy Brandon Tuma. “Spatial and temporal heterogeneity in diffusion”. In: *American journal of sociology* 99.3 (1993), pp. 614–639.

[222] Thomas E Turner, Santiago Schnell, and Kevin Burrage. “Stochastic approaches for modelling in vivo reactions”. In: *Computational biology and chemistry* 28.3 (2004), pp. 165–178.

[223] Irving R Epstein and Bing Xu. “Reaction–diffusion processes at the nano-and microscales”. In: *Nature nanotechnology* 11.4 (2016), pp. 312–319.

[224] Cyrus K Aidun and Jonathan R Clausen. “Lattice-Boltzmann method for complex flows”. In: *Annual review of fluid mechanics* 42 (2010), pp. 439–472.

[225] Xiaoyi He and Li-Shi Luo. “Theory of the lattice Boltzmann method: From the Boltzmann equation to the lattice Boltzmann equation”. In: *Physical review E* 56.6 (1997), p. 6811.

[226] AA Mohamad. *Lattice boltzmann method*. Vol. 70. Springer, 2011.

[227] Michael P Howard, Arash Nikoubashman, and Jeremy C Palmer. “Modeling hydrodynamic interactions in soft materials with multiparticle collision dynamics”. In: *Current Opinion in Chemical Engineering* 23 (2019), pp. 34–43.

[228] M Cristina Marchetti et al. “Hydrodynamics of soft active matter”. In: *Reviews of modern physics* 85.3 (2013), p. 1143.

[229] Antonius Petrus Johannes Jansen. *An introduction to kinetic Monte Carlo simulations of surface reactions*. Vol. 856. Springer, 2012.

[230] Tim P Schulze. “Efficient kinetic monte carlo simulation”. In: *Journal of Computational Physics* 227.4 (2008), pp. 2455–2462.

[231] David R Foss and John F Brady. “Brownian dynamics simulation of hard-sphere colloidal dispersions”. In: *Journal of Rheology* 44.3 (2000), pp. 629–651.

[232] Donald L Ermak and J Andrew McCammon. “Brownian dynamics with hydrodynamic interactions”. In: *The Journal of chemical physics* 69.4 (1978), pp. 1352–1360.

[233] Gary A Huber and J Andrew McCammon. “Brownian dynamics simulations of biological molecules”. In: *Trends in chemistry* 1.8 (2019), pp. 727–738.

[234] Ian Snook. *The Langevin and generalised Langevin approach to the dynamics of atomic, polymeric and colloidal systems*. Elsevier, 2006.

[235] Max Innerbichler et al. “White-noise fluctuation theorem for Langevin dynamics”. In: *New Journal of Physics* 24.11 (2022), p. 113028.

[236] Alexandre Dhotel et al. “Molecular motions in functional self-assembled nanostructures”. In: *International journal of molecular sciences* 14.2 (2013), pp. 2303–2333.

[237] Karthikeyan Subramani, Ameen Khraisat, and Anne George. “Self-assembly of proteins and peptides and their applications in bionanotechnology”. In: *Current Nanoscience* 4.2 (2008), pp. 201–207.

[238] Zhe Gong et al. “Patchy particles made by colloidal fusion”. In: *Nature* 550.7675 (2017), pp. 234–238.

[239] Krishnendu Das, Luca Gabrielli, and Leonard J Prins. “Chemically fueled self-assembly in biology and chemistry”. In: *Angewandte Chemie International Edition* 60.37 (2021), pp. 20120–20143.

[240] Stefano Angioletti-Uberti et al. “Mobile linkers on DNA-coated colloids: valency without patches”. In: *Phys. Rev. Lett.* 113.12 (2014), p. 128303.

[241] Lorenzo Di Michele, Pritam Kumar Jana, and Bortolo Matteo Mognetti. “Steric interactions between mobile ligands facilitate complete wrapping in passive endocytosis”. In: *Physical Review E* 98.3 (2018), p. 032406.

[242] Pedro A. Sánchez et al. “Kinetically limited valence of colloidal particles with surface mobile DNA linkers”. In: *J. Mol. Liq.* 382 (2023), p. 121895. ISSN: 0167-7322. DOI: `https://doi.org/10.1016/j.molliq.2023.121895`.

[243] Sumit Roy and Pramod P Pillai. “What Triggers the Dynamic Self-Assembly of Molecules and Materials?” In: *Langmuir* 39.37 (2023), pp. 12967–12974.

[244] Johan M Winne, Ludwik Leibler, and Filip E Du Prez. “Dynamic covalent chemistry in polymer networks: a mechanistic perspective”. In: *Polymer Chemistry* 10.45 (2019), pp. 6091–6108.

[245] Emilie Moulin, Gabriela Cormos, and Nicolas Giuseppone. “Dynamic combinatorial chemistry as a tool for the design of functional materials and devices”. In: *Chemical Society Reviews* 41.3 (2012), pp. 1031–1049.

[246] Norbert Kern and Daan Frenkel. “Fluid–fluid coexistence in colloidal systems with short-ranged strongly directional attraction”. In: *J. Chem. Phys.* 118.21 (2003), pp. 9882–9889.

[247] Flavio Romano, Eduardo Sanz, and Francesco Sciortino. “Role of the range in the fluid-crystal coexistence for a patchy particle model”. In: *The Journal of Physical Chemistry B* 113.46 (2009), pp. 15133–15136.

[248] Flavio Romano, Eduardo Sanz, and Francesco Sciortino. “Phase diagram of a tetrahedral patchy particle model for different interaction ranges”. In: *The Journal of Chemical Physics* 132.18 (2010).

[249] John Russo et al. “The physics of empty liquids: From patchy particles to water”. In: *Reports on Progress in Physics* 85.1 (2022), p. 016601.

[250] Christoph Gögelein et al. “Fluid-fluid and fluid-solid transitions in the Kern-Frenkel model from Barker-Henderson thermodynamic perturbation theory”. In: *The Journal of Chemical Physics* 136.9 (2012).

[251] D Rosenbaum, PC Zamora, and CF Zukoski. “Phase behavior of small attractive colloidal particles”. In: *Physical review letters* 76.1 (1996), p. 150.

[252] Abraham George and W William Wilson. “Predicting protein crystallization from a dilute solution property”. In: *Acta Crystallographica Section D: Biological Crystallography* 50.4 (1994), pp. 361–365.

[253] Étienne Duguet et al. “Patchy colloidal particles for programmed self-assembly”. In: *Comptes Rendus Chimie* 19.1-2 (2016), pp. 173–182.

[254] Nicolas Rolland et al. “New patchy particle model with anisotropic patches for molecular dynamics simulations: Application to a coarse-grained model of cellulose Nanocrystal”. In: *Journal of chemical theory and computation* 16.6 (2020), pp. 3699–3711.

[255] MS Wertheim. “Thermodynamic perturbation theory of polymerization”. In: *The Journal of chemical physics* 87.12 (1987), pp. 7323–7331.

[256] Walter G Chapman, George Jackson, and Keith E Gubbins. “Phase equilibria of associating fluids: chain molecules with multiple bonding sites”. In: *Molecular Physics* 65.5 (1988), pp. 1057–1079.

[257] Peter J Lu et al. “Gelation of particles with short-range attraction”. In: *Nature* 453.7194 (2008), pp. 499–503.

[258] Hongjun Liu et al. “Vapor-liquid coexistence of fluids with attractive patches: An application of Wertheim’s theory of association”. In: *The Journal of chemical physics* 130.4 (2009).

[259] Emanuela Bianchi et al. “Phase diagram of patchy colloids: Towards empty liquids”. In: *Physical review letters* 97.16 (2006), p. 168301.

[260] Francesco Sciortino and Emanuela Zaccarelli. “Reversible gels of patchy particles”. In: *Current Opinion in Solid State and Materials Science* 15.6 (2011), pp. 246–253.

[261] Walter G Chapman et al. “SAFT: Equation-of-state solution model for associating fluids”. In: *Fluid Phase Equilibria* 52 (1989), pp. 31–38.

[262] Cristiano De Michele, Tommaso Bellini, and Francesco Sciortino. “Self-assembly of bifunctional patchy particles with anisotropic shape into polymers chains: Theory, simulations, and experiments”. In: *Macromolecules* 45.2 (2012), pp. 1090–1106.

[263] Francesco Sciortino. “Entropy in self-assembly”. In: *La Rivista del Nuovo Cimento* 42 (2019), pp. 511–548.

[264] Khanh Thuy Nguyen, Francesco Sciortino, and Cristiano De Michele. “Self-assembly-driven nematization”. In: *Langmuir* 30.16 (2014), pp. 4814–4819.

[265] Cristiano De Michele, Rolf Schilling, and Francesco Sciortino. “Dynamics of uniaxial hard ellipsoids”. In: *Physical review letters* 98.26 (2007), p. 265702.

[266] Maik Hadorn et al. “Specific and reversible DNA-directed self-assembly of oil-in-water emulsion droplets”. In: *Proc. Natl. Acad. Sci.* 109.50 (2012), pp. 20320–20325.

[267] Paul A Beales and T Kyle Vanderlick. “Application of nucleic acid–lipid conjugates for the programmable organisation of liposomal modules”. In: *Advances in colloid and interface science* 207 (2014), pp. 290–305.

[268] Lucia Parolini et al. “Volume and porosity thermal regulation in lipid mesophases by coupling mobile ligands to soft membranes”. In: *Nature communications* 6.1 (2015), p. 5948.

[269] Stephan Jan Bachmann et al. “Melting transition in lipid vesicles functionalised by mobile DNA linkers”. In: *Soft Matter* 12.37 (2016), pp. 7804–7817.

[270] Stef AJ van der Meulen and Mirjam E Leunissen. “Solid colloids with surface-mobile DNA linkers”. In: *J. Am. Chem. Soc.* 135.40 (2013), pp. 15129–15134.

[271] Xiuyang Xia et al. “Linker-mediated self-assembly of mobile DNA-coated colloids”. In: *Sci. Adv.* 6.21 (2020), eaaz6921.

[272] Bortolo Matteo Mognetti, Pietro Cicuta, and Lorenzo Di Michele. “Programmable interactions with biomimetic DNA linkers at fluid membranes and interfaces”. In: *Rep. Prog. Phys.* 82.11 (2019), p. 116601.

[273] Stefano Angioletti-Uberti, Bortolo M Mognetti, and Daan Frenkel. “Theory and simulation of DNA-coated colloids: a guide for rational design”. In: *Phys. Chem. Chem. Phys.* 18.9 (2016), pp. 6373–6393.

[274] Stephan Jan Bachmann, Marius Petitzon, and Bortolo Matteo Mognetti. “Bond formation kinetics affects self-assembly directed by ligand–receptor interactions”. In: *Soft matter* 12.47 (2016), pp. 9585–9592.

[275] Patrick Varilly et al. “A general theory of DNA-mediated and other valence-limited colloidal interactions”. In: *J. Chem. Phys.* 137.9 (2012), p. 094108.

[276] Stefano Angioletti-Uberti et al. “Communication: A simple analytical formula for the free energy of ligand–receptor-mediated interactions”. In: *The Journal of chemical physics* 138.2 (2013).

[277] Mirjam E Leunissen and Daan Frenkel. “Numerical study of DNA-functionalized microparticles and nanoparticles: Explicit pair potentials and their implications for phase behavior”. In: *The Journal of Chemical Physics* 134.8 (2011).

[278] Lorenzo Di Michele et al. “Effect of inert tails on the thermodynamics of DNA hybridization”. In: *Journal of the American Chemical Society* 136.18 (2014), pp. 6538–6541.

[279] John SantaLucia Jr. “A unified view of polymer, dumbbell, and oligonucleotide DNA nearest-neighbor thermodynamics”. In: *Proceedings of the National Academy of Sciences* 95.4 (1998), pp. 1460–1465.

[280] Lea-Laetitia Pontani et al. “Immiscible lipids control the morphology of patchy emulsions”. In: *Soft Matter* 9.29 (2013), pp. 7150–7157.

[281] Yinghao Wu et al. “Cooperativity between trans and cis interactions in cadherin-mediated junction formation”. In: *Proceedings of the National Academy of Sciences* 107.41 (2010), pp. 17592–17597.

[282] Connor J Thompson et al. “Cadherin cis and trans interactions are mutually cooperative”. In: *Proceedings of the National Academy of Sciences* 118.10 (2021), e2019845118.

[283] Jiawen Chen et al. “A computational model for kinetic studies of cadherin binding and clustering”. In: *Biophysical journal* 111.7 (2016), pp. 1507–1518.

[284] Lawrence Shapiro and William I Weis. “Structure and biochemistry of cadherins and catenins”. In: *Cold Spring Harbor perspectives in biology* 1.3 (2009), a003053.

[285] Carlo Ciatto et al. “T-cadherin structures reveal a novel adhesive binding mechanism”. In: *Nature structural & molecular biology* 17.3 (2010), pp. 339–347.

[286] Camila A Saez Cabezas et al. “Gelation of plasmonic metal oxide nanocrystals by polymer-induced depletion attractions”. In: *Proceedings of the National Academy of Sciences* 115.36 (2018), pp. 8925–8930.

[287] Beth A Lindquist et al. “On the formation of equilibrium gels via a macroscopic bond limitation”. In: *The Journal of Chemical Physics* 145.7 (2016).

[288] Zachary M Sherman et al. “Plasmonic response of complex nanoparticle assemblies”. In: *Nano Letters* 23.7 (2023), pp. 3030–3037.

[289] Jiho Kang et al. “Modular mixing in plasmonic metal oxide nanocrystal gels with thermoreversible links”. In: *The Journal of Chemical Physics* 158.2 (2023).

[290] Ryan B Jadrich, Delia J Milliron, and Thomas M Truskett. “Colloidal gels”. In: *The Journal of Chemical Physics* 159.9 (2023).

[291] Allison M Green et al. “Assembling inorganic nanocrystal gels”. In: *Nano Letters* 22.4 (2022), pp. 1457–1466.

[292] Michael P Howard et al. “Effects of linker flexibility on phase behavior and structure of linked colloidal gels”. In: *The Journal of Chemical Physics* 154.7 (2021).

[293] Michael P Howard et al. "Wertheim's thermodynamic perturbation theory with double-bond association and its application to colloid–linker mixtures". In: *The Journal of Chemical Physics* 154.2 (2021).

[294] Jiho Kang et al. "Colorimetric quantification of linking in thermoreversible nanocrystal gel assemblies". In: *Science Advances* 8.7 (2022), eabm7364.

[295] Camila A Saez Cabezas et al. "Universal gelation of metal oxide nanocrystals via depletion attractions". In: *Nano Letters* 20.5 (2020), pp. 4007–4013.

[296] Manuel N Dominguez et al. "Assembly of linked nanocrystal colloids by reversible covalent bonds". In: *Chemistry of Materials* 32.23 (2020), pp. 10235–10245.

[297] Jiho Kang et al. "Structural control of plasmon resonance in molecularly linked metal oxide nanocrystal gel assemblies". In: *ACS nano* (2023).

[298] Zachary M Sherman et al. "Colloidal nanocrystal gels from thermodynamic principles". In: *Accounts of Chemical Research* 54.4 (2021), pp. 798–807.

[299] Thomas M FitzSimons, Eric V Anslyn, and Adrianne M Rosales. "Effect of pH on the properties of hydrogels cross-linked via dynamic thia-michael addition bonds". In: *ACS Polymers Au* 2.2 (2021), pp. 129–136.

[300] Thomas M FitzSimons et al. "Preferential control of forward reaction kinetics in hydrogels crosslinked with reversible conjugate additions". In: *Macromolecules* 53.10 (2020), pp. 3738–3746.

[301] Kushal Thapa et al. "Photothermal Modulation of Dynamic Covalent Poly (ethylene glycol)/PEDOT Composite Hydrogels for On-Demand Drug Delivery". In: *ACS Applied Materials & Interfaces* 15.45 (2023), pp. 52180–52196.

[302] Murari Singh et al. "Linker-templated structure tuning of optical response in plasmonic nanoparticle gels". In: *The Journal of Physical Chemistry C* 126.39 (2022), pp. 16885–16893.

[303] Asish Pal, Aasheesh Srivastava, and Santanu Bhattacharya. “Role of Capping Ligands on the Nanoparticles in the Modulation of Properties of a Hybrid Matrix of Nanoparticles in a 2D Film and in a Supramolecular Organogel”. In: *Chemistry–A European Journal* 15.36 (2009), pp. 9169–9182.

[304] Morgan Delarue et al. “mTORC1 controls phase separation and the biophysical properties of the cytoplasm by tuning crowding”. In: *Cell* 174.2 (2018), pp. 338–349.

[305] Martina Bonucci, Tong Shu, and Liam J Holt. “How it feels in a cell”. In: *Trends in Cell Biology* (2023).

[306] Salman F Banani et al. “Biomolecular condensates: organizers of cellular biochemistry”. In: *Nature reviews Molecular cell biology* 18.5 (2017), pp. 285–298.

[307] Theodore Hueckel, Glen M Hocky, and Stefano Sacanna. “Total synthesis of colloidal matter”. In: *Nat. Rev. Mat.* 6.11 (2021), pp. 1053–1069.

[308] You-Jin Kim et al. “Advances in Colloidal Building Blocks: Toward Patchy Colloidal Clusters”. In: *Adv. Mat.* (2022), p. 2203045.

[309] Mingxin He et al. “Colloidal diamond”. In: *Nature* 585.7826 (2020), pp. 524–529.

[310] A Paul Alivisatos et al. “Organization of’nanocrystal molecules’ using DNA”. In: *Nature* 382.6592 (1996), pp. 609–611.

[311] Paul L Biancaniello, Anthony J Kim, and John C Crocker. “Colloidal interactions and self-assembly using DNA hybridization”. In: *Phys. Rev. Lett.* 94.5 (2005), p. 058302.

[312] Matthew R Jones, Nadrian C Seeman, and Chad A Mirkin. “Programmable materials and the nature of the DNA bond”. In: *Science* 347.6224 (2015), p. 1260901.

[313] Marie-Pierre Valignat et al. “Reversible self-assembly and directed assembly of DNA-linked micrometer-sized colloids”. In: *Proc. Natl. Acad. Sci.* 102.12 (2005), pp. 4225–4229.

[314] John Russo, Piero Tartaglia, and Francesco Sciortino. "Reversible gels of patchy particles: role of the valence". In: *J. Chem. Phys.* 131.1 (2009), p. 014504.

[315] Zhongmin Zhang and Kateri H DuBay. "The Sequence of a Step-Growth Copolymer Can Be Influenced by Its Own Persistence Length". In: *J. Phys. Chem. B* 125.13 (2021), pp. 3426–3437.

[316] Matthew N O'Brien et al. "Programming colloidal crystal habit with anisotropic nanoparticle building blocks and DNA bonds". In: *J. Am. Chem. Soc.* 138.44 (2016), pp. 14562–14565.

[317] Debapriya Banerjee et al. "Assembly of particle strings via isotropic potentials". In: *J. Chem. Phys.* 150.12 (2019), p. 124903.

[318] Marjolein Dijkstra and Erik Luijten. "From predictive modelling to machine learning and reverse engineering of colloidal self-assembly". In: *Nature Mat.* 20.6 (2021), pp. 762–773.

[319] Yee-Hung M Chan, Peter Lenz, and Steven G Boxer. "Kinetics of DNA-mediated docking reactions between vesicles tethered to supported lipid bilayers". In: *Proc. Natl. Acad. Sci.* 104.48 (2007), pp. 18913–18918.

[320] Robert J Rawle et al. "Vesicle fusion observed by content transfer across a tethered lipid bilayer". In: *Biophys. J* 101.8 (2011), pp. L37–L39.

[321] Minsub Chung, Bon Jun Koo, and Steven G Boxer. "Formation and analysis of topographical domains between lipid membranes tethered by DNA hybrids of different lengths". In: *Faraday discussions* 161 (2013), pp. 333–345.

[322] Kalthoum Ben M'Barek et al. "Phagocytosis of immunoglobulin-coated emulsion droplets". In: *Biomaterials* 51 (2015), pp. 270–277.

[323] Nina A Elbers et al. "Bulk scale synthesis of monodisperse PDMS droplets above 3 μm and their encapsulation by elastic shells". In: *Chem. Mat.* 27.5 (2015), pp. 1709–1719.

[324] Ivan Coluzza et al. “Design and folding of colloidal patchy polymers”. In: *Soft Matter* 9.3 (2013), pp. 938–944.

[325] Ivan Coluzza et al. “Sequence controlled self-knotting colloidal patchy polymers”. In: *Phys. Rev. Lett.* 110.7 (2013), p. 075501.

[326] Indrani Chakraborty et al. “Self-assembly dynamics of reconfigurable colloidal molecules”. In: *ACS Nano* 16.2 (2022), pp. 2471–2480.

[327] Pinar Akcora et al. “Anisotropic self-assembly of spherical polymer-grafted nanoparticles”. In: *Nature materials* 8.4 (2009), pp. 354–359.

[328] Victor Pryamtisyn et al. “Modeling the anisotropic self-assembly of spherical polymer-grafted nanoparticles”. In: *The Journal of chemical physics* 131.22 (2009), p. 221102.

[329] Tsung-Yeh Tang and Gaurav Arya. “Anisotropic three-particle interactions between spherical polymer-grafted nanoparticles in a polymer matrix”. In: *Macromolecules* 50.3 (2017), pp. 1167–1183.

[330] Nathan A Mahynski and Athanassios Z Panagiotopoulos. “Grafted nanoparticles as soft patchy colloids: Self-assembly versus phase separation”. In: *The Journal of Chemical Physics* 142.7 (2015), p. 074901.

[331] Richard Swinbank and R James Purser. “Fibonacci grids: A novel approach to global modelling”. In: *Q. J. R. Meteorol. Soc.* 132.619 (2006), pp. 1769–1793.

[332] Joshua A Anderson and Sharon C Glotzer. “The development and expansion of HOOMD-blue through six years of GPU proliferation”. In: *arXiv preprint arXiv:1308.5587* 26 (2013).

[333] Søren Toxvaerd and Jeppe C Dyre. *Communication: Shifted forces in molecular dynamics.* 2011.

[334] Joshua A Anderson, Chris D Lorenz, and Alex Travesset. "General purpose molecular dynamics simulations fully implemented on graphics processing units". In: *J. Comp. Phys.* 227.10 (2008), pp. 5342–5359.

[335] Joshua A Anderson, Jens Glaser, and Sharon C Glotzer. "HOOMD-blue: A Python package for high-performance molecular dynamics and hard particle Monte Carlo simulations". In: *Comp. Mat. Sci.* 173 (2020), p. 109363.

[336] Stephen Thomas et al. "Routine million-particle simulations of epoxy curing with dissipative particle dynamics". In: *J. Chem. Theor. Comput.* 17.03 (2018), p. 1840005.

[337] Nicholas Metropolis and Stanislaw Ulam. "The monte carlo method". In: *Journal of the American statistical association* 44.247 (1949), pp. 335–341.

[338] Daniel T Gillespie. "Stochastic simulation of chemical kinetics". In: *Annu. Rev. Phys. Chem.* 58 (2007), pp. 35–55.

[339] Douglas Barrick. *Biomolecular thermodynamics: From theory to application.* CRC Press, 2017.

[340] Roy J Glauber. "Time-dependent statistics of the Ising model". In: *Journal of mathematical physics* 4.2 (1963), pp. 294–307.

[341] Mark EJ Newman and Gerard T Barkema. *Monte Carlo methods in statistical physics.* Clarendon Press, 1999.

[342] Marilyn E Ferrari and Victor A Bloomfield. "Scattering and diffusion of mononucleosomal DNA: effects of counterion valence and salt, and DNA concentration". In: *Macromolecules* 25.20 (1992), pp. 5266–5276.

[343] Ilya Koltover, Kathrin Wagner, and Cyrus R Safinya. "DNA condensation in two dimensions". In: *Proc. Natl. Acad. Sci.* 97.26 (2000), pp. 14046–14051.

[344] Jens Glaser et al. “Strong scaling of general-purpose molecular dynamics simulations on GPUs”. In: *Comp. Phys. Comm.* 192 (2015), pp. 97–107.

[345] Carolyn L Phillips, Joshua A Anderson, and Sharon C Glotzer. “Pseudo-random number generation for Brownian Dynamics and Dissipative Particle Dynamics simulations on GPU devices”. In: *J. Comp. Phys.* 230.19 (2011), pp. 7191–7201.

[346] Ben Leimkuhler and Charles Matthews. *Molecular dynamics*. Vol. 36. Springer, 2015.

[347] Michael P Howard et al. “Efficient neighbor list calculation for molecular simulation of colloidal systems using graphics processing units”. In: *Comp. Phys. Comm.* 203 (2016), pp. 45–52.

[348] Michael P Howard et al. “Quantized bounding volume hierarchies for neighbor search in molecular simulations on graphics processing units”. In: *Comp. Mat. Sci.* 164 (2019), pp. 139–146.

[349] Pauli Virtanen et al. “SciPy 1.0: Fundamental Algorithms for Scientific Computing in Python”. In: *Nature Methods* 17 (2020), pp. 261–272. DOI: `10.1038/s41592-019-0686-2`.

[350] Bradley Efron and Robert J Tibshirani. *An introduction to the bootstrap*. CRC press, 1994.

[351] Anthony Trubiano and Miranda Holmes-Cerfon. “Thermodynamic stability versus kinetic accessibility: Pareto fronts for programmable self-assembly”. In: *Soft Matter* 17.28 (2021), pp. 6797–6807.

[352] Jorg Klingelhofer et al. “Dynamic interplay between adhesive and lateral E-cadherin dimers”. In: *Molecular and cellular biology* 22.21 (2002), pp. 7449–7458.

[353] Kevin Suffoletto, Deekshitha Jetta, and Susan Z Hua. “E-cadherin mediated lateral interactions between neighbor cells necessary for collective migration”. In: *Journal of Biomechanics* 71 (2018), pp. 159–166.

[354] Deborah Leckband and Anil Prakasam. “Mechanism and dynamics of cadherin adhesion”. In: *Annu. Rev. Biomed. Eng.* 8 (2006), pp. 259–287.

[355] William M Brieher, Martin Pruschy, Barry M Gumbiner, et al. “Lateral clustering of the adhesive ectodomain: a fundamental determinant of cadherin function”. In: *Current Biology* 7.5 (1997), pp. 308–315.

[356] Liong Seng Tee, Sukehiro Gotoh, and Warren E Stewart. “Molecular parameters for normal fluids. Lennard-Jones 12-6 Potential”. In: *Industrial & Engineering Chemistry Fundamentals* 5.3 (1966), pp. 356–363.

[357] Jean-Pierre Hansen and Loup Verlet. “Phase transitions of the Lennard-Jones system”. In: *physical Review* 184.1 (1969), p. 151.

[358] JJ Nicolas et al. “Equation of state for the Lennard-Jones fluid”. In: *Molecular Physics* 37.5 (1979), pp. 1429–1454.

[359] BJTJ Smit. “Phase diagrams of Lennard-Jones fluids”. In: *The Journal of chemical physics* 96.11 (1992), pp. 8639–8640.

[360] Vania MM Braga. “Cell–cell adhesion and signalling”. In: *Current opinion in cell biology* 14.5 (2002), pp. 546–556.

[361] Barry M Gumbiner. “Cell adhesion: the molecular basis of tissue architecture and morphogenesis”. In: *Cell* 84.3 (1996), pp. 345–357.

[362] Daniel A Hammer and Matthew Tirrell. “Biological adhesion at interfaces”. In: *Annual Review of Materials Science* 26.1 (1996), pp. 651–691.

[363] Amelia Ahmad Khalili and Mohd Ridzuan Ahmad. “A review of cell adhesion studies for biomedical and biological applications”. In: *International journal of molecular sciences* 16.8 (2015), pp. 18149–18184.

[364] Christiane A Helm, Wolfgang Knoll, and Jacob N Israelachvili. “Measurement of ligand-receptor interactions.” In: *Proceedings of the National Academy of Sciences* 88.18 (1991), pp. 8169–8173.

[365] BNJ Persson. “On the mechanism of adhesion in biological systems”. In: *The Journal of chemical physics* 118.16 (2003), pp. 7614–7621.

[366] Cheng Zhu, Gang Bao, and Ning Wang. “Cell mechanics: mechanical response, cell adhesion, and molecular deformation”. In: *Annual review of biomedical engineering* 2.1 (2000), pp. 189–226.

[367] Arpita Upadhyaya and Alexander van Oudenaarden. “Biomimetic systems for studying actin-based motility”. In: *Current Biology* 13.18 (2003), R734–R744.

[368] Michele Ciavarella et al. “The role of adhesion in contact mechanics”. In: *Journal of the Royal Society Interface* 16.151 (2019), p. 20180738.

[369] Alexander D Bershadsky, Nathalie Q Balaban, and Benjamin Geiger. “Adhesion-dependent cell mechanosensitivity”. In: *Annual review of cell and developmental biology* 19.1 (2003), pp. 677–695.

[370] Andy Aman and Tatjana Piotrowski. “Cell migration during morphogenesis”. In: *Developmental biology* 341.1 (2010), pp. 20–33.

[371] Wendy Thomas. “Catch bonds in adhesion”. In: *Annu. Rev. Biomed. Eng.* 10 (2008), pp. 39–57.

[372] Wendy E Thomas, Viola Vogel, and Evgeni Sokurenko. “Biophysics of catch bonds”. In: *Annu. Rev. Biophys.* 37 (2008), pp. 399–416.

[373] Samuel Hertig and Viola Vogel. “Catch bonds”. In: *Current Biology* 22.19 (2012), R823–R825.

[374] Bryan T Marshall et al. “Direct observation of catch bonds involving cell-adhesion molecules”. In: *Nature* 423.6936 (2003), pp. 190–193.

[375] V Barsegov and D Thirumalai. “Dynamics of unbinding of cell adhesion molecules: transition from catch to slip bonds”. In: *Proceedings of the National Academy of Sciences* 102.6 (2005), pp. 1835–1839.

[376] Sally A Kim et al. “Calcium-dependent dynamics of cadherin interactions at cell–cell junctions”. In: *Proceedings of the National Academy of Sciences* 108.24 (2011), pp. 9857–9862.

[377] Deborah Leckband and Sanjeevi Sivasankar. “Mechanism of homophilic cadherin adhesion”. In: *Current opinion in cell biology* 12.5 (2000), pp. 587–592.

[378] Sophie Chappuis-Flament et al. “Multiple cadherin extracellular repeats mediate homophilic binding and adhesion”. In: *The Journal of cell biology* 154.1 (2001), pp. 231–243.

[379] Han L Lim et al. “Smart hydrogels as functional biomimetic systems”. In: *Biomaterials Science* 2.5 (2014), pp. 603–618.

[380] Leonid Ionov. “Biomimetic hydrogel-based actuating systems”. In: *Advanced Functional Materials* 23.36 (2013), pp. 4555–4570.

[381] Roger Y Tam, Laura J Smith, and Molly S Shoichet. “Engineering cellular microenvironments with photo-and enzymatically responsive hydrogels: toward biomimetic 3D cell culture models”. In: *Accounts of chemical research* 50.4 (2017), pp. 703–713.

[382] Donghyuk Kim et al. “Microfluidics-based in vivo mimetic systems for the study of cellular biology”. In: *Accounts of chemical research* 47.4 (2014), pp. 1165–1173.

[383] Dorothea Brüggemann, Johannes P Frohnmayer, and Joachim P Spatz. “Model systems for studying cell adhesion and biomimetic actin networks”. In: *Beilstein journal of nanotechnology* 5.1 (2014), pp. 1193–1202.

[384] Pia Streicher et al. “Integrin reconstituted in GUVs: a biomimetic system to study initial steps of cell spreading”. In: *Biochimica et Biophysica Acta (BBA)-Biomembranes* 1788.10 (2009), pp. 2291–2300.

[385] Erich Sackmann and Ana-Sunčana Smith. “Physics of cell adhesion: some lessons from cell-mimetic systems”. In: *Soft matter* 10.11 (2014), pp. 1644–1659.

[386] Maria B Rahmany and Mark Van Dyke. “Biomimetic approaches to modulate cellular adhesion in biomaterials: A review”. In: *Acta biomaterialia* 9.3 (2013), pp. 5431–5437.

[387] Alexei Boulbitch, Zeno Guttenberg, and Erich Sackmann. “Kinetics of membrane adhesion mediated by ligand–receptor interaction studied with a biomimetic system”. In: *Biophysical Journal* 81.5 (2001), pp. 2743–2751.

[388] Daniel J Cohen, Martijn Gloerich, and W James Nelson. “Epithelial self-healing is recapitulated by a 3D biomimetic E-cadherin junction”. In: *Proceedings of the National Academy of Sciences* 113.51 (2016), pp. 14698–14703.

[389] M Lisa Manning. “Essay: Collections of deformable particles present exciting challenges for soft matter and biological physics”. In: *Physical Review Letters* 130.13 (2023), p. 130002.

[390] Sangwoo Kim and Sascha Hilgenfeldt. “A simple landscape of metastable state energies for two-dimensional cellular matter”. In: *Soft Matter* 15.2 (2019), pp. 237–242.

[391] Ian M Gemp, Richard W Carthew, and Sascha Hilgenfeldt. “Cadherin-dependent cell morphology in an epithelium: constructing a quantitative dynamical model”. In: *PLoS computational biology* 7.7 (2011), e1002115.

[392] Sangwoo Kim and Sascha Hilgenfeldt. “Cell shapes and patterns as quantitative indicators of tissue stress in the plant epidermis”. In: *Soft matter* 11.37 (2015), pp. 7270–7275.

[393] Sascha Hilgenfeldt, Sinem Erisken, and Richard W Carthew. "Physical modeling of cell geometric order in an epithelial tissue". In: *Proceedings of the National Academy of Sciences* 105.3 (2008), pp. 907–911.

[394] Guangnan Meng et al. "The free-energy landscape of clusters of attractive hard spheres". In: *Science* 327.5965 (2010), pp. 560–563.

[395] Johannes Kästner. "Umbrella sampling". In: *Wiley Interdisciplinary Reviews: Computational Molecular Science* 1.6 (2011), pp. 932–942.

[396] Amy Wang, Alexander R Dunn, and William I Weis. "Mechanism of the cadherin–catenin F-actin catch bond interaction". In: *Elife* 11 (2022), e80130.

[397] Sergei Izrailev et al. "Steered molecular dynamics". In: *Computational Molecular Dynamics: Challenges, Methods, Ideas: Proceedings of the 2nd International Symposium on Algorithms for Macromolecular Modelling, Berlin, May 21–24, 1997*. Springer. 1999, pp. 39–65.

[398] Shaon Chakrabarti, Michael Hinczewski, and D Thirumalai. "Phenomenological and microscopic theories for catch bonds". In: *Journal of structural biology* 197.1 (2017), pp. 50–56.

[399] Zachary M Sherman et al. "Inverse methods for design of soft materials". In: *The Journal of chemical physics* 152.14 (2020).

[400] Sanket Kadulkar et al. "Machine learning–assisted design of material properties". In: *Annual Review of Chemical and Biomolecular Engineering* 13 (2022), pp. 235–254.

[401] Michael Rubinstein, Ralph H Colby, et al. *Polymer physics*. Vol. 23. Oxford university press New York, 2003.

[402] Yongxiang Gao, Juntae Kim, and Matthew E Helgeson. "Microdynamics and arrest of coarsening during spinodal decomposition in thermoreversible colloidal gels". In: *Soft Matter* 11.32 (2015), pp. 6360–6370.

[403] PN Segre et al. “Glasslike kinetic arrest at the colloidal-gelation transition”. In: *Physical Review Letters* 86.26 (2001), p. 6042.

[404] Emanuela Zaccarelli. “Colloidal gels: Equilibrium and non-equilibrium routes”. In: *Journal of Physics: Condensed Matter* 19.32 (2007), p. 323101.

[405] Francesco Sciortino and Emanuela Zaccarelli. “Equilibrium gels of limited valence colloids”. In: *Current opinion in colloid & interface science* 30 (2017), pp. 90–96.

[406] Mehdi Bouzid and Emanuela Del Gado. “Mechanics of soft gels: Linear and nonlinear response”. In: *Handbook of Materials Modeling: Applications: Current and Emerging Materials* (2020), pp. 1719–1746.

[407] Guilherme de Oliveira Reis et al. “Irreversible hardening of a colloidal gel under shear: The smart response of natural rubber latex gels”. In: *Journal of colloid and interface science* 539 (2019), pp. 287–296.

[408] Emanuela Zaccarelli et al. “Gelation as arrested phase separation in short-ranged attractive colloid–polymer mixtures”. In: *Journal of Physics: Condensed Matter* 20.49 (2008), p. 494242.

[409] Aaron PR Eberle, Norman J Wagner, and Ramon Castaneda-Priego. “Dynamical arrest transition in nanoparticle dispersions with short-range interactions”. In: *Physical review letters* 106.10 (2011), p. 105704.

[410] Emanuela Zaccarelli et al. “Model for reversible colloidal gelation”. In: *Physical review letters* 94.21 (2005), p. 218301.

[411] Daniel de las Heras, José Maria Tavares, and Margarida M Telo da Gama. “Phase diagrams of binary mixtures of patchy colloids with distinct numbers and types of patches: The empty fluid regime”. In: *The Journal of chemical physics* 134.10 (2011).

[412] J Russo et al. “Re-entrant phase behaviour of network fluids: A patchy particle model with temperature-dependent valence”. In: *The Journal of chemical physics* 135.3 (2011).

[413] Lorenzo Rovigatti, José Maria Tavares, and Francesco Sciortino. “Self-assembly in chains, rings, and branches: a single component system with two critical points”. In: *Physical review letters* 111.16 (2013), p. 168302.

[414] John Russo et al. “Reentrant phase diagram of network fluids”. In: *Physical review letters* 106.8 (2011), p. 085703.

[415] Jan Mewis and Norman J Wagner. *Colloidal suspension rheology.* Cambridge university press, 2012.

[416] Hajime Tanaka. “Viscoelastic phase separation in biological cells”. In: *Communications Physics* 5.1 (2022), p. 167.

[417] Jeong-Mo Choi, Alex S Holehouse, and Rohit V Pappu. “Physical principles underlying the complex biology of intracellular phase transitions”. In: *Annual review of biophysics* 49 (2020), pp. 107–133.

[418] Barbara Ruzicka et al. “Observation of empty liquids and equilibrium gels in a colloidal clay”. In: *Nature materials* 10.1 (2011), pp. 56–60.

[419] Silvia Biffi et al. “Phase behavior and critical activated dynamics of limited-valence DNA nanostars”. In: *Proceedings of the National Academy of Sciences* 110.39 (2013), pp. 15633–15637.

[420] Lorenzo Rovigatti, Francesca Bomboi, and Francesco Sciortino. “Accurate phase diagram of tetravalent DNA nanostars”. In: *The Journal of Chemical Physics* 140.15 (2014).

[421] Javier Fernandez-Castanon et al. “Small-angle neutron scattering and molecular dynamics structural study of gelling DNA nanostars”. In: *The Journal of chemical physics* 145.8 (2016).

[422] Silvia Biffi et al. “Equilibrium gels of low-valence DNA nanostars: a colloidal model for strong glass formers”. In: *Soft Matter* 11.16 (2015), pp. 3132–3138.

[423] Dan T Nguyen and Omar A Saleh. “Tuning phase and aging of DNA hydrogels through molecular design”. In: *Soft Matter* 13.32 (2017), pp. 5421–5427.

[424] Nathaniel Conrad et al. “Emulsion imaging of a DNA nanostar condensate phase diagram reveals valence and electrostatic effects”. In: *The Journal of Chemical Physics* 157.23 (2022).

[425] Francesca Bomboi et al. “Equilibrium gels of trivalent DNA-nanostars: Effect of the ionic strength on the dynamics”. In: *The European Physical Journal E* 38 (2015), pp. 1–8.

[426] Javier Fernandez-Castanon, Francesca Bomboi, and Francesco Sciortino. “Binding branched and linear DNA structures: From isolated clusters to fully bonded gels”. In: *The Journal of Chemical Physics* 148.2 (2018).

[427] Nathaniel Conrad et al. “Increasing valence pushes DNA nanostar networks to the isostatic point”. In: *Proceedings of the National Academy of Sciences* 116.15 (2019), pp. 7238–7243.

[428] Enrico Lattuada et al. “Spatially uniform dynamics in equilibrium colloidal gels”. In: *Science Advances* 7.49 (2021), eabk2360.

[429] Enrico Lattuada, Tommaso Pietrangeli, and Francesco Sciortino. “Interpenetrating gels in binary suspensions of DNA nanostars”. In: *The Journal of Chemical Physics* 157.13 (2022).

[430] Nikola A Dudukovic and Charles F Zukoski. “Evidence for equilibrium gels of valence-limited particles”. In: *Soft Matter* 10.39 (2014), pp. 7849–7856.

[431] Eric Dickinson and Leif Eriksson. “Particle flocculation by adsorbing polymers”. In: *Advances in Colloid and Interface Science* 34 (1991), pp. 1–29.

[432] Jie Chen, Steven R Kline, and Yun Liu. "From the depletion attraction to the bridging attraction: The effect of solvent molecules on the effective colloidal interactions". In: *The Journal of chemical physics* 142.8 (2015).

[433] Junhua Luo et al. "Gelation of large hard particles with short-range attraction induced by bridging of small soft microgels". In: *Soft Matter* 11.12 (2015), pp. 2494–2503.

[434] Chuanzhuang Zhao et al. "Macrogel induced by microgel: Bridging and depletion mechanisms". In: *Soft Matter* 8.26 (2012), pp. 7036–7043.

[435] Amita Singh et al. "Linking Semiconductor Nanocrystals into Gel Networks through All-Inorganic Bridges". In: *Angewandte Chemie International Edition* 54.49 (2015), pp. 14840–14844.

[436] Vladimir Sayevich et al. "3D assembly of all-inorganic colloidal nanocrystals into gels and aerogels". In: *Angewandte Chemie International Edition* 55.21 (2016), pp. 6334–6338.

[437] Vladimir Sayevich et al. "Chloride and Indium-Chloride-Complex Inorganic Ligands for Efficient Stabilization of Nanocrystals in Solution and Doping of Nanocrystal Solids". In: *Advanced Functional Materials* 26.13 (2016), pp. 2163–2175.

[438] Vladimir Lesnyak et al. "CdTe nanocrystals capped with a tetrazolyl analogue of thioglycolic acid: aqueous synthesis, characterization, and metal-assisted assembly". In: *Acs Nano* 4.7 (2010), pp. 4090–4096.

[439] Christopher N Bowman and Christopher J Kloxin. "Covalent adaptable networks: reversible bond structures incorporated in polymer networks". In: *Angewandte Chemie International Edition* 18.51 (2012), pp. 4272–4274.

[440] Matthew J Webber et al. "Supramolecular biomaterials". In: *Nature materials* 15.1 (2016), pp. 13–26.

[441] Rudy J Wojtecki, Michael A Meador, and Stuart J Rowan. “Using the dynamic bond to access macroscopically responsive structurally dynamic polymers”. In: *Nature materials* 10.1 (2011), pp. 14–27.

[442] Yinghua Jin et al. “Recent advances in dynamic covalent chemistry”. In: *Chemical Society Reviews* 42.16 (2013), pp. 6634–6654.

[443] Victor Segui Barragan et al. “Dipolar ligands tune plasmonic properties of tin-doped indium oxide nanocrystals”. In: *Nano Letters* 23.17 (2023), pp. 7983–7989.

[444] James F Reuther, Samuel D Dahlhauser, and Eric V Anslyn. “Tunable orthogonal reversible covalent (TORC) bonds: Dynamic chemical control over molecular assembly”. In: *Angewandte Chemie International Edition* 58.1 (2019), pp. 74–85.

[445] Helen M Seifert, Karina Ramirez Trejo, and Eric V Anslyn. “Four simultaneously dynamic covalent reactions. Experimental proof of orthogonality”. In: *Journal of the American Chemical Society* 138.34 (2016), pp. 10916–10924.

[446] Marlon Gouveia, CS Dias, and JM Tavares. “Percolation in binary mixtures of linkers and particles: Chaining vs branching”. In: *The Journal of Chemical Physics* 157.16 (2022).

[447] James E Carpenter and Yamil J Colón. “Atomistic simulation of soft porous coordination polymers”. In: *The Journal of Chemical Physics* 158.7 (2023).

[448] Stefan Borsley and Euan R Kay. “Dynamic covalent assembly and disassembly of nanoparticle aggregates”. In: *Chemical Communications* 52.58 (2016), pp. 9117–9120.

[449] Caixia Ding et al. “Dually responsive injectable hydrogel prepared by in situ cross-linking of glycol chitosan and benzaldehyde-capped PEO-PPO-PEO”. In: *Biomacromolecules* 11.4 (2010), pp. 1043–1051.

[450] John D Weeks, David Chandler, and Hans C Andersen. “Role of repulsive forces in determining the equilibrium structure of simple liquids”. In: *The Journal of chemical physics* 54.12 (1971), pp. 5237–5247.

[451] David Michael Heyes and Hisashi Okumura. “Some physical properties of the Weeks–Chandler–Andersen fluid”. In: *Mol. Sim.* 32.01 (2006), pp. 45–50.

[452] Marvin Bishop, MH Kalos, and HL Frisch. “Molecular dynamics of polymeric systems”. In: *The Journal of Chemical Physics* 70.3 (1979), pp. 1299–1304.

[453] Gary S Grest and Kurt Kremer. “Molecular dynamics simulation for polymers in the presence of a heat bath”. In: *Physical Review A* 33.5 (1986), p. 3628.

[454] Arash Nikoubashman, Andrey Milchev, and Kurt Binder. “Dynamics of single semiflexible polymers in dilute solution”. In: *The Journal of chemical physics* 145.23 (2016).

[455] Arash Nikoubashman and Michael P Howard. “Equilibrium dynamics and shear rheology of semiflexible polymers in solution”. In: *Macromolecules* 50.20 (2017), pp. 8279–8289.

[456] Stefan Paquay and Remy Kusters. “A method for molecular dynamics on curved surfaces”. In: *Biophysical journal* 110.6 (2016), pp. 1226–1233.

[457] H Kamberaj, RJ Low, and MP Neal. “Time reversible and symplectic integrators for molecular dynamics simulations of rigid molecules”. In: *The Journal of chemical physics* 122.22 (2005).

[458] Francesco Sciortino et al. “Combinatorial-entropy-driven aggregation in DNA-grafted nanoparticles”. In: *ACS nano* 14.5 (2020), pp. 5628–5635.

[459] Jean-Pierre Hansen and Ian Ranald McDonald. *Theory of simple liquids: with applications to soft matter*. Academic press, 2013.

[460] Ryan B Jadrich et al. “Origin and detection of microstructural clustering in fluids with spatial-range competitive interactions”. In: *Physical Review E* 91.4 (2015), p. 042312.

[461] Tsutomu Furuya and Tsuyoshi Koga. “Molecular simulation of networks formed by end-linking of tetra-arm star polymers: Effects of network structures on mechanical properties”. In: *Polymer* 189 (2020), p. 122195.

[462] Demetris E Apostolides, Takamasa Sakai, and Costas S Patrickios. “Dynamic covalent star poly (ethylene glycol) model hydrogels: A new platform for mechanically robust, multifunctional materials”. In: *Macromolecules* 50.5 (2017), pp. 2155–2164.

[463] Andrew S Lyon, William B Peeples, and Michael K Rosen. “A framework for understanding the functions of biomolecular condensates across scales”. In: *Nature Reviews Molecular Cell Biology* 22.3 (2021), pp. 215–235.

[464] Peiguo Yang et al. “G3BP1 is a tunable switch that triggers phase separation to assemble stress granules”. In: *Cell* 181.2 (2020), pp. 325–345.

[465] Jonas Van Den Berg, Arnold J Boersma, and Bert Poolman. “Microorganisms maintain crowding homeostasis”. In: *Nature Reviews Microbiology* 15.5 (2017), pp. 309–318.

[466] Sho Asakura and Fumio Oosawa. “Interaction between particles suspended in solutions of macromolecules”. In: *Journal of polymer science* 33.126 (1958), pp. 183–192.

[467] R John Ellis. “Macromolecular crowding: obvious but underappreciated”. In: *Trends in biochemical sciences* 26.10 (2001), pp. 597–604.

[468] Huan-Xiang Zhou, Germán Rivas, and Allen P Minton. “Macromolecular crowding and confinement: biochemical, biophysical, and potential physiological consequences”. In: *Annu. Rev. Biophys.* 37 (2008), pp. 375–397.

[469] Guilherme Nettesheim et al. “Macromolecular crowding acts as a physical regulator of intracellular transport”. In: *Nature Physics* 16.11 (2020), pp. 1144–1151.

[470] Adrian F Pegoraro, Paul Janmey, and David A Weitz. “Mechanical properties of the cytoskeleton and cells”. In: *Cold Spring Harbor perspectives in biology* 9.11 (2017), a022038.

[471] Michele Di Pierro et al. “Anomalous diffusion, spatial coherence, and viscoelasticity from the energy landscape of human chromosomes”. In: *Proceedings of the National Academy of Sciences* 115.30 (2018), pp. 7753–7758.

[472] Xiaona Fang and Jin Wang. “Nonequilibrium thermodynamics in cell biology: Extending equilibrium formalism to cover living systems”. In: *Annual review of biophysics* 49 (2020), pp. 227–246.

[473] Anthony A Hyman and Clifford P Brangwynne. “Beyond stereospecificity: liquids and mesoscale organization of cytoplasm”. In: *Developmental cell* 21.1 (2011), pp. 14–16.

[474] Kathryn A Rosowski et al. “Elastic ripening and inhibition of liquid–liquid phase separation”. In: *Nature physics* 16.4 (2020), pp. 422–425.

[475] Subhadip Biswas, Biswaroop Mukherjee, and Buddhapriya Chakrabarti. “Thermodynamics predicts a stable microdroplet phase in polymer–gel mixtures undergoing elastic phase separation”. In: *Soft Matter* 18.42 (2022), pp. 8117–8123.

[476] Daniel SW Lee, Ned S Wingreen, and Clifford P Brangwynne. “Chromatin mechanics dictates subdiffusion and coarsening dynamics of embedded condensates”. In: *Biophysical Journal* 120.3 (2021), 318a.

[477] Yaojun Zhang et al. “Mechanical frustration of phase separation in the cell nucleus by chromatin”. In: *Physical review letters* 126.25 (2021), p. 258102.

[478] Meta Heidenreich et al. “Designer protein assemblies with tunable phase diagrams in living cells”. In: *Nature Chemical Biology* 16.9 (2020), pp. 939–945.

[479] Paul J Flory. *Principles of polymer chemistry*. Cornell University Press, 1953.

[480] Salman F Banani et al. “Compositional control of phase-separated cellular bodies”. In: *Cell* 166.3 (2016), pp. 651–663.

[481] Tyler S Harmon et al. "Intrinsically disordered linkers determine the interplay between phase separation and gelation in multivalent proteins". In: *elife* 6 (2017), e30294.

[482] Pilong Li et al. "Phase transitions in the assembly of multivalent signalling proteins". In: *Nature* 483.7389 (2012), pp. 336–340.

[483] Dan Bracha et al. "Mapping local and global liquid phase behavior in living cells using photo-oligomerizable seeds". In: *Cell* 175.6 (2018), pp. 1467–1480.

[484] Yongdae Shin et al. "Spatiotemporal control of intracellular phase transitions using light-activated optoDroplets". In: *Cell* 168.1 (2017), pp. 159–171.

[485] Kohji Murase et al. "Gibberellin-induced DELLA recognition by the gibberellin receptor GID1". In: *Nature* 456.7221 (2008), pp. 459–463.

[486] Takafumi Miyamoto et al. "Rapid and orthogonal logic gating with a gibberellin-induced dimerization system". In: *Nature chemical biology* 8.5 (2012), pp. 465–470.

[487] Ask Hjorth Larsen et al. "The atomic simulation environment—a Python library for working with atoms". In: *Journal of Physics: Condensed Matter* 29.27 (2017), p. 273002.

[488] Davide Loi, Stefano Mossa, and Leticia F Cugliandolo. "Effective temperature of active matter". In: *Physical Review E* 77.5 (2008), p. 051111.

[489] Christina M Caragine, Nikitas Kanellakopoulos, and Alexandra Zidovska. "Mechanical stress affects dynamics and rheology of the human genome". In: *Soft Matter* 18.1 (2022), pp. 107–116.

[490] Joshua A Riback et al. "Stress-triggered phase separation is an adaptive, evolutionarily tuned response". In: *Cell* 168.6 (2017), pp. 1028–1040.

[491] Daniel SW Lee et al. "Size distributions of intracellular condensates reflect competition between coalescence and nucleation". In: *Nature Physics* 19.4 (2023), pp. 586–596.

[492] Eric D Siggia. “Late stages of spinodal decomposition in binary mixtures”. In: *Physical review A* 20.2 (1979), p. 595.

[493] Ilya M Lifshitz and Vitaly V Slyozov. “The kinetics of precipitation from supersaturated solid solutions”. In: *Journal of physics and chemistry of solids* 19.1-2 (1961), pp. 35–50.

[494] Bradley R Parry et al. “The bacterial cytoplasm has glass-like properties and is fluidized by metabolic activity”. In: *Cell* 156.1 (2014), pp. 183–194.

[495] Predrag Bursac et al. “Cytoskeletal remodelling and slow dynamics in the living cell”. In: *Nature materials* 4.7 (2005), pp. 557–561.

[496] Emad Moeendarbary et al. “The cytoplasm of living cells behaves as a poroelastic material”. In: *Nature materials* 12.3 (2013), pp. 253–261.

[497] Hervé Turlier et al. “Equilibrium physics breakdown reveals the active nature of red blood cell flickering”. In: *Nature physics* 12.5 (2016), pp. 513–519.

[498] Gabor Csardi, Tamas Nepusz, et al. “The igraph software package for complex network research”. In: *InterJournal, complex systems* 1695.5 (2006), pp. 1–9.

[499] Anthony KL Leung. “Poly (ADP-ribose): a dynamic trigger for biomolecular condensate formation”. In: *Trends in cell biology* 30.5 (2020), pp. 370–383.

[500] Yuan Lin et al. “Formation and maturation of phase-separated liquid droplets by RNA-binding proteins”. In: *Molecular cell* 60.2 (2015), pp. 208–219.

[501] Clifford P Brangwynne et al. “Cytoplasmic diffusion: molecular motors mix it up”. In: *The Journal of cell biology* 183.4 (2008), pp. 583–587.

[502] Linhong Deng et al. “Fast and slow dynamics of the cytoskeleton”. In: *Nature materials* 5.8 (2006), pp. 636–640.

[503] Ming Guo et al. “Probing the stochastic, motor-driven properties of the cytoplasm using force spectrum microscopy”. In: *Cell* 158.4 (2014), pp. 822–832.

[504] Avinash Patel et al. “ATP as a biological hydrotrope”. In: *Science* 356.6339 (2017), pp. 753–756.

[505] David Zwicker et al. “Growth and division of active droplets provides a model for protocells”. In: *Nature Physics* 13.4 (2017), pp. 408–413.

[506] Baptiste Guilhas et al. “ATP-driven separation of liquid phase condensates in bacteria”. In: *Molecular Cell* 79.2 (2020), pp. 293–303.

[507] Saumya Saurabh et al. “ATP-responsive biomolecular condensates tune bacterial kinase signaling”. In: *Science Advances* 8.7 (2022), eabm6570.

[508] Rikki M Garner et al. “Vast heterogeneity in cytoplasmic diffusion rates revealed by nanorheology and Doppelgänger simulations”. In: *Biophysical journal* 122.5 (2023), pp. 767–783.

[509] Dajun Sang et al. “Condensed-phase signaling can expand kinase specificity and respond to macromolecular crowding”. In: *Molecular cell* 82.19 (2022), pp. 3693–3711.

[510] William M Jacobs, Aleks Reinhardt, and Daan Frenkel. “Rational design of self-assembly pathways for complex multicomponent structures”. In: *Proceedings of the National Academy of Sciences* 112.20 (2015), pp. 6313–6318.

[511] Paul M Dodd, Pablo F Damasceno, and Sharon C Glotzer. “Universal folding pathways of polyhedron nets”. In: *Proceedings of the National Academy of Sciences* 115.29 (2018), E6690–E6696.

[512] KD Danov et al. “Coalescence dynamics of deformable Brownian emulsion droplets”. In: *Langmuir* 9.7 (1993), pp. 1731–1740.

[513] Volkan Yesilyurt et al. “Mixed reversible covalent crosslink kinetics enable precise, hierarchical mechanical tuning of hydrogel networks”. In: *Advanced materials* 29.19 (2017), p. 1605947.

[514] Jake Song et al. “Dynamics of dual-junction-functionality associative polymer networks with ion and nanoparticle metal-coordinate cross-link junctions”. In: *Journal of Rheology* 66.6 (2022), pp. 1333–1345.

[515] Hugo Le Roy et al. “Valence can control the nonexponential viscoelastic relaxation of multivalent reversible gels”. In: *arXiv preprint arXiv:2112.07454* (2021).

[516] Yen H Tran et al. “Strain-stiffening gels based on latent crosslinking”. In: *Soft Matter* 13.47 (2017), pp. 9007–9014.

[517] Fabio Trovato and Valentina Tozzini. “Diffusion within the cytoplasm: a mesoscale model of interacting macromolecules”. In: *Biophysical journal* 107.11 (2014), pp. 2579–2591.

[518] W Abdul, P Bera, and J Mondal. “On the Spatial Positioning of Ribosomes around chromosome in E. coli Cytoplasm”. In: (2023).

[519] John E Hesketh and IF Pryme. “Interaction between mRNA, ribosomes and the cytoskeleton.” In: *Biochemical journal* 277.Pt 1 (1991), p. 1.

[520] U Bommer et al. “Ribosomes and polysomes”. In: *Subcellular Fractionation-A Practical Approach* (1997), pp. 271–301.

[521] Alexander Rich, Jonathan R Warner, and Howard M Goodman. “The structure and function of polyribosomes”. In: (1963).

[522] Thomas J Lampo et al. “Cytoplasmic RNA-protein particles exhibit non-Gaussian subdiffusive behavior”. In: *Biophysical journal* 112.3 (2017), pp. 532–542.

[523] Kurt Binder et al. “Confinement effects on phase behavior of soft matter systems”. In: *Soft Matter* 4.8 (2008), pp. 1555–1568.

[524] Simon Alberti, Amy Gladfelter, and Tanja Mittag. “Considerations and challenges in studying liquid-liquid phase separation and biomolecular condensates”. In: *Cell* 176.3 (2019), pp. 419–434.

[525] Michele Ceriotti, Giovanni Bussi, and Michele Parrinello. “Langevin equation with colored noise for constant-temperature molecular dynamics simulations”. In: *Physical review letters* 102.2 (2009), p. 020601.

[526] Michele Ceriotti, Giovanni Bussi, and Michele Parrinello. “Colored-noise thermostats à la carte”. In: *Journal of Chemical Theory and Computation* 6.4 (2010), pp. 1170–1180.